

# Cannon balls from Bremervörde (D)

A characterization of historic cannon balls using SEM and  
LA-ICPMS microchemistry

Tonny B. Thomsen, Nynke T. Keulen, Benjamin D. Heredia  
& Sebastian N. Malkki

# **Cannon balls from Bremervörde (D)**

A characterization of historic cannon balls using SEM and  
LA-ICPMS microchemistry

Tonny B. Thomsen, Nynke T. Keulen, Benjamin D. Heredia  
& Sebastian N. Malkki

## Summary

A total of 41 historic cannon balls from the 16<sup>th</sup> and 17<sup>th</sup> centuries were analysed by SEM (AQM and BSE) and LA-ICPMS with the aim of grouping the cannon balls using their textural and chemical-compositional attributes. With emphasis on using typical textures occurring in the cannon balls, the general composition of the sample material, trace element chemistry of carefully selected and omnipresent Fe-rich phases, and a principal component analysis (PCA) methodology, the cannon ball can be divided into at least three, but likely four groups with distinct and reasonably noticeable attributes. The report includes the results from this reconnaissance study, which constitutes a first attempt to characterize such materials using a combination of electronic microscopy and LA-ICPMS instrumentation and method setup.

## Dansk resume

Kanonkugler anvendt i det 16. og 17. århundrede er blevet analyseret vha. SEM og LA-ICPMS for at undersøge om det er muligt på baggrund af deres teksturelle karakteristika og kemiske sammensætning at skelne imellem kanonkuglerne, for derved at kunne gruppere de respektive kanonkugler mhp. en arkæologisk fortolkning af brugen, oprindelsen og eftermælet for kanonkuglerne. Sekundært var det et mål at undersøge kanonkuglernes proveniens, det vil sige fra hvilke miner eller malm-områder kanonkuglerne kunne tænkes at de oprindeligt er udgravet fra. Hvis metoderne brugt ifm. produktion af kanonkuglerne har udslettet ethvert proveniens kendetegn, så undersøge proveniensen for fabrikationen af kanonkuglerne, dvs. hvor og måske hvordan kanonkuglerne er fremstillet. Denne rapport indeholder kun data for den første del af undersøgelserne rettet imod en gruppering af kanonkuglerne, da den tid som var allokeret til projektet kun tillod at gennemføre dette delmål. Kanonkuglerne formodes anvendt i forskellige krige, og er en del af Bachmann-Museum Bremervördes 102 stk. store samling af kanonkugler fra denne historiske tidsperiode.

Til undersøgelserne blev anvendt automated quantitative mineral mapping (AQM) og BSE imaging vha. Skanning-Elektron Mikroskopi (SEM) og efterfølgende Laser Ablation Inductively Coupled Plasma Mass Spectrometry (LA-ICPMS). Med disse analyseinstrumenter er kanonkuglerne blevet karakteriseret tekturelt og den kemiske sammensætning bestemt.

Resultaterne af analyserne viser at det er muligt med denne instrument-sammensætning at inddеле de analyserede prøver i mindst 3, men formentlig 4 grupper baseret på typiske teksturer, der forekommer i kanonkuglerne, samt nogle karakteristiske forhold for den kemiske sammensætning af kanonkuglernes jern-rigeste faser. Foruden SEM data og billeder samt kemiske sporelement-forhold er der også inddraget principal component analysis (PCA) til karakterisering af kanonkuglernes beskaffenhed mhp. en tilstrækkelig pålidelig gruppering af kanonkuglerne.

Resultaterne fra dette rekognoseringsprojekt bidrager til forståelsen af, hvordan man på baggrund af teksturelle og kemiske data kan differentiere imellem de forskellige typer af historiske kanonkugler, som i deres udgangspunkt måske ligner hinanden. En række yderligere analyser anbefales dog for at kunne indarbejde proveniensanalysen i karaktereringen af sådanne materialer for derigennem at få det bedst mulige grundlag for en videnskabelig robust fortolkning.

# Content

<b>1.</b>	<b>Rationale for the project</b>	<b>6</b>
<b>2.</b>	<b>Analytical techniques used</b>	<b>8</b>
<b>3.</b>	<b>Results</b>	<b>12</b>
<b>4.</b>	<b>Concluding remarks</b>	<b>25</b>
<b>5.</b>	<b>Recommendations for future work</b>	<b>26</b>
<b>6.</b>	<b>Acknowledgements</b>	<b>27</b>
<b>7.</b>	<b>Electronically appendices (supplementary files)</b>	<b>28</b>
<b>8.</b>	<b>References</b>	<b>29</b>

# 1. Rationale for the project

The Bachmann-Museum in Bremervörde, Germany, hosts a collection of 102 historic cannon balls discovered throughout the region. The cannon balls were utilized in various battles during the period from 1547 to 1674. The 102 specimens are composed predominantly of iron (97), lead (2), iron+lead (1), and 2 are stony cannon balls. The condition of the cannon balls greatly varies from almost intact original surfaces to slightly corroded or almost completely degraded material.

Some of the cannon balls can be assigned to entries in the access books. However, this is not possible for all the cannon balls found. For 62 of the iron cannon balls more or less accurate information exist for the place of discovery. This is typically in the vicinity of the Bremervörde Castle grounds near the former army path, or in the surrounding area (Fig. 1). Those cannon balls were most probably shot out from the castle's cannons. Other cannon balls have a somewhat unclear origin with respect to their archeological context. Some of them do not fit any cannon type known to be used. The calibers of these cannon balls in the inventory lists are just as diverse as those in the museum's collection, making it difficult to obtain further information from there. In addition, the inventory of the castle shrunk severely during 1657-1660 as a result of besieging by Denmark.

It is most likely that some of the cannon balls were produced by the intruding opponent. At this time, the iron ore material used for cannon balls was most likely cast fairly close to the location where it was mined using production methods characteristic of those facilities. The ore material and/or manufacturing processes of these cannon balls, as well as of the locally German-produced cannon balls, may have different chemical characteristics that can be used to differentiate between the various kinds of cannon balls.

It was the main purpose of this project to gain new knowledge about the cannon balls regarding the type variation of the cannon balls, thereby enabling the differentiation between them. If this differentiation was possible from the new results, a secondary target was to fingerprint or try to constrain the provenance of the cannon balls, including the differentiation between the production methods used for the cannon balls, which would tell something about the original site(s) for the manufacturing of the cannon balls.

In the project, we have used two different analytical techniques that produce complementary chemical and textural data to investigate what can be revealed from such data in terms of fingerprinting information usable for the interpretation of the archeological context for the cannon balls. To our knowledge, this project is the first study on the historic cannon balls from Bremervörde, where the composition of the cannon ball material is investigated using modern Scanning Electron Microscopy (SEM) and Laser Ablation ICP Mass Spectrometry (LA-ICPMS) techniques. The analytical methods and results of this reconnaissance study are reported here with supplementary data and (high-resolution) images given in associated files. The focus of the analytical work was on chemical and

textural imaging of the sample material using SEM, followed by microanalyses of selected chemical phases by LA-ICPMS.



NIBIS®Kartenserver

copyright © Landesamt für Bergbau, Energie und Geologie

L:EG

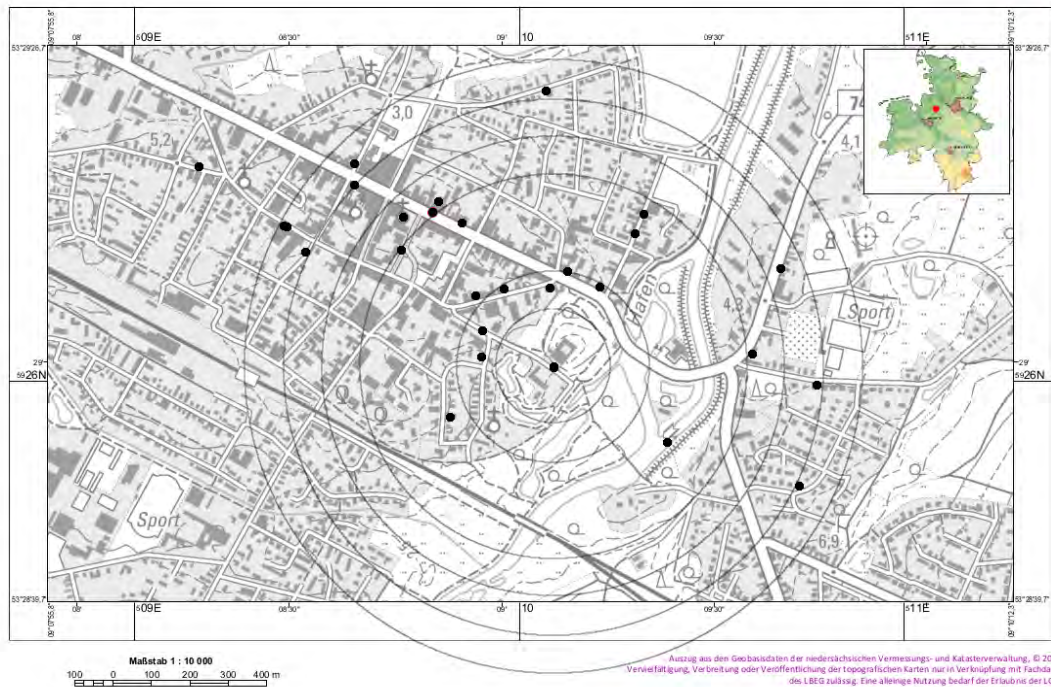


**Figure 1:** At top, a photo of some of the cannon balls from the collection at the Bachmann-Museum, Bremervörde in northern Lower Saxony. The figure below is a map of the city of Bremervörde on a 1:10,000 scale with discovery locations (black dots) relative to the Vörde Castle for some of the cannon balls of the Museum's archaeological collection.

## 2. Analytical techniques used

In disciplines like materials science, geoscience and akin, *in situ* microanalyses of crystalline materials are routinely carried out using analytical techniques like Scanning Electron Microscopy (SEM) and Laser Ablation Inductively Coupled Plasma Mass Spectrometry (LA-ICPMS) to provide information about the texture of the analysed materials and their chemical composition (i.e., elemental or isotopic abundances). In this project we have used SEM, LA-ICPMS, and optical microscopy, to characterise the textural appearance and the chemistry of the materials sampled, either drilled out from the cannon balls or sent as the raw cannon balls material stored at the museum.

A set of 41 cannon ball samples (Appendix A) were mounted in epoxy and analysed in the Scanning Electron Microscope (SEM). The purpose was to obtain images for the texture and measure the approximate composition of the samples (chemistry and mineralogy). The images were also used as documentation for the Laser Ablation Inductively Coupled Plasma Mass Spectrometry (LA-ICP-MS) analyses, where trace elemental compositions were determined. Part of the samples consist of flakes of the cannon ball, which were taken from the outermost layer. Other samples were drilled out of rust-cleaned cannon balls; these samples generally consist of very small pieces.

**Sample preparation** at GEUS included encapsulating selected pieces or all the cannon ball sample materials available into epoxy mounts of 40 mm in diameter using a Struers CitoPress-30 hot mounting press. The epoxy mounts were polished by routine procedures using Struers polishing instrumentation and diamond paste. The mounts were used for the subsequent analyses. The samples that consisted of drilled-out cannon balls material required chemical cleaning to remove the WD-40 used as lubricant during the drilling, as WD-40 contaminates the SEM and LA-ICPMS. The epoxy mounts were first imaged by optical microscopy, then analysed by SEM followed by LA-ICPMS.

**Optical microscopy** was used exclusively for acquiring overview pictures of the mounts. These were used to manoeuvre during SEM and LA-ICPMS analysis, and for reference to the back-scattered (BSE) and automated mineral images obtained by the SEM as well as for the analyses obtained by LA-ICPMS. All optical, BSE and AQM (see below) images are included into Appendix B.

**SEM analyses** were used in two ways, viz. back-scattered imaging and automated quantitative mineral mapping (AQM). **Automated quantitative mineral mapping (AQM)** was performed on the SEM at the Geological Survey of Denmark and Greenland (GEUS), using the ZEISS Mineralogic software platform (Fig. 2). All samples had representative areas imaged with a back-scattered electron contrast detector (BSE), which shows the material/density contrast in the samples, with the most dense/heavy material in white and lighter material in dark grey tones. Individual images are placed in a mosaic and saved as the BSE-map of the sample (Appendix B). Energy dispersive spectrometry (EDS) was applied to analyse the chemistry of the samples. The chemistry in each



analytical point analysed by the EDS detectors was interpreted as a mineral phase and each analytical point forms one pixel in a false coloured mineral map (MIN) (see Appendix B). Further details on the software and applied methodology can be found in Keulen et al. (2020). From the MIN map, we can extract the bulk mineralogy for the samples (reported in Appendix C), where only minerals/phases present in concentrations larger than 0.5 area% are shown.

The samples were analysed without coating at 30 Pa vacuum, 12-15 kV acceleration voltage, 120  $\mu\text{m}^2$  aperture, 275 kcps throughput rate and a dwell time of 0.015-0.025 seconds. The spot size used for the analysis varied from 0.5 to 20  $\mu\text{m}$  (though mainly 2 or 5  $\mu\text{m}$ ) depending on the resolution needed for the optimal analysis results.

### ***Limitations of the AQM and EDS technique***

The **AQM** software has a first-match routine. This means that if a mineral in the list fits two descriptions, always the first mineral from the list that matches the chemistry is used in the classification. Thus, the order of mineral list items is important. Here, we applied the following order: first we selected the Fe-silicates from the sample, then a range of metals that often occurs in iron ores and potentially may be used as tracers: Sn, Co, Cr, V, Ti, Pb, Ni, Mn, Cu, Zn. Subsequently, the samples were investigated for the presence of phosphorus and sulfur. All these elements had a threshold value of 5 wt%. As a next step the iron content in the samples was mapped in steps of 10 wt% from 30% to 100% of iron in iron-oxides/hydroxides with pure iron as a last step. This shows the amount of rusting or oxidation (more oxygen, less iron), but also if the iron is pure or occurs as magnetite ( $\text{Fe}_3\text{O}_4$ ) or hematite ( $\text{Fe}_2\text{O}_3$ ). Finally, other silicates, especially quartz are coloured. The order of minerals in the Excel sheets matches this mineral list.

Hydrogen cannot be detected with **EDS** detectors. Thus, the chemical analysis cannot separate iron-hydroxides from iron-oxides. Various iron-rust minerals contain hydroxides, which will show in the EDS/AQM results as oxides. The various  $\text{FeO}_x$  minerals can therefore be various types of rust as well as oxidized iron. Here, they will be described as  $\text{FeO}_x$  and iron oxides/hydroxides.

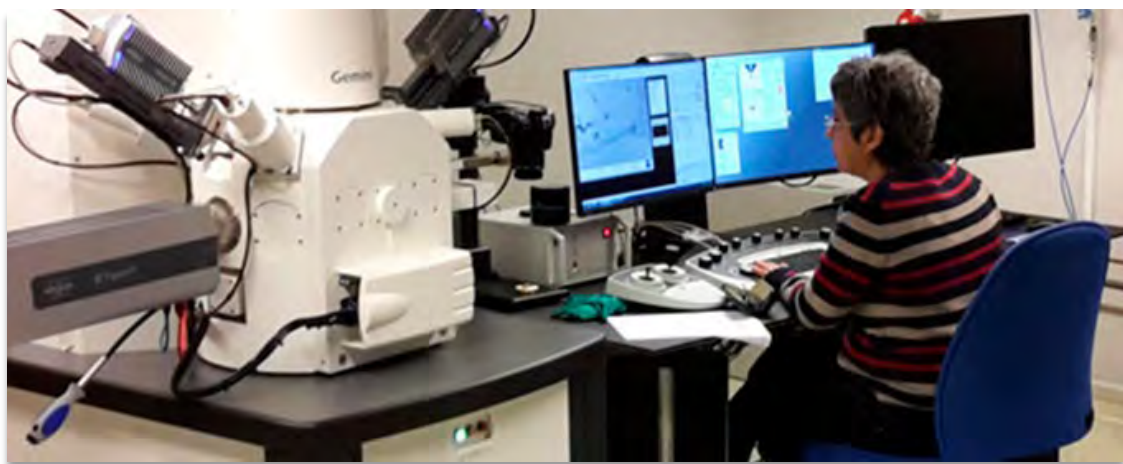


**Figure 2:** The Scanning Electron Microscopy laboratory at GEUS.

**Laser ablation inductively coupled plasma mass spectrometry (LA-ICPMS)** is used to measure the trace element concentrations of selected Fe-rich phases in the cannon ball samples. A NWR213 solid state Nd:YAG laser ablation system from Elemental Scientific Lasers (ESL) mounted with a standard TV2 ablation cell was coupled to an ELEMENT 2 double-focusing single-collector magnetic sector-field ICPMS from Thermo-Fisher Scientific (Fig. 3). The mass spectrometer is equipped with a Jet interface pump system and used X-type (jet) sampler and H-type skimmer Ni cones (thus Ni was not included into the analyses), and a quartz torch shielded with a grounded Pt electrode. Operating conditions and data acquisition parameters are listed in Appendix D.

The laser was heated up for at least 15 minutes before operation, providing stable laser output energy and flat ablation craters by the “resonator-flat” laser beam. Prior to loading, samples and standards were carefully cleaned using ethanol and an ultrasonic bath to remove surface contamination. The ablation cell with the custom-made sample holder was flushed with helium gas to minimize and stabilize the gas blank level. Helium was used as carrier gas and was mixed with argon gas ca. 0.5 m before entering the mass spectrometer. The mass spectrometer was run for at least one hour before analysis to stabilise and minimise the Hg and Pb background signal.

The ICP-MS was optimised for dry plasma conditions through continuous linear ablation of the NIST612 glass and the GJ-1 zircon standards. The signal-to-noise ratios were maximised for isotopes in the entire mass range of interest (i.e., Sc to Pb) while opting for low element-oxide production levels by minimising the  $^{238}\text{UO}/^{238}\text{U}$  ratios. To optimise the top peak location for all elements, a mass offset correction procedure was employed. Instrumental drift was minimized by using a standard-sample-standard analysis protocol, bracketing 6 sample analyses by 3 measurements of the primary standard BCR-2.

The quality of the standard measurements was controlled by regular measurements of the reference standards NIST-610, NIST-614 glasses and the BHVO-2 basalt glass as well as a synthetic Fe-rich standard (E363) made from meteorite material (van Kooten et al. 2022). All standards yielded averaged internal 2SE uncertainties of <10 % for all elements with concentrations above 1-2 ppm, except for Cr and Sc (<20%). Average accuracies for most elements above 1-2 ppm was within 5-10% deviation from reference values, whereas the accuracy for elements with abundances below 2 ppm typically showed up to 20-25 % deviation (Fig. 4). Data were acquired from single spot analyses of 25  $\mu\text{m}$  in diameter, using nominal laser fluence of  $\sim 3.5 \text{ J/cm}^2$  and a pulse rate of 10 Hz. Total acquisition time for single analyses were ca. 150 sec., including pre-ablation (5 pulses) followed by 60 sec. gas blank, then by laser ablation for 40 sec. and washout for 40 sec. Factory-supplied software from Thermo-Fisher Scientific was used for the acquisition of the transient data, obtained through pre-set spot locations. Data reduction was performed off-line through the software Lolite version 2.5 (Hellstrom et al. 2008, Paton et al. 2011) using the Trace\_Elements\_IS routine and  $^{57}\text{Fe}$  as the internal standard element assuming 70 wt% Fe for all Fe-rich (Fe70-100) phases measured on the sample.



**Figure 3:** The Laser Ablation ICP-MS facility at GEUS (the laser ablation instrument in front).

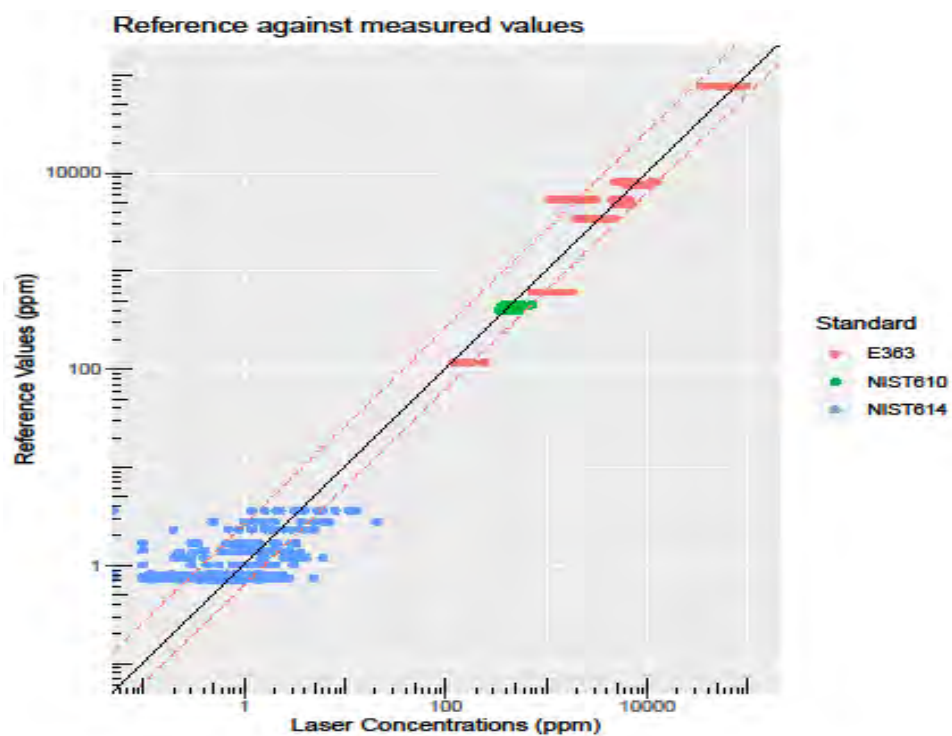


**Figure 4:** Diagram showing the accuracy for the measured elements in the reference standards E363, NIST610 and NIST614 that were included in the analyses. The solid line represents the “perfect fit” (i.e., 100% accuracy) of the data, with the dashed lines along the solid line denoting the 10% accuracy-offset compared to published values for the reference standards.

## 3. Results

Below are listed some of the attributes that were identified from the produced analyses. It is not intended to be an ultimate reporting of *all* possible results that can emerge from the new data. It is merely what we at GEUS were able to deduce from the data and images produced in the time available, and that we considered useful for interpretation with regards to the purposes of the study. A more detailed investigation of the data will most probably reveal further and more detailed information.

In general, we have focused our efforts on targeting the differentiation question only. This is because early in the project it became apparent that a profound investigation of the provenance for the geological origin of the Fe-ores in terms of a geographical or a geological fingerprinting was not possible. These limitations were due to the time available for the study and the lack of background information for comparison work. A complete investigation of provenance and Fe-ore fingerprinting will require a substantially deeper background study acquiring sufficient background information and data like comparable Fe-ore materials from relevant areas in question (e.g., Norway, Sweden, Denmark and Germany). In section 5, we have briefly described the requirement for a profound background study to be able to carry out such a fingerprinting of the cannon balls.

### 3.1. Results based on Scanning Electron Microscopy

The **SEM analyses** produced BSE and automated mineral (chemical) phase images (see Appendix B+C). Two different ways to divide the samples into subgroups were employed. First, we made a division based on *textural* features, these are best observed on the BSE images. Secondly, we made a division based on the *bulk composition* of the samples, these are easiest recognizable from the AQM maps (phase image).

#### ***Division 1: samples grouped by textural features***

Based on their texture, samples could be divided into four groups (see Figure 5 for illustration of the most common textures). Note that for the sample material that were drilled out of the cannon balls, the textural analyses are much less certain, because the investigated surfaces are a lot smaller than for the large flakes and pieces that were collected from the other cannon ball samples.

**A: 5843; 5872; 5913; 5933:**

These samples contain large amounts of iron-silicate minerals and show no signs of quenching. Possible interpretation: The cannon balls lack evidence of a cast-made iron production process and is most likely derived directly from an iron-ore. The material might be iron slags.

**B:** 5847; 5895; 5897; 5903:

These samples have spherical and vermicular dendritic textures (see Fig. 5), but also contain subhedral iron oxide grains (melts at around 1400 °C), sulfides, iron-silicate and silicate minerals (the latter melt at around 1200 °C), which would indicate that the sample has not been fully but only partially melted.

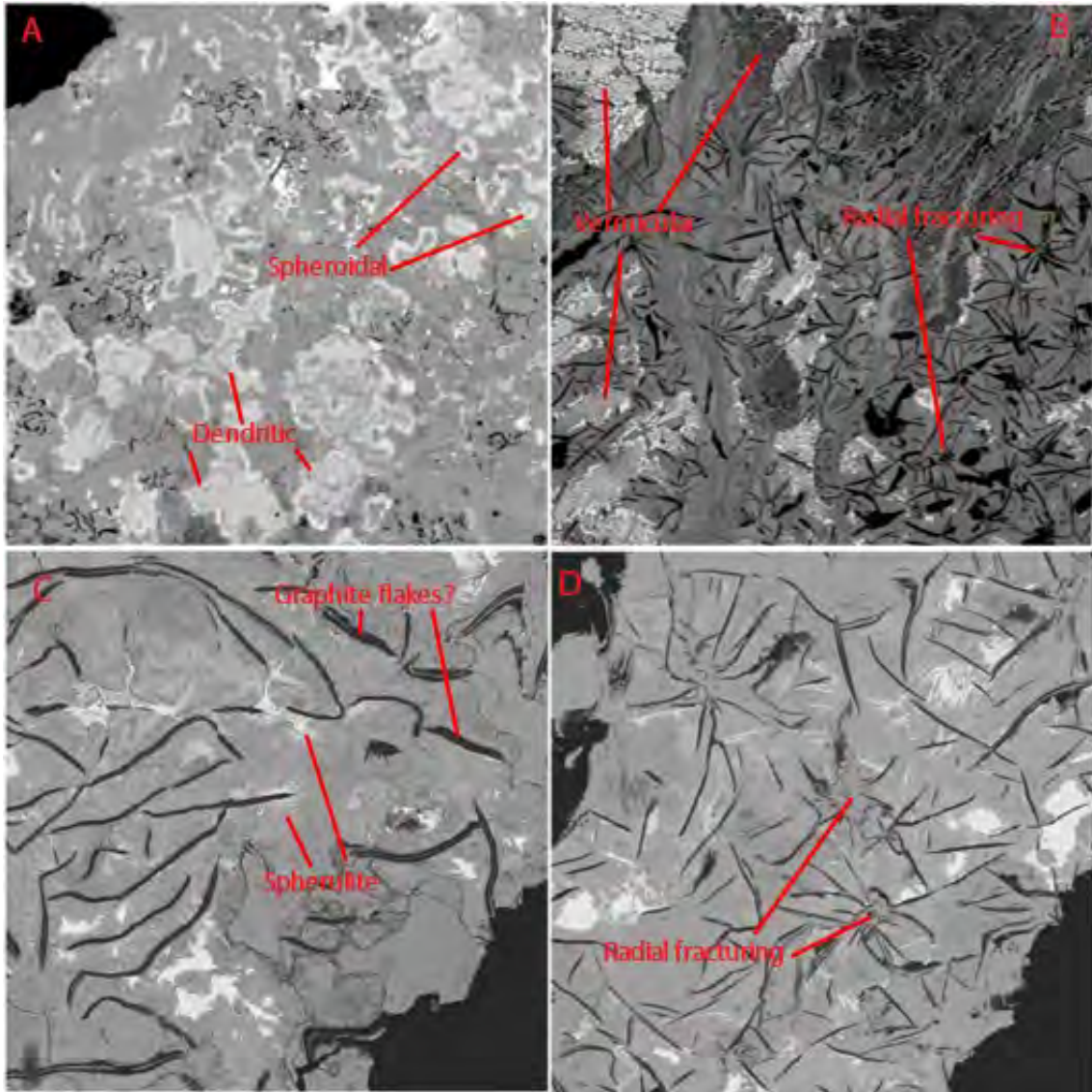


**Figure 5:** Examples of textures observed in the BSE images of the cannon balls. A: Sample 5852 (group C in division 1), field of view 1.75 mm. B: Sample 5891 (group B in division 1), field of view 2.2 mm. C: Sample 5855 (group B in division 1), field of view 0.5 mm. D: Sample 5890 (group B in division 1), field of view 0.5 mm.

**C:** 1063; 5825; 5826; 5831; 5833; 5840; 5844; 5845; 5851; 5852; 5855; 5867; 5868; 5870epoxy; 5877; 5890; 5891; 5894; 5905; 5911; 5923; 5930:

These samples show clear melting and quenching textures including spherulites/spheroidal textures, dendritic textures and radial fracturing (Figure 5). Furthermore, the samples contain no silicate minerals and are very iron-rich leading to the conclusion that they

have been melted. In addition, sample 5923, among others, shows a variation in iron oxide/hydroxide content from the edges and towards the center of the sample which corresponds very well with this sample being melted and subsequently cooled. Black lamella occurring in many of these samples could be graphite flakes, which are common constituents in cast iron (Figure 5).

**D:** 5837; 5846; 5857; 5870; 5871; 5893; 5898; 5899; 5904; 5910; 5934:

Samples containing high amounts of pure iron that is very uniform with little to no additional textural information.

## ***Division 2: samples grouped by bulk composition from SEM***

At least three distinct cannon ball types appear to be present based on the mineral phase images: **(A)** cannon balls that include a substantial amount of phosphoric chemical phases; **(B and D)** cannon balls that are almost exclusively composed of iron (ore) and essentially no other constituents, and **(C)** cannon balls that are composed by various “impurity” constituents (compared to the pure iron cannon balls) and that in some cases resemble slag material.

In this division into subgroups, samples are distinguished mainly by their bulk composition as determined in area % by AQM (Fig. 6 and Appendix C). Note that the metals e.g., “Zinc” means that the phase detected contains at least 5 % Zn. Most of the material can still be iron or an iron-oxide/hydroxide, e.g., 95 % FeOx + 5 % Zinc. It was possible to make three subgroups based on this criterion. Results for the AQM analyses are given below.

### ***A) Samples with more than 50 area% pure iron***

1063; 5825; 5831; 5833; 5837; 5846; 5857; 5870; 5871; 5893; 5898; 5899; 5904; 5905; 5910; 5911; 5913; 5934:

The above samples (sorted by descending iron content) all contain more than 50% pure iron and up to a maximum of 88% pure iron in sample 5893. Some samples (e.g., 5905 and 5825) also contain phosphides. Some samples, 5934 and 5899, contain minor amounts of other metals (e.g., zinc) within the pure iron.

### ***B) Samples with less than 50 area% pure iron***

5826; 5840; 5844; 5845; 5847; 5851; 5851; 5855; 5867; 5877; 5890; 5891; 5894; 5903; 5923:

Samples 5826,5844,5891,5894,5923,5851,5890,5855 and 5877 contain none to small amounts of other phases than pure iron and iron oxides/hydroxides (FeOx) with varying amount of Fe and O. The remaining samples in this group contain a significant number of phosphides (e.g., 5867) and silicate mineral phases.

### ***C) Samples with no pure iron (only iron oxides)***

5843; 5852; 5868; 5870epoxy; 5872; 5895; 5897; 5930; 5933:

The third group of samples contains no pure iron in their bulk composition but do have high amounts of iron oxides/hydroxides. This group does in general also contain more silicate phases than groups A and B. Sample 5868 is very diverse in its composition and contains both sulphides, phosphides, silicates, FeOx and some metals.

### **3.1.1. Remarks to the SEM results**

Note that sample 5870 was analysed twice, once on material derived from the outer part of the cannon ball (i.e., the “5870epoxy”) and once from drilled out material from within the cannon ball (i.e., the “5870”).

Although they are from the same sample, these two samples did not show the same criteria, neither in terms of texture, nor in terms of composition. Consequently, they were allocated to different groups. This demonstrates that significant differences exist even between sample pieces collected from the same sample; here from the outer crust of the sample material and from material drilled from within the cannon ball sample, respectively. The drilled sample material from within the cannon balls is less oxidized/rusty, but also shows less melting and quenching textures. It is thus likely that the largest variation in texture is observed at the outer rim of the cannon balls. This shows that comparison between the drilled sample material and pieces from the outer parts of the cannon balls can appear very different. This introduces an additional parameter increasing the uncertainty of the results, and it can in fact be questioned if it is reasonable to directly compare data that is obtained from the cannon balls in too differing ways or that originate from different parts of the cannon balls.

Future sampling of similar cannon ball materials should therefore be performed systematically and with great caution and must include the reporting from where the material is sampled from on the cannon balls, comparable to how it is listed in Appendix A

The samples 5867, 5868, 5870, 5897, 5903, and 5913 are examples of cannon balls that show a very large textural variation within the analysed area. The same may apply more generally to several of the cannon ball samples, i.e., they are very inhomogeneous in composition, even when looking only at the outermost layer of the cannon ball. Compositions should therefore be cautiously compared, rather to be taken as a list of included phases with an absolute number representing the entire composition of the cannon ball.

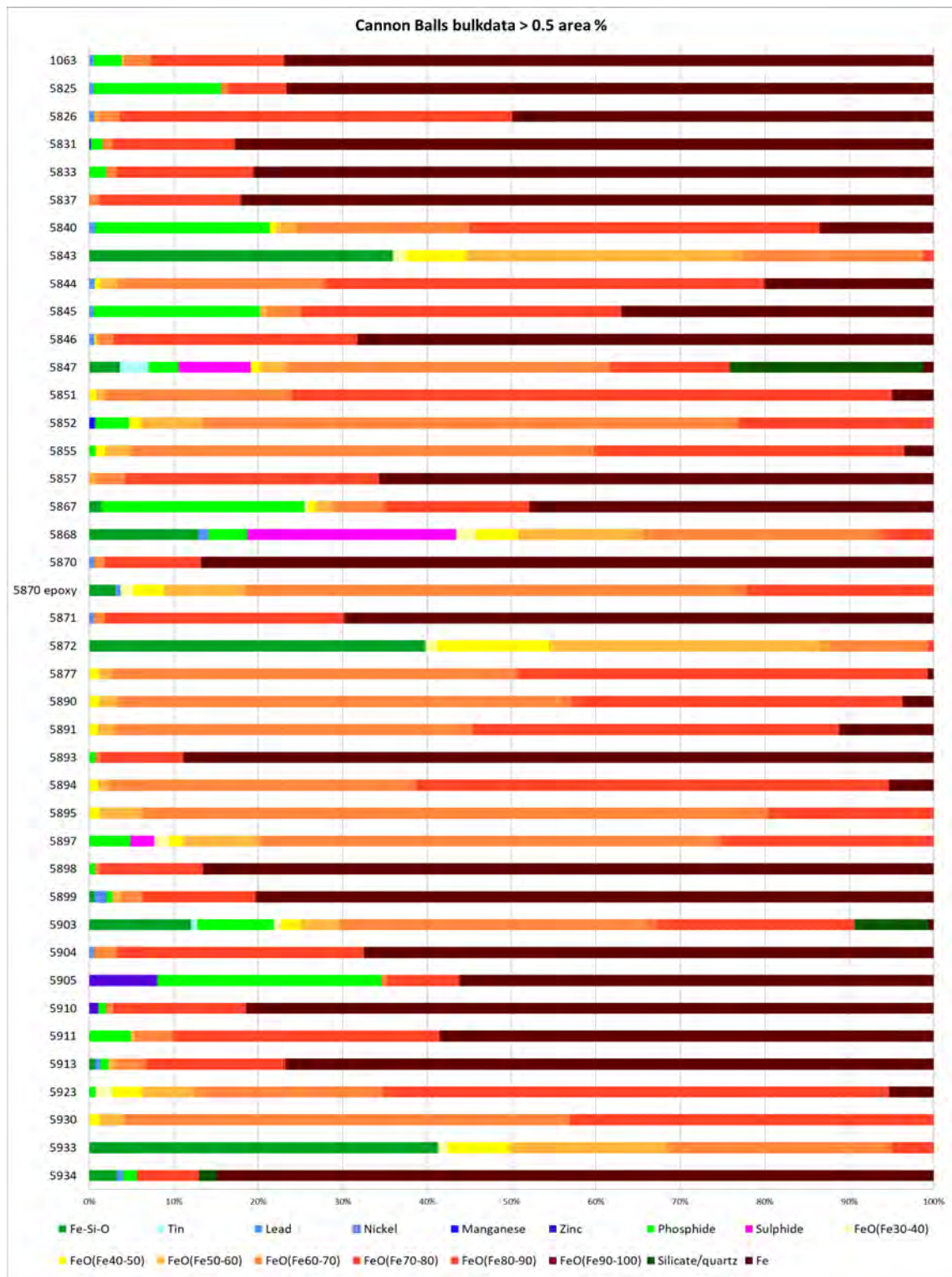


**Figure 6:** Stacked bar chart with all the 41 cannon ball samples measured based on their bulk composition (normalised to 100% for phases above 0.5 area%). The colour codes correspond to those used on the mineral maps in Appendix B. The legend is explained under the Division 2 subgrouping in section 3.1.



## 3.2. Results based on laser ablation ICP-MS analysis

The **LA-ICPMS analyses** focused on the *iron-rich* chemical phases in the sample material, with emphasis on the s Fe70-100 phases that consist of 70 to 100 % iron determined by AQM. The reason for selecting this chemical phase range was their omnipresence, which provided a good basis for comparison between the cannon balls, thus giving the best conditions to differentiate between them. The results are reported in Appendix E.

Three criteria were to be achieved for the chemical phases to be applicable for the aim of the study, viz. (1) the chemical phases used should preferably occur in all the cannon balls, (2) they should be sufficiently abundant in all cannon balls, and (3) the phases should be big enough and relatively fresh enough to be analysed by the LA-ICPMS system. In all samples, these criteria were fulfilled by the iron-rich phases with >50-60 % pure iron. Amongst those, phases in the Fe70-100 chemical range were assessed to be the most reliable targets for the analyses, presumably producing the most robust results. In addition to the Fe70-100 analyses, a few analyses of other phases occurring in the sample material, like phosphor-rich phases, were analysed, but no emphasis was put on the interpretation of these phases as they appeared in a relatively few samples.

The 30 elements selected for the LA-ICPMS analyses included the metals **Sc, Ti, V, Cr, Mn, Fe, Co, Cu, Zn, Mo, Sn, Sb, Hf, W, Hg, Pb** and the rare earth elements (**REE**) that include **La, Ce, Pr, Nd, Sm, Eu, Cd, Tb, Dy, Ho, Er, Tm, Yb, Lu**. In particular, the transition metals were anticipated to give usable results for the distinction between the cannon balls. The REE were included because they are frequently used for provenance studies in geological investigations. Hg was included to monitor the Hg content of the cannon balls to avoid pollution of the instrumentation.

### 3.2.1. Chemical variations

In general, the LA-ICPMS analyses of the Fe-rich phases show that the elements **V, Mn, Co, Cu, Zn, Mo** and **W** carry the most prosperous potential regarding the distinction between the individual cannon balls, whereas the elements Sc, Ti, Cr, and the REE appear to be less useful. In certain samples the elements Sn, Sb and Pb indicate that they might be used for distinguishing between at least some of the cannon balls, however they behave somewhat erratic and appear to be less useful for the general differentiation. Based on the elemental data alone, the cannon balls can be separated into at least 3 groups, which generally follow the textural division 1 of the SEM analyses.

The resulting product of the “direct” and/or “bloomery” method for partially smelting iron ores (e.g., Blakelock et al. 2009; Buchwald 2005) produces a mixed range of textures and various chemical compositions. Major elements were not analysed with the ICP-MS in this study, so trace elemental compositions were calculated based on an assumed iron abundance of 70 wt% Fe for all cannon balls. For all samples, rare earth element (REE) concentrations were too low, mostly below the limits of detection for the mass

spectrometer. Thus, the REE are not included in the below description or in the statistical treatment of the data.

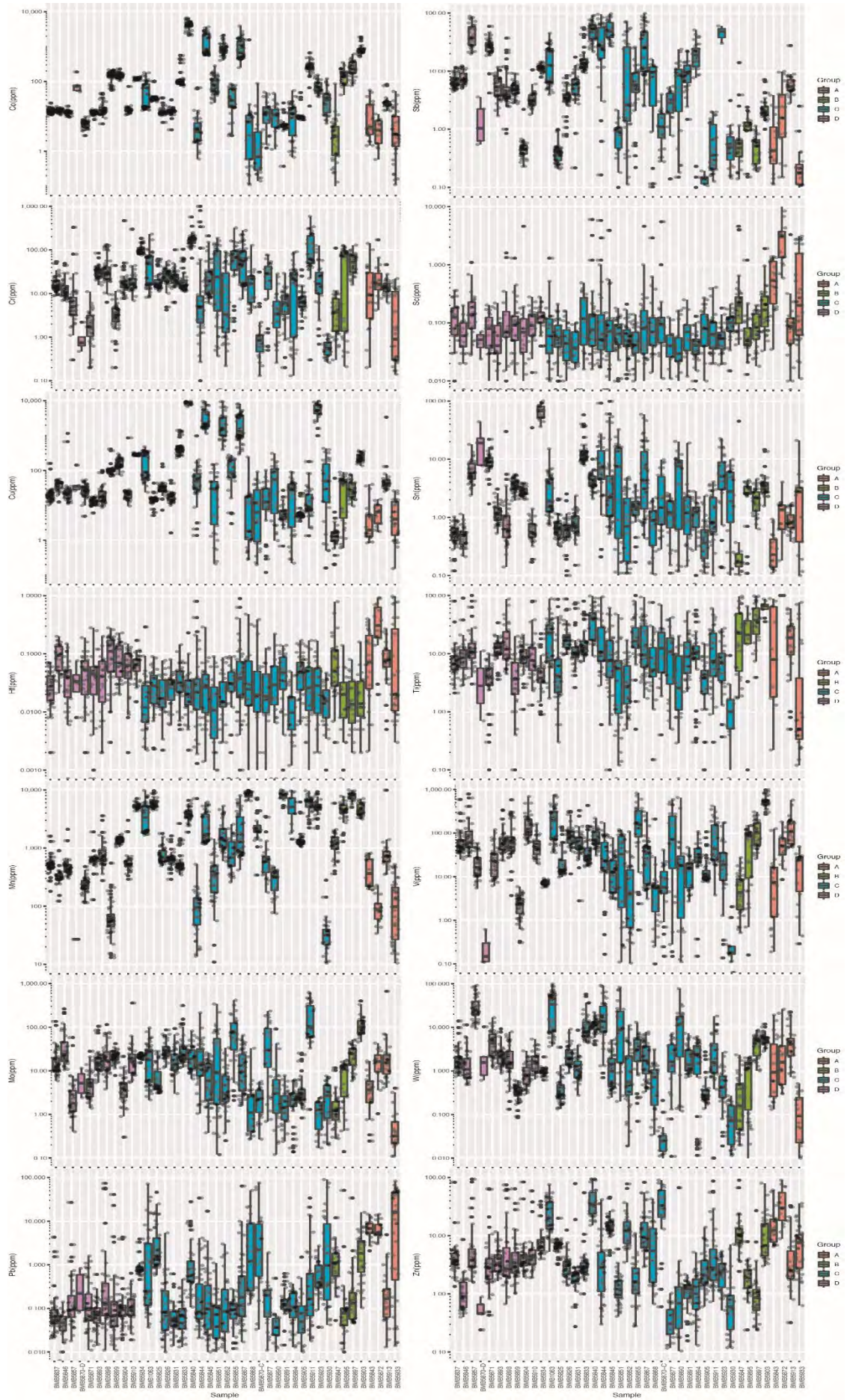
### 3.2.2. Trace element variations

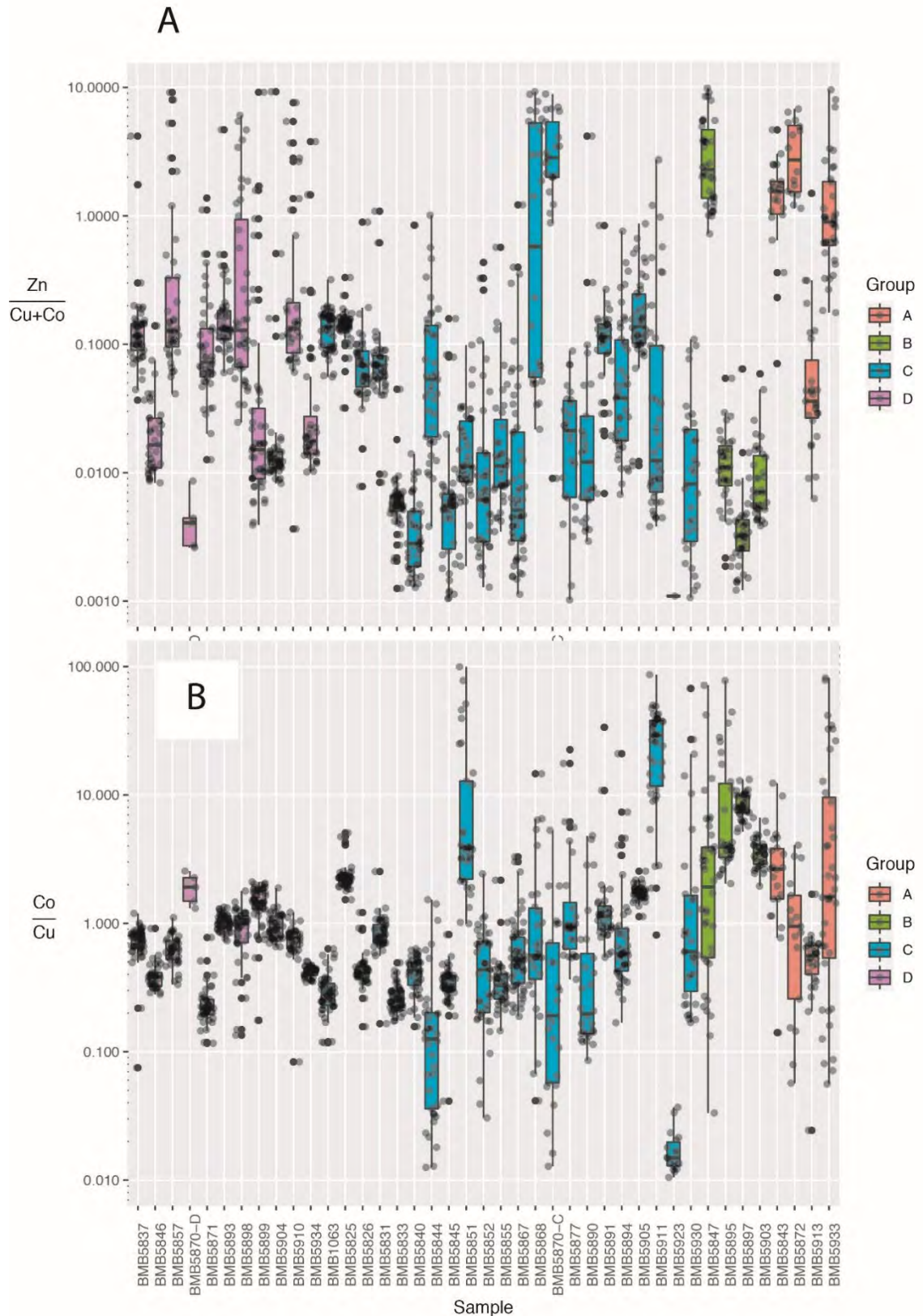
The LA-ICPMS analyses predominately included the iron-rich phases, and the plots presented here do not include any other chemical phases. We realized fairly early that the chemical data produced from the cannon ball samples in general followed a comparable pattern as for the Division 1 of the SEM analyses (i.e., the separation based on the textural variations). Thus, we have chosen to keep this division in the below description of the cannon balls' chemical characteristics.

Figure 7 show boxplots summarising of all the elements considered here as useful discriminators, viz. Sc, Ti, V, Cr, Mn, Co, Cu, Zn, Mo, Sn, Sb, Hf, W and Pb. It is noticeable that **Group A** (samples 5843, 5872, 5913 and 5933) does not show a great variation in Co, Cu, and Pb. **Group B** (samples 5847, 5895, 5897 and 5903) shows a great variation in Ti, whereas **Group C** (samples 1063, 5825, 5826, 5831, 5833, 5840, 5844, 5845, 5851, 5852, 5855, 5867, 5868, 5870epoxy, 5877, 5890, 5891, 5894, 5905, 5911, 5923, 5930) has a large variation in Mo, and **Group D** (5837, 5846, 5857, 5870, 5871, 5893, 5898, 5899, 5904, 5910, 5934) shows large variation in Sb. All samples from group A, B and D show nearly constant concentrations of Hf, Sc and Mo. When looking at the some of the element ratios (e.g., Fig. 8A), it is observed that some samples of groups B and C contains an order of magnitude less and some samples of group A an order of magnitude more of the Zn/(Cu+Co) ratio than group D (i.e., the samples containing a high amount of pure iron). Furthermore, the ratio Co/Cu approximates the unity for Group D, despite the variation for the remaining groups (A, B, C; Fig. 8B). The group A can be clearly distinguished using e.g., the ratios Sc/Mn and Pb/Cu (Fig. 8C and D), whereas the use of W in relation to any other elements (e.g., the W/Ti in Fig. 8E) appear to be less applicable for the discrimination between the cannon balls.

Here, it should be noted that although we have investigated many ratios, we emphasized on those ratios that we assume would provide the most relevant information for the aim of this study. However, for the time allocated we were not able to perform a deeper analysis including all possible ratio constellations that potentially could give additional or supporting results, and which could ultimately provide a more thorough interpretation of the chemical data set produced. Thus, although single elements can be allocated to two or more groups, it is the joined results that we have used to interpretate to where a particular sample should be allocated.

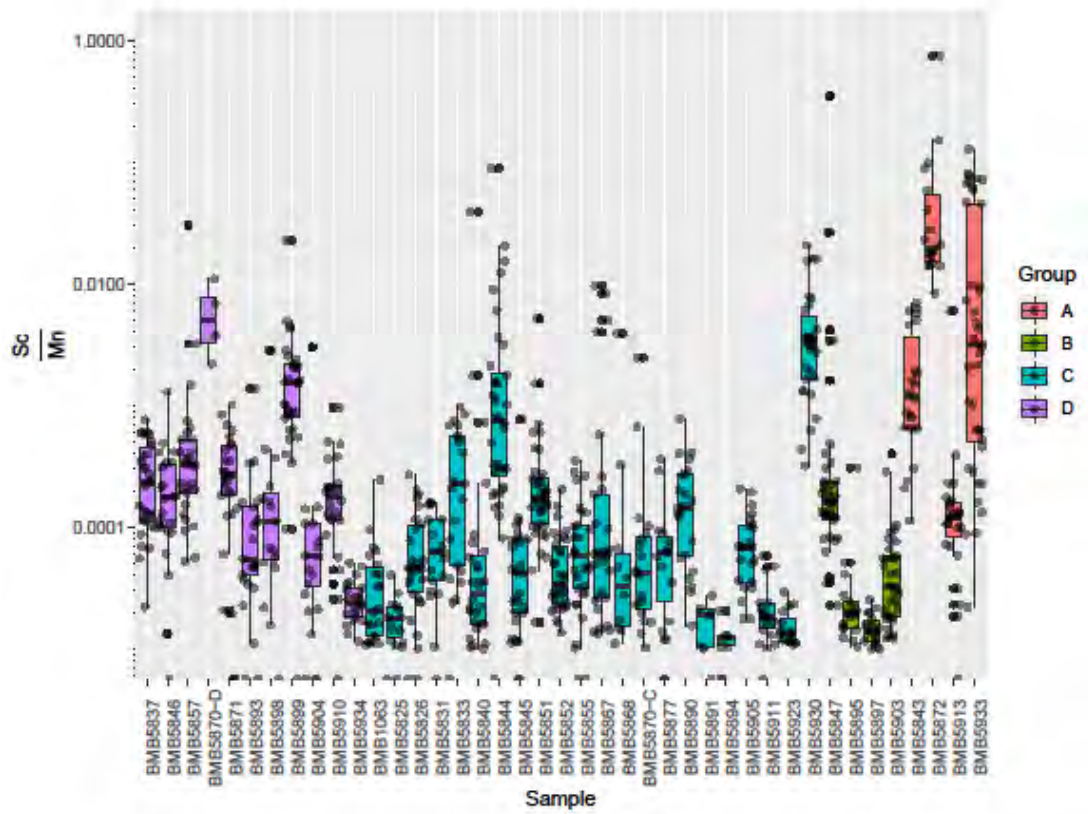
**Figure 7 (on next page):** Box and whisker diagrams for the cannon ball samples, showing the abundance spreading (coloured boxes) and the median values with associated uncertainties (vertical lines) for each sample measured by the LA-ICPMS. The differentiation into separate groups is based on the SEM Division 1 described in section 3.1.



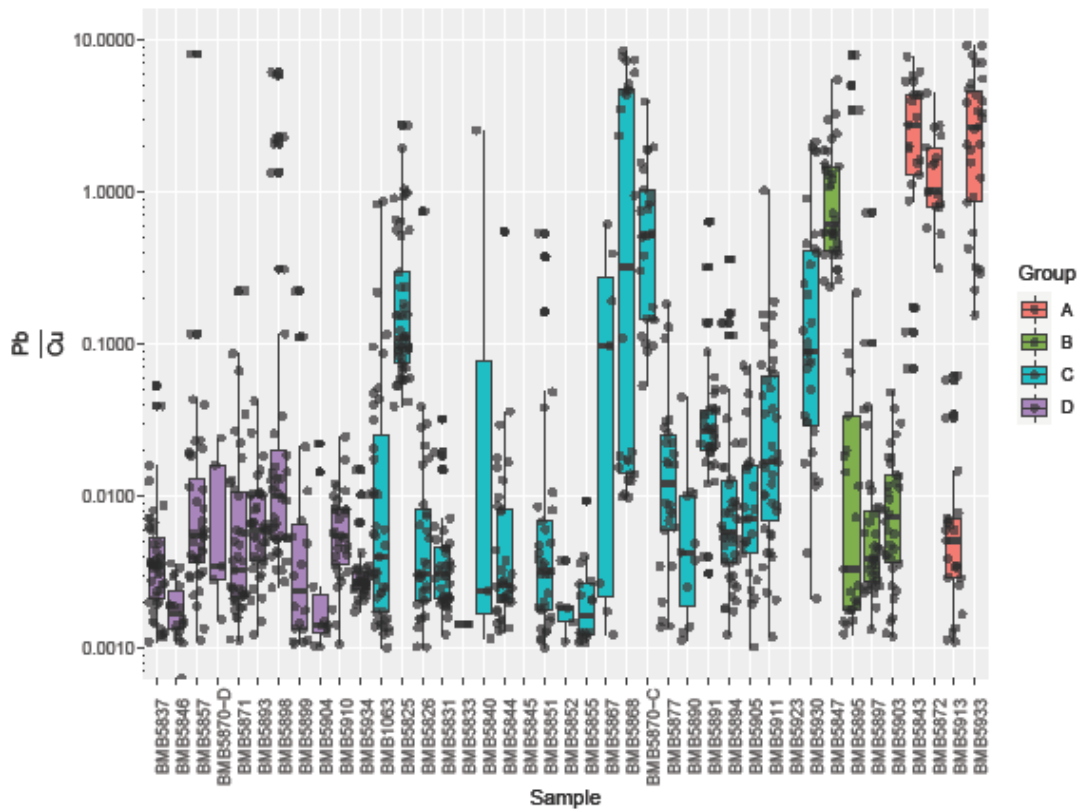


**Figure 8 (p. 20-22):** Box and whisker plots for the cannon ball samples expressed as sample ratios between elements. **A:** Zn/Cu+Co ratio. **B:** Co/Cu ratio. **C:** Sc/Mn ratio. **D:** Pb/Cu ratio. **E:** W/Ti ratio. Further descriptions are provided in the text. Note that some samples of each of the textural division have similar ratios but have an unlike spreading of the individual data points.

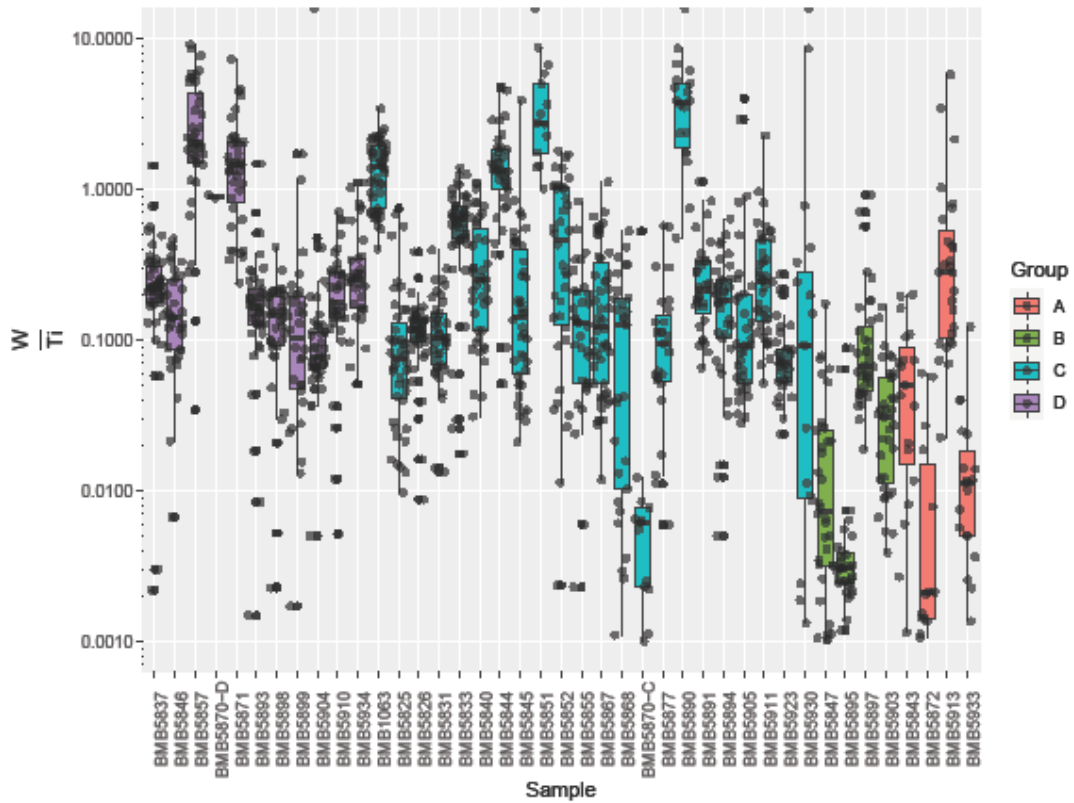
C



D



# E



When plotting concentrations in bivariate diagrams, it shows noticeable positive element ratio correlations. For instance, the  $Pb/(Co+Cu)$  against  $W/(Co+Cu)$  on Fig. 9 chiefly show a positive correlation as observed in the semimajor axis of the ellipse containing the 95% of data (ca. 2 sigma in the confidence interval). Moreover, the density plots show the distribution of the numerical values in the data, in which groups A, C and D have  $W/(Co+Cu)$  values close to 0.1 whereas group B has values close to 0.01, i.e., an order of magnitude less. For the  $Pb/(Co+Cu)$ , it is observed in the density plots that modal values range from 0.01 to 0.02 for Groups C and D, for group A modal values of ca. 1.00, and a bimodal distribution for Group B.

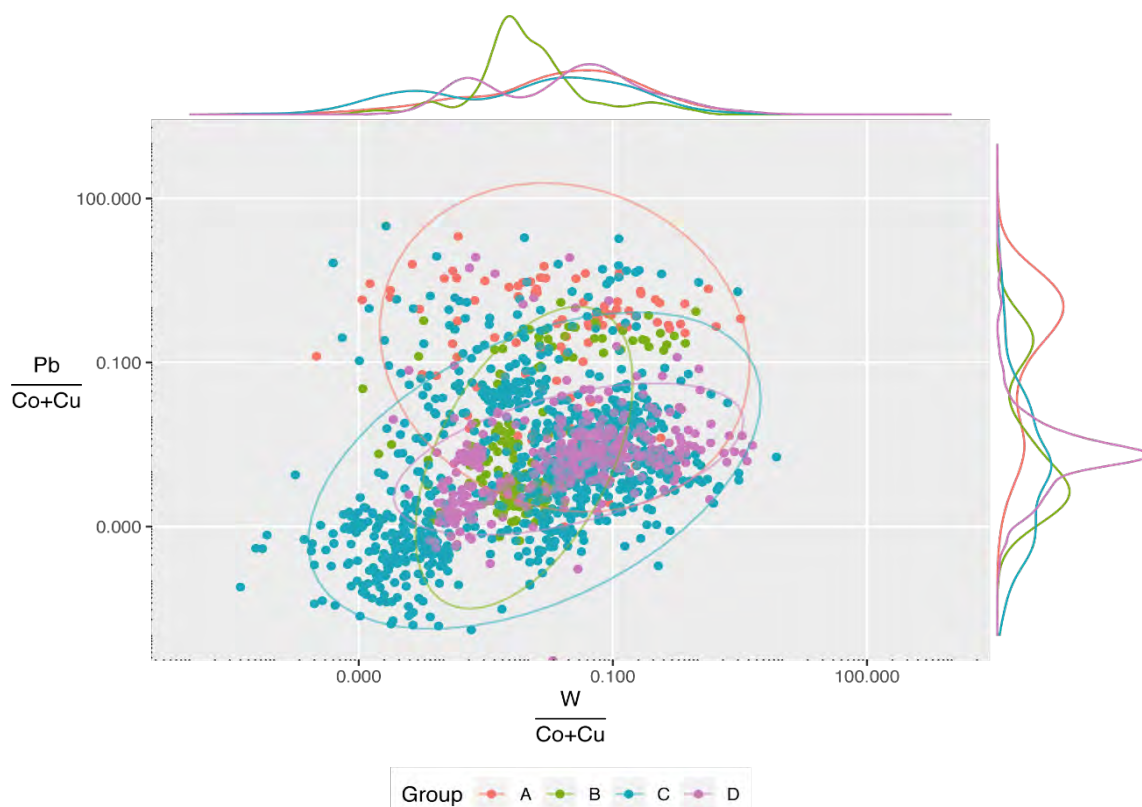


**Figure 9:** Bivariate diagram of the ratios for  $Pb/(Co+Cu)$  against  $W/(Co+Cu)$ , showing a major positive correlating between and within the samples in particular for group C and D samples. Density plots show the distribution of individual data points within each sample. Group A appears different compared to the other three groups.

### 3.2.3. Principal Component Analysis (PCA)

As described above, the produced set of data is fairly complex, and thus challenging for a possible explanation of the chemical variability of the cannon balls. An attempt to deal with the challenge of possible interpretations for the chemical variations linked to the textures, a method for reducing the dimensions of the chemical data was selected by looking at principal components though preserving some statistical information (e.g., variability) as much as possible. Mathematically, variables maximising the variance of seemingly uncorrelated components can be assessed by linear transformations. These new linear variables (or principal components) are reduced to solving an eigenvector problem (e.g., Jolliffe and Cadima, 2016). In this exercise, the data set was divided into  $p$ -numerical variables (i.e., variations in the analysed chemical elements) for each of the  $n$ -number of samples. All vectors are then defined in the  $p \times n$  matrix, seeking for the linear combination with maximum variance.

When performing principal component analysis (PCA), the largest eigenvalue of the given component is of great interest since the eigenvalue can be associated to the variances of the linear combinations (see Jolliffe and Cadima, 2016 for details about the mathematics). We thus selected major metals that show a consistent concentration

above the limits of detection for the mass spectrometer, viz. Sc, Ti, V, Cr, Mn, Co, Cu, Zn, Mo, Sn, Sb, Hf, W and Pb, as described above. All elements were calculated to ppm level.

Amongst these 14 elements, concentrations of Sc and Hf were generally constant. Thus, we expect lesser variations in the chemical exchange in these two elements for all cannon balls. However, it was opted to use all elemental concentrations for producing two dimensional components, namely PC1 and PC2, explaining 57.2% of the total variance. As shown on the bivariate diagram of Fig. 10, the standardised PC1 explains 45.29% of the variance whilst the PC2 only explains 11.91% variance in the set of data. This is most probably due to the presence of outliers, which increase the uncertainty in the linear transformation. Although it is observed variable degrees in the covariances, two main groups can be observed, namely one where Co, Cu and Mn suggest highly correlated variables, and one including Sn, Cr, Zn, V, W, Hf, Mo and Ti, with less prominent, one-dimensional correlated variables.

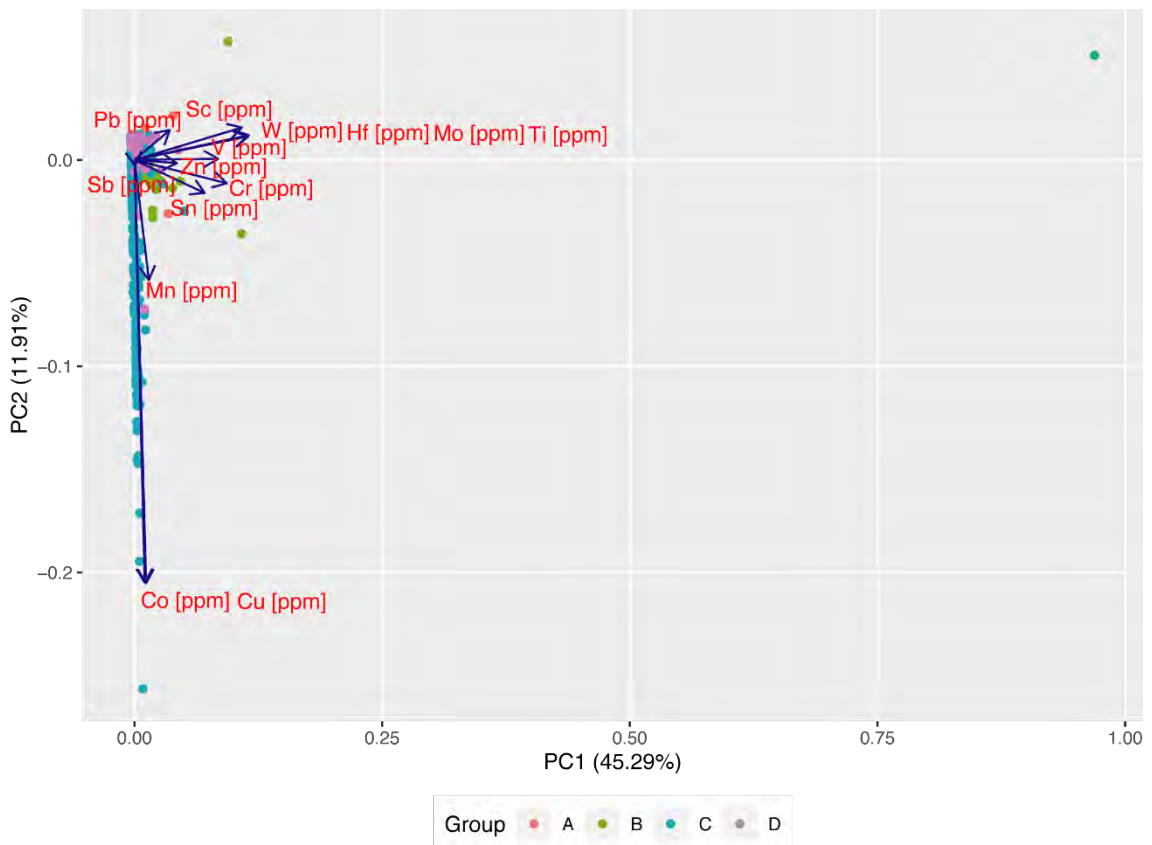


**Figure 10:** Bivariate diagram with the result of our principal component analysis (PCA). It includes the first two principal components (PC1 and PC2) and shows the variables in form of vectors and sample points for each of the cannon ball samples. The samples proximity to a given vector may indicate how influenced that sample is by the given vector. For instance, samples of group C are very much influenced by the variables Co and Cu, whereas samples of group B are influenced by Sn. The PCA analysis supports our observations from the variation diagrams in Fig. 7, 8 and 9.



## 4. Concluding remarks

Based on the analyses carried out by SEM and LA-ICPMS, the cannon balls can optimally be divided into 4 separate groups, whereof at least 3 groups show distinctly different textural and chemical features. This division, however, must be taken as indicative only based on the somewhat limited data material received, which furthermore demonstrated a large compositional and textural variation, and moreover, for some samples were in a condition difficult for carrying out microchemical analyses.

Nevertheless, although the results in parts only allow for a somewhat uncertain interpretation, this study demonstrates that analysis using the technical constellation of AQM + BSE imaging by SEM combined with microchemistry analysis of the most Fe-rich phases by LA-ICPMS on sample material from historic cannon balls made predominantly of iron, can provide sufficiently reliable textural, compositional, and microchemical results that can be used for discriminating between single cannon ball materials. As the textural and microchemical variation within the cannon balls are formed by two at least semi-independent processes, i.e., the smelting and casting process vs. the source of the iron ore, respectively, the division into the four different groups with their own history might prove to be rather robust. The threshold of when such analyses can or cannot be applied is, however, not possible to assess based on the sample material employed in this study.

The aim of the study to fingerprint the cannon ball sample material in order to allocate them to distinct ore locations or rock domains within Scandinavia or the German countries have not been undertaken, mostly due to a significant lack of background information to where our analyses could be compared. However, together with a more profound background study of potential provenance locations in terms of possible mining and manufacturing sites for the cannon balls, this study constitutes a plinth for further investigations to ultimately be able to fingerprint the cannon balls' provenance geographically as well as geologically. To get a sufficiently robust analytical background data material it might be beneficial to supplement the data from this study with more analyses of the same kind and/or additional isotopic data from analytical facilities that can offer analyses of a higher quality and resolution.

This report provides some suggestions how the data can be interpreted and how to work further on with the data material produced in this study. It was not the scope of this work to provide in-depth results, but merely to test if the employed techniques can be used for separating the cannon ball samples into distinct groups, and for making a plinth for future analyses helpful for the differentiation and in turn for future provenance investigations of the cannon balls. Seen in this view, we think that this report constitutes a reasonably solid platform for further investigations of iron-rich cannon ball materials.

## 5. Recommendations for future work

With the above results as benchmark, we have below listed a few recommendations for further investigations that are considered to benefit the study of the cannon balls in terms of type differentiation and provenance:

- **Bayesian models and Principal Component Analysis (PCA)**

This study provides several methods how to compare and group the samples (e.g., texture, composition, LA-ICPMS trace element data), including some first PCA analysis. It is, however, beyond the time allocated to this study to deliver a more profound PCA analysis. To obtain a more complete grouping, a multi-variate statistics analysis could thus be performed. Statistical analysis using especially Bayesian models (e.g., Longman et al. 2018) would presumably be very beneficial for the isotope (ICPMS) analyses. Through this kind of analysis, it might be possible to resolve plausible sources of iron ore and perhaps even sequential mixing of the source material used in the cannon balls. A clear division and grouping of sources would allow resolving the principal components. These constraints on the parametrisation of the variances and covariances in the chemical data could advocate a better characterization of the raw materials from which the cannon balls are manufactured.

- **Profound background study for fingerprinting the provenance/origin**

For the study of provenance/origin of ore locations, a more substantial literature study is required. During this work we suggested to contact the geological surveys of Norway (NGU) and Sweden (SGU) for background and chemical data on Fe-ores and their locations (mines) in the time period of question. Similar, for institutions within the historic/archeological field for data material to compare to the data produced herein. Without this data material there is no baseline data material to compare the analyses to, and it is at best very difficult (if not impossible) to determine any provenance location of the Fe-ore material from which the cannon balls were produced.

- **Isotope fingerprinting of the cannon balls**

Despite the efforts of elucidating the geochemistry of the cannon balls, data still limit the identification of the iron source. It is well known that lead (Pb) isotopes provide unique insights on the origin of a geological sample, ranging from tracing the sources and subsequential contribution from other sources by means of pollution and/or mixing. Naturally occurring Pb is composed of the isotopes  $^{208}\text{Pb}$  (52%),  $^{207}\text{Pb}$  (ca. 23%),  $^{206}\text{Pb}$  (24%) and  $^{204}\text{Pb}$  (1%). Whereas  $^{208}\text{Pb}$  is the final radioactive decay product of  $^{232}\text{Th}$ ,  $^{206}\text{Pb}$  the final product of  $^{238}\text{U}$ , and  $^{207}\text{Pb}$  the final product of  $^{235}\text{U}$  through radioactive decay, the  $^{204}\text{Pb}$  is a non-radiogenic isotope (i.e., not a product of radioactive decay). Combining radiogenic and non-radiogenic isotopes of the same element (e.g.,  $\mu$ -values of Pb) offers the option to investigate the natural geological sources of dissimilar materials and the rate of mixing processes that produced changes in the original isotopic composition of the source material. For this kind of provenance study characterizing the cannon balls' origin and affiliation to potential ore locations, analyses using instrumentation that offer a higher sensitivity and resolution is required. This can be a multi-collector ICPMS, ion probe (SIMS) or thermal ionization mass spectrometry (TIMS), or akin techniques.

## **6. Acknowledgements**

Mojgan Alaei, Høgni Vesturklett and Carsten Guvad from GEUS are thanked for their hard work with the careful sample preparation and cleaning of the cannon ball materials.

## **7. Electronically appendices (supplementary files)**

Appendix. A. Sample list and Analyses at GEUS

Appendix. B. Optical microscopy, BSE and AQM images

Appendix. C. AQM (SEM) results

Appendix. D. LA-ICPMS operating and data acquisition parameters

Appendix. E. LA-ICPMS results

## 8. References

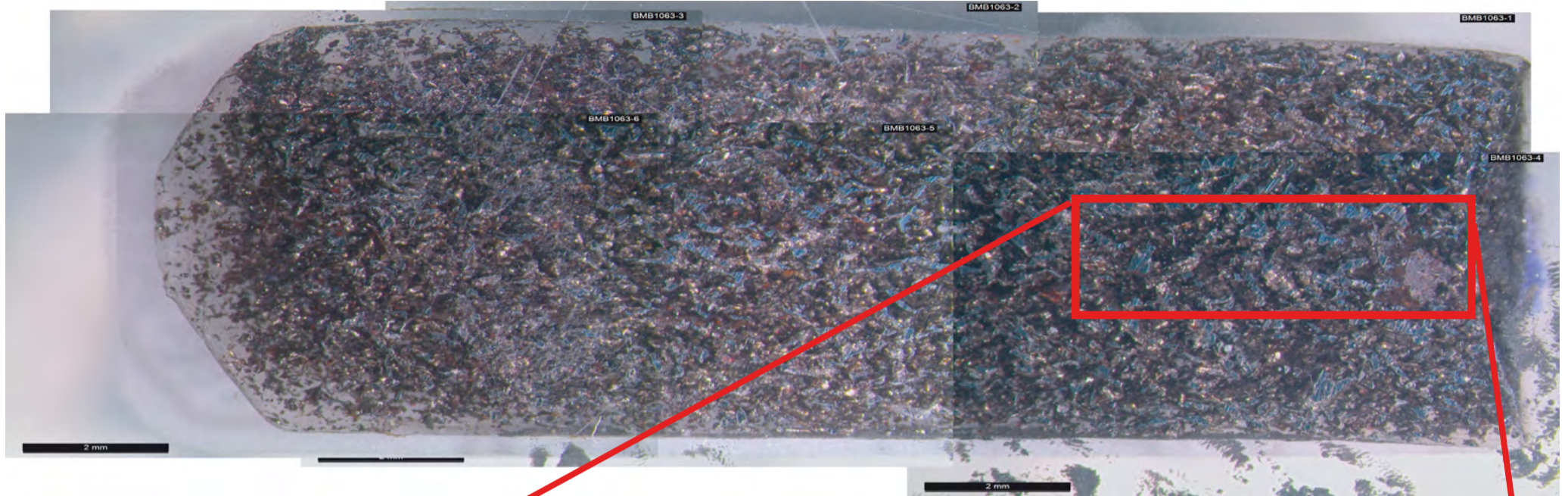
- Blakelock, E., Martinon-Torres, M., Veldhuijzen, H.A., Young, T. 2009. Slag inclusions in iron objects and the quest for provenance: an experiment and a case study. *J. Archeol. Sc.* 36, 1745-1757.
- Buchwald, V.F. 2005. Iron and Steel in Ancient Times. *Historisk-filosofiske Skrifter*. Det Kongelige Danske Videnskabernes Selskab, Copenhagen.
- Hellstrom, J, Paton C, Woodhead J, Hergt J (2008) *Iolite: Software for spatially resolved LA-(quad and MC) ICPMS analysis*. In: Sylvester P (editor) *Laser Ablation ICP-MS in the Earth Sciences: Current Practices and Outstanding Issues*, 343–348, Mineral. Assoc. of Canada, Quebec, Canada.
- Jackson SE, Pearson NJ, Griffin WL, Belousova EA (2004) The application of laser ablation-inductively coupled plasma-mass spectrometry to in situ U–Pb zircon geochronology. *Chemical Geology* 211, 47-69.
- Jolliffe, I.T., Cadima, J. 2016. Principal component analysis: a review and recent developments. *Phil. Trans. R.Soc. A* 374: 20150202.
- Keulen N, Malkki SN, Graham S (2020) Automated Quantitative Mineralogy Applied to Metamorphic Rocks. *Minerals* 10, 47, 29pp. DOI: 10.3390/min10010047
- Longman, J. Veres, D. Ersek, V, Phillips, D.L., Chauvel, C., Tamas, C.G. 2018. Quantitative assessment of Pb sources in isotopic mixtures using a Bayesian mixing model. *Scientific Reports* 8
- Paton C, Hellstrom JC, Paul P, Woodhead JD, Hergt JM (2011) *Iolite: Freeware for the visualisation and processing of mass spectrometric data*. *Journal of Analytical Atomic Spectrometry* 26, 2508-2518.
- Paton C, Woodhead JD, Hellstrom JC, Hergt JM, Greig A, Maas R (2010) Improved laser ablation U-Pb zircon geochronology through robust downhole fractionation correction. *Geochemistry Geophysics Geosystems* 11, 1-36.
- Petrus JA, Kamber BS (2012) *VizualAge: A Novel Approach to Laser Ablation ICP-MS U-Pb Geochronology Data Reduction*. *Geostandards and Geoanalytical Research* 36, 247-270.
- van Kooten E, Kubik E, Siebert J, Heredia BD, Thomsen TB, Moynier F (2022) Metal compositions of carbonaceous chondrites. *Geochimica Cosmochimica Acta*.



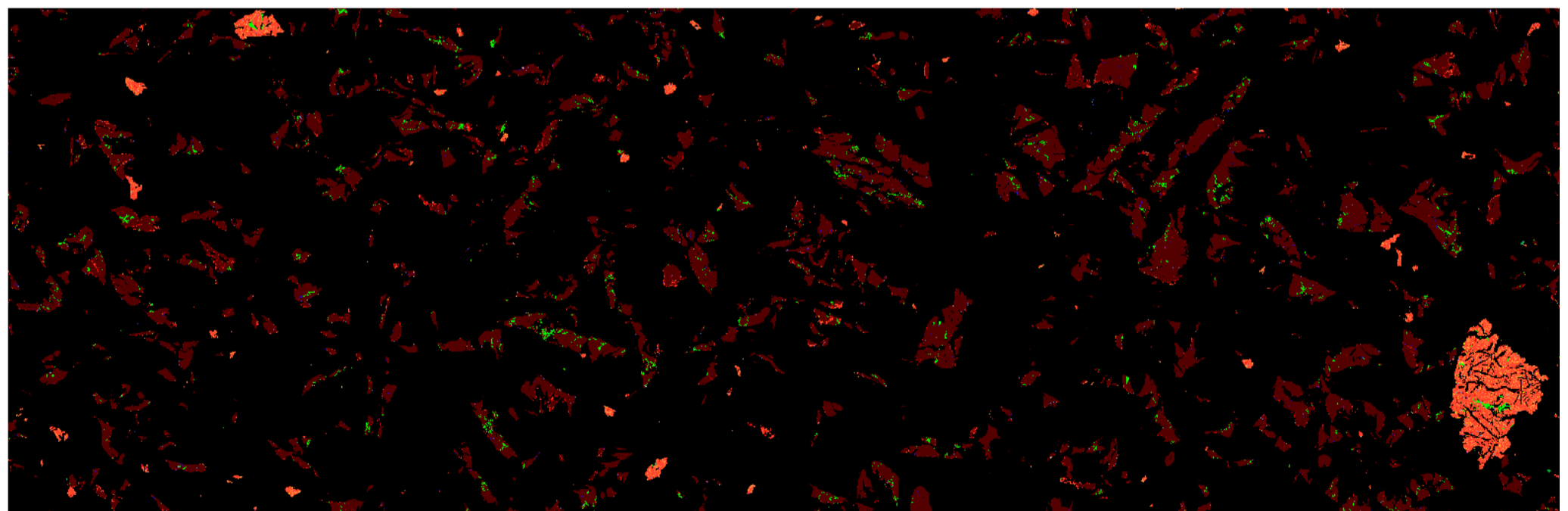
## **Appendix B – Optical microscopy, BSE and AQM images**

# BMB1063

Optical microscopy image



BSE image



Chromium	FeO(Fe30-40)	FeO(Fe70-80)	Lead	Silicate/quartz	Vanadium	Unclassified
Cobalt	FeO(Fe40-50)	FeO(Fe80-90)	Manganese	Sulphate/Sulphide	Zinc	
Copper	FeO(Fe50-60)	FeO(Fe90-100)	Nickel	Tin	Not Analysed	
Fe	FeO(Fe60-70)	Fe-Si-O	Phosphate/phosphide	Titanium	Not Classified	500µm

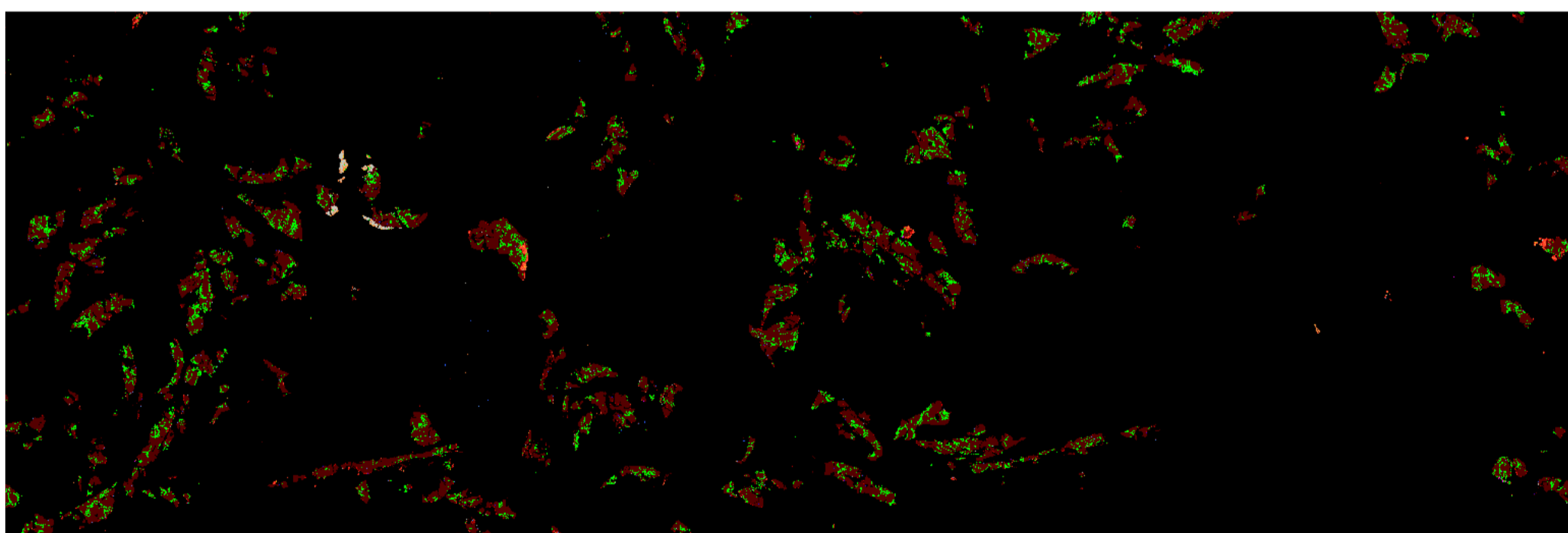
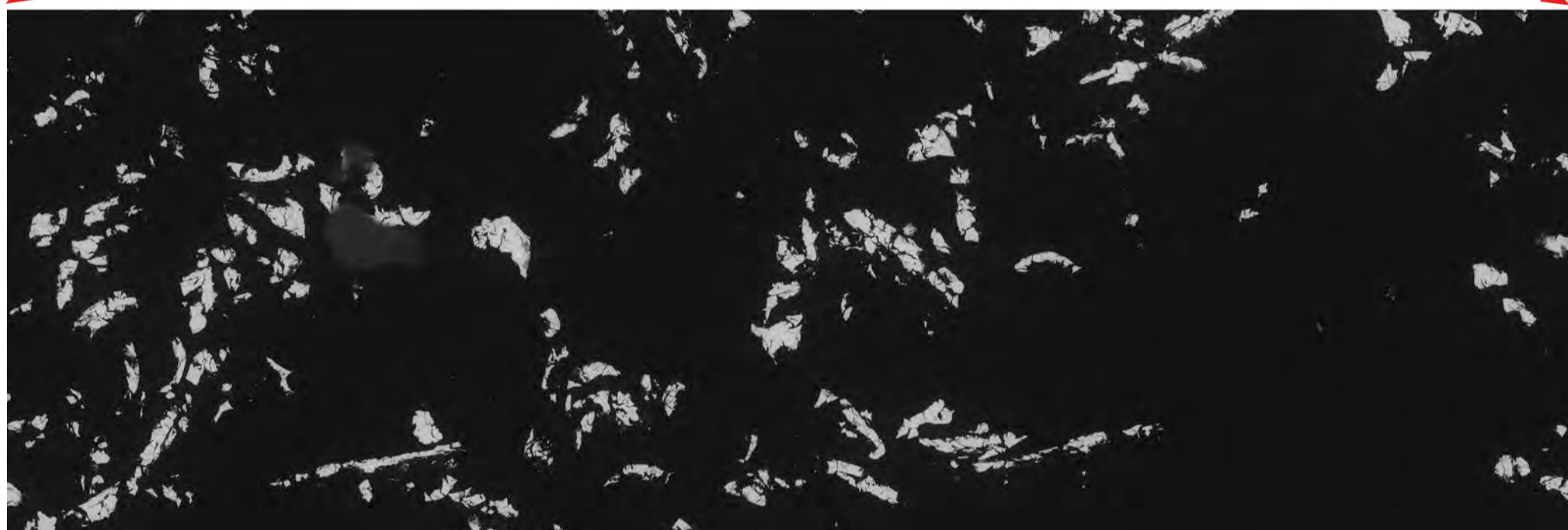
Mineral phases image



Optical microscopy image



BSE image

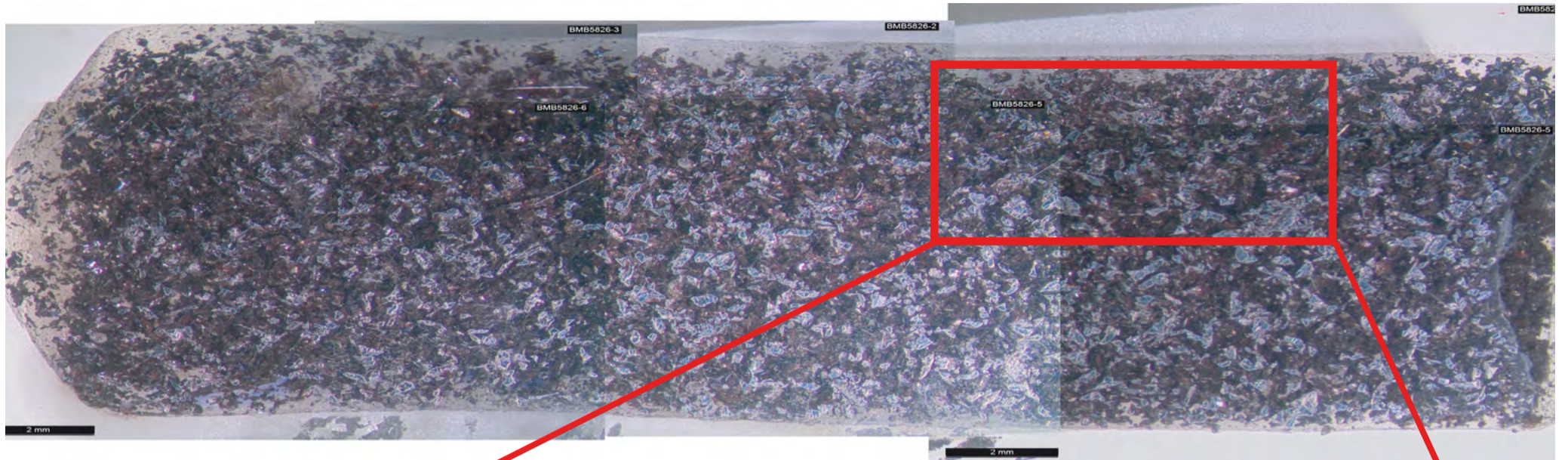


Chromium	FeO(Fe30-40)	FeO(Fe70-80)	Lead	Silicate/quartz	Vanadium	Unclassified
Cobalt	FeO(Fe40-50)	FeO(Fe80-90)	Manganese	Sulphate/Sulphide	Zinc	
Copper	FeO(Fe50-60)	FeO(Fe90-100)	Nickel	Tin	Not Analysed	500µm
Fe	FeO(Fe60-70)	Fe-Si-O	Phosphate/phosphide	Titanium	Not Classified	

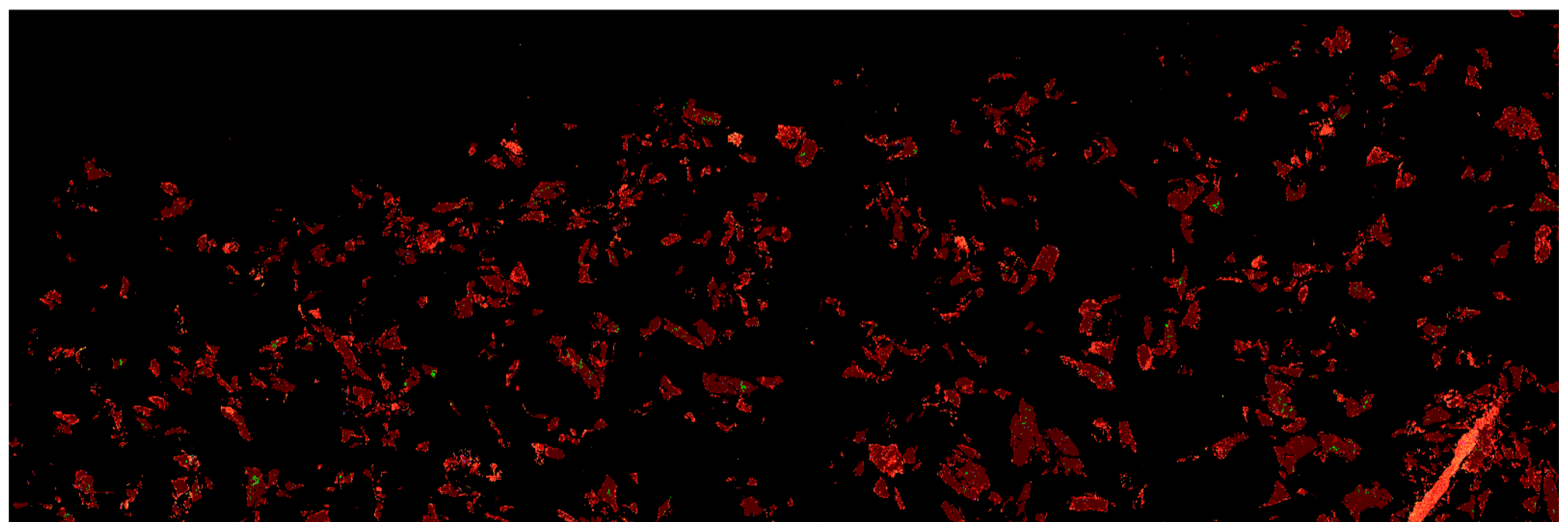
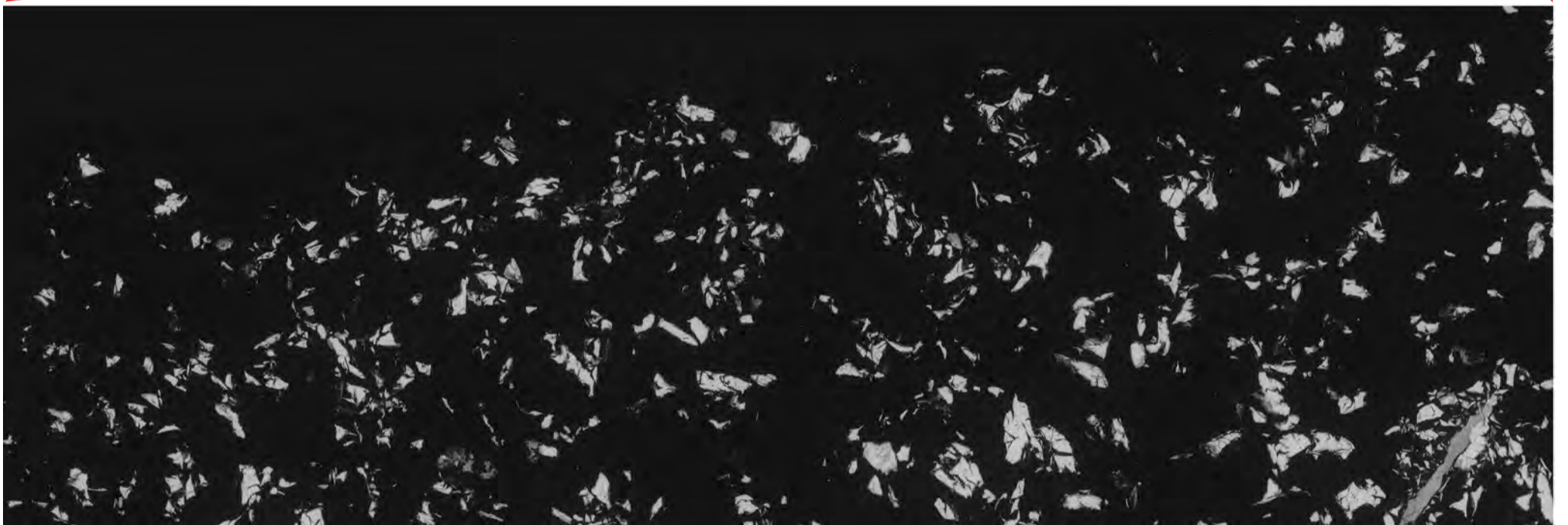
Mineral phases image

# BMB5826

Optical microscopy image



BSE image



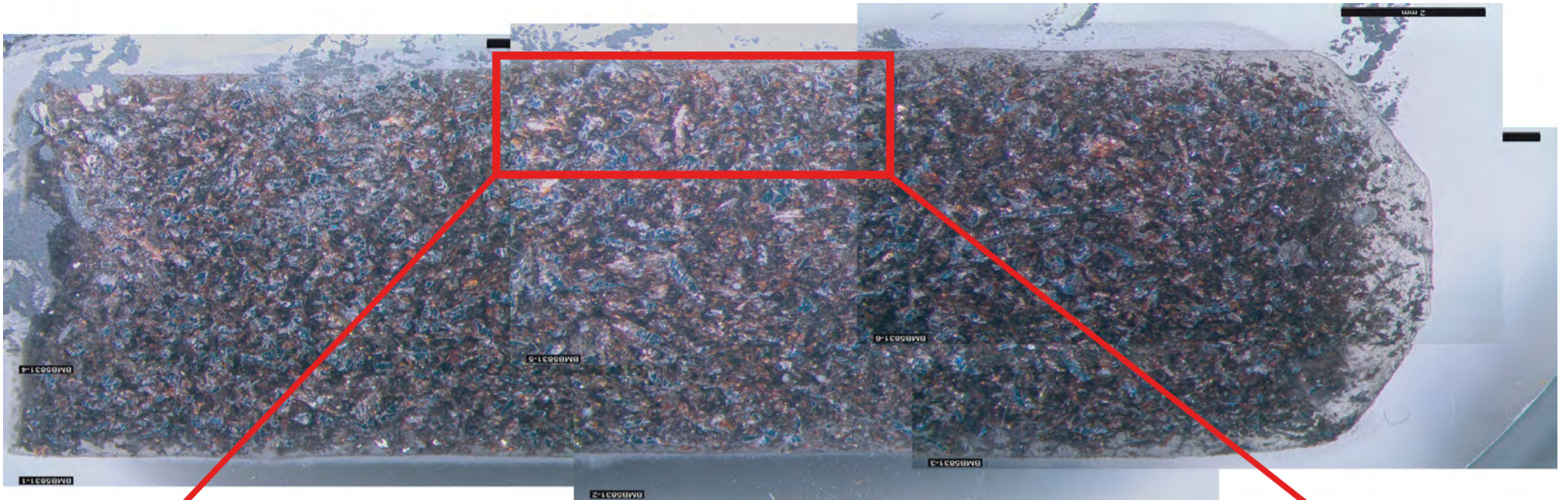
Chromium	FeO(Fe40-50)	FeO(Fe80-90)	Manganese	Sulphate/Sulphide	Zinc
Copper	FeO(Fe50-60)	FeO(Fe90-100)	Nickel	Tin	Not Analysed
Fe	FeO(Fe60-70)	Fe-Si-O	Phosphate/phosphide	Titanium	Not Classified
FeO(Fe30-40)	FeO(Fe70-80)	Lead	Silicate/quartz	Vanadium	Unclassified

500µm

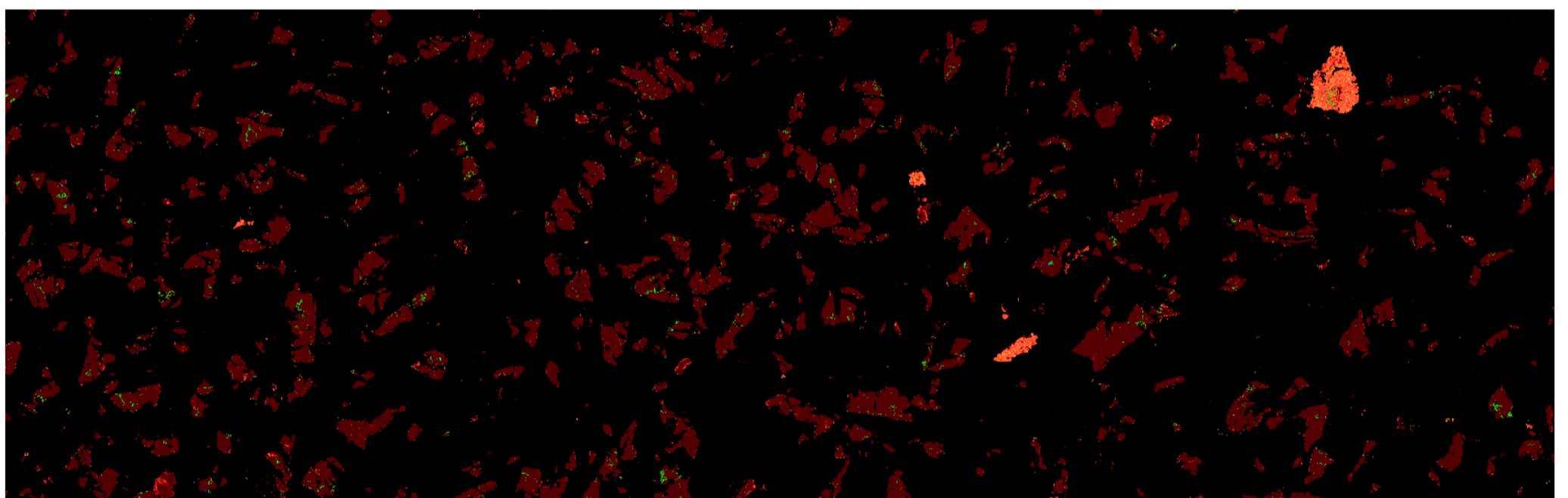
Mineral phases image

# BMB5831

Optical microscopy image



BSE image



Chromium	FeO(Fe30-40)	FeO(Fe70-80)	Lead	Sulphate/Sulphide	Zinc
Cobalt	FeO(Fe40-50)	FeO(Fe80-90)	Manganese	Tin	Not Classified
Copper	FeO(Fe50-60)	FeO(Fe90-100)	Nickel	Titanium	Unclassified
Fe	FeO(Fe60-70)	Fe-Si-O	Phosphate/phosphide	Vanadium	

500µm

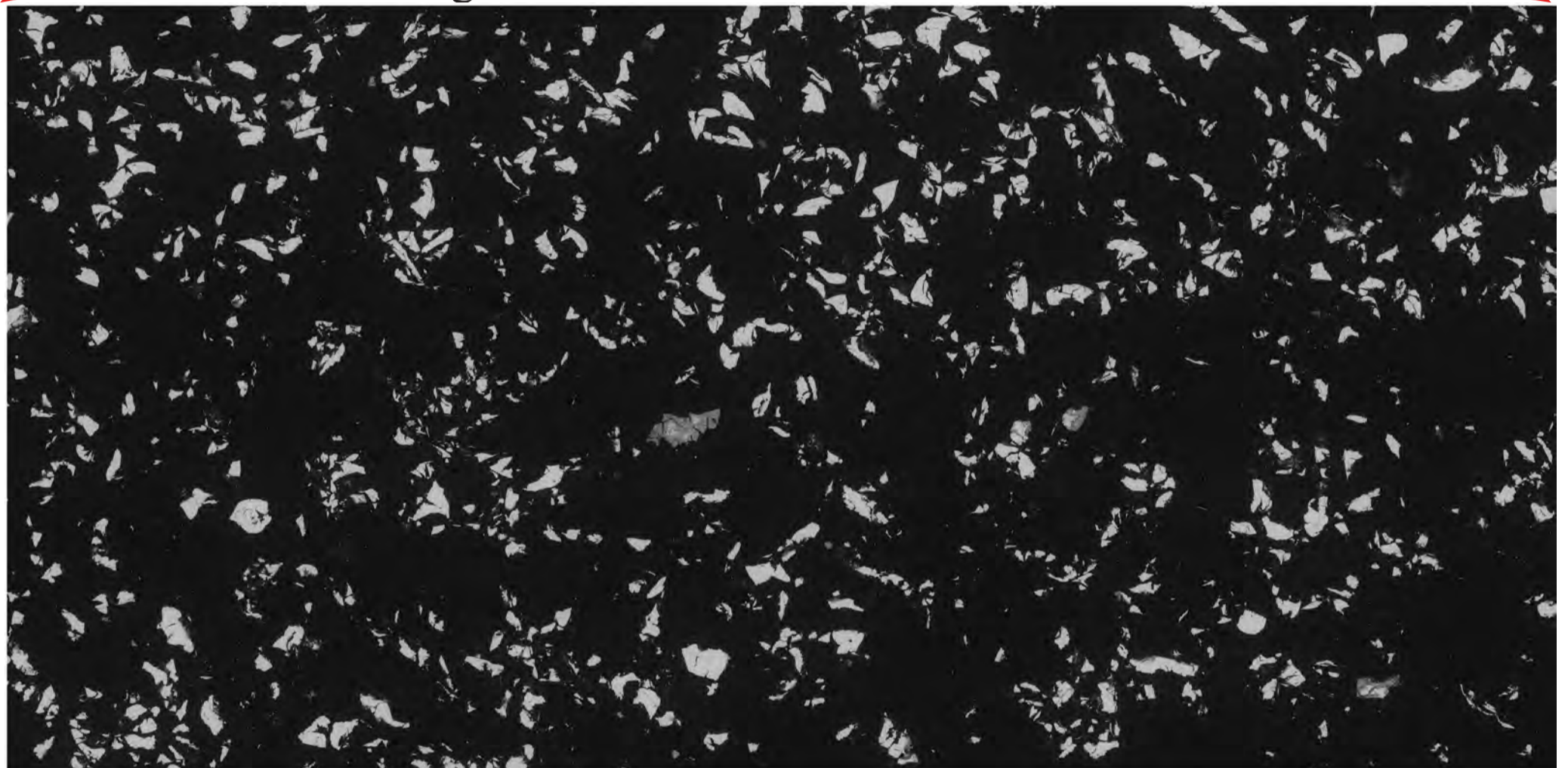
Mineral phases image

Optical microscopy image

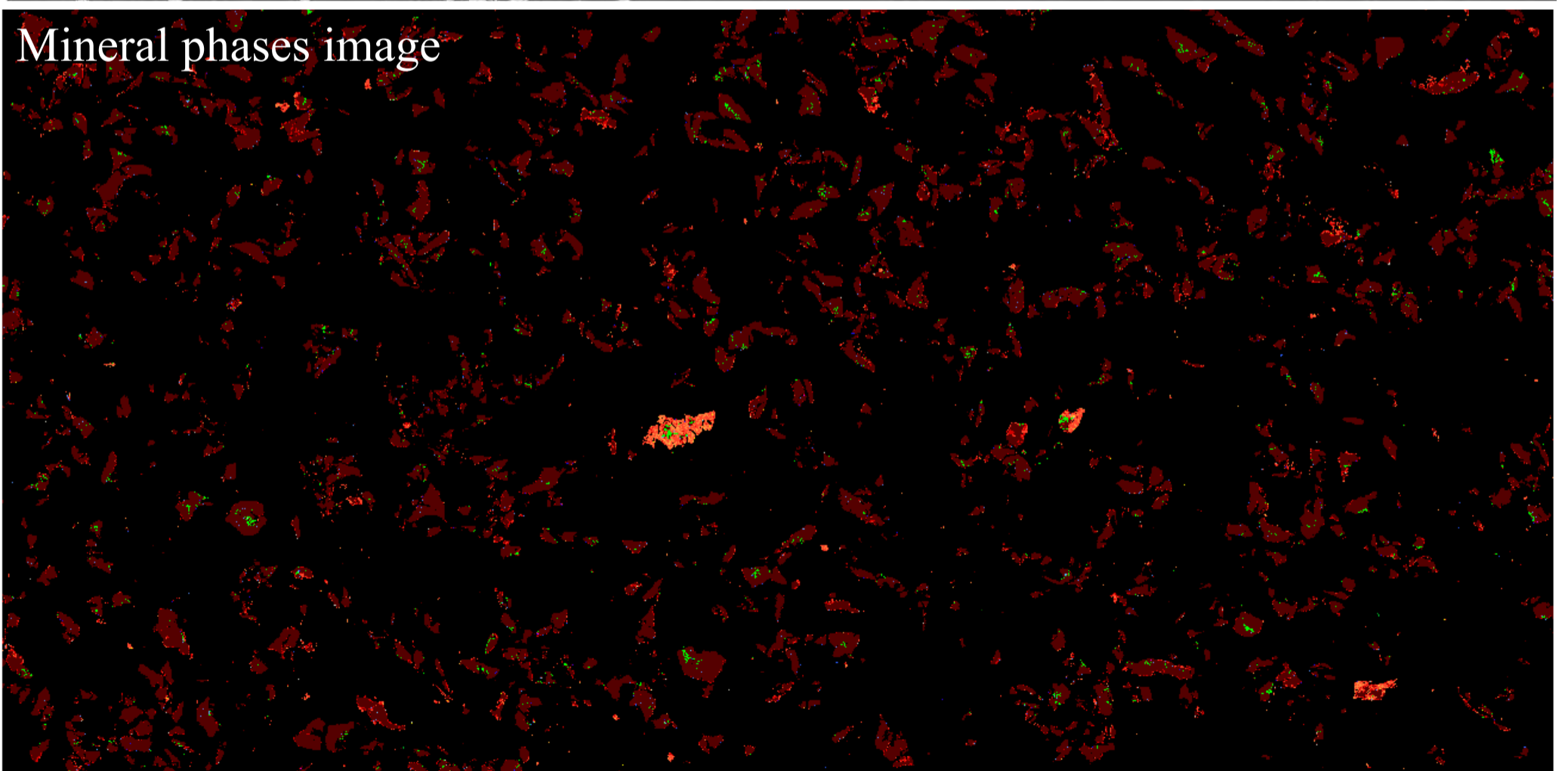
BMB5833



BSE image



Mineral phases image



Chromium	FeO(Fe40-50)	FeO(Fe80-90)	Manganese	Sulphate/Sulphide	Zinc
Copper	FeO(Fe50-60)	FeO(Fe90-100)	Nickel	Tin	Not Analysed
Fe	FeO(Fe60-70)	Fe-Si-O	Phosphate/phosphide	Titanium	Not Classified
FeO(Fe30-40)	FeO(Fe70-80)	Lead	Silicate/quartz	Vanadium	Unclassified

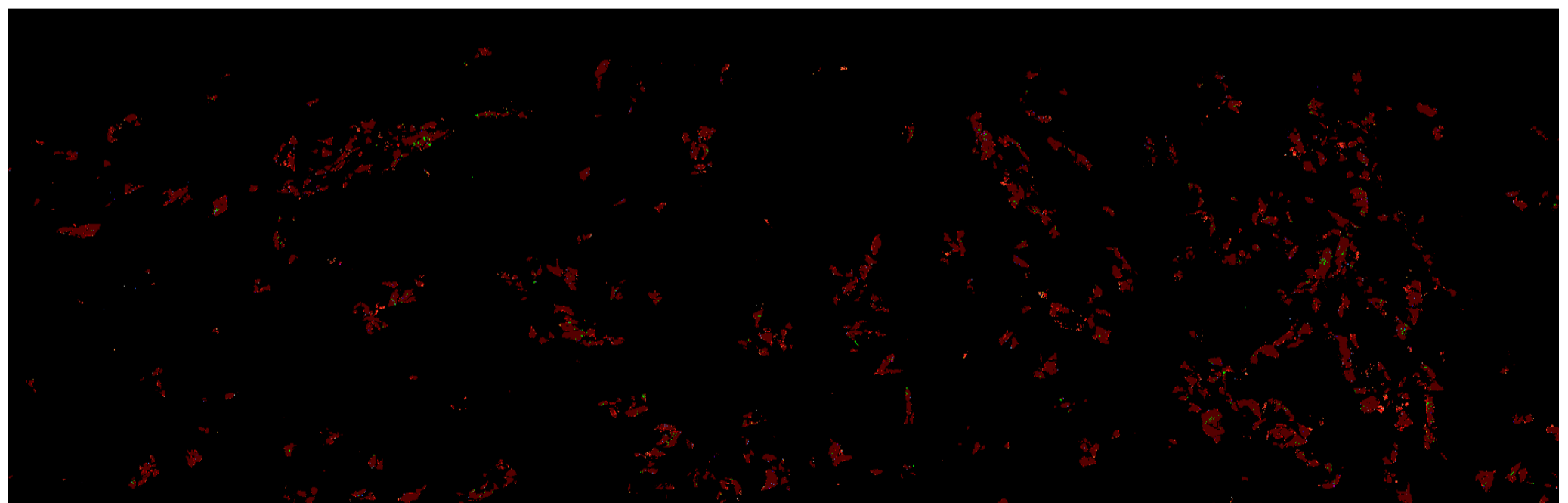
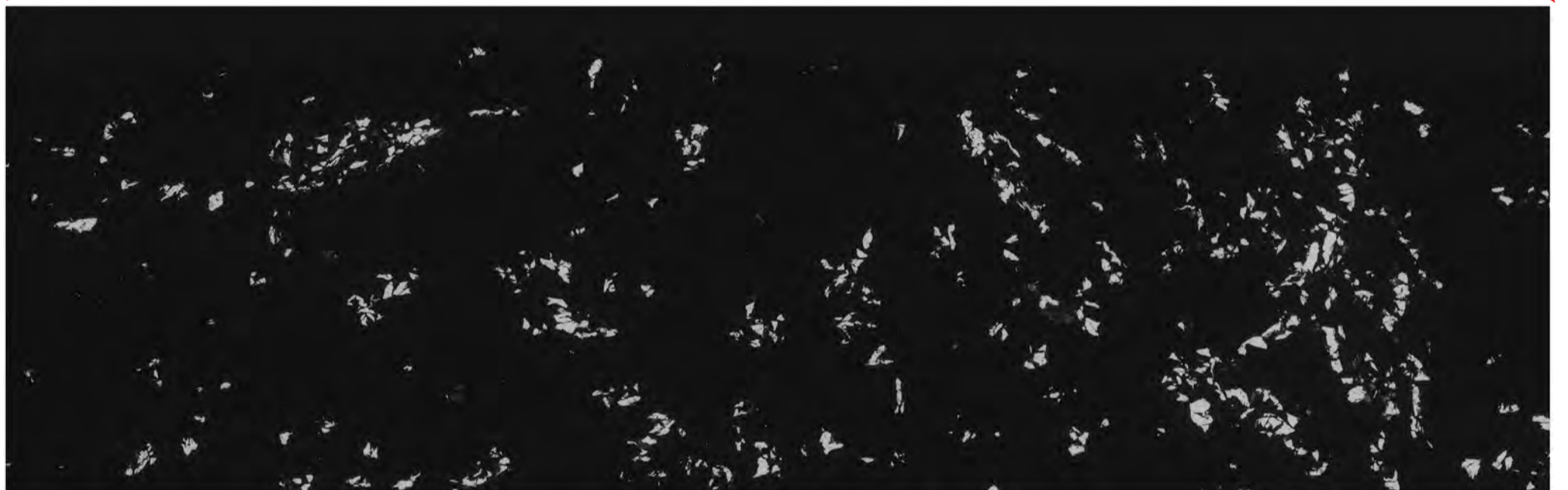
500µm

# BMB5837

Optical microscopy image



BSE image



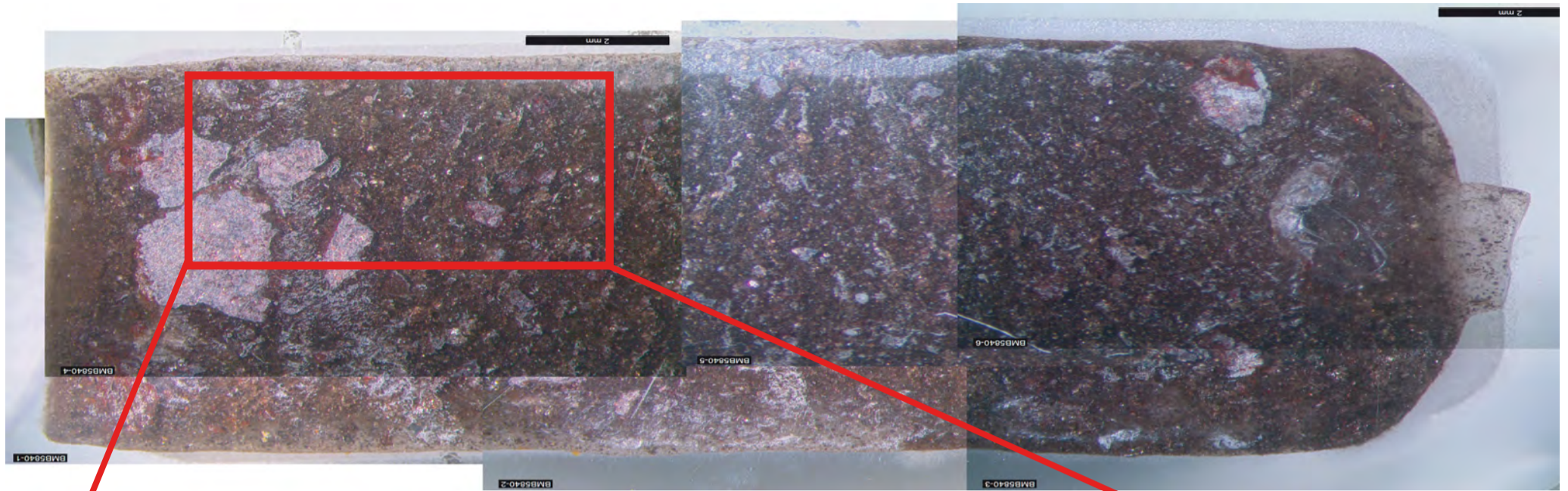
Chromium	FeO(Fe40-50)	FeO(Fe80-90)	Manganese	Sulphate/Sulphide	Zinc
Copper	FeO(Fe50-60)	FeO(Fe90-100)	Nickel	Tin	Not Classified
Fe	FeO(Fe60-70)	Fe-Si-O	Phosphate/phosphide	Titanium	Unclassified
FeO(Fe30-40)	FeO(Fe70-80)	Lead	Silicate/quartz	Vanadium	

500µm

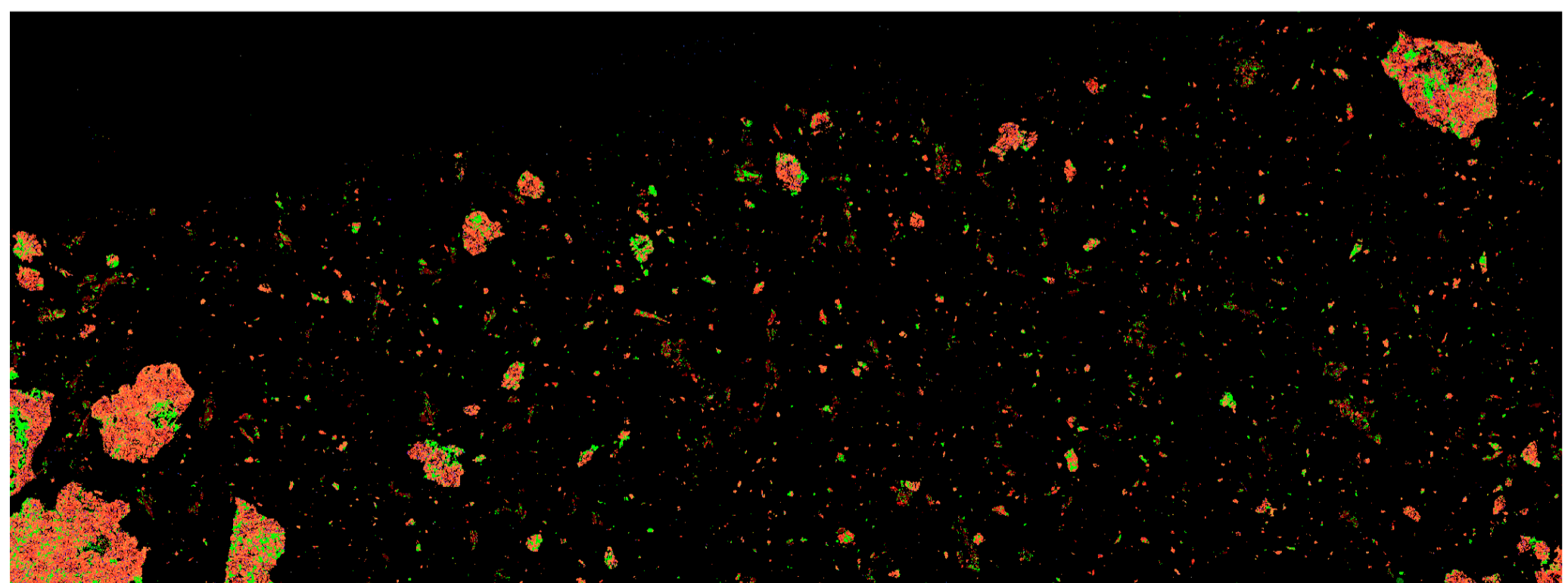
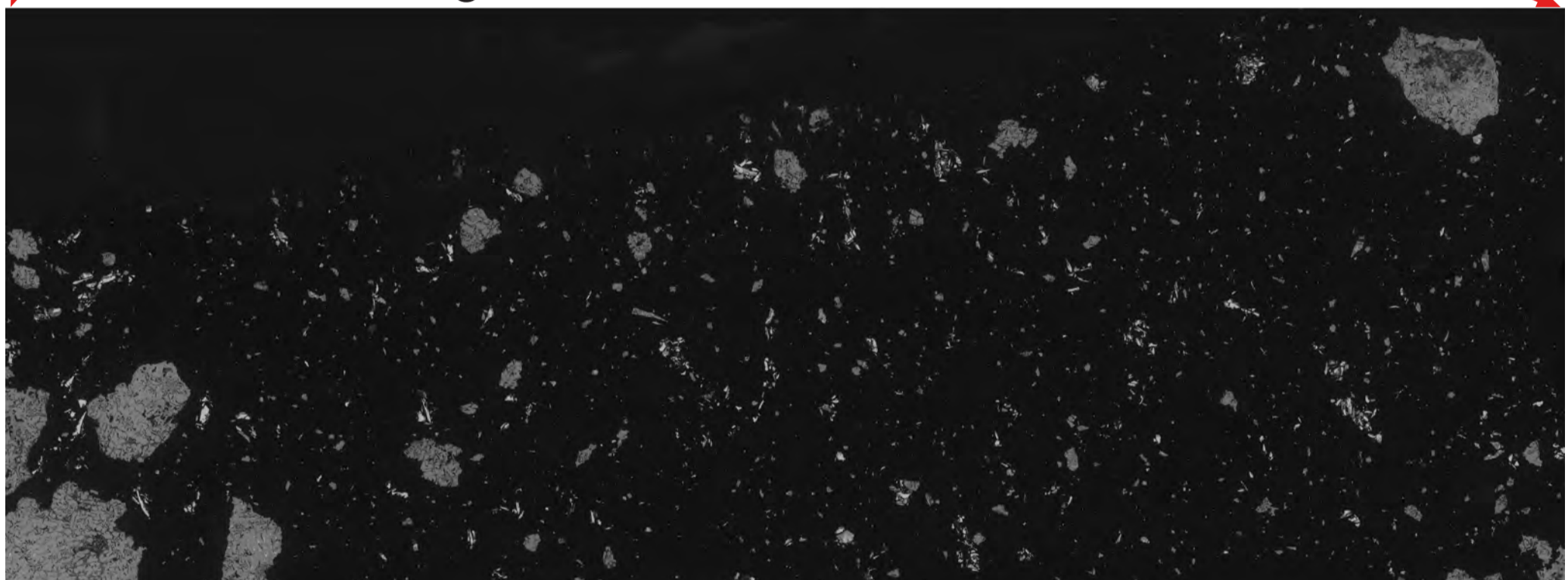
Mineral phases image

# BMB5840

Optical microscopy image



BSE image

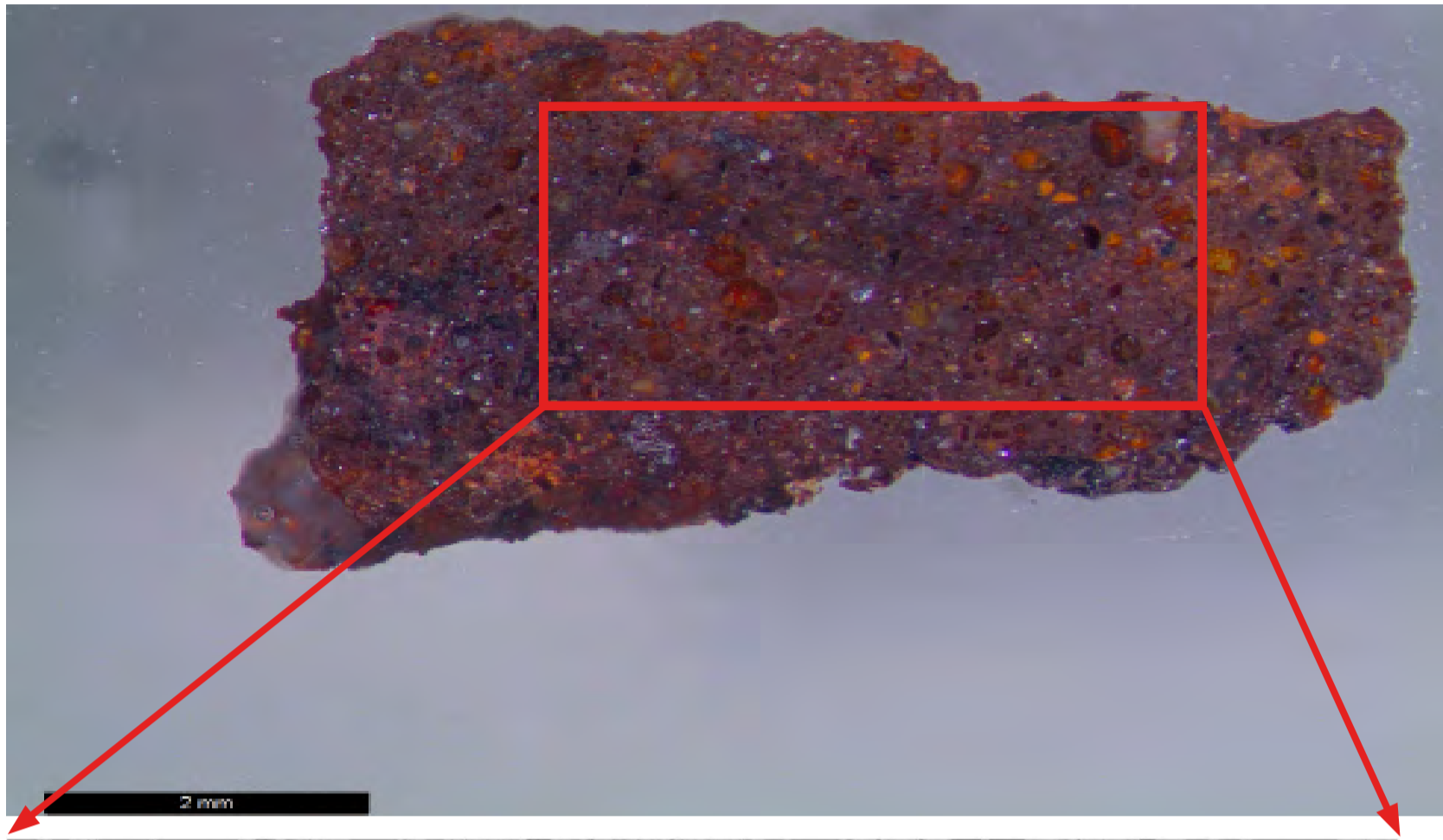


Chromium	FeO(Fe30-40)	FeO(Fe70-80)	Lead	Silicate/quartz	Vanadium	Unclassified
Cobalt	FeO(Fe40-50)	FeO(Fe80-90)	Manganese	Sulphate/Sulphide	Zinc	
Copper	FeO(Fe50-60)	FeO(Fe90-100)	Nickel	Tin	Not Analysed	500µm
Fe	FeO(Fe60-70)	Fe-Si-O	Phosphate/phosphide	Titanium	Not Classified	

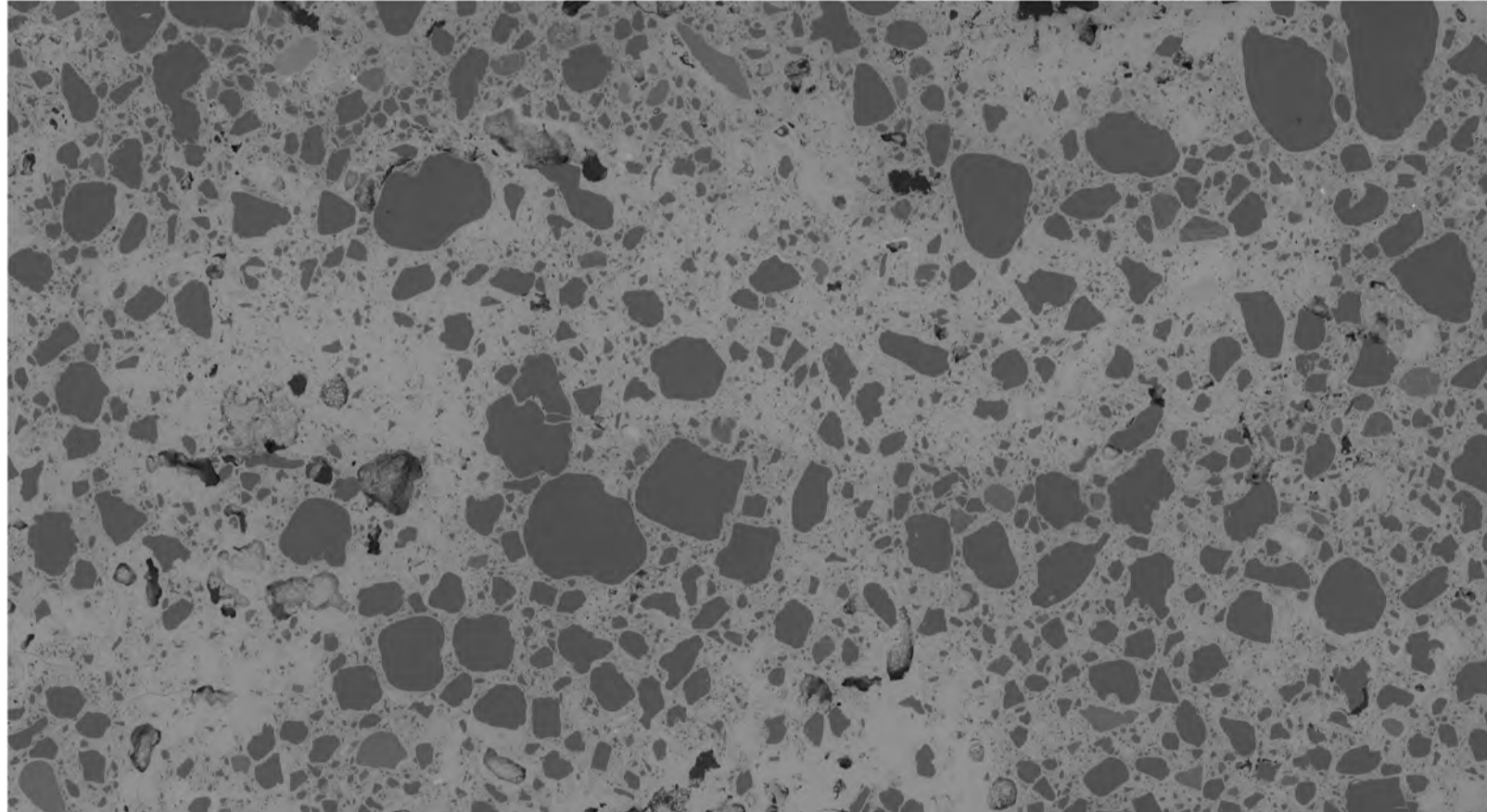
Mineral phases image

Optical microscopy image

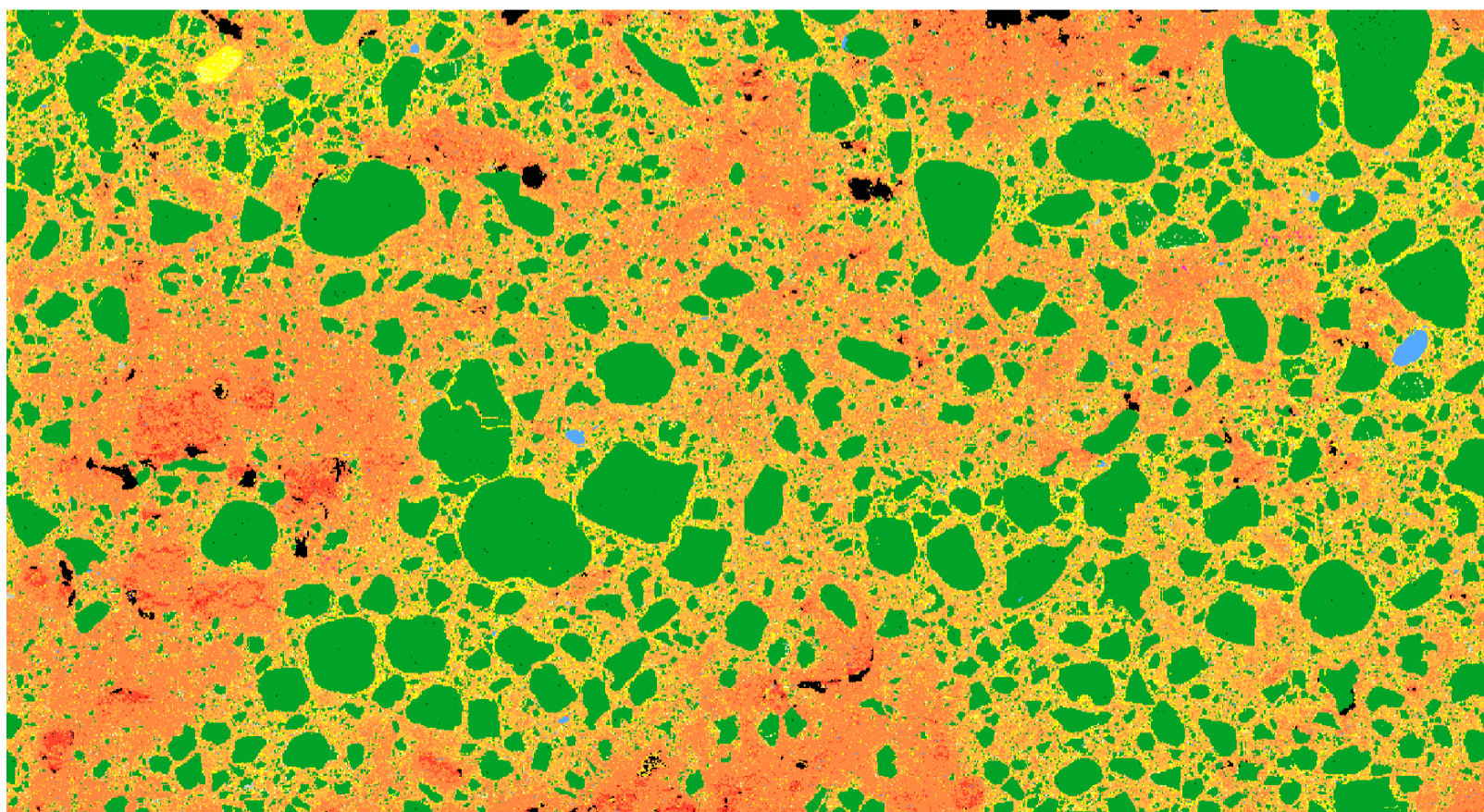
BMB5843



BSE image



Mineral phases image

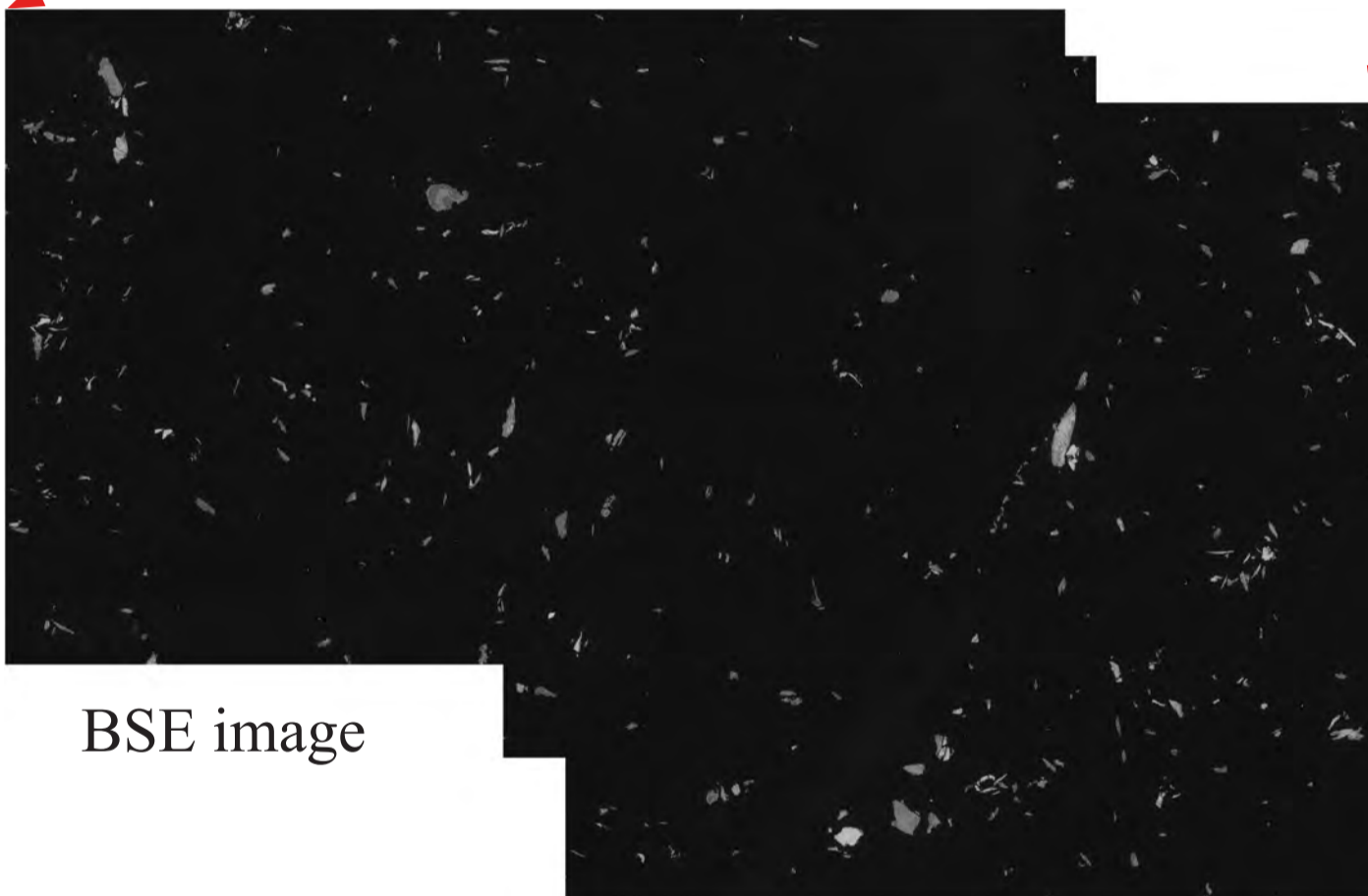
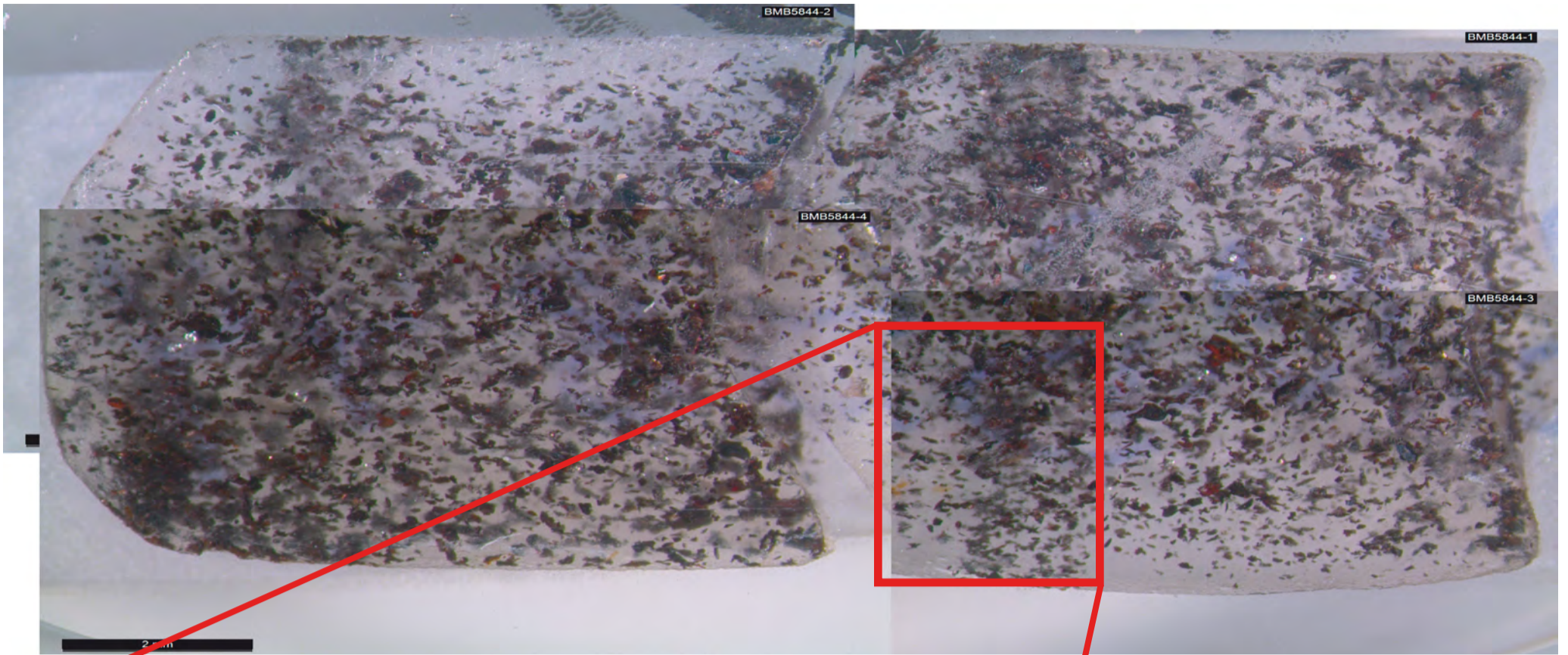


Chromium	Copper	FeO(Fe30-40)	FeO(Fe40-50)	FeO(Fe50-60)	FeO(Fe60-70)	FeO(Fe70-80)	FeO(Fe80-90)	Fe-Si-O
Lead	Phosphate/phosphide	Silicate/quartz	Sulphate/Sulphide	Titanium	Zinc	Not Classified	Unclassified	

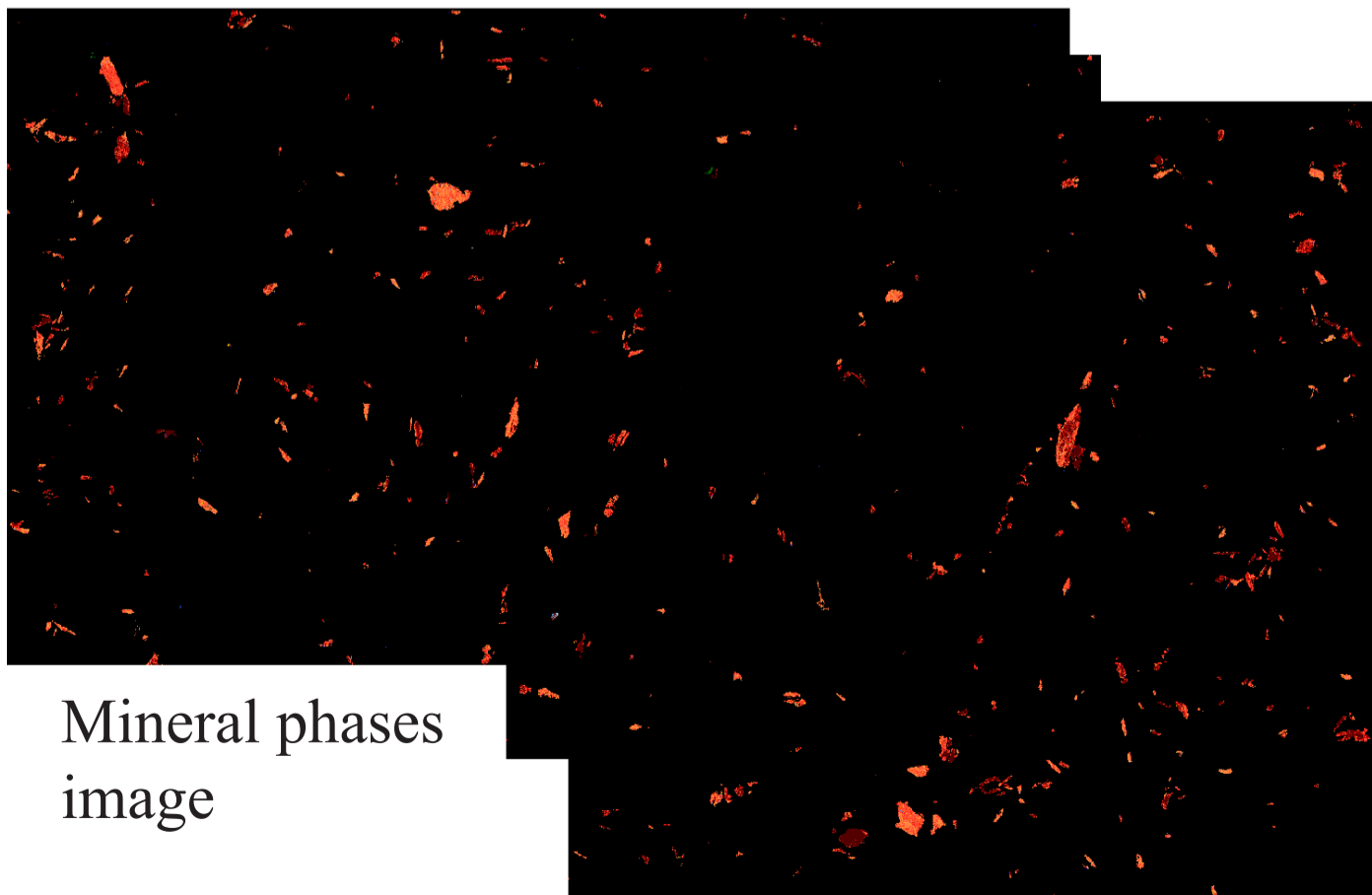
200µm

Optical microscopy image

BMB5844



BSE image



Mineral phases image

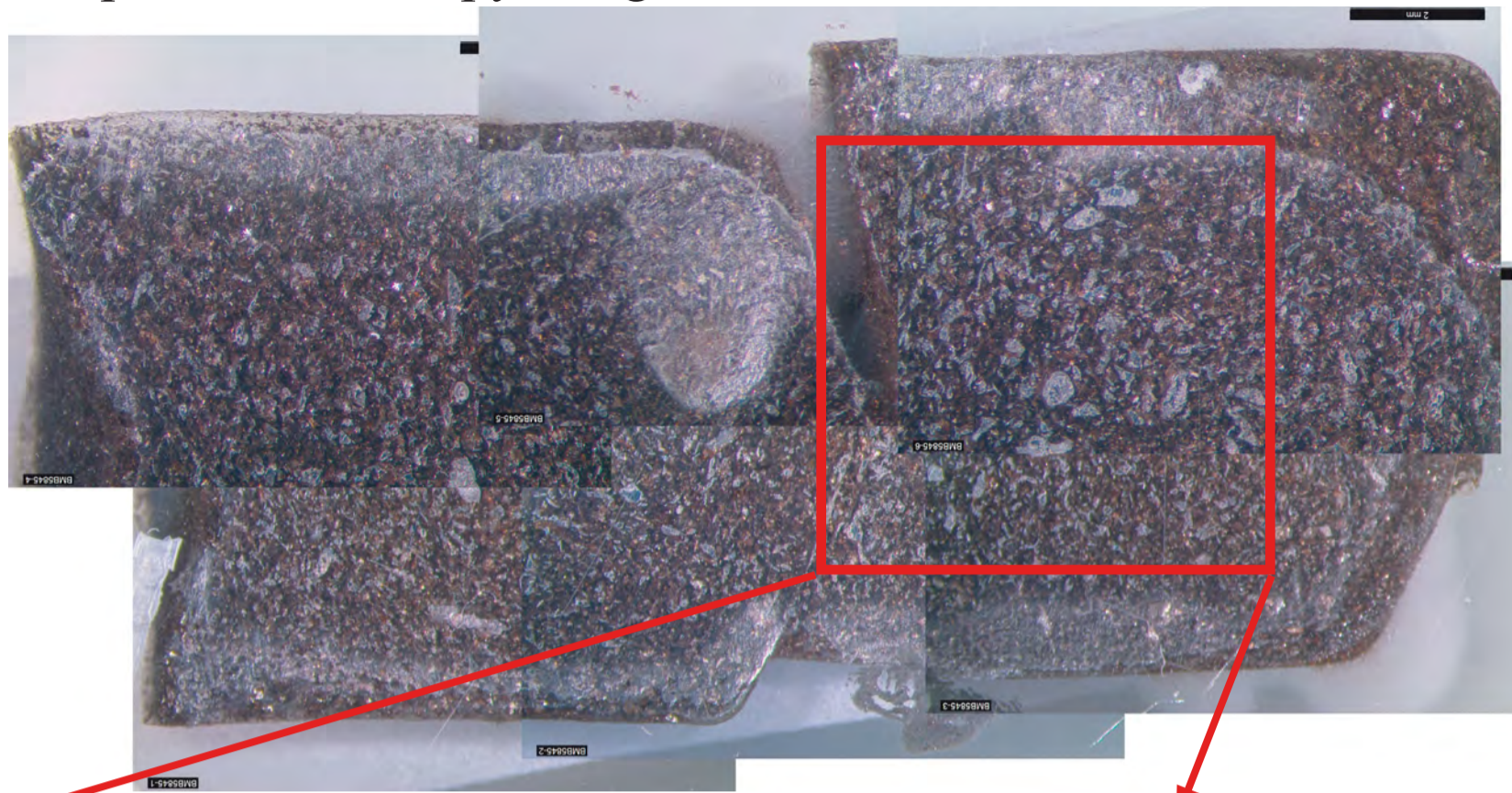
- |                   |                     |
|-------------------|---------------------|
| Chromium          | FeO(Fe40-50)        |
| Copper            | FeO(Fe50-60)        |
| Fe                | FeO(Fe60-70)        |
| FeO(Fe30-40)      | FeO(Fe70-80)        |
| FeO(Fe80-90)      | Manganese           |
| FeO(Fe90-100)     | Nickel              |
| Fe-Si-O           | Phosphate/phosphide |
| Lead              | Silicate/quartz     |
| Sulphate/Sulphide | Zinc                |
| Tin               | Not Classified      |
| Titanium          | Unclassified        |
| Vanadium          |                     |

500µm

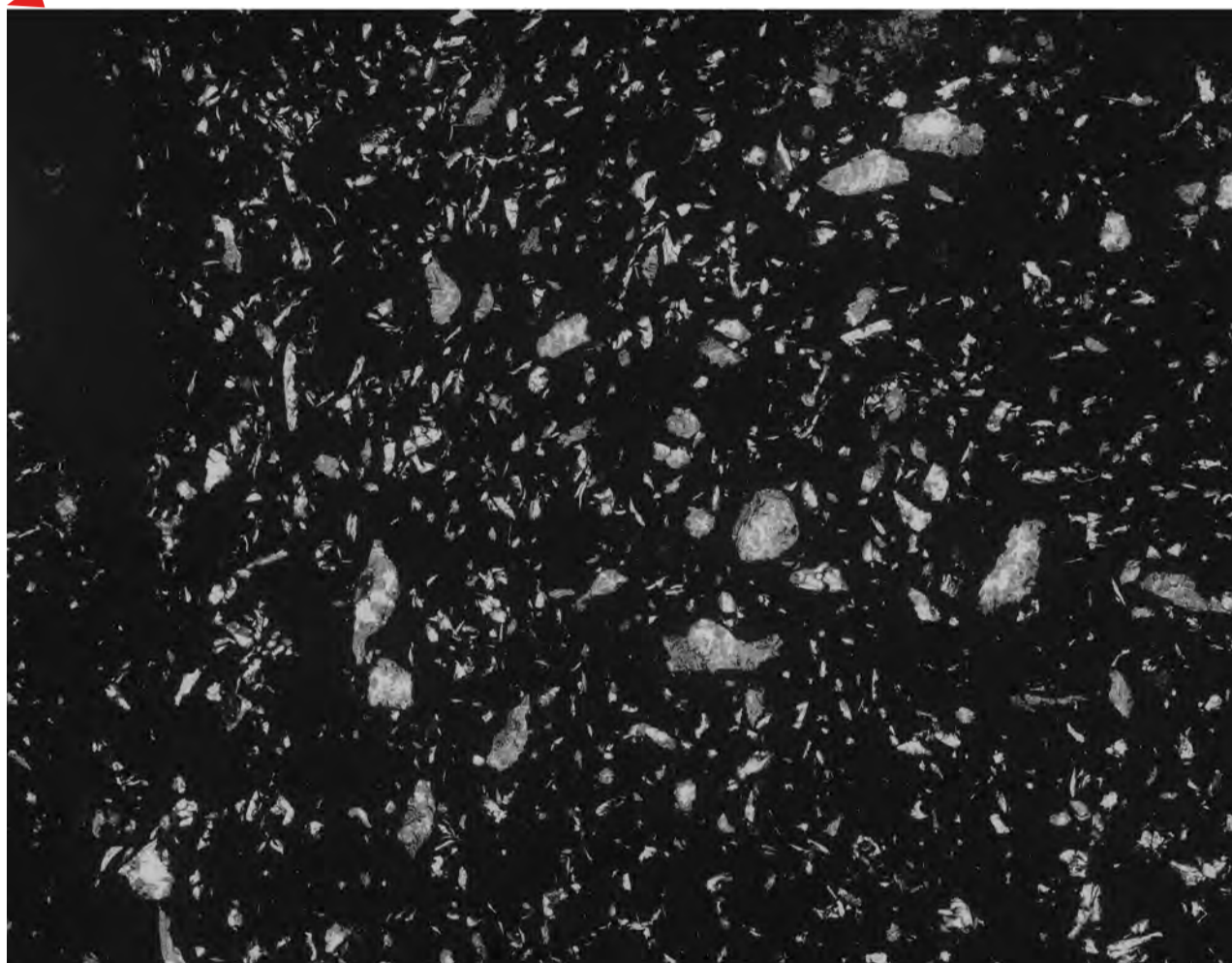


Optical microscopy image

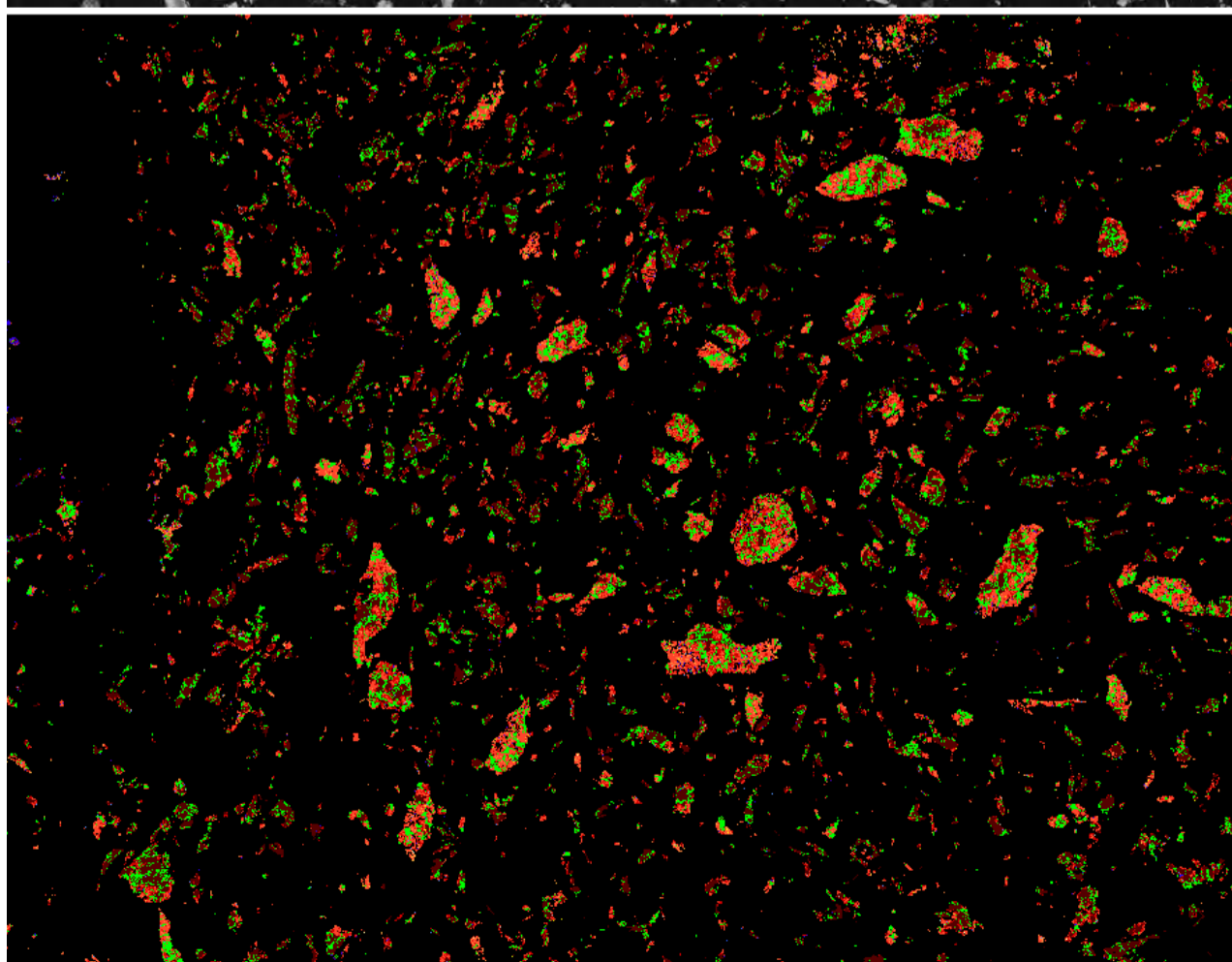
BMB5845



BSE image



Mineral phases image

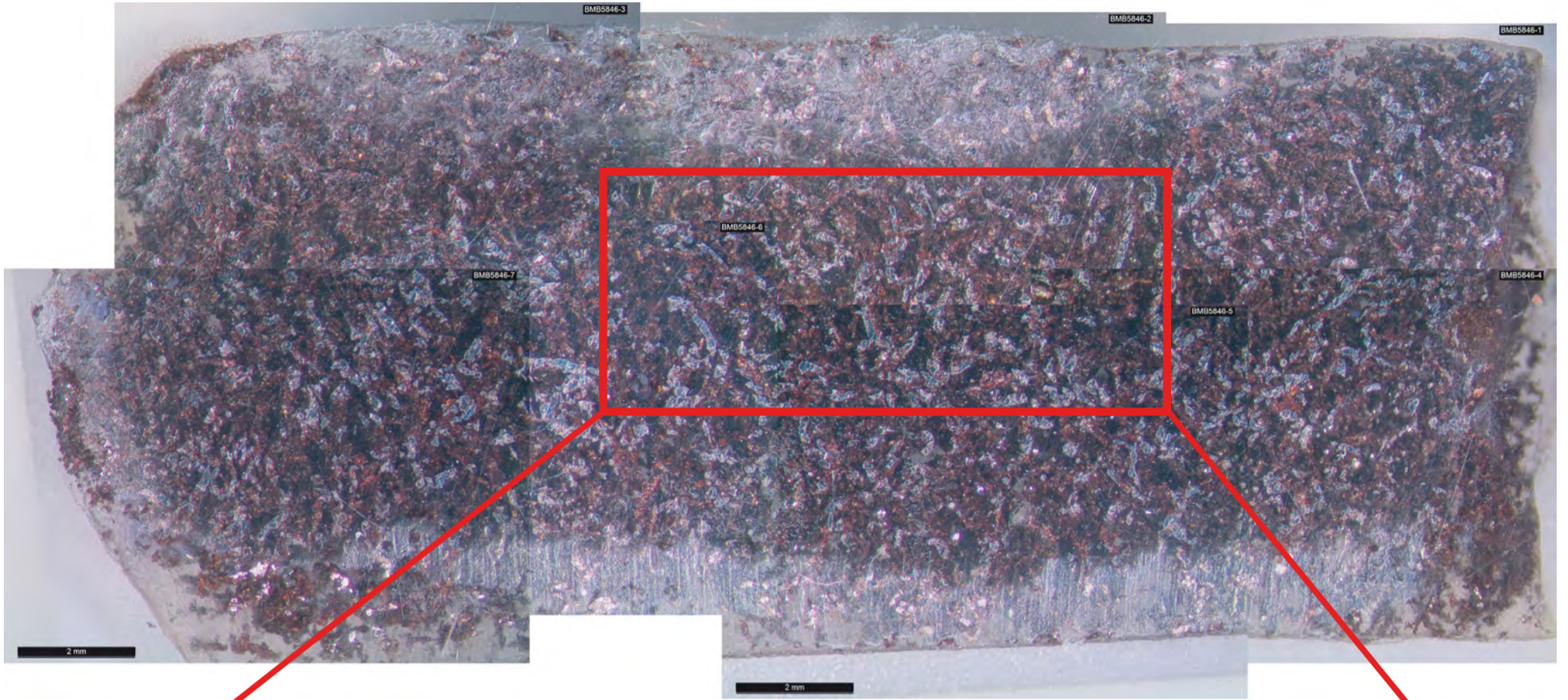


- |                   |                     |
|-------------------|---------------------|
| Chromium          | FeO(Fe30-40)        |
| Cobalt            | FeO(Fe40-50)        |
| Copper            | FeO(Fe50-60)        |
| Fe                | FeO(Fe60-70)        |
| FeO(Fe70-80)      | Lead                |
| FeO(Fe80-90)      | Manganese           |
| FeO(Fe90-100)     | Nickel              |
| Fe-Si-O           | Phosphate/phosphide |
| Silicate/quartz   | Zinc                |
| Sulphate/Sulphide | Not Analysed        |
| Tin               | Not Classified      |
| Titanium          | Unclassified        |

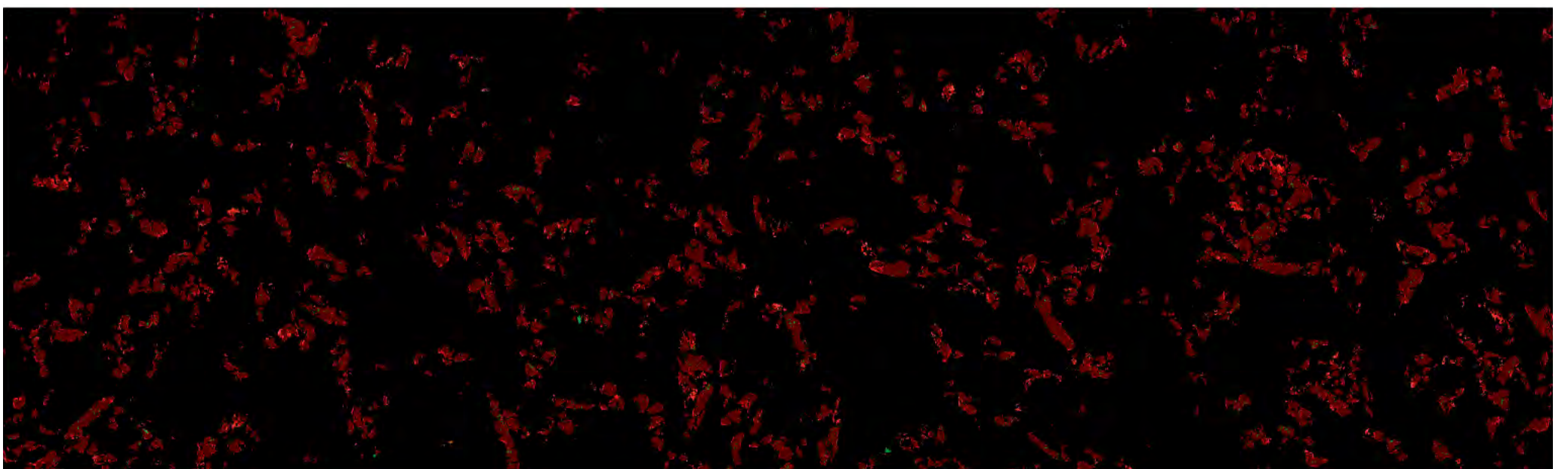
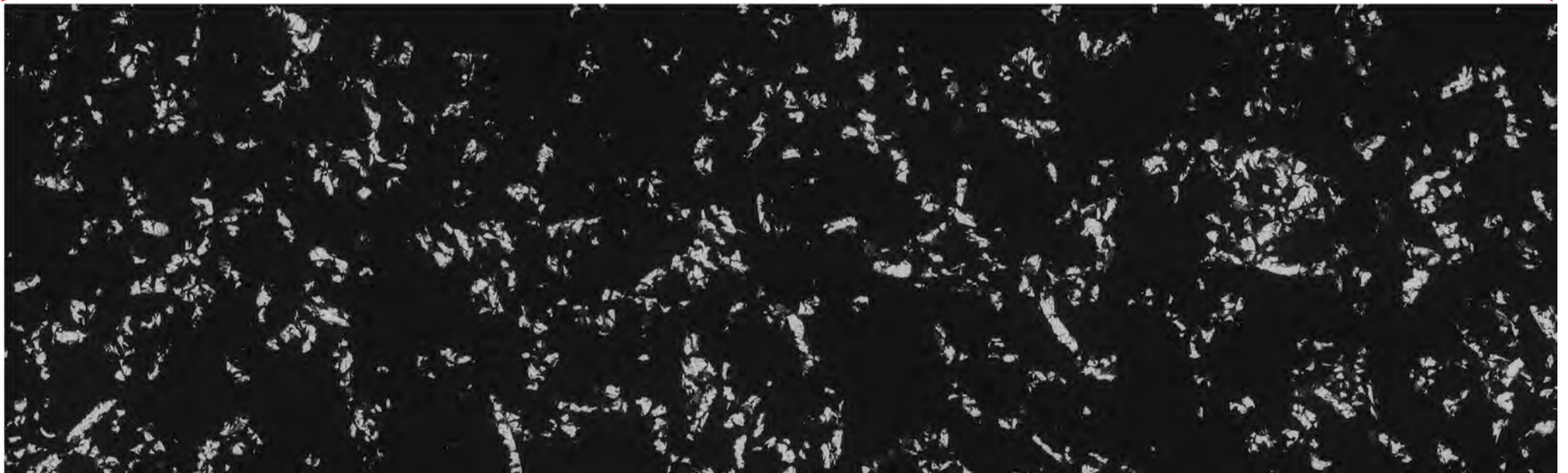
500µm

# BMB5846

Optical microscopy image



BSE image



Cobalt	FeO(Fe40-50)	FeO(Fe80-90)	Manganese	Sulphate/Sulphide	Zinc
Copper	FeO(Fe50-60)	FeO(Fe90-100)	Nickel	Tin	Not Analysed
Fe	FeO(Fe60-70)	Fe-Si-O	Phosphate/phosphide	Titanium	Not Classified
FeO(Fe30-40)	FeO(Fe70-80)	Lead	Silicate/quartz	Vanadium	Unclassified

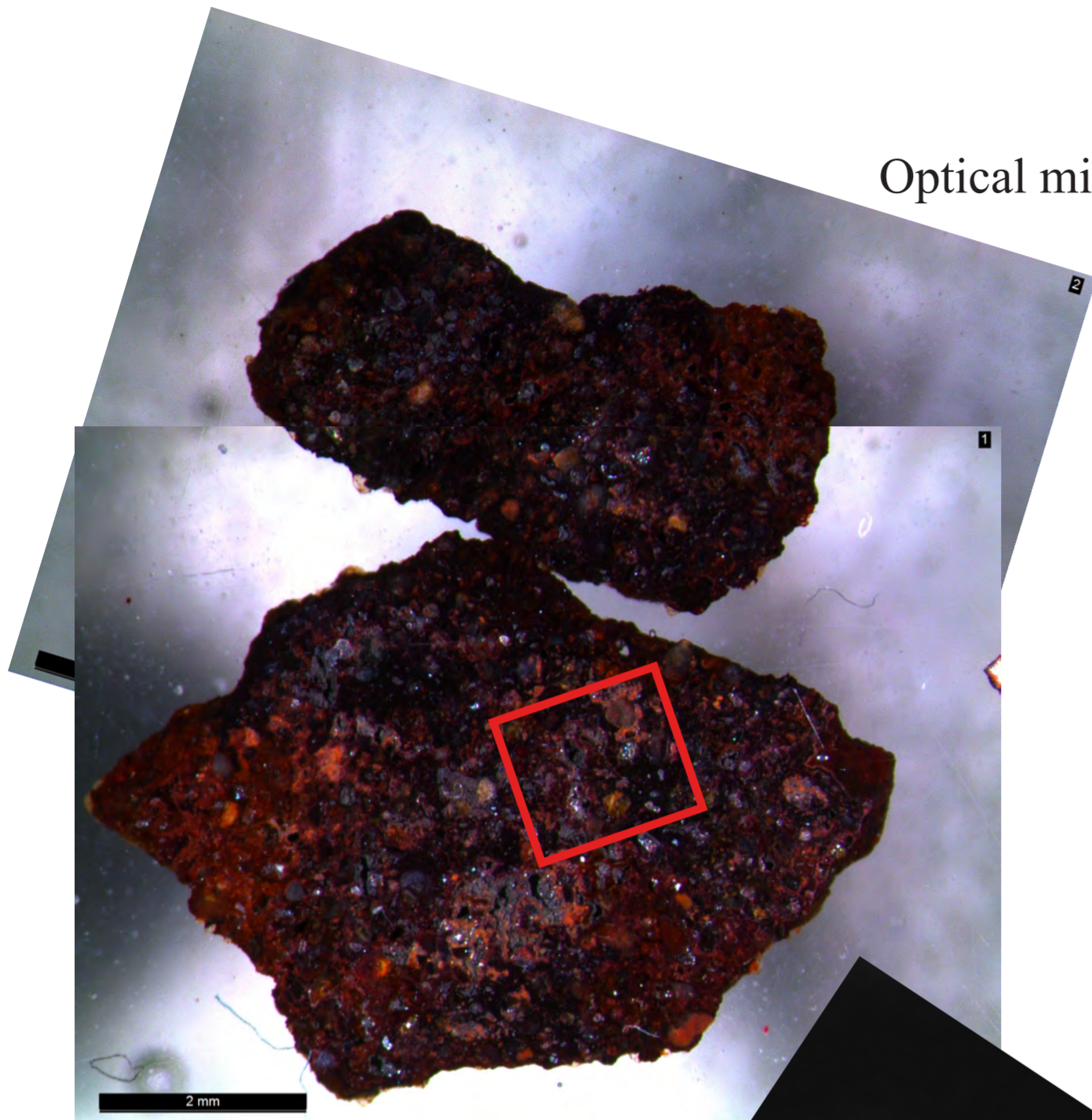
500µm

Mineral phases image

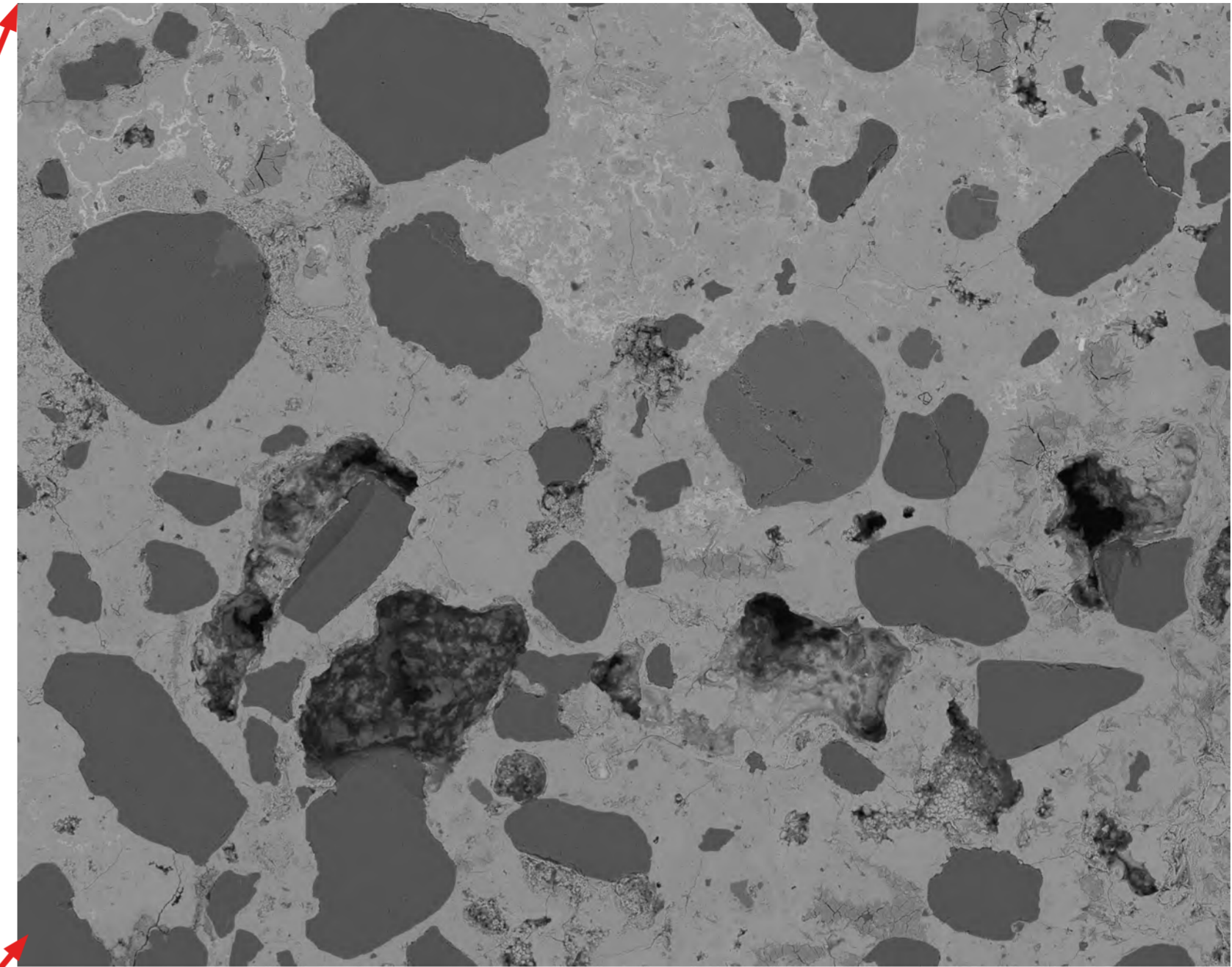
BMB5847

BMB5847

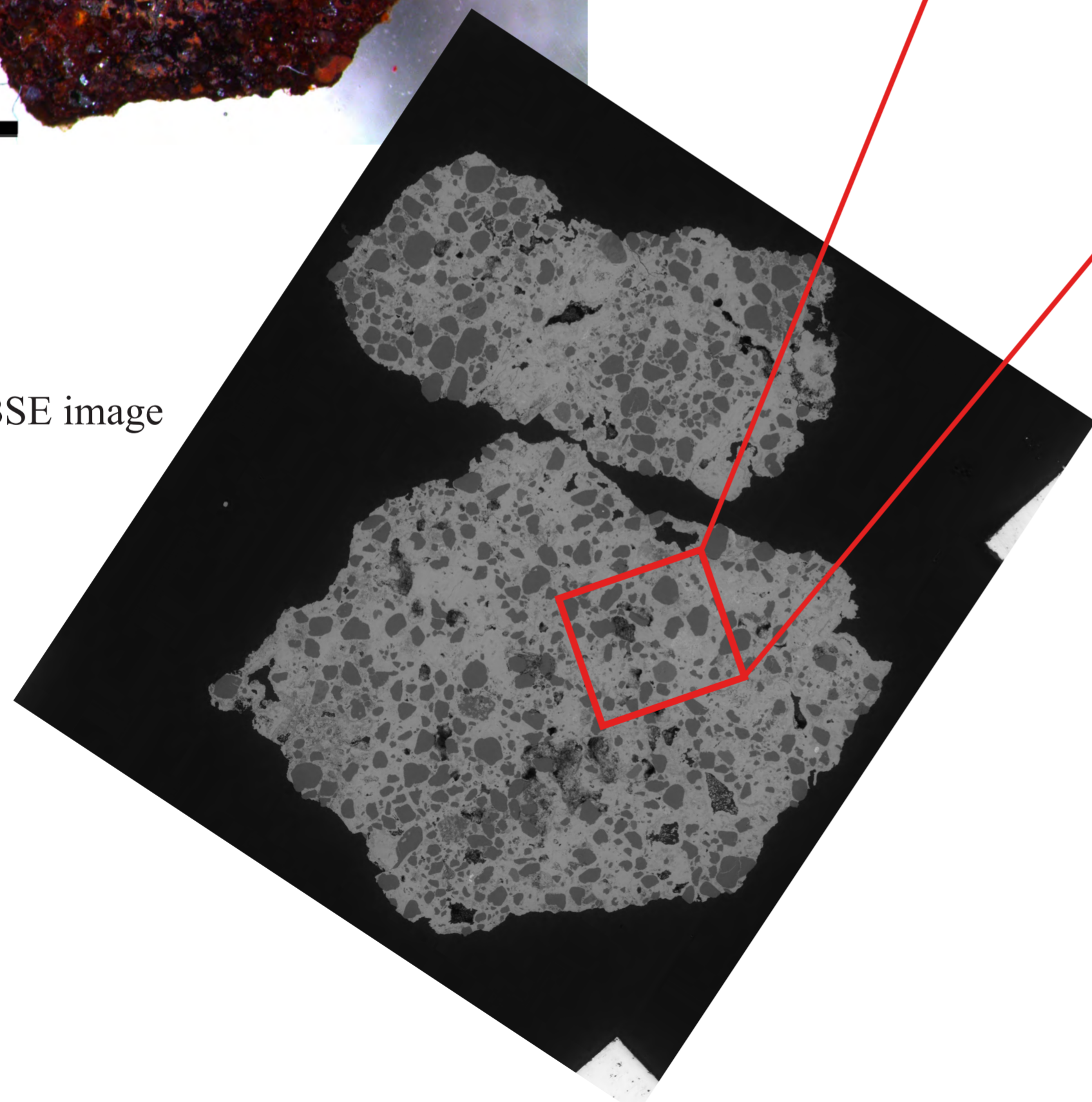
Optical microscopy image



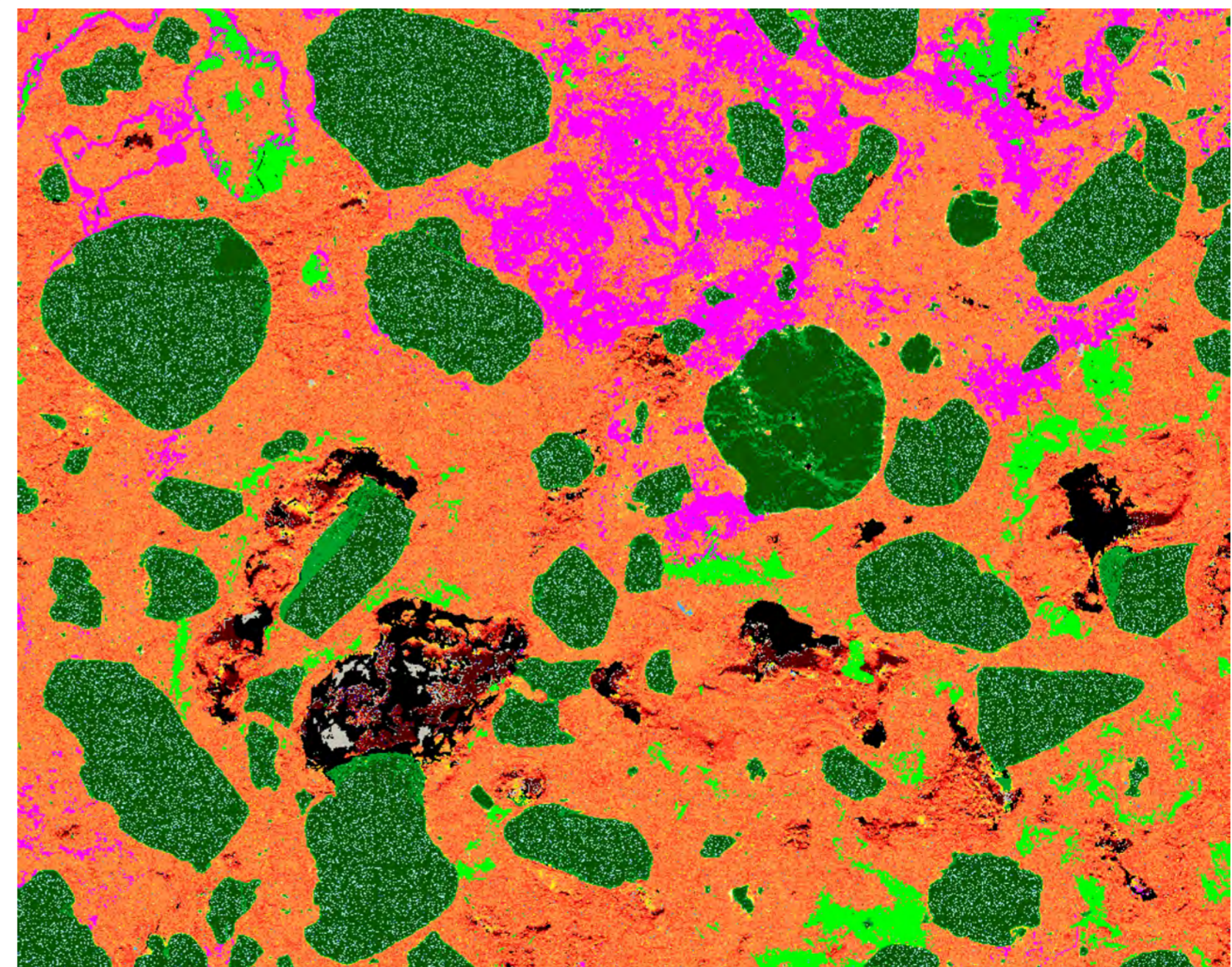
BSE image



BSE image



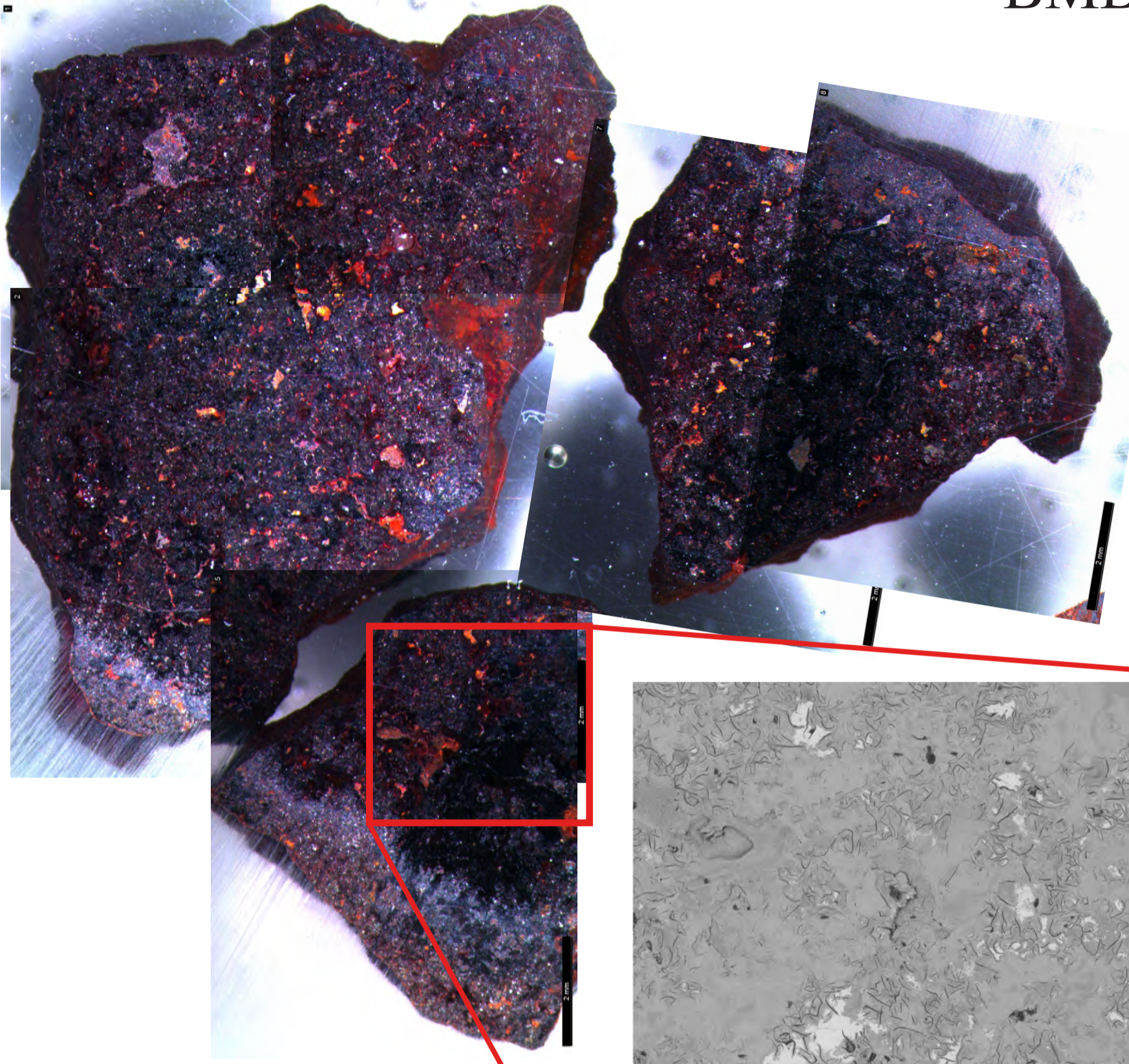
Mineral phases image



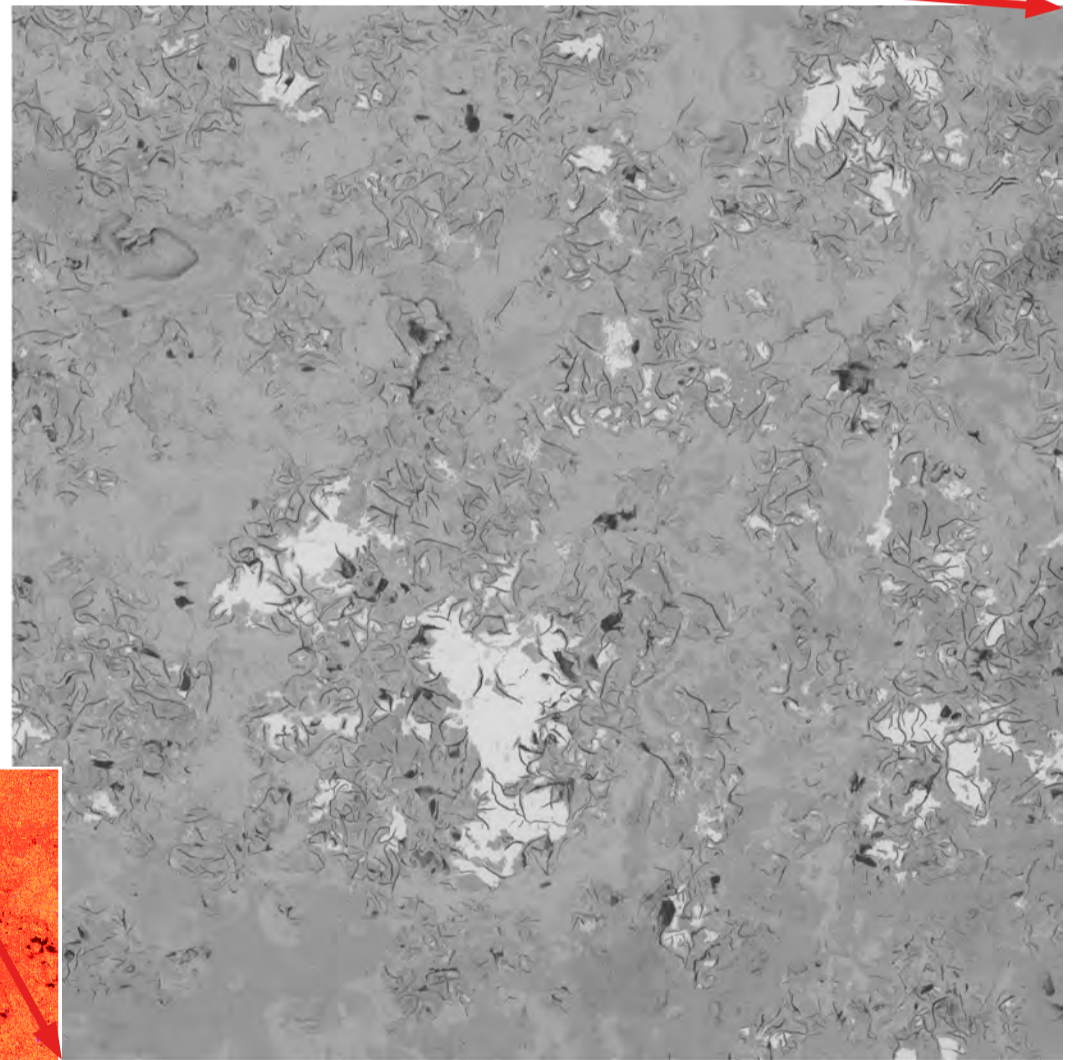
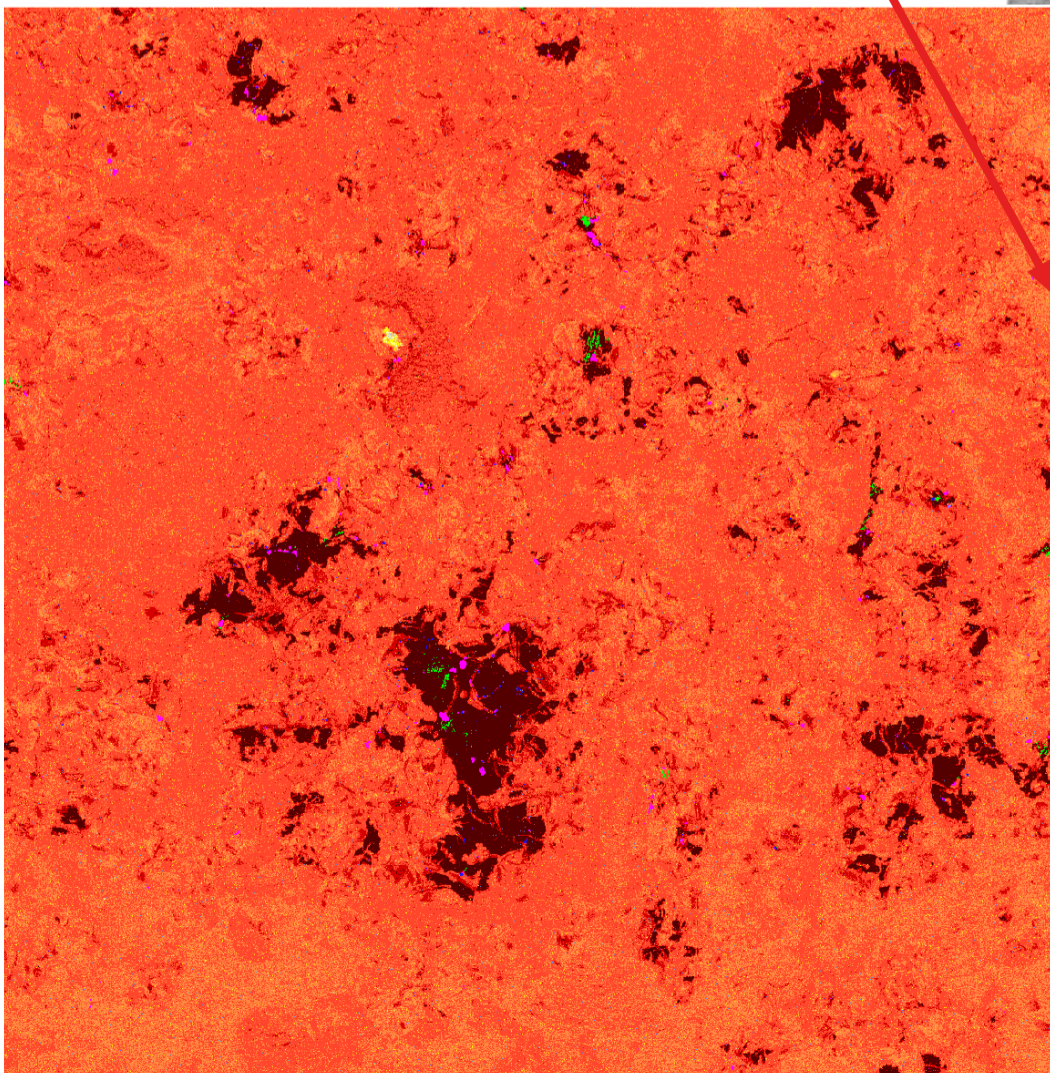
Chromium	Cobalt	Copper	Fe	FeO(Fe30-40)	FeO(Fe40-50)	FeO(Fe50-60)
FeO(Fe60-70)	FeO(Fe70-80)	FeO(Fe80-90)	Fe-Si-O	Lead	Manganese	Nickel
Phosphate/phosphide	Silicate/quartz	Sulphate/Sulphide	Tin	Titanium	Vanadium	Zinc
Not Analysed	Not Classified	Unclassified				

Optical microscopy image

BMB5851



Mineral phases image



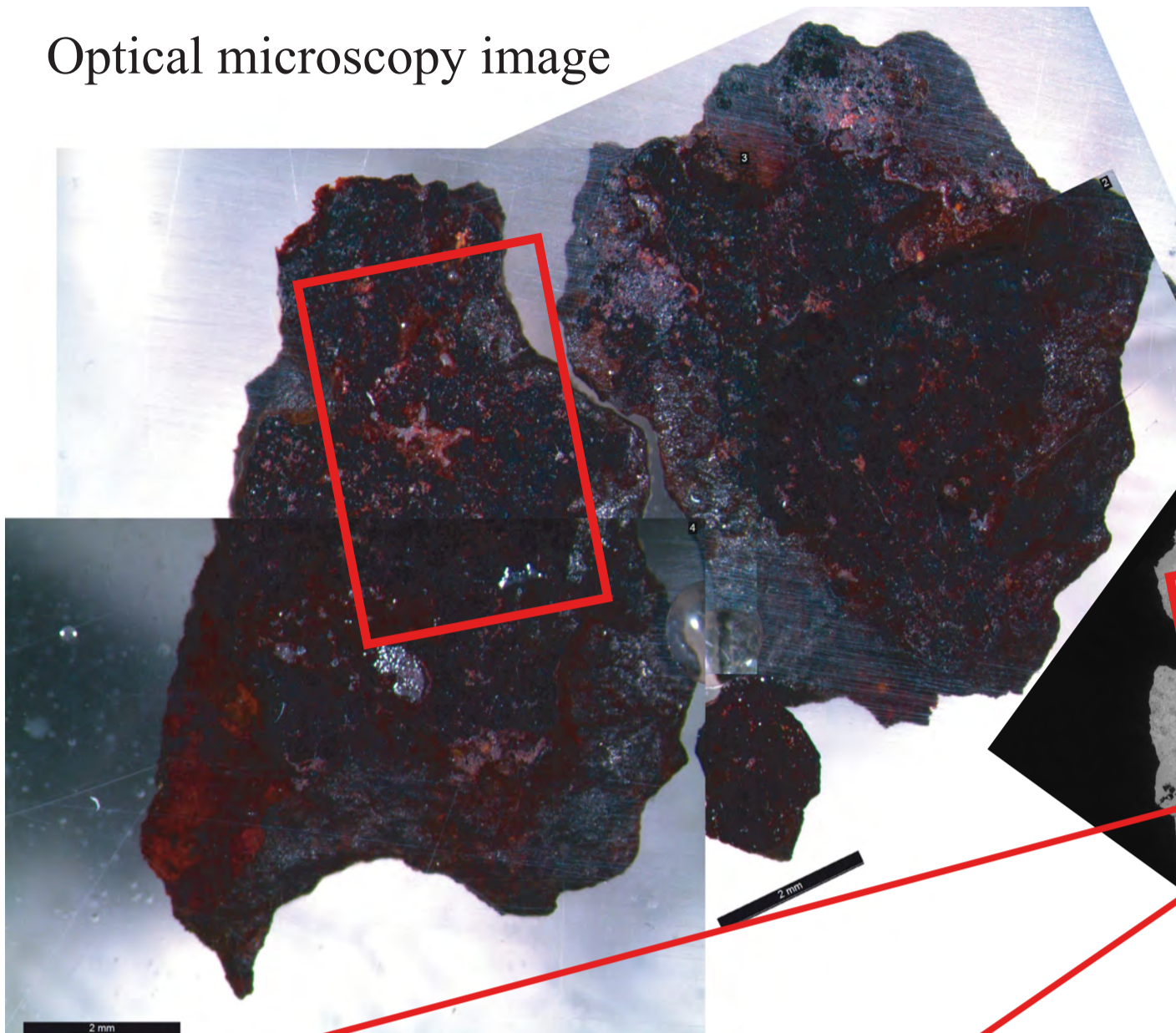
BSE image

100µm

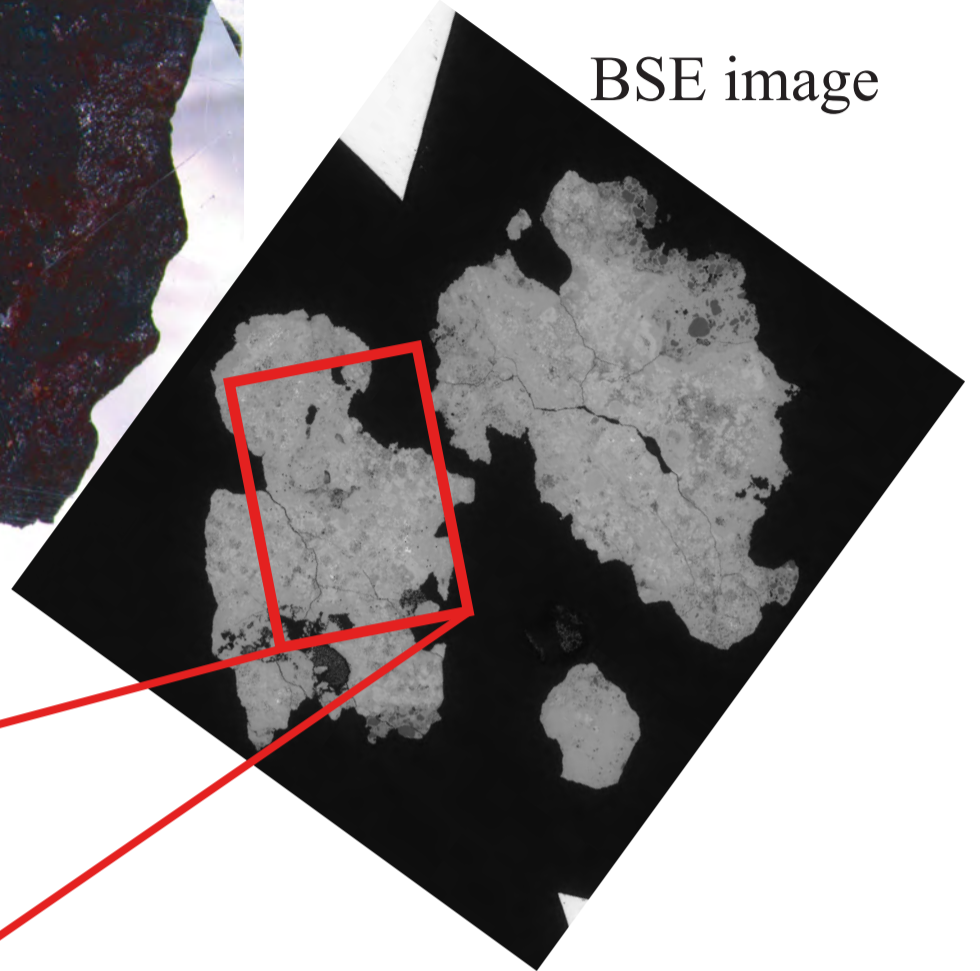
- |                   |                     |
|-------------------|---------------------|
| Chromium          | FeO(Fe30-40)        |
| Cobalt            | FeO(Fe40-50)        |
| Copper            | FeO(Fe50-60)        |
| Fe                | FeO(Fe60-70)        |
| FeO(Fe70-80)      | Lead                |
| FeO(Fe80-90)      | Manganese           |
| FeO(Fe90-100)     | Nickel              |
| Fe-Si-O           | Phosphate/phosphide |
| Silicate/quartz   | Zinc                |
| Sulphate/Sulphide | Not Analysed        |
| Tin               | Not Classified      |
| Titanium          | Unclassified        |

BMB5852

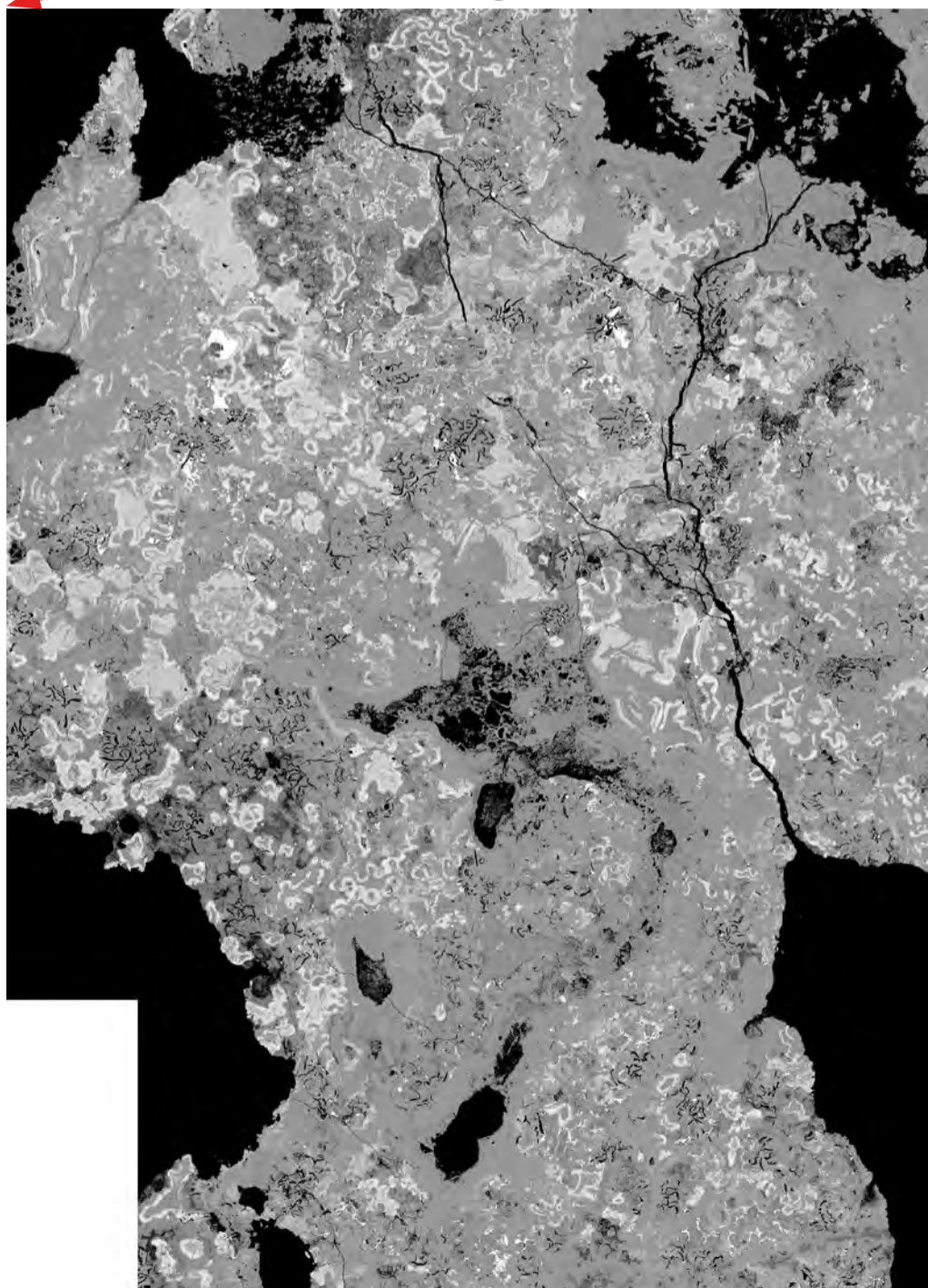
Optical microscopy image



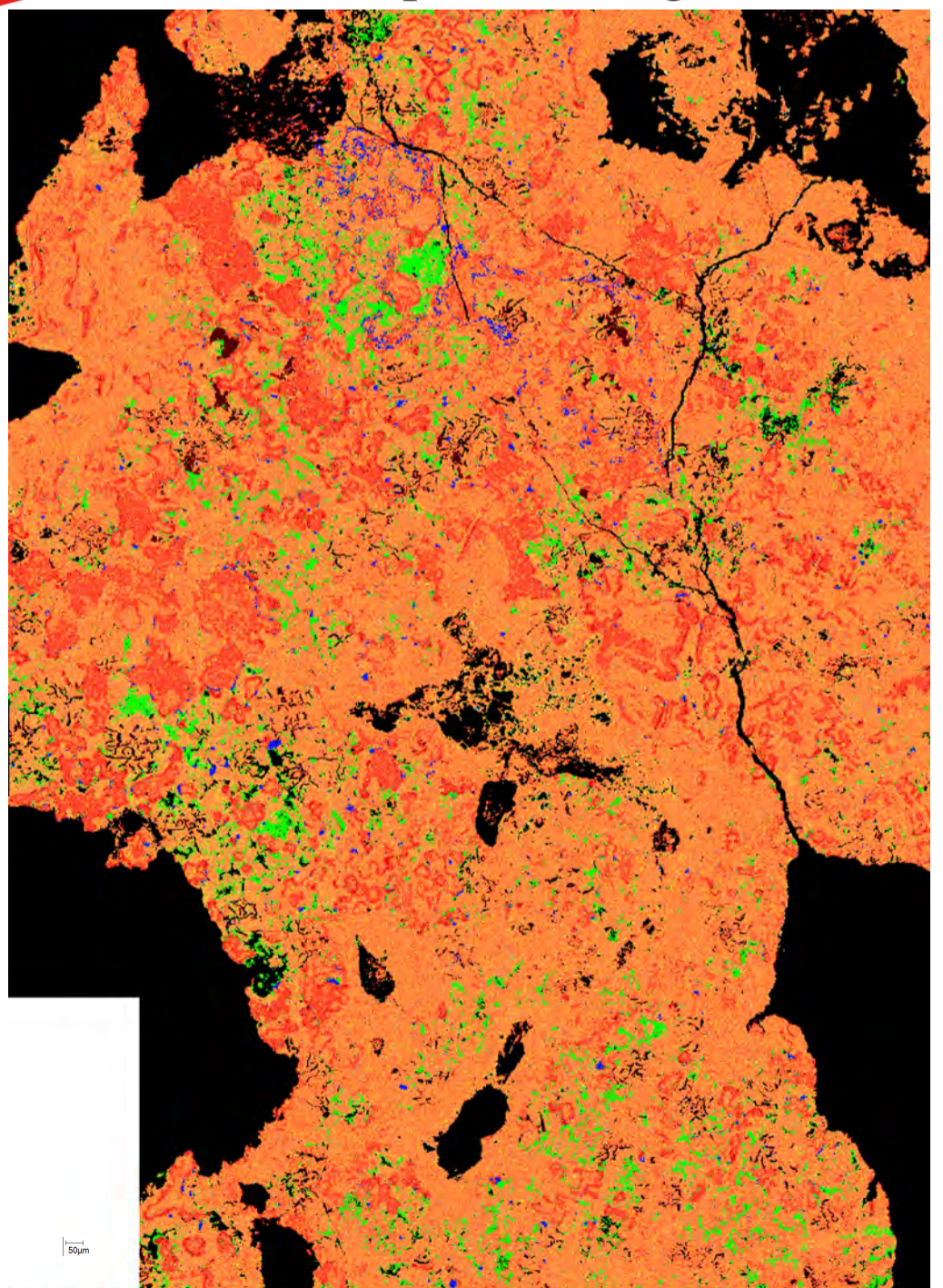
BSE image



BSE image



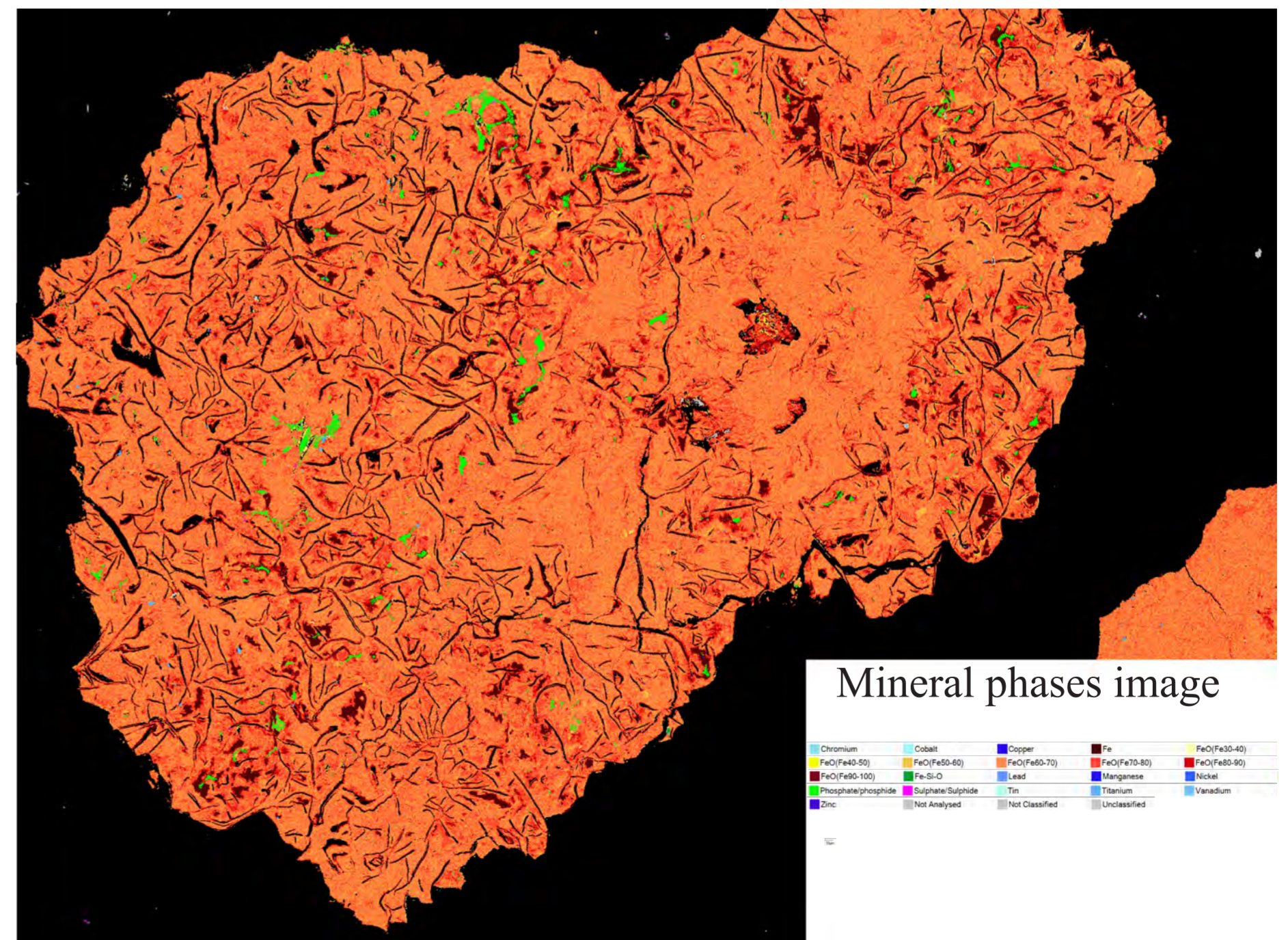
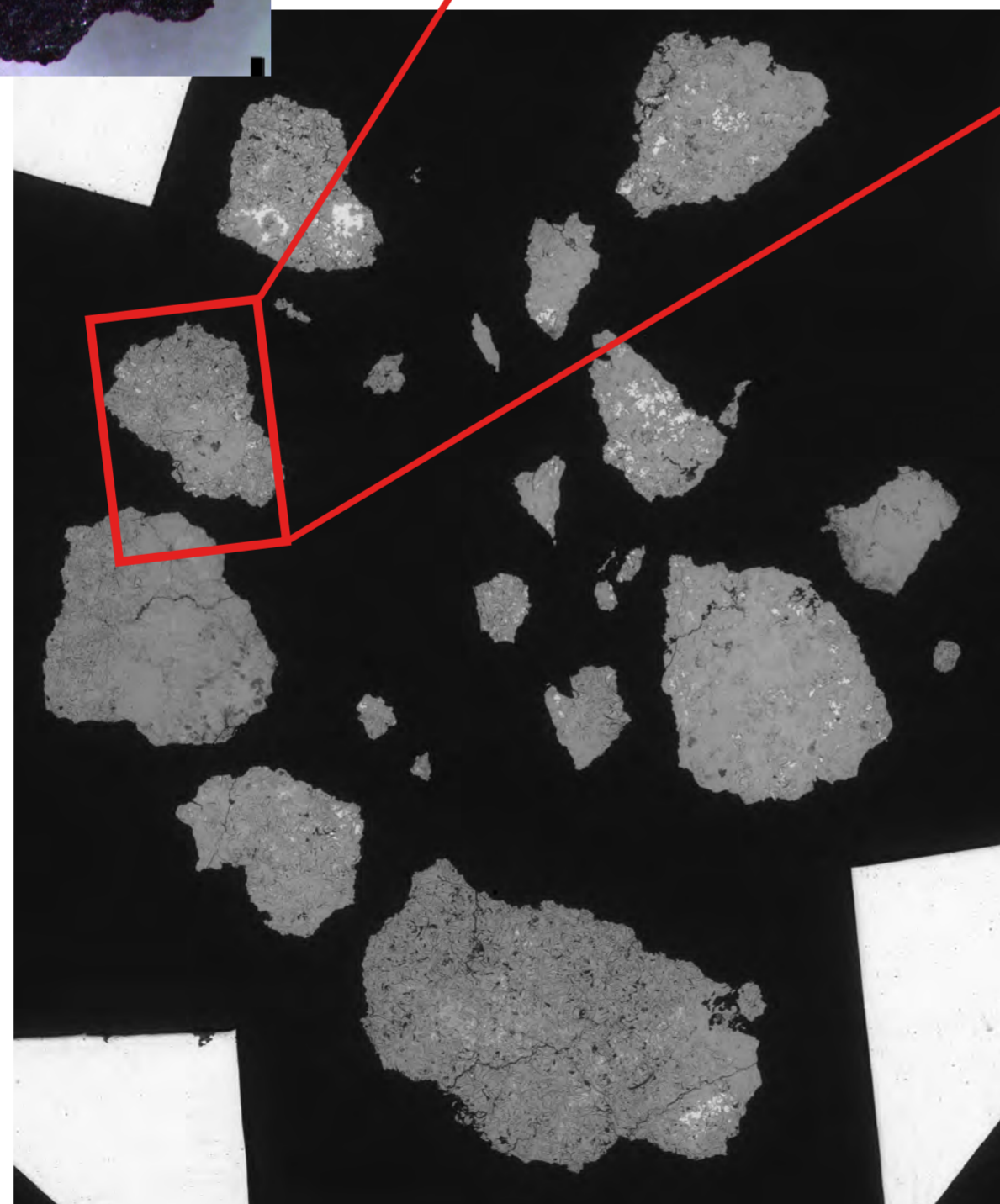
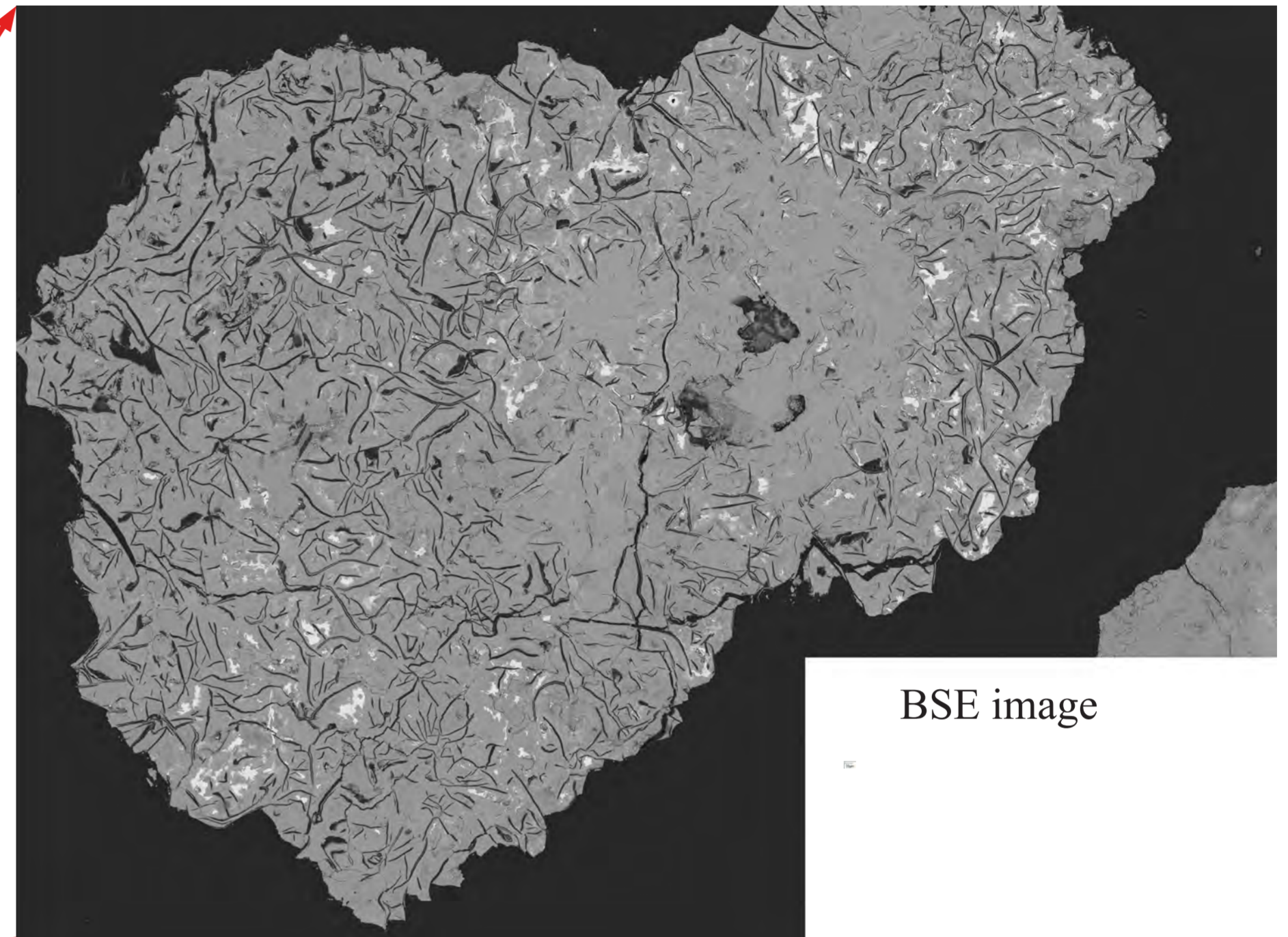
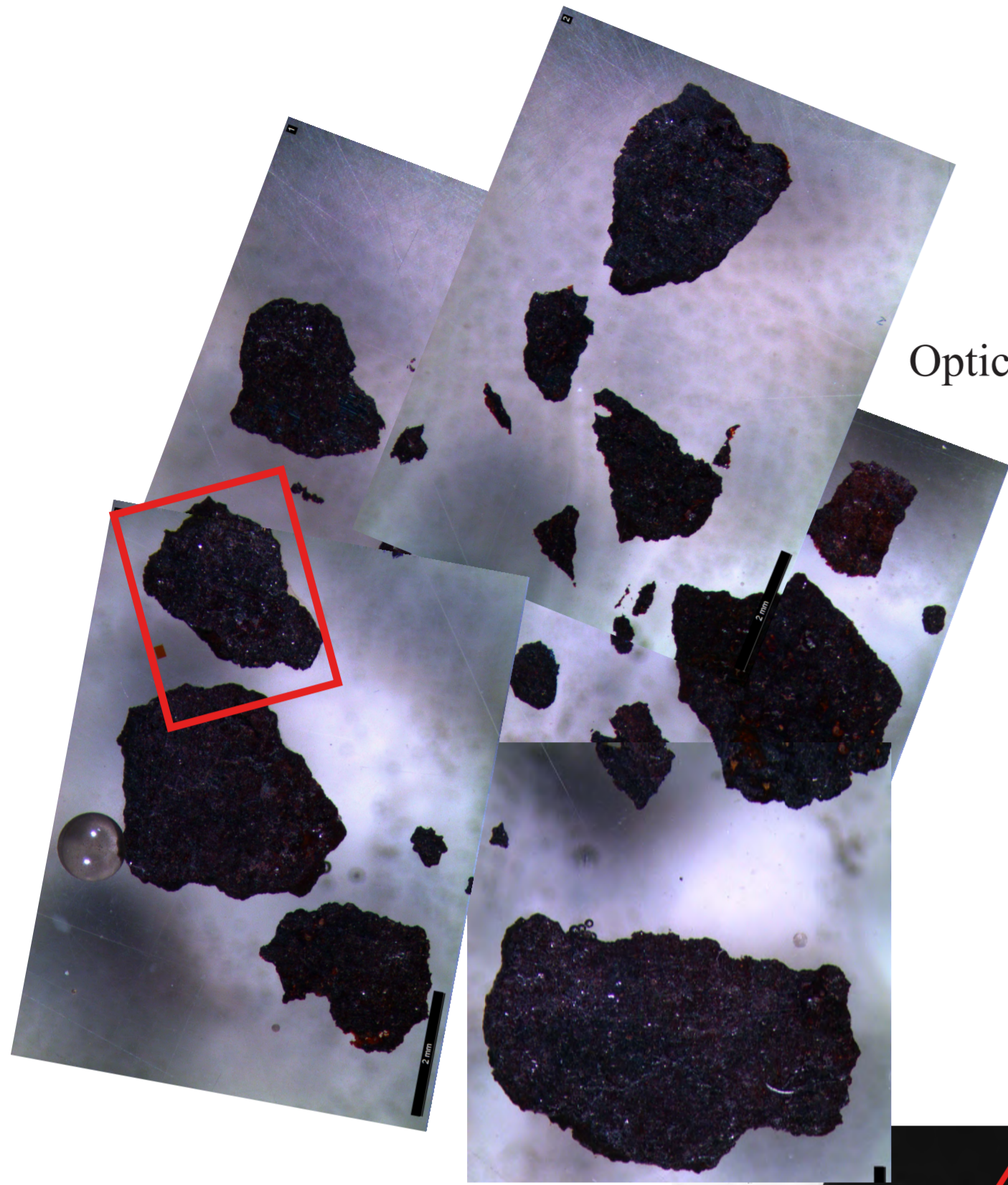
Mineral phases image



Chromium	Copper	FeO(Fe30-40)	FeO(Fe50-60)	FeO(Fe70-80)	FeO(Fe90-100)	Lead	Nickel
Cobalt	Fe	FeO(Fe40-50)	FeO(Fe60-70)	FeO(Fe80-90)	Fe-Si-O	Manganese	Phosphate/phosphide
Sulphate/Sulphide	Titanium	Zinc	Not Classified	Unclassified			
Tin	Vanadium	Not Analysed					

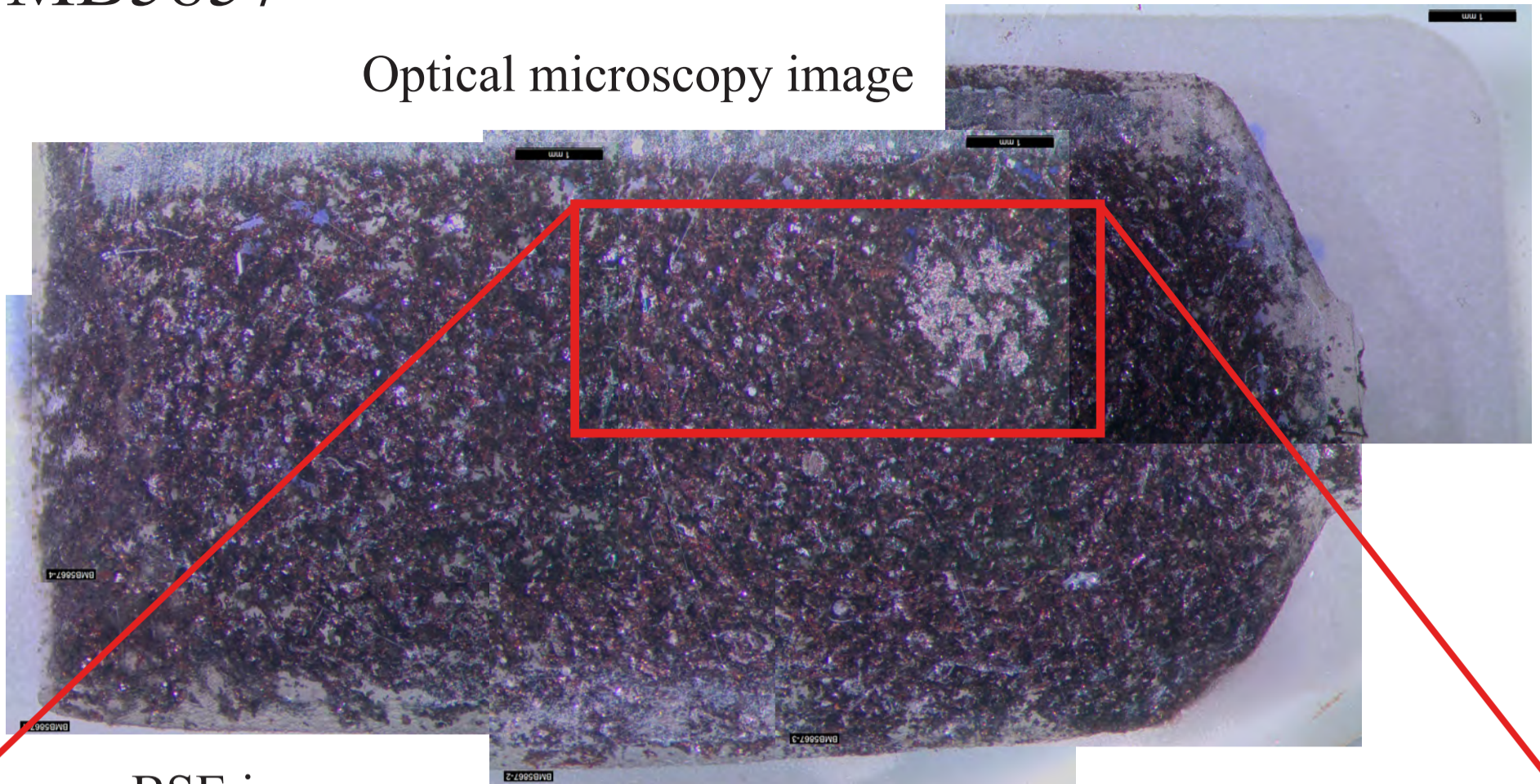
BMB5855

BMB5855

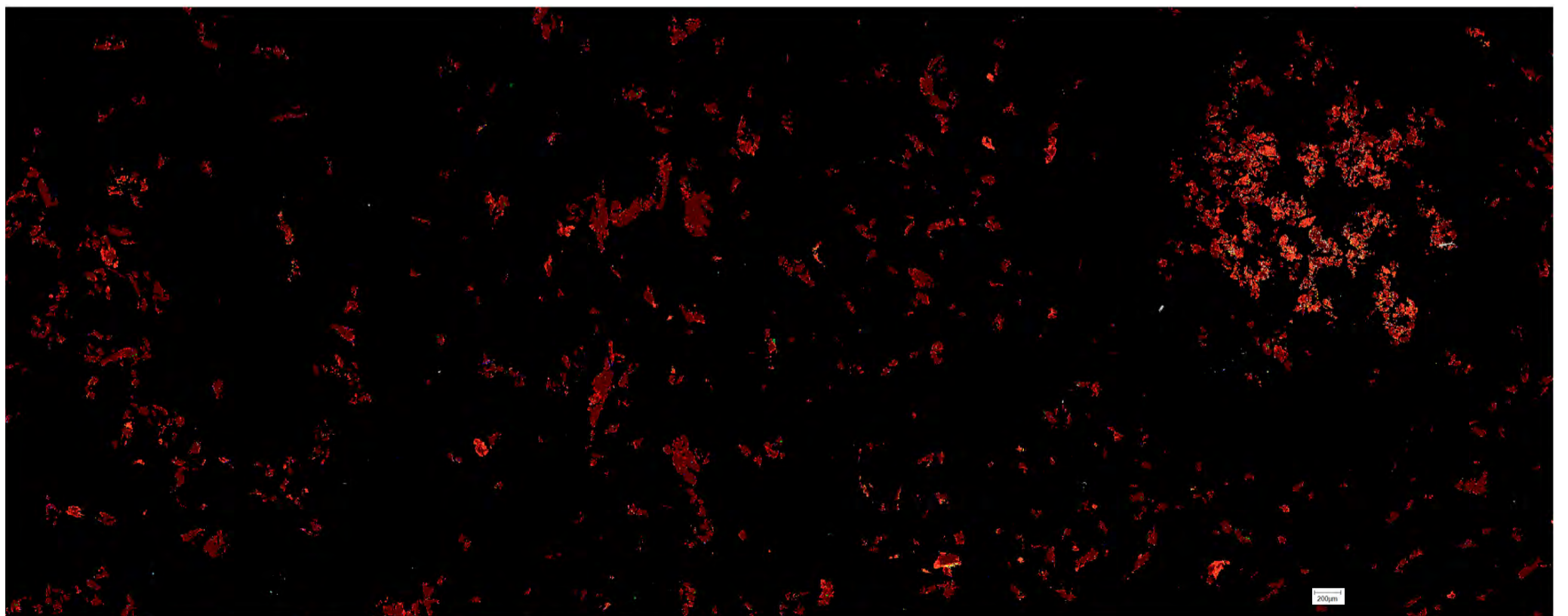
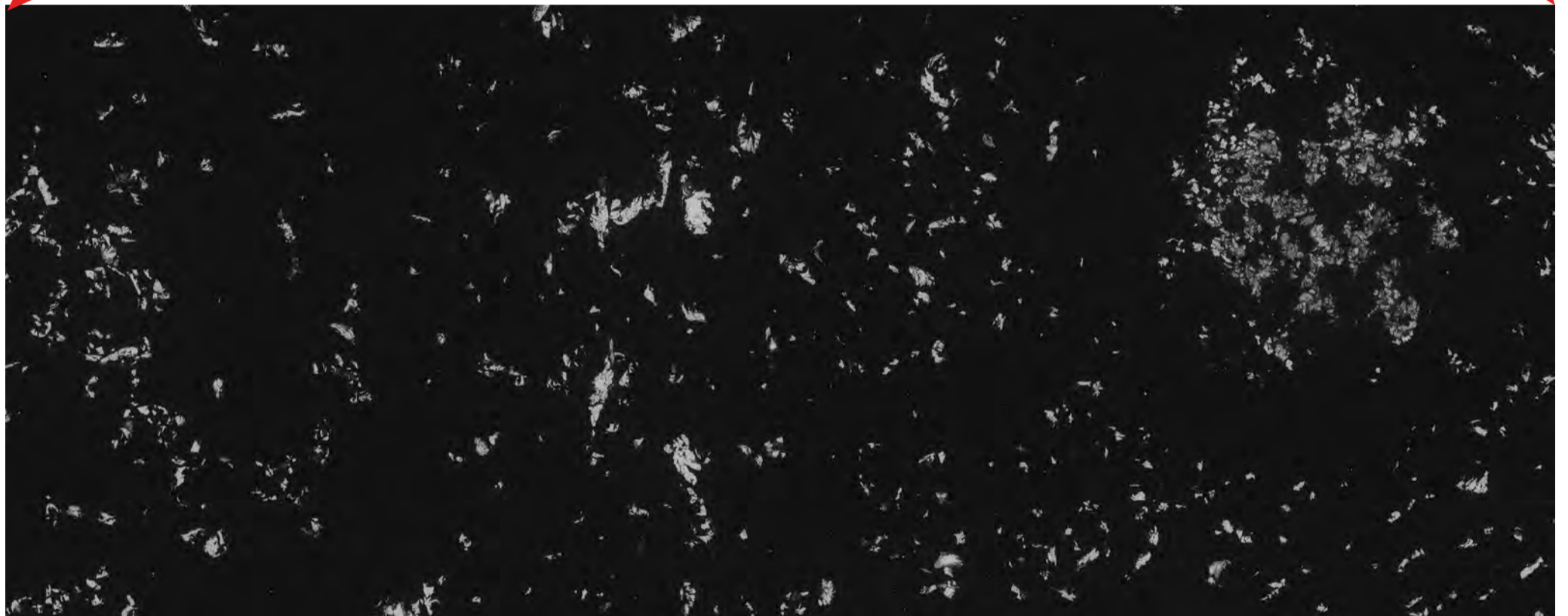


# BMB5857

Optical microscopy image



BSE image

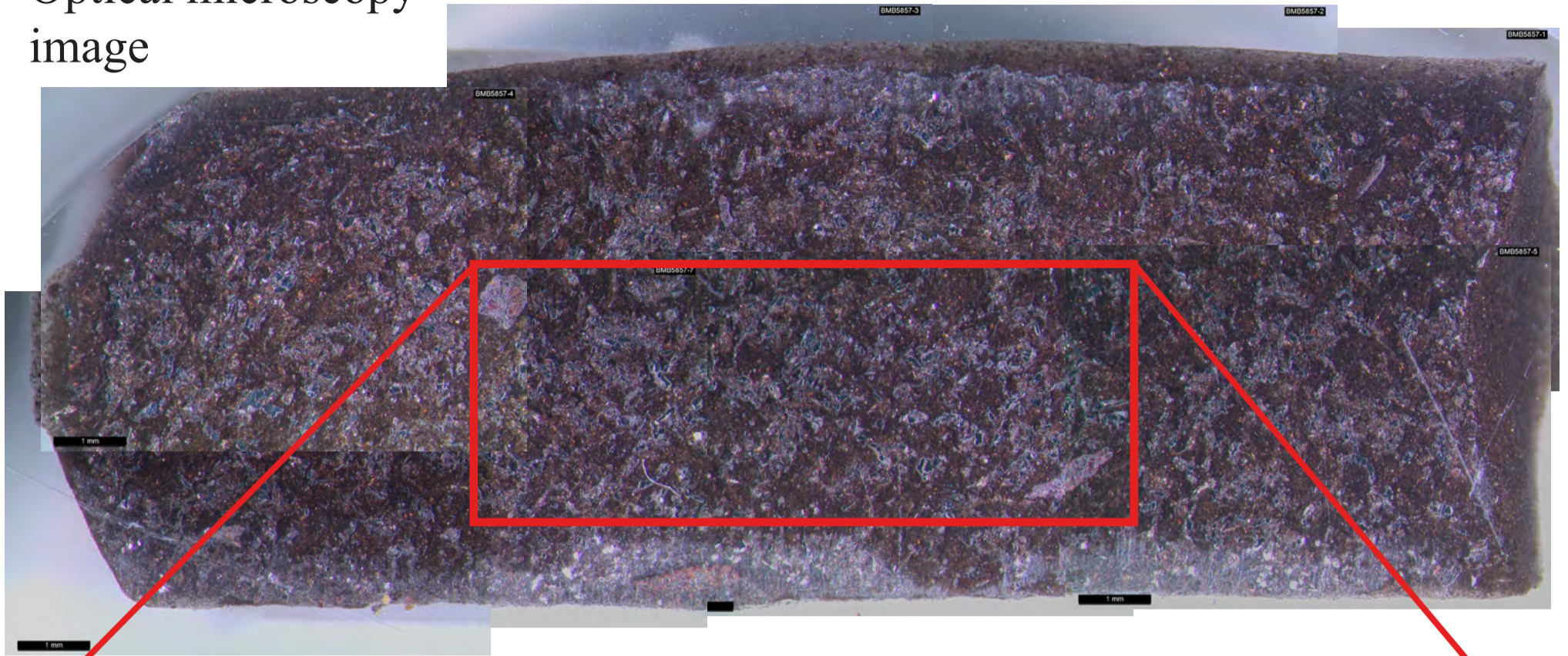


Chromium Copper Fe FeO(Fe30-40) FeO(Fe40-50) FeO(Fe50-60) FeO(Fe60-70) FeO(Fe70-80) FeO(Fe80-90) FeO(Fe90-100) Fe-Si-O Lead Manganese Nickel  
Phosphate/phosphide Silicate/quartz Sulphate/Sulphide Tin Titanium Vanadium Zinc Not Analysed Not Classified Unclassified

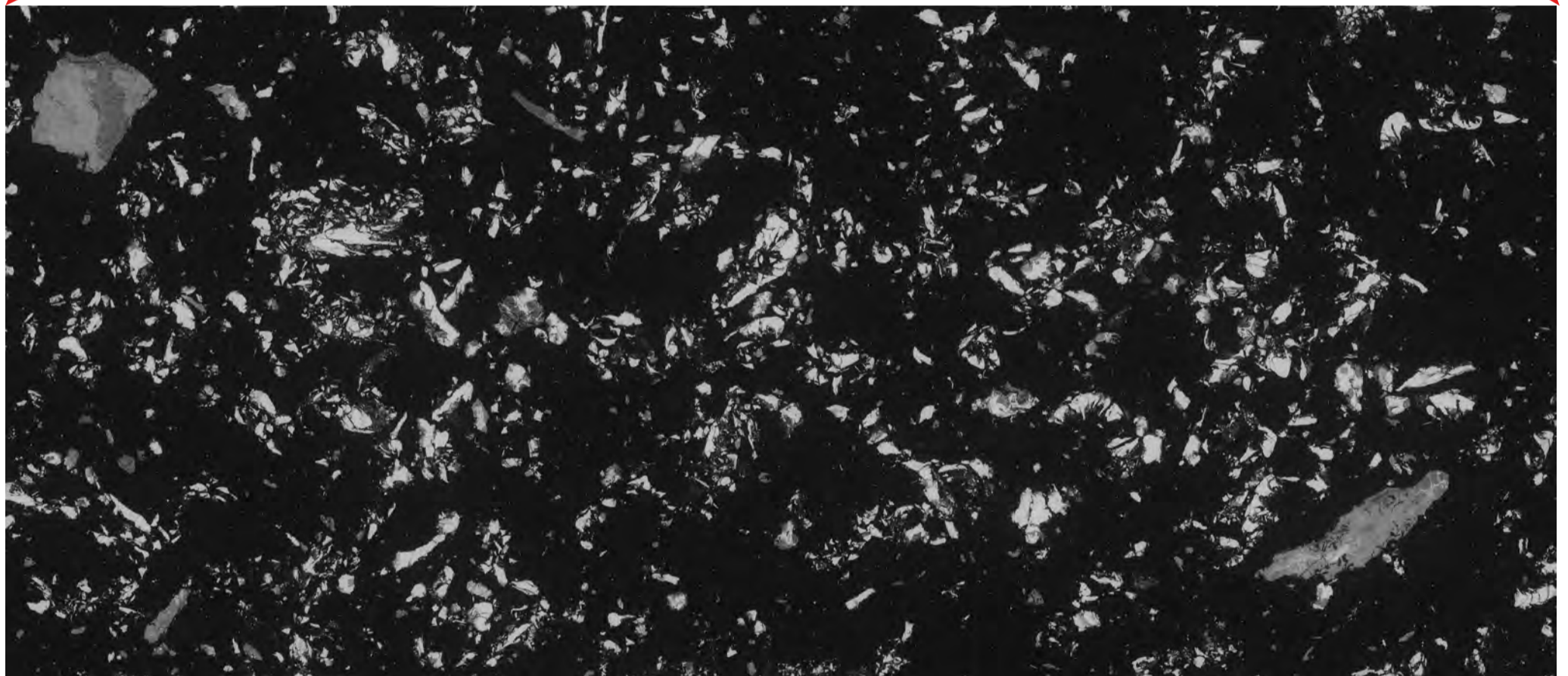
Mineral phases image

# BMB5867

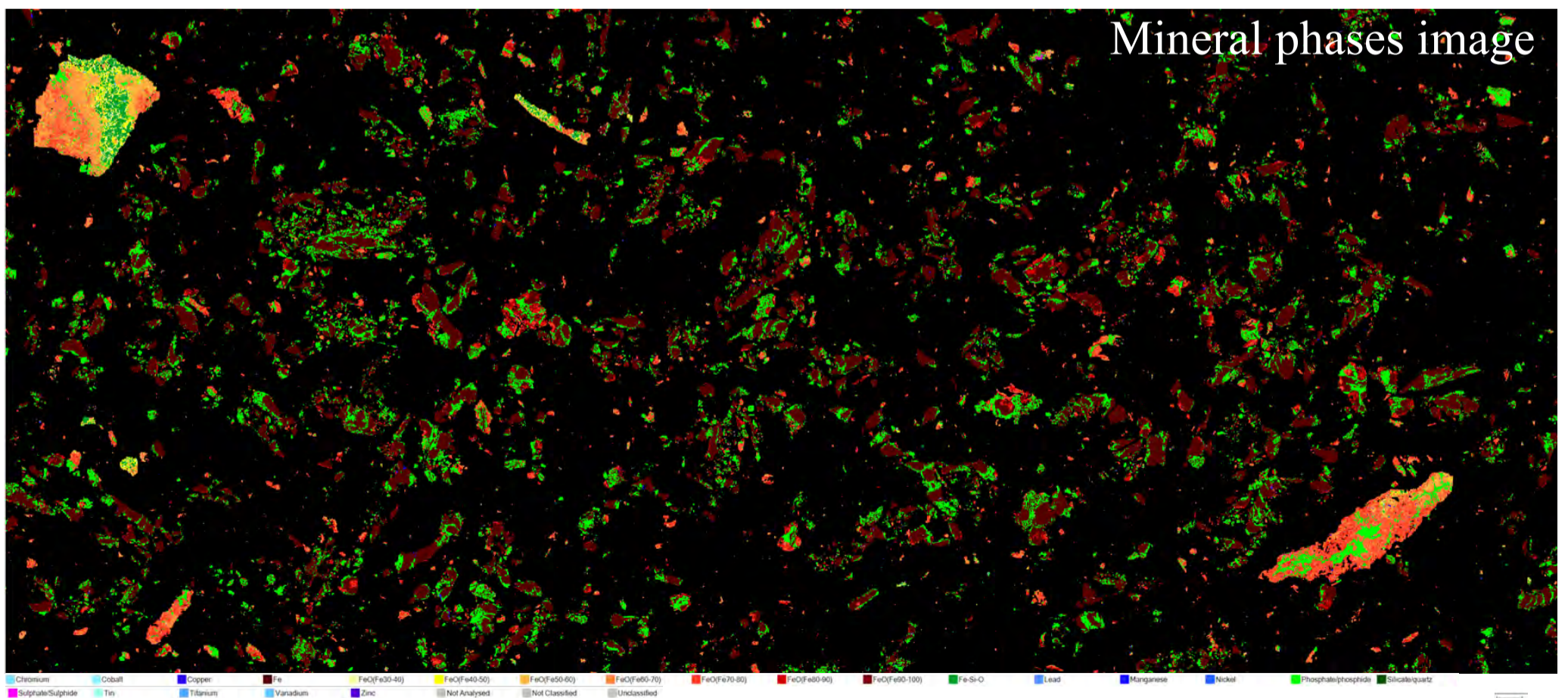
Optical microscopy image



BSE image



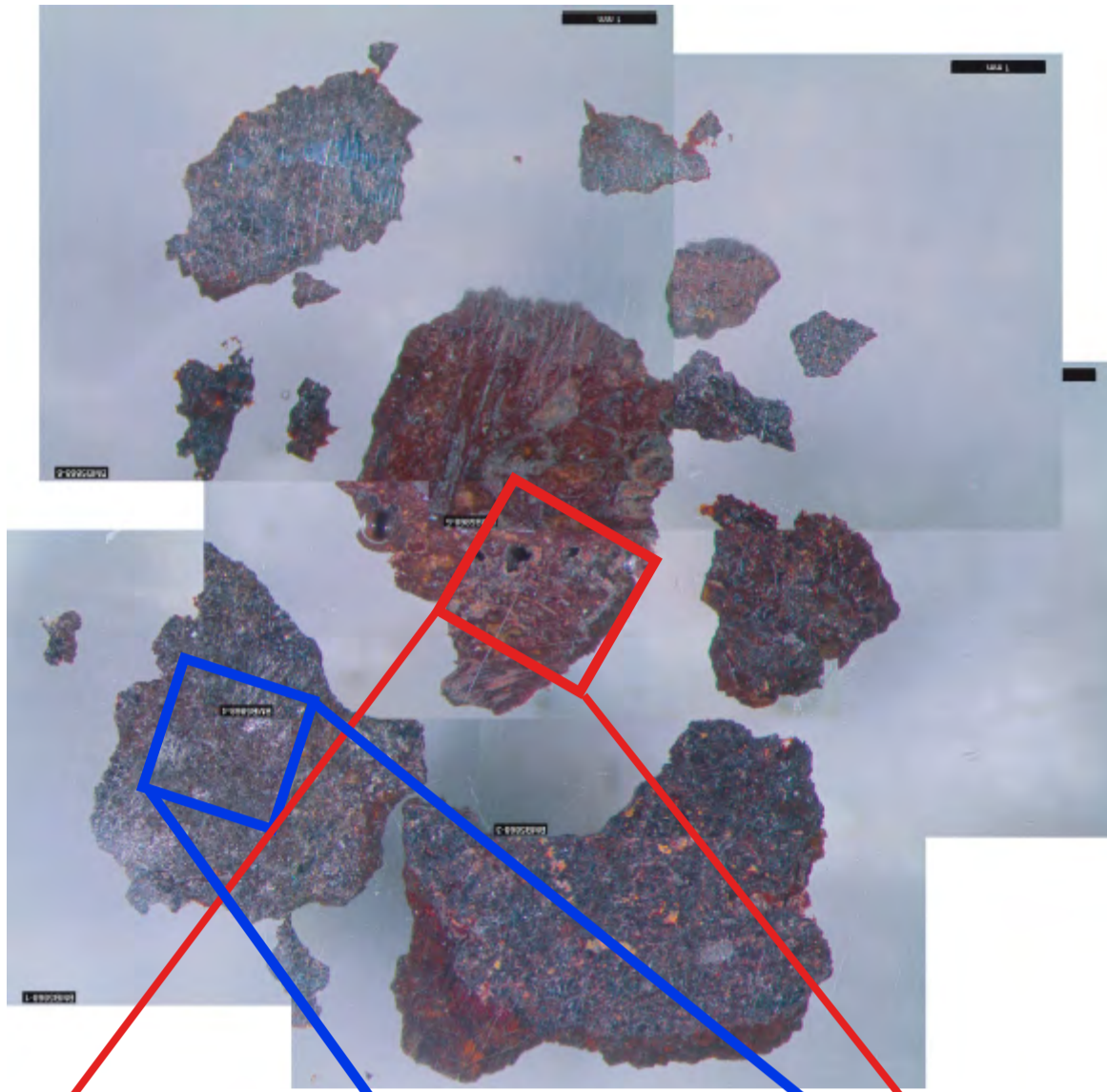
Mineral phases image



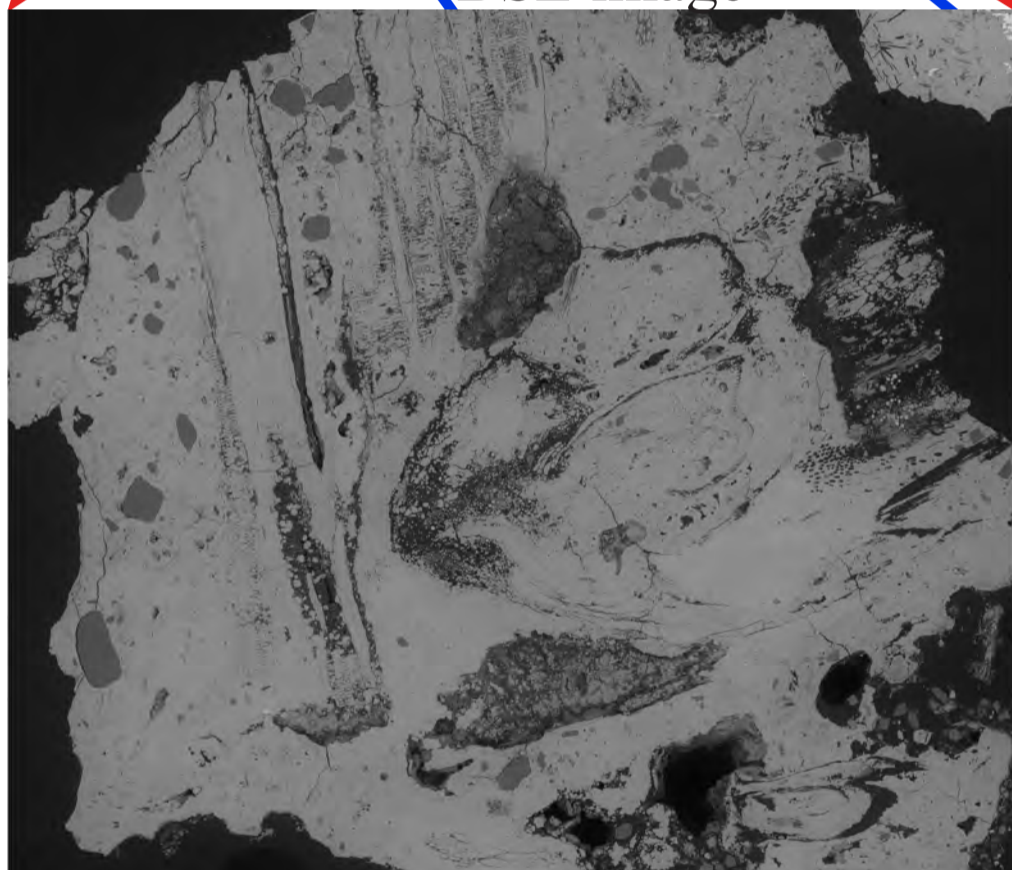


# BMB5868

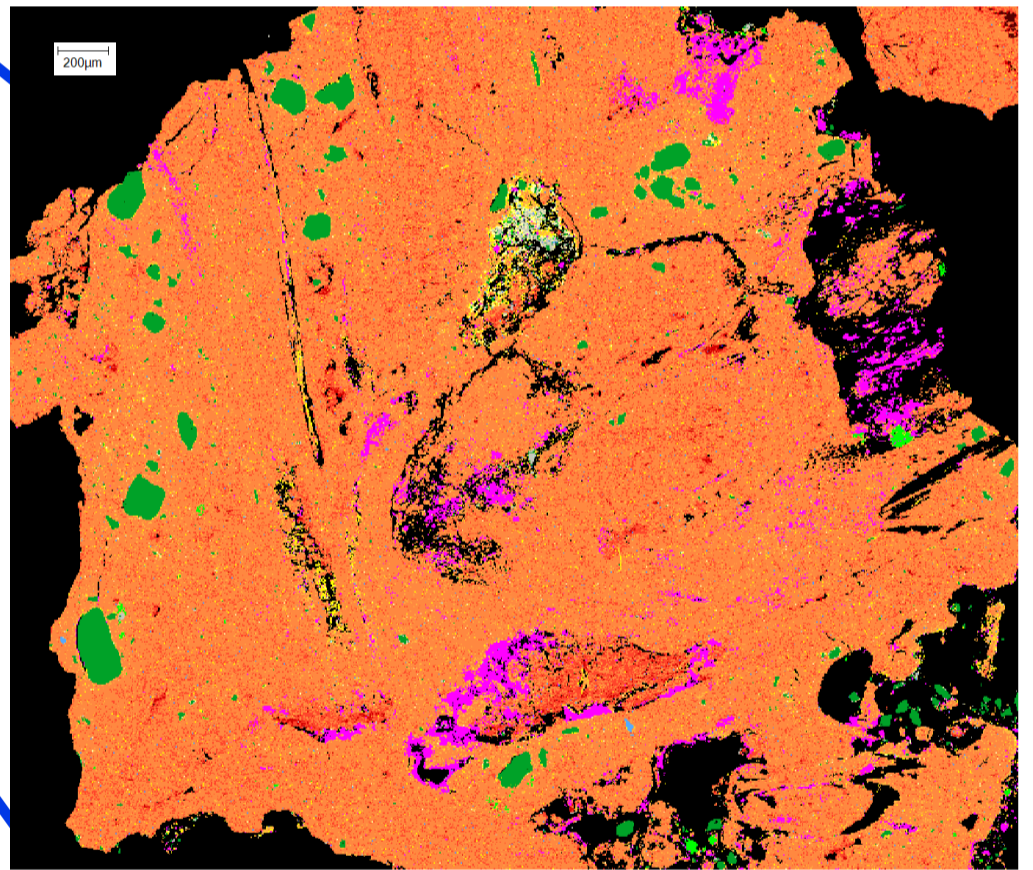
Optical microscopy image



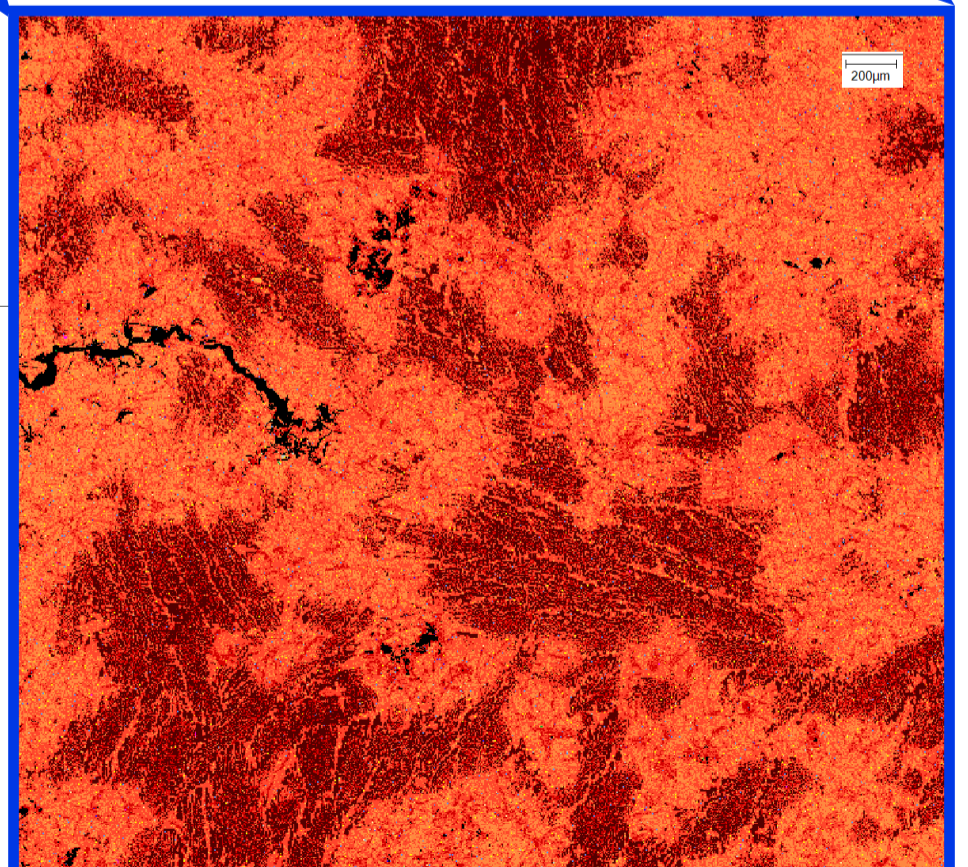
BSE image



Mineral phases images

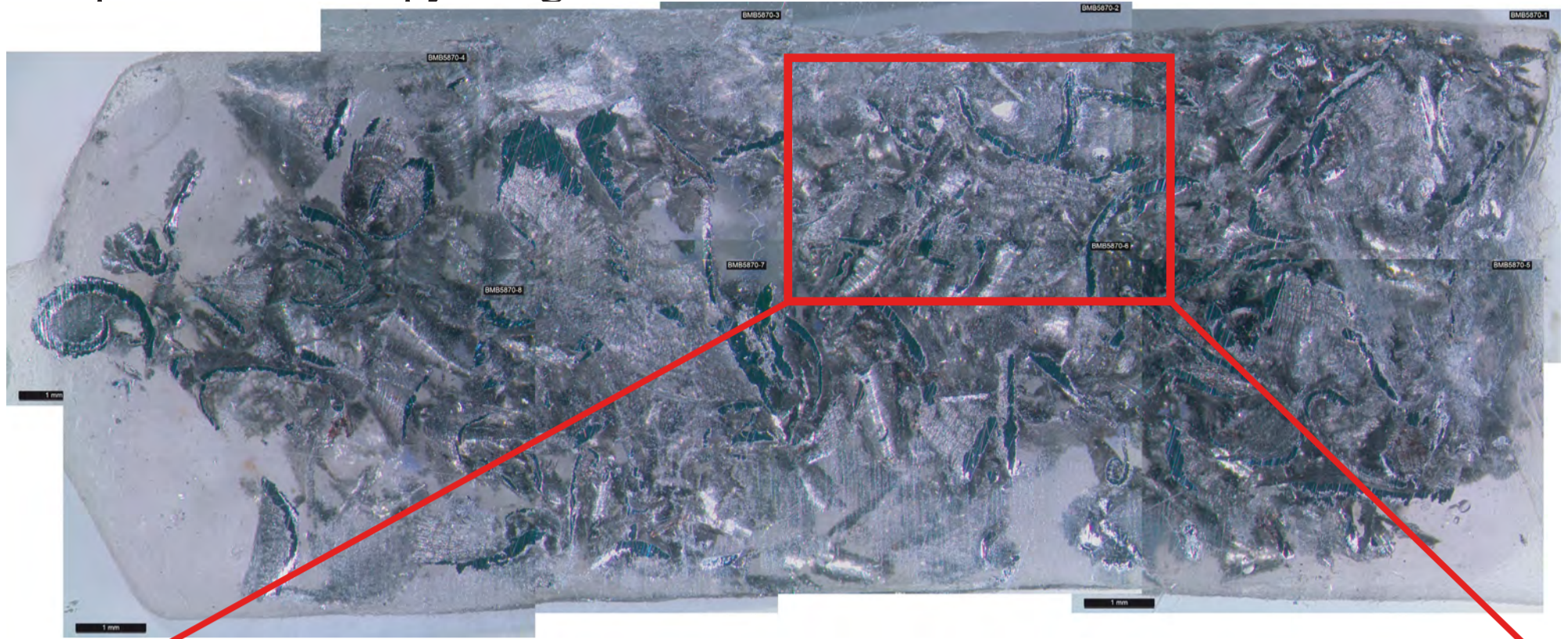


Chromium	Cobalt	Copper	Fe	FeO(Fe30-40)	FeO(Fe40-50)
FeO(Fe50-60)	FeO(Fe60-70)	FeO(Fe70-80)	FeO(Fe80-90)	FeO(Fe90-100)	Fe-Si-O
Lead	Manganese	Nickel	Phosphate/phosphide	Silicate/quartz	Sulphate/Sulphide
Tin	Titanium	Zinc	Not Analysed	Not Classified	Unclassified

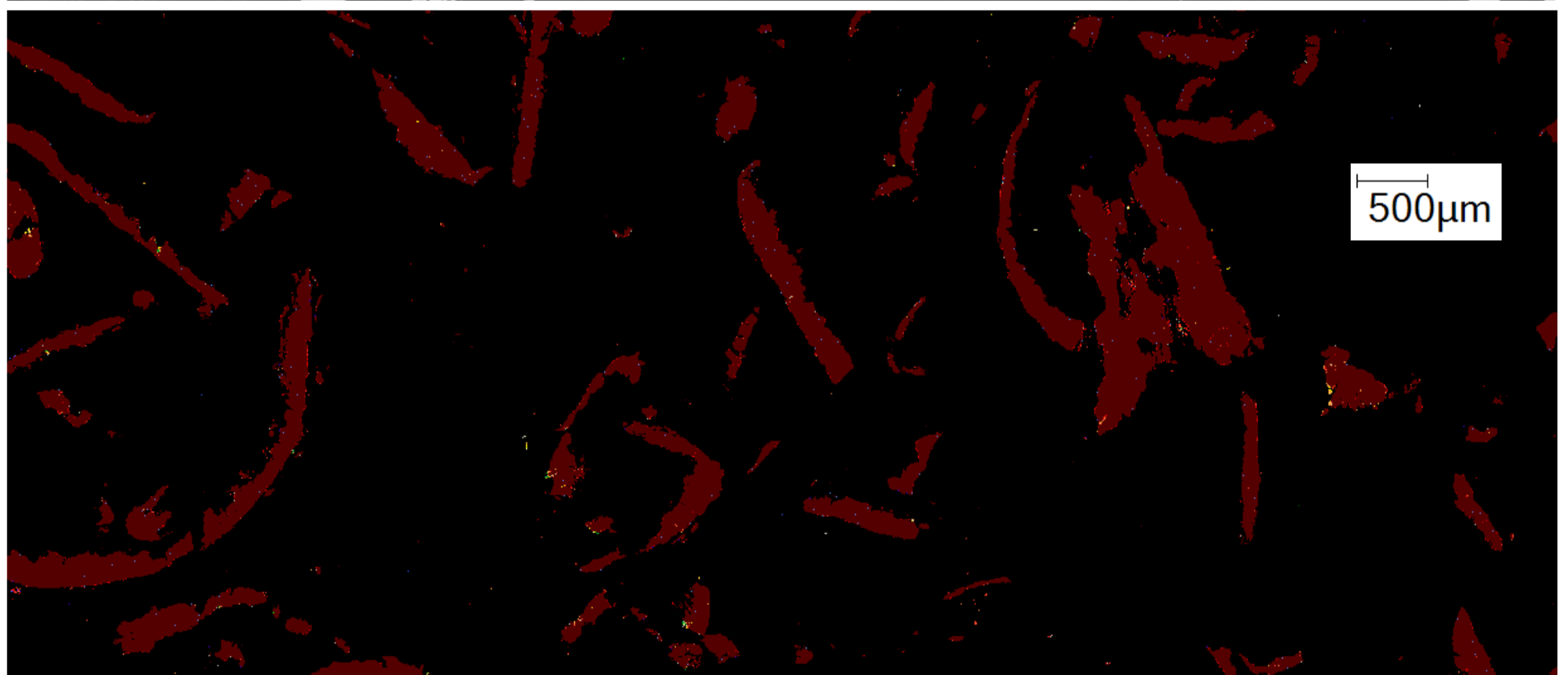


# BMB5870

Optical microscopy image

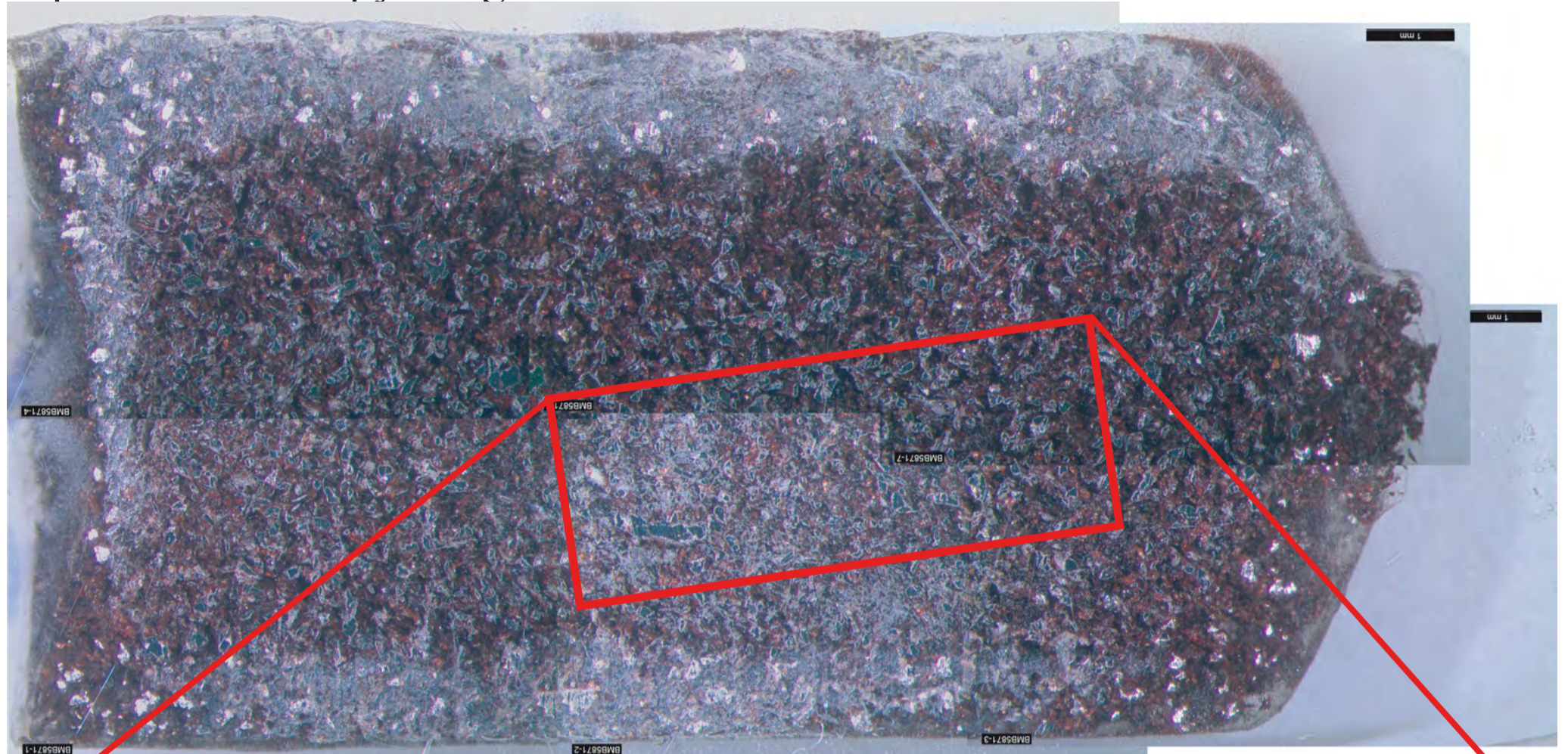


BSE image

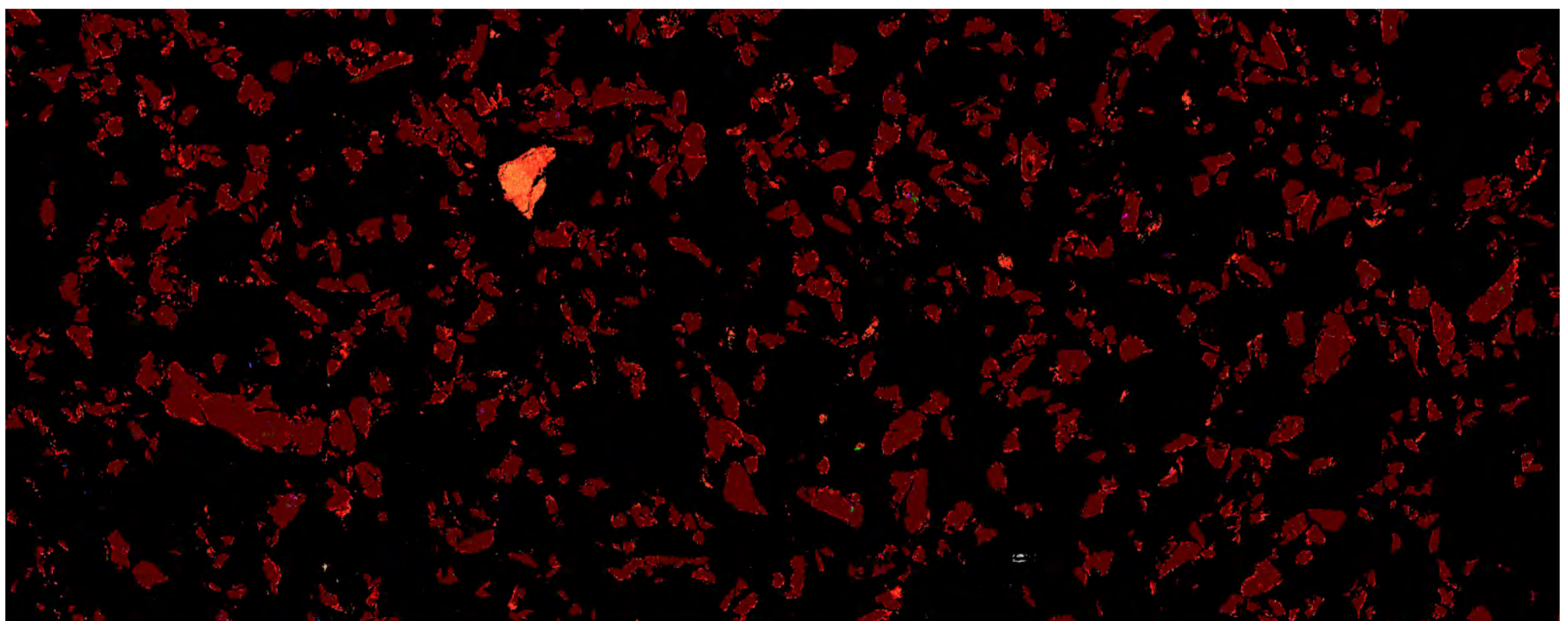
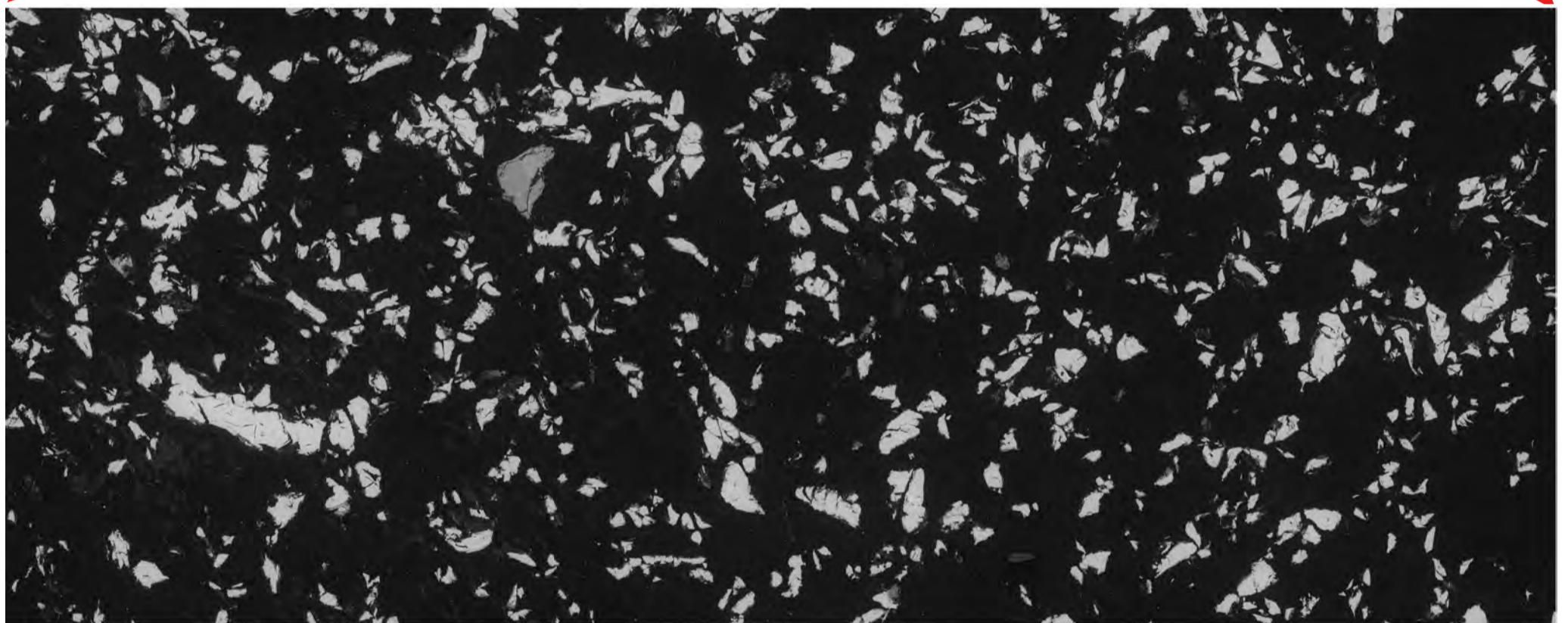


Chromium	FeO(Fe30-40)	FeO(Fe60-70)	FeO(Fe90-100)	Manganese	Silicate/quartz	Zinc
Copper	FeO(Fe40-50)	FeO(Fe70-80)	Fe-Si-O	Nickel	Tin	Not Classified
Fe	FeO(Fe50-60)	FeO(Fe80-90)	Lead	Phosphate/phosphide	Titanium	Unclassified

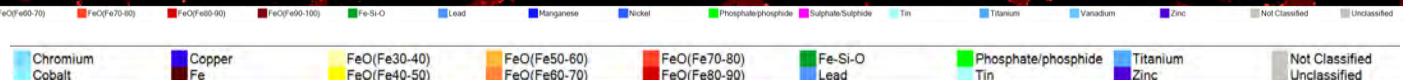
Optical microscopy image



BSE image

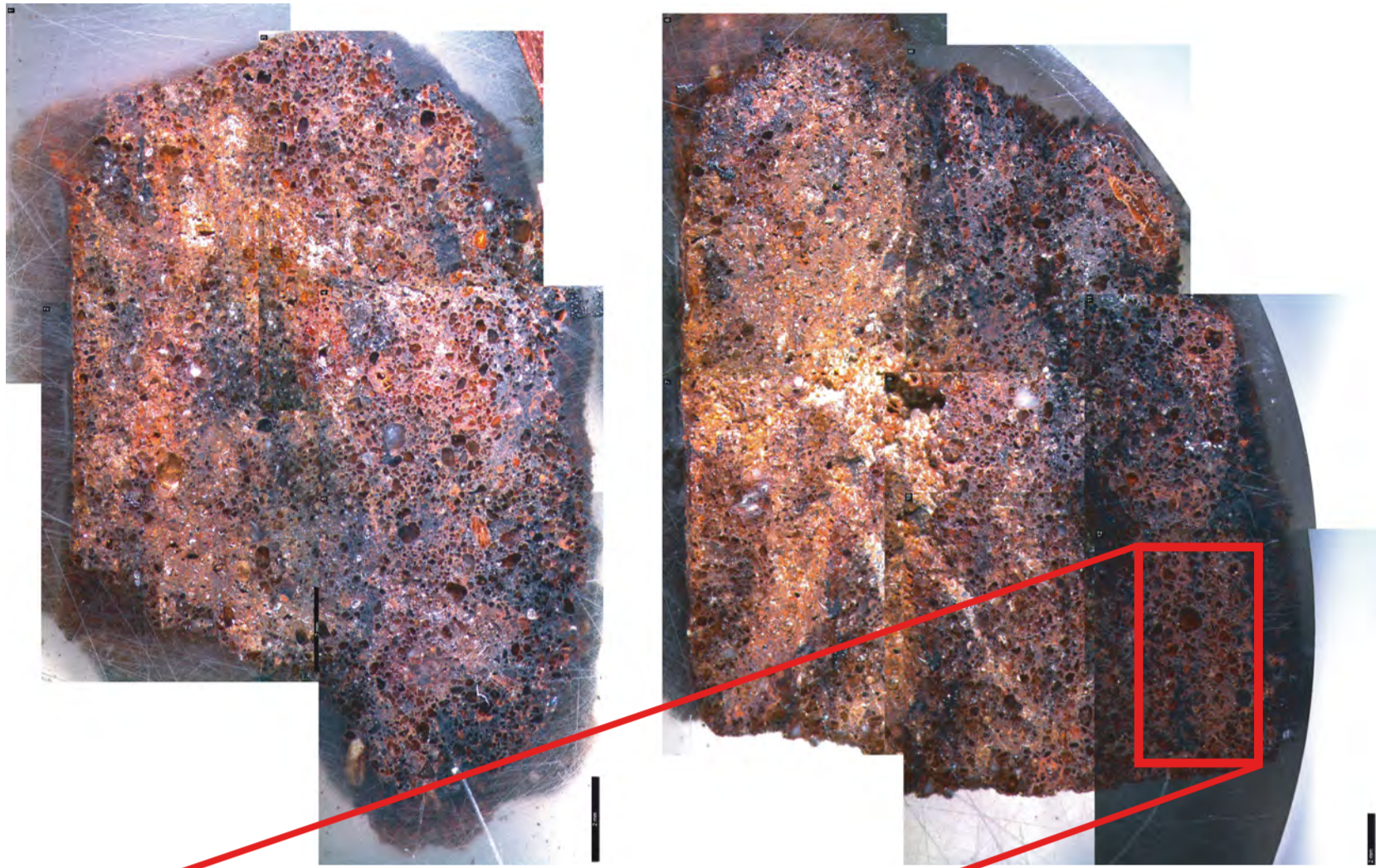


Mineral phases image



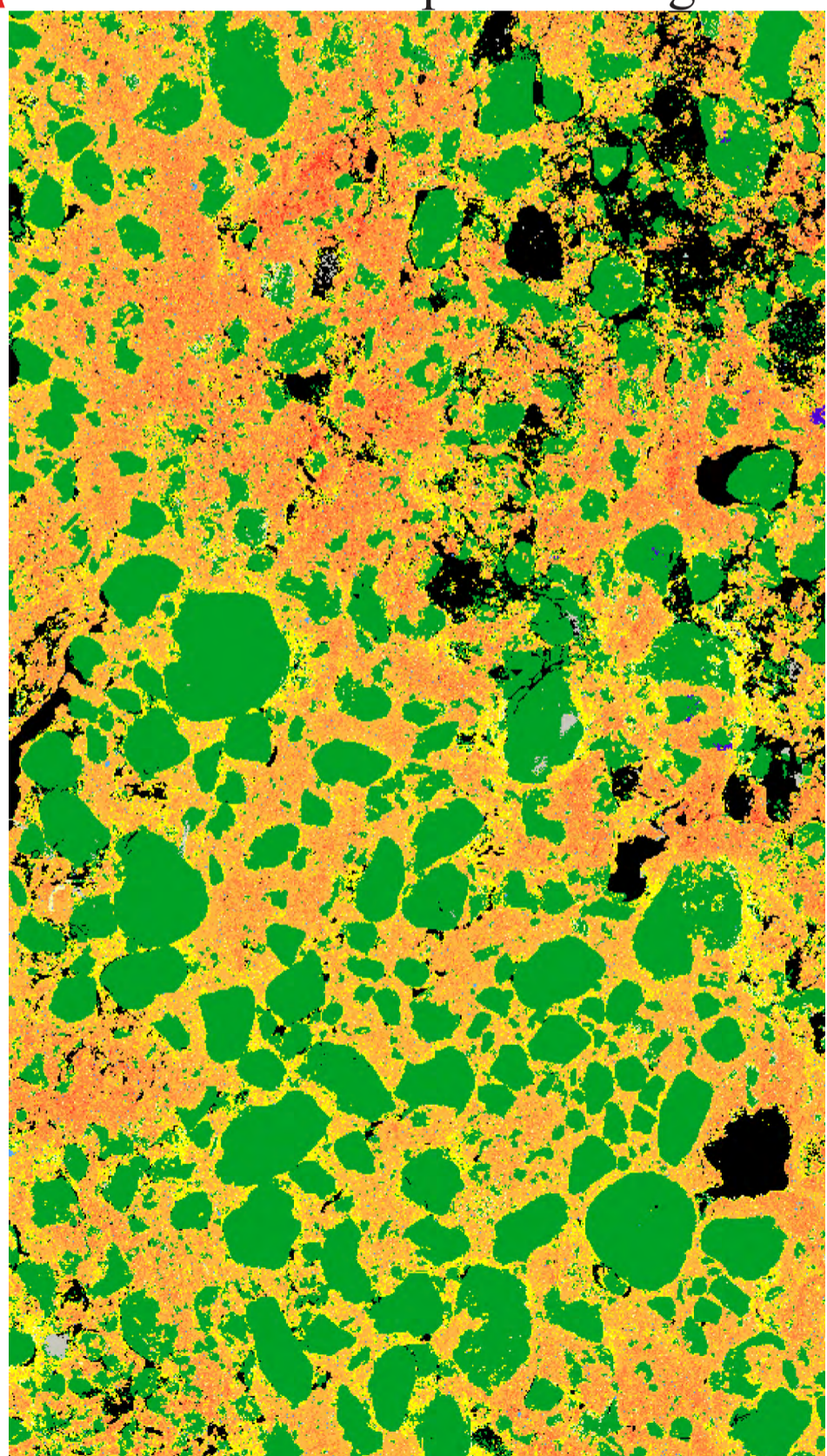
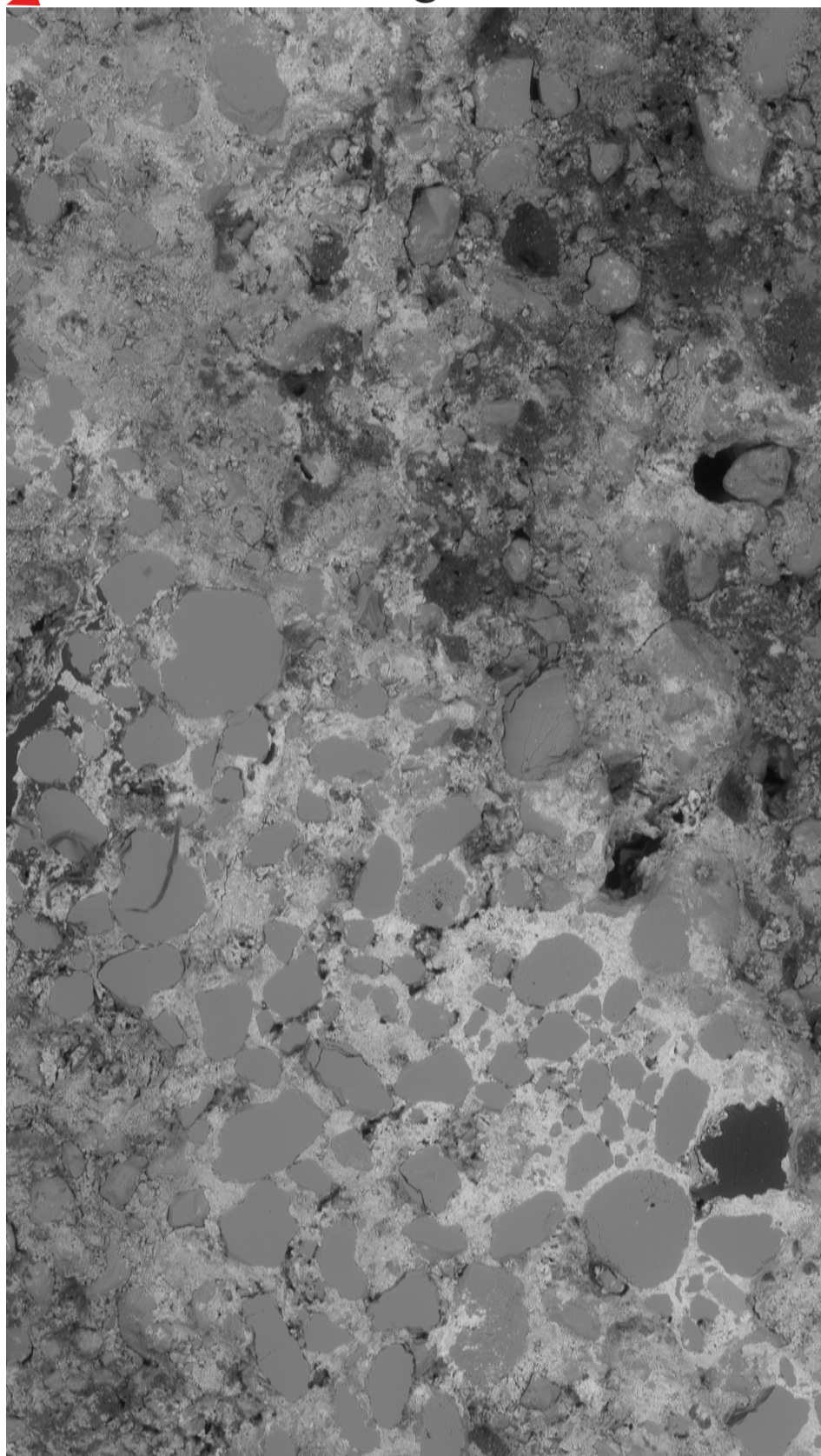
Optical microscopy image

BMB5872



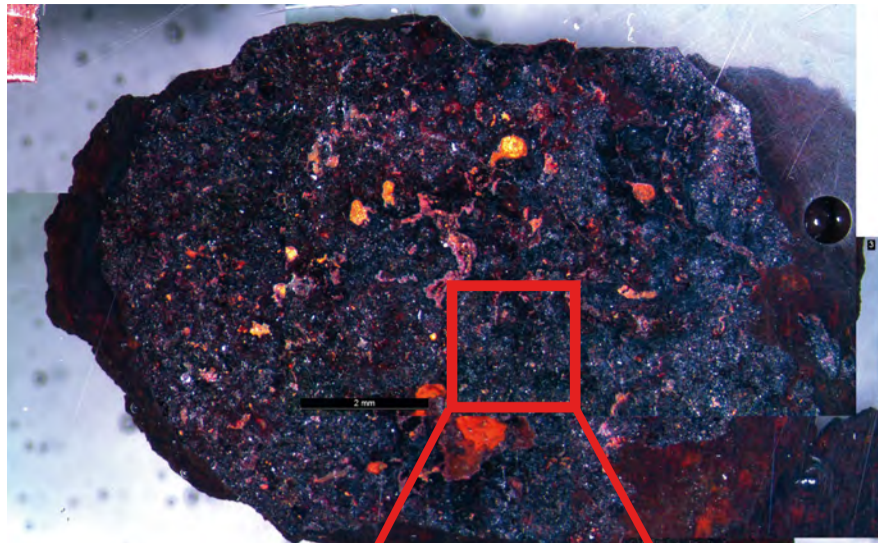
BSE image

Mineral phases image

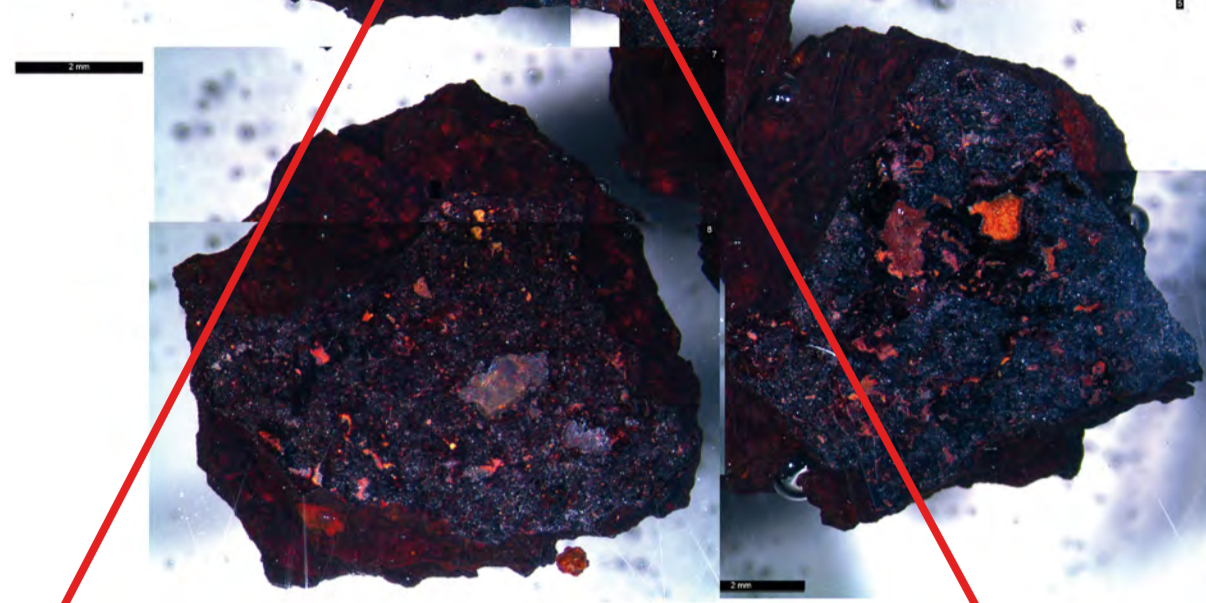


Chromium	Copper	FeO(Fe30-40)	FeO(Fe50-60)	FeO(Fe70-80)	Fe-Si-O	Phosphate/phosphide	Titanium	Not Classified
Cobalt	Fe	FeO(Fe40-50)	FeO(Fe60-70)	FeO(Fe80-90)	Lead	Tin	Zinc	

# BMB5877

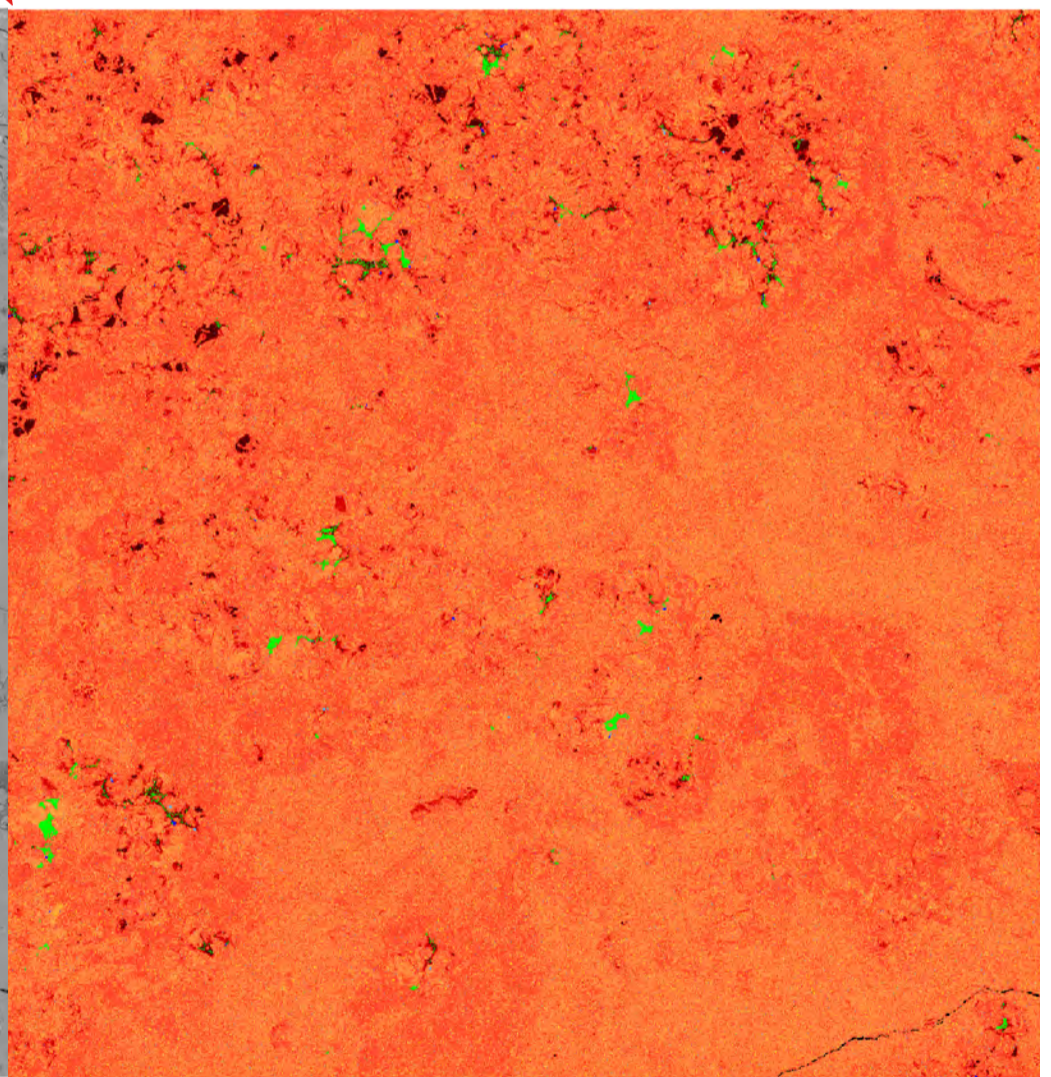
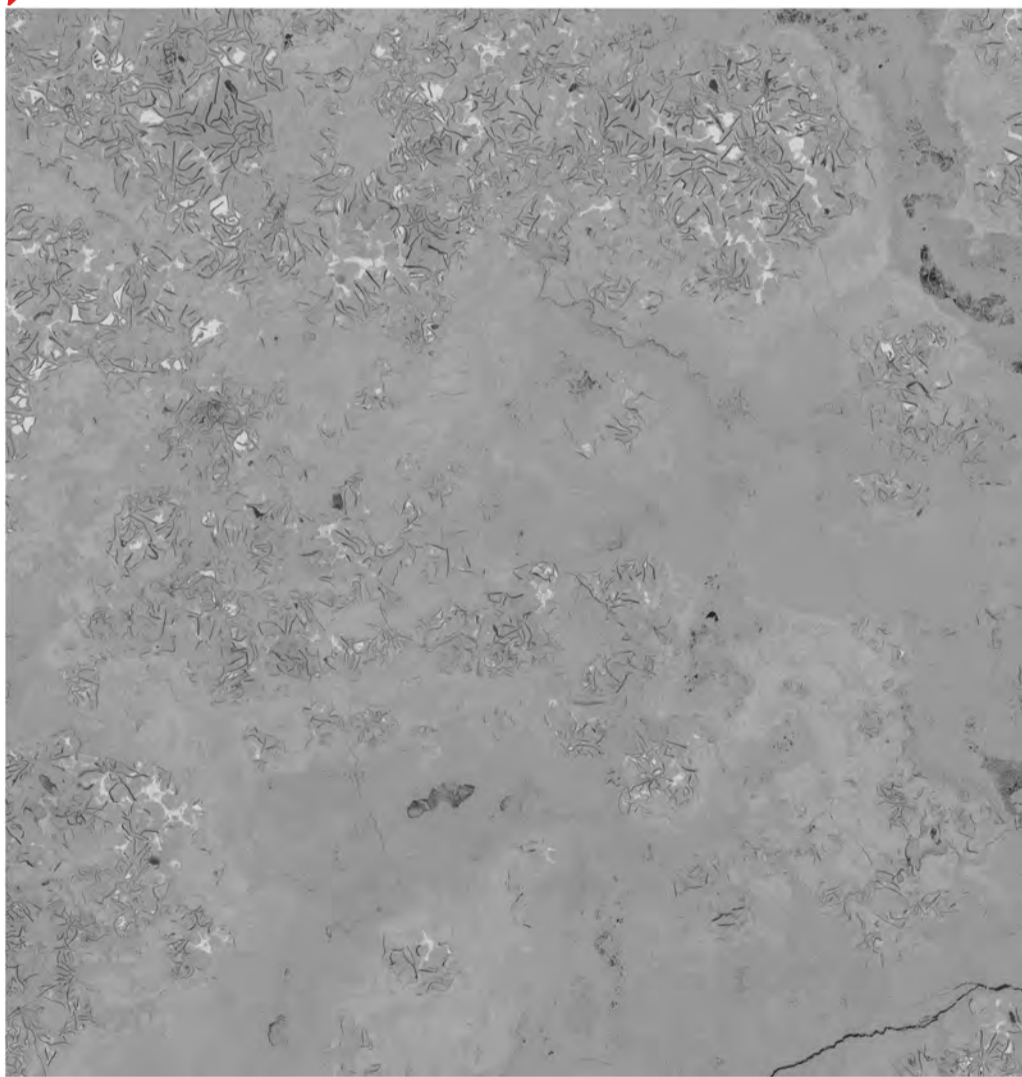


Optical microscopy image



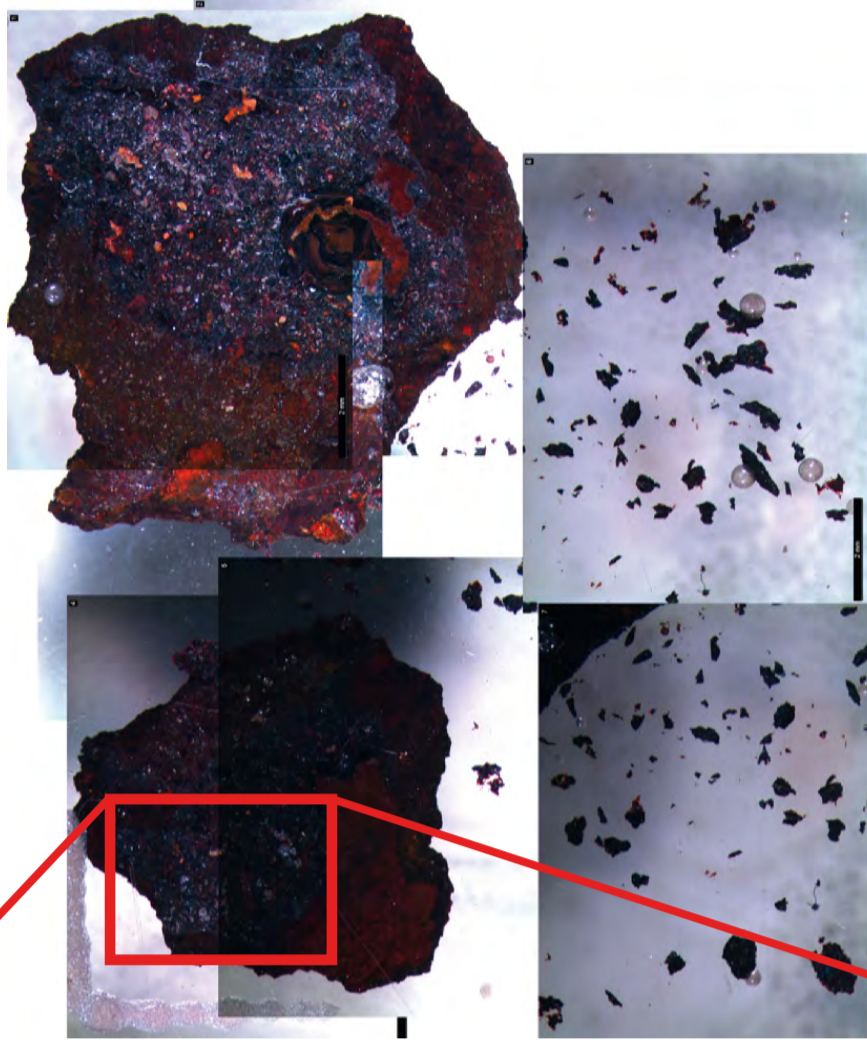
BSE image

Mineral phases image

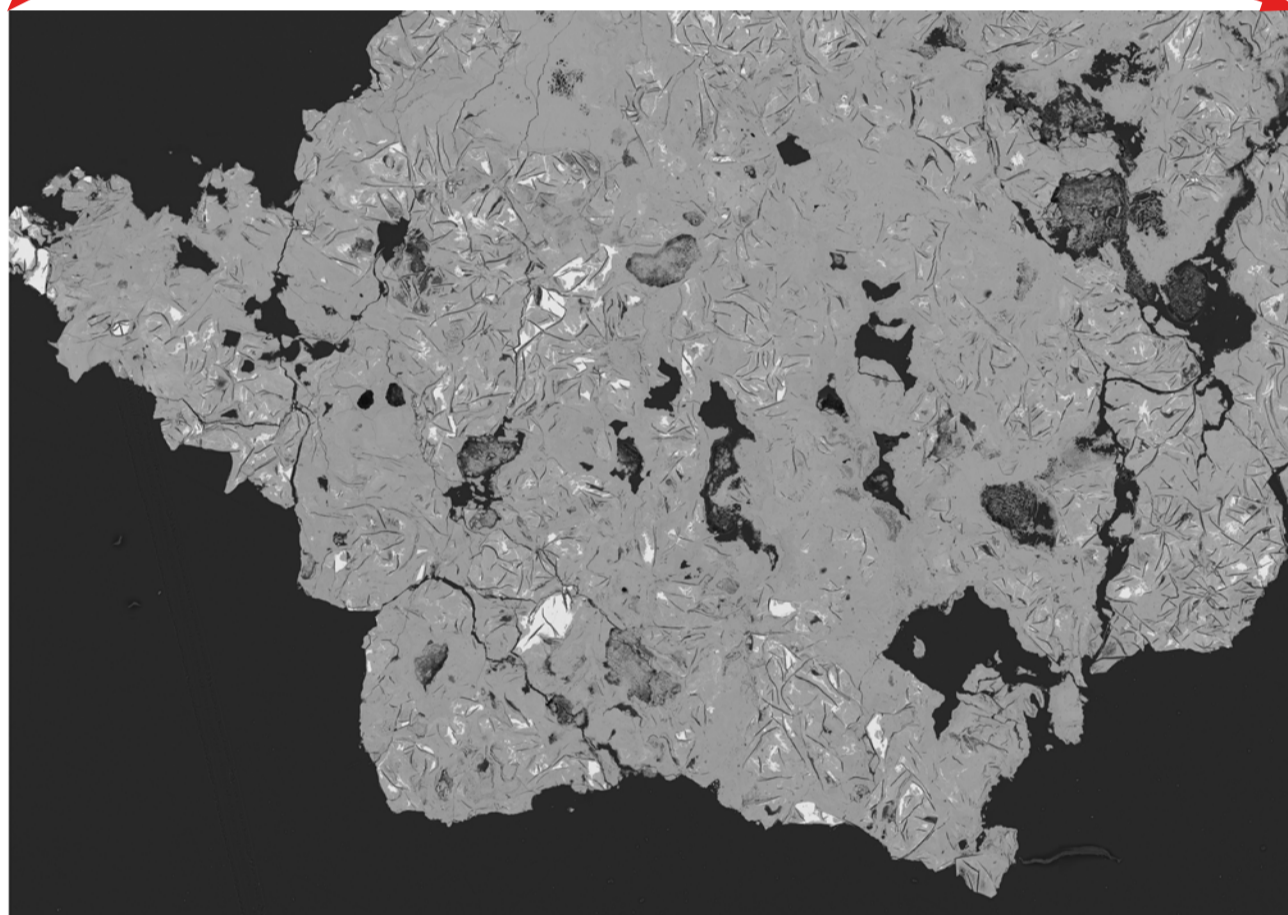


Chromium	Cobalt	Copper	Fe	FeO(Fe30-40)	FeO(Fe40-50)
FeO(Fe50-60)	FeO(Fe60-70)	FeO(Fe70-80)	FeO(Fe80-90)	FeO(Fe90-100)	Fe-Si-O
Lead	Manganese	Nickel	Phosphate/phosphide	Sulphate/Sulphide	Titanium
Vanadium	Zinc	Not Analysed	Not Classified	Unclassified	100µm

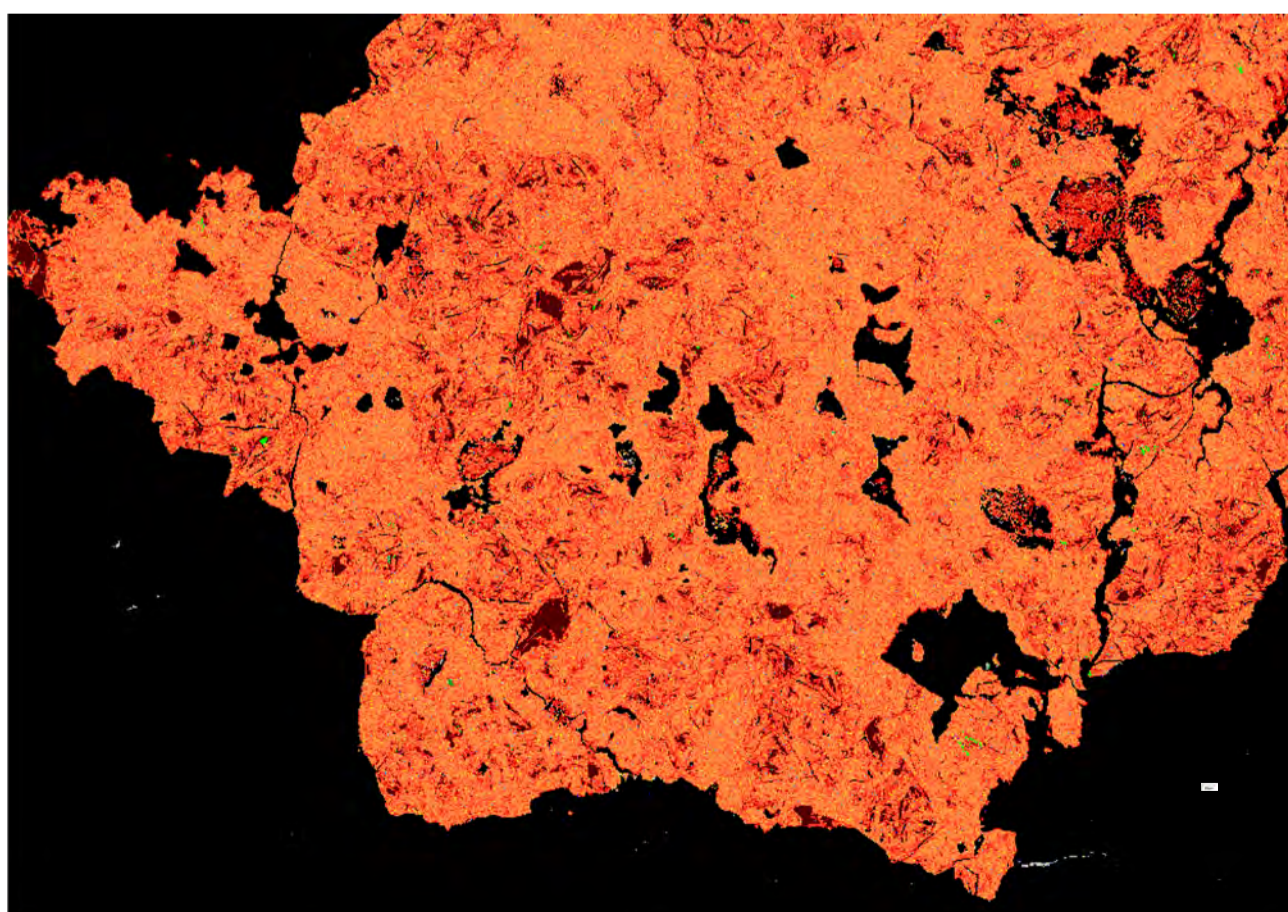
# BMB5890



Optical microscopy image



BSE image

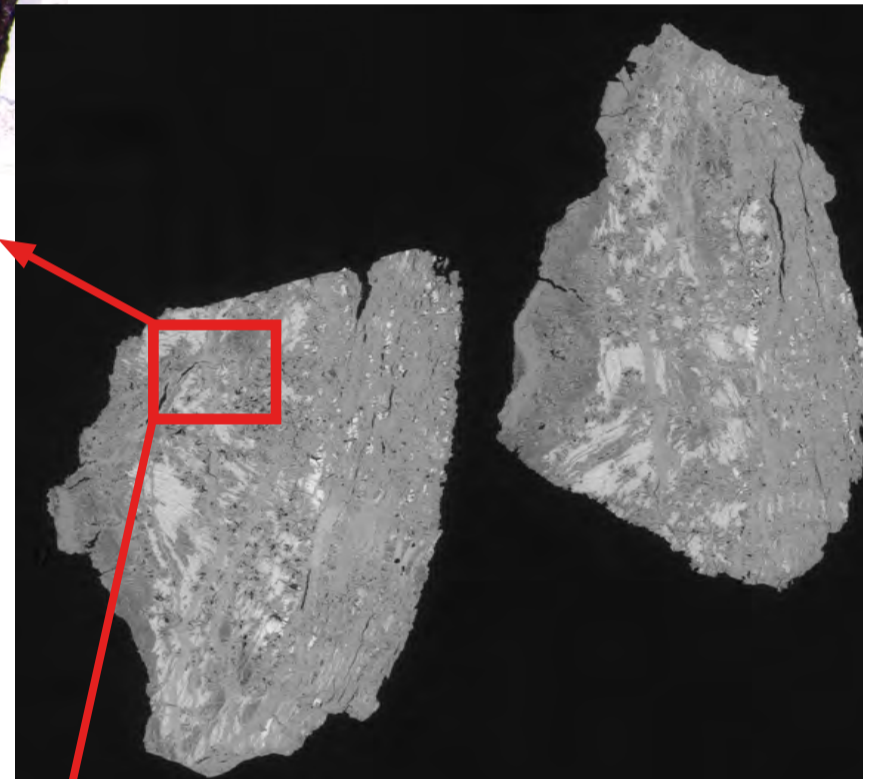
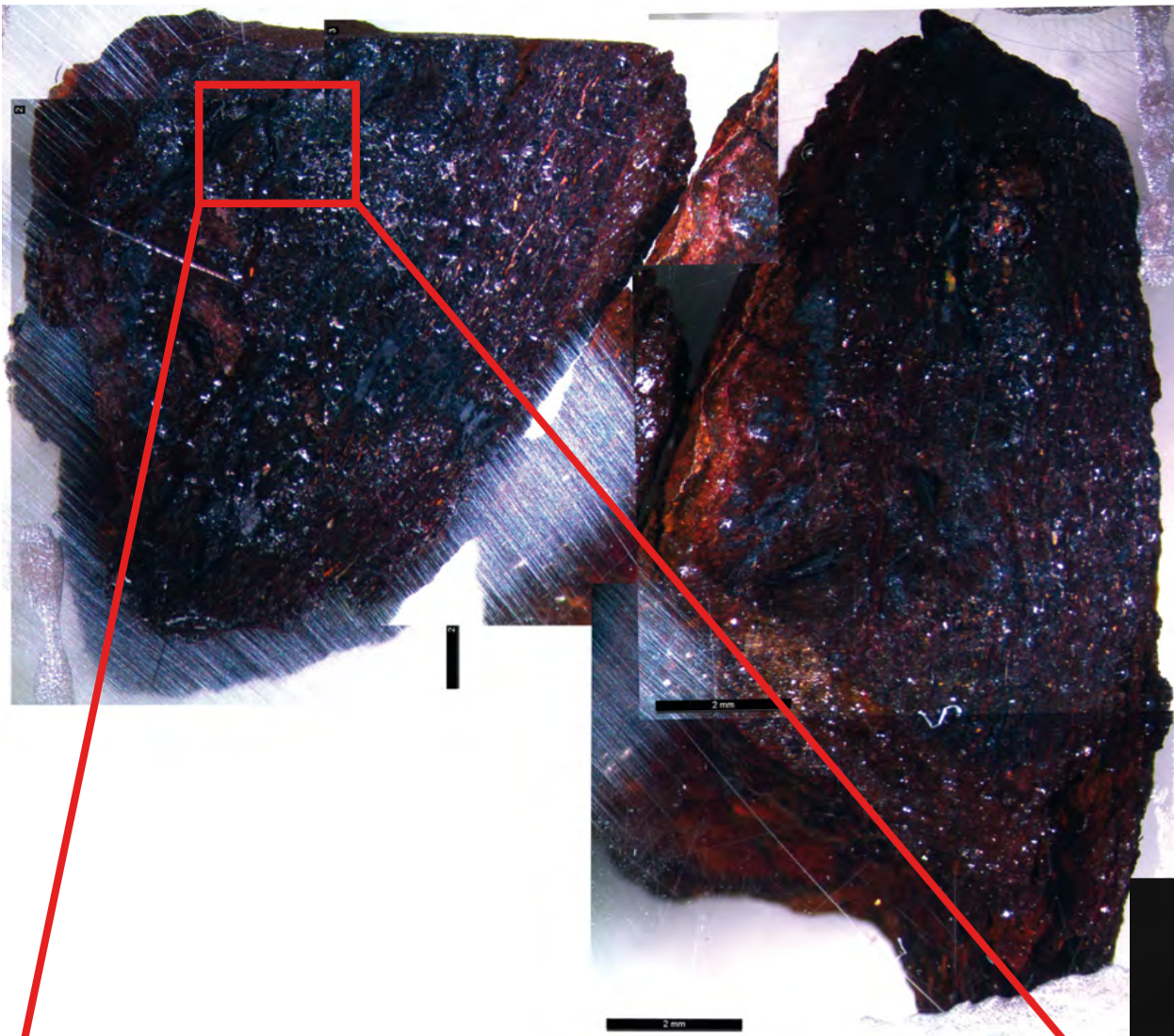


Mineral phases image

Chromium	Cobalt	Copper	Fe	FeU(FeSU-4U)
FeU(FeU-5U)	FeU(FeU-6U)	FeU(FeU-7U)	FeU(FeU-8U)	FeU(FeU-9U)
FeU(FeU-10U)	Fe-Si-U	Lead	Manganese	Nickel
Phosphate/phosphide	Sulphate/sulphide	Ti in	Titanium	Zinc
Not Analysed	Not Classified	Unclassified		

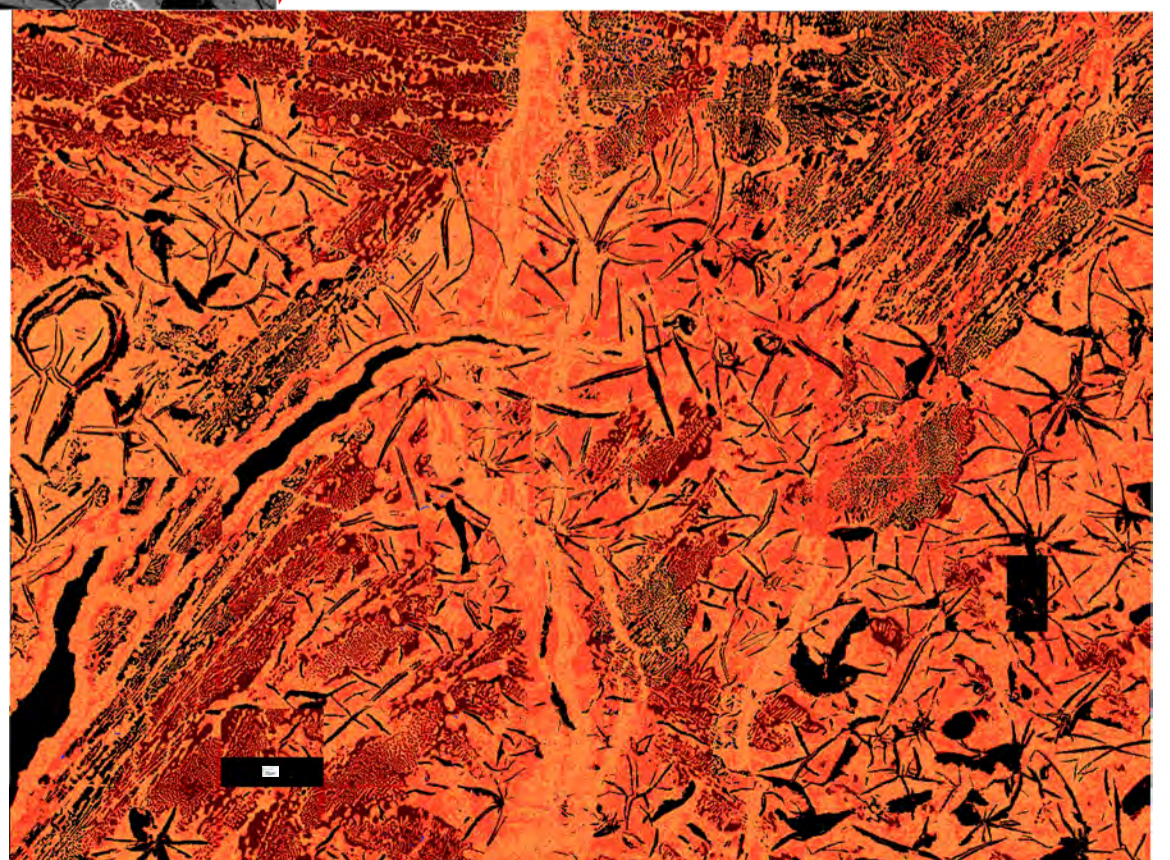
# BMB5891

Optical microscopy image



BSE images

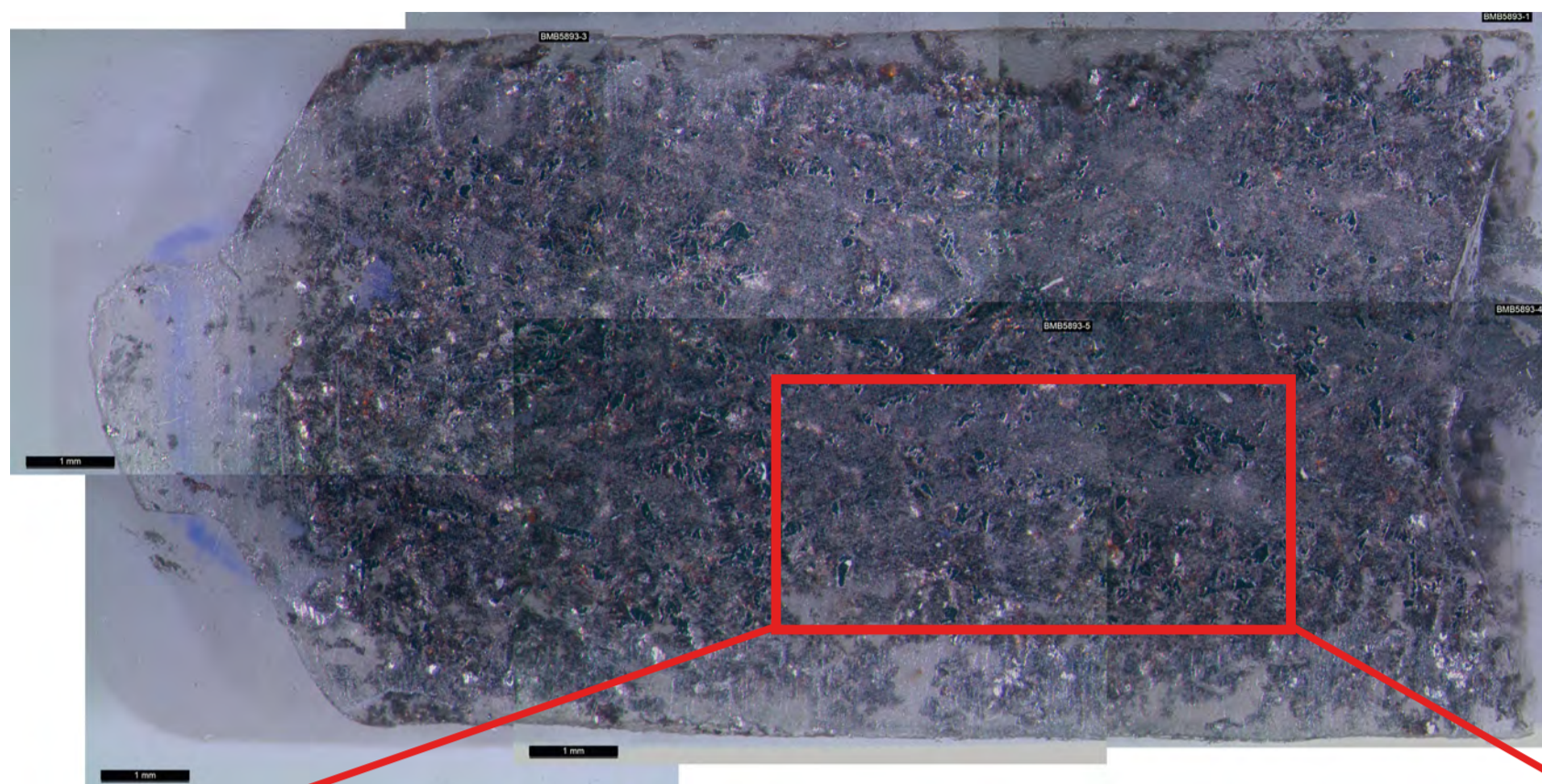
Mineral phases image



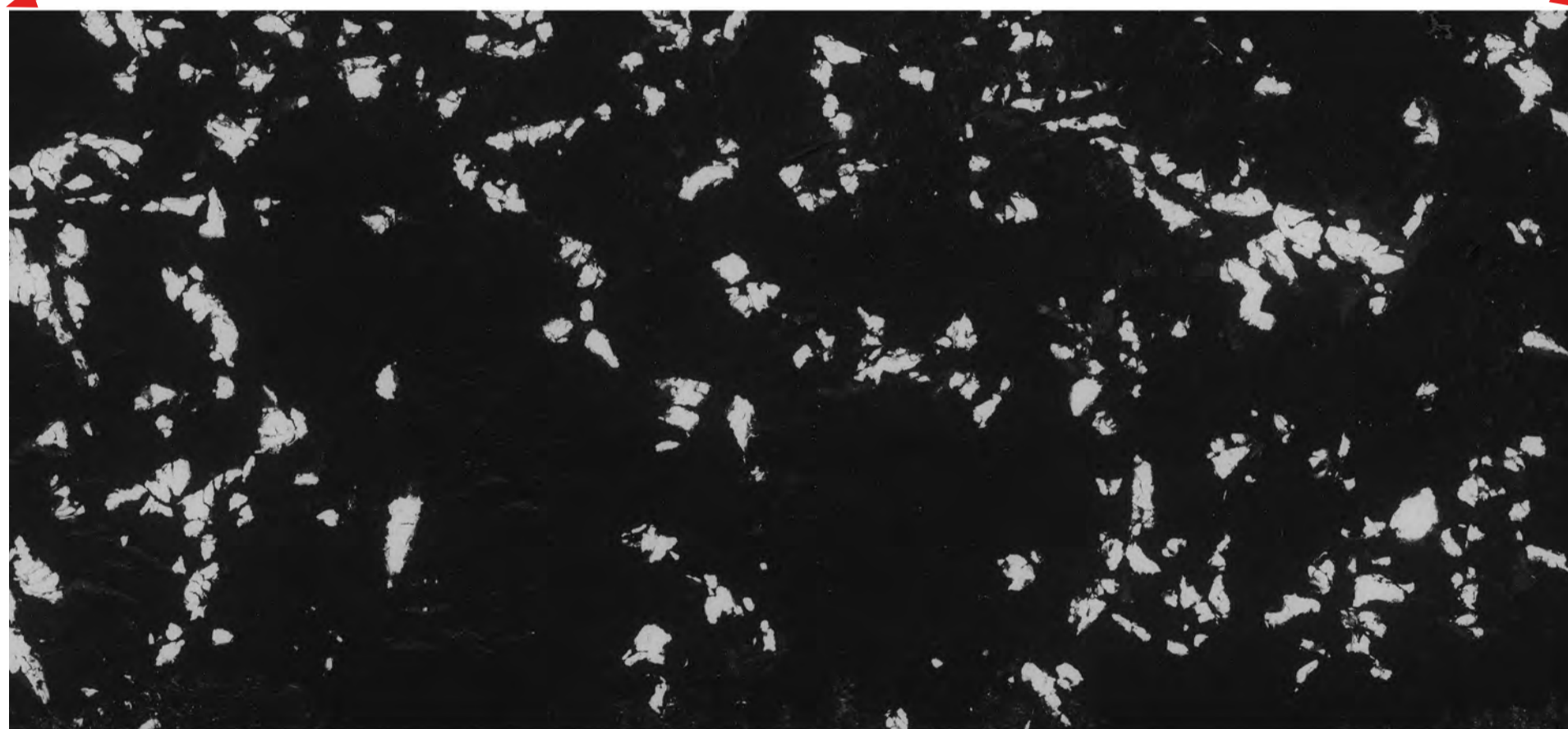
Chromium	Copper	Fe	FeO(Fe30-40)	FeO(Fe40-50)
FeO(Fe60-70)	FeO(Fe70-80)	FeO(Fe80-90)	FeO(Fe90-100)	Lead
Manganese	Nickel	Phosphate/phosphide	Sulphate/Sulphide	Tin
Titanium	Vanadium	Zinc	Not Analysed	Not Classified

Optical microscopy image

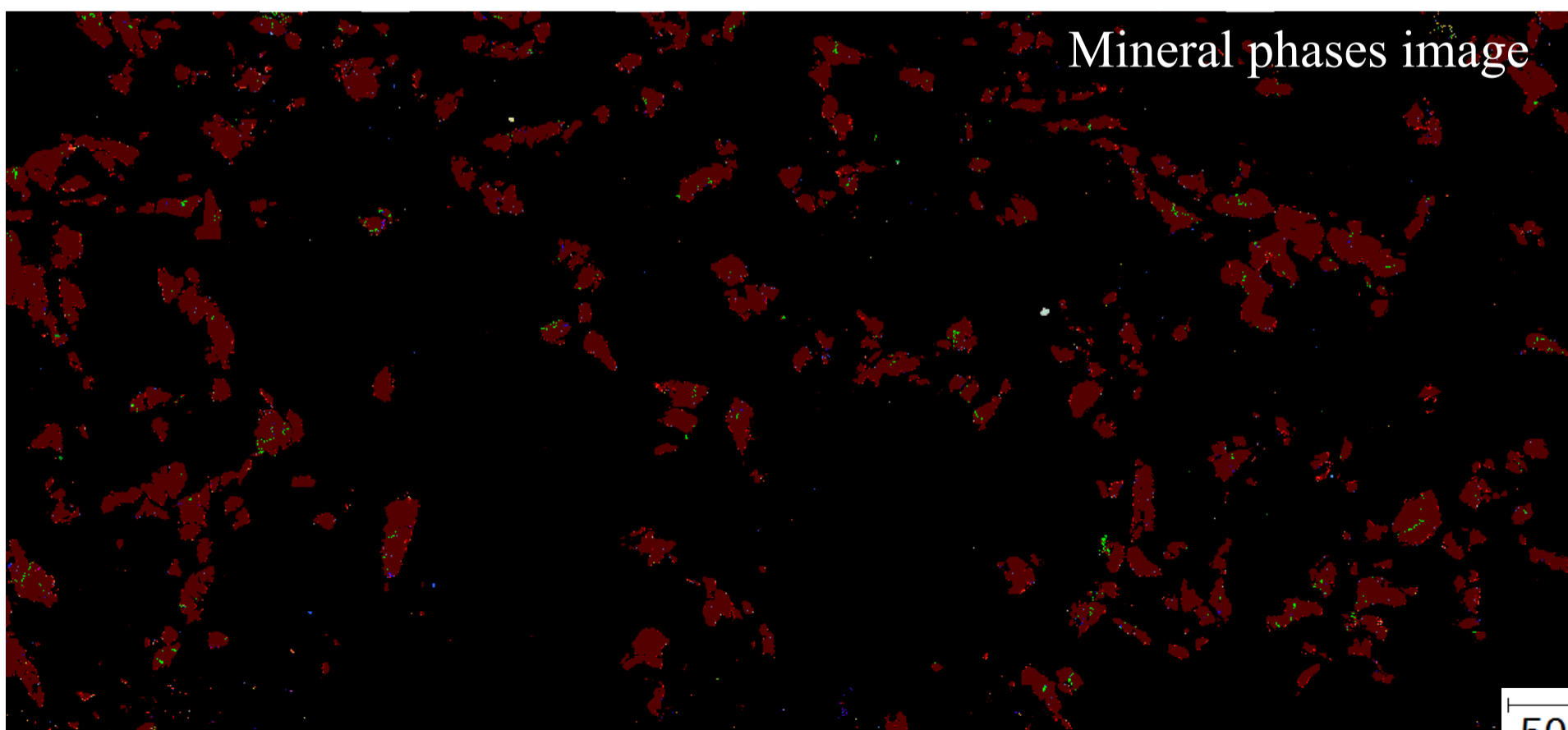
BMB5893



BSE image



Mineral phases image

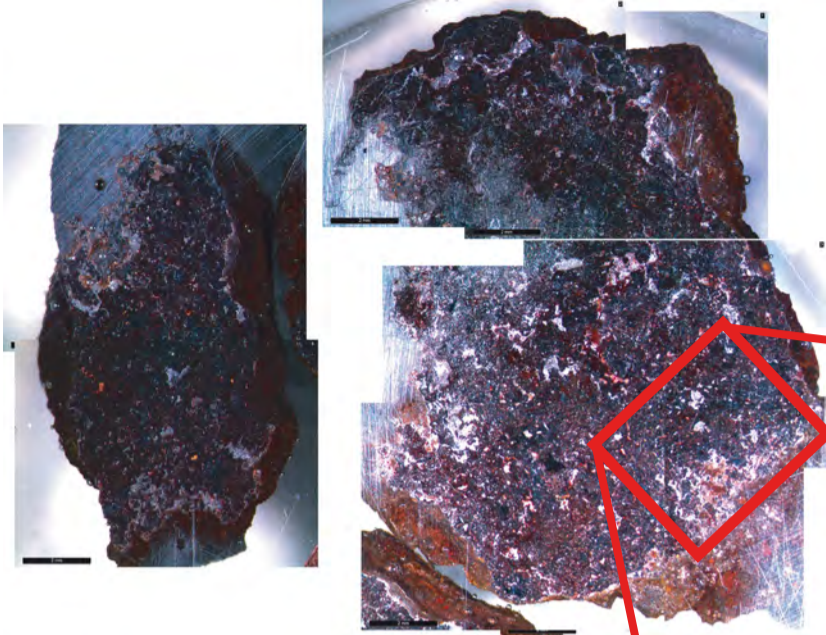


Chromium	FeO(Fe30-40)	FeO(Fe60-70)	FeO(Fe90-100)	Manganese	Silicate/quartz	Titanium
Copper	FeO(Fe40-50)	FeO(Fe70-80)	Fe-Si-O	Nickel	Sulphate/Sulphide	Vanadium
Fe	FeO(Fe50-60)	FeO(Fe80-90)	Lead	Phosphate/phosphide	Tin	Zinc
						Not Analysed
						Not Classified
						Unclassified

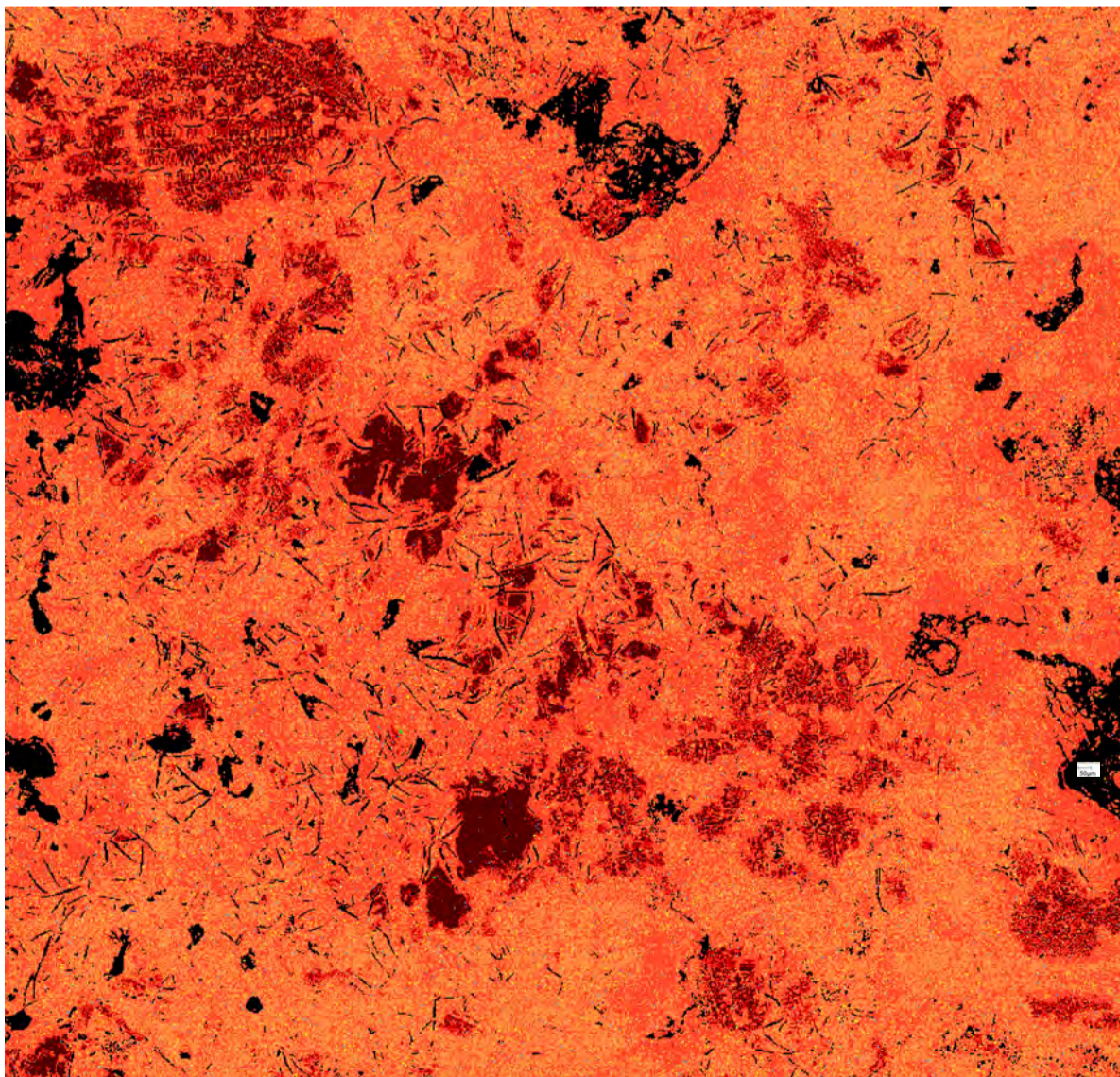
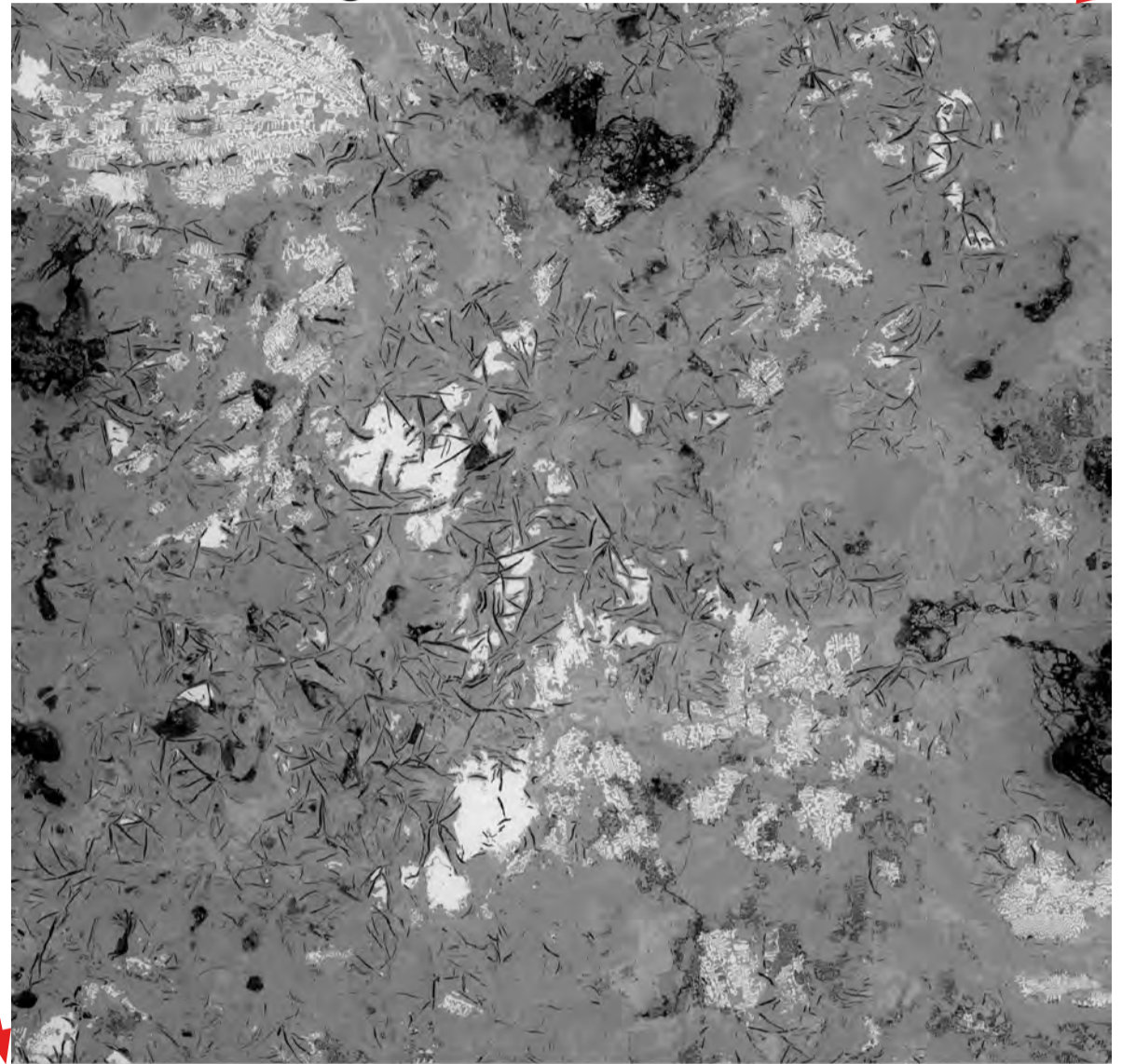
500μm



Optical microscopy image



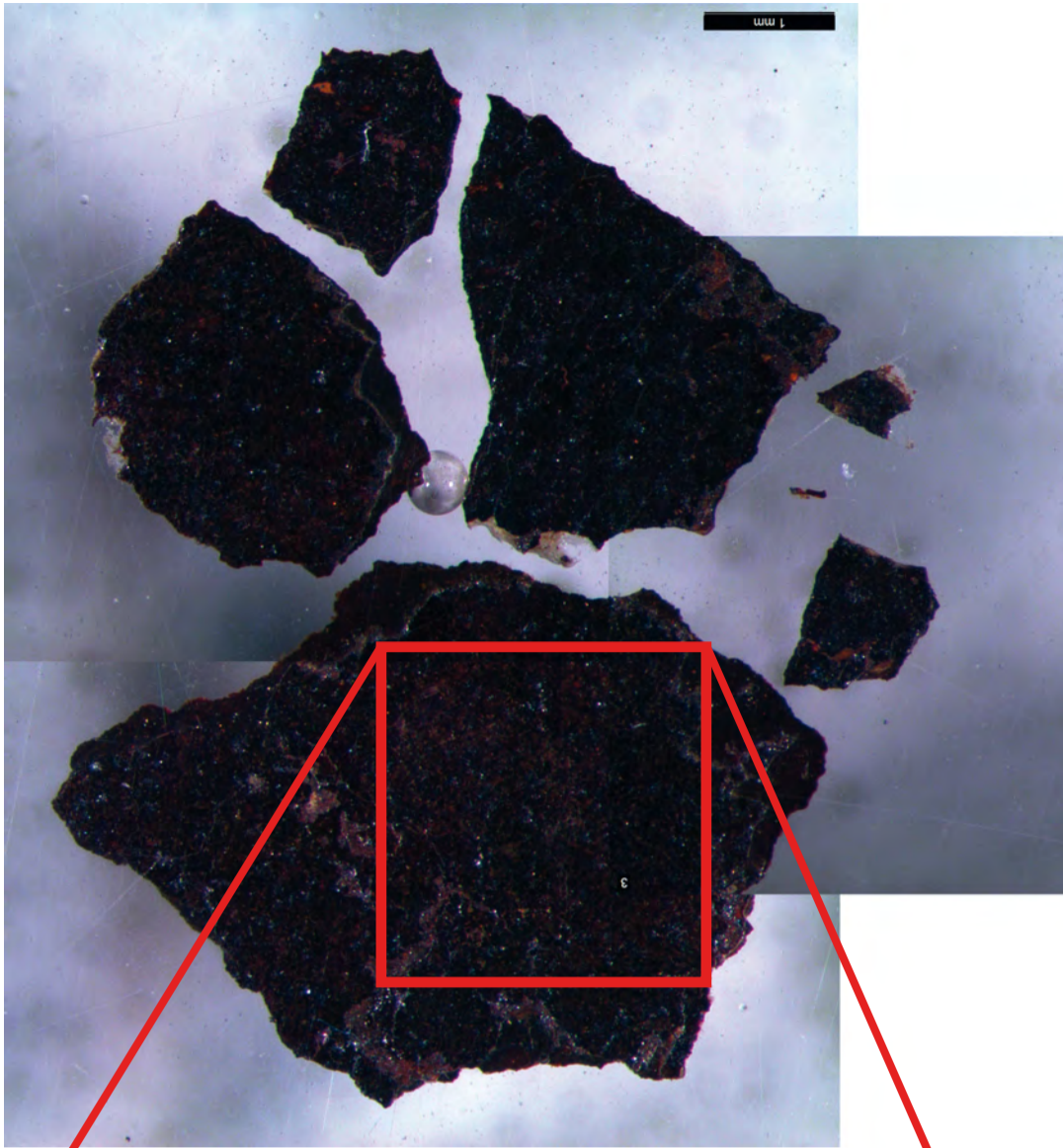
BSE image



Mineral phases image

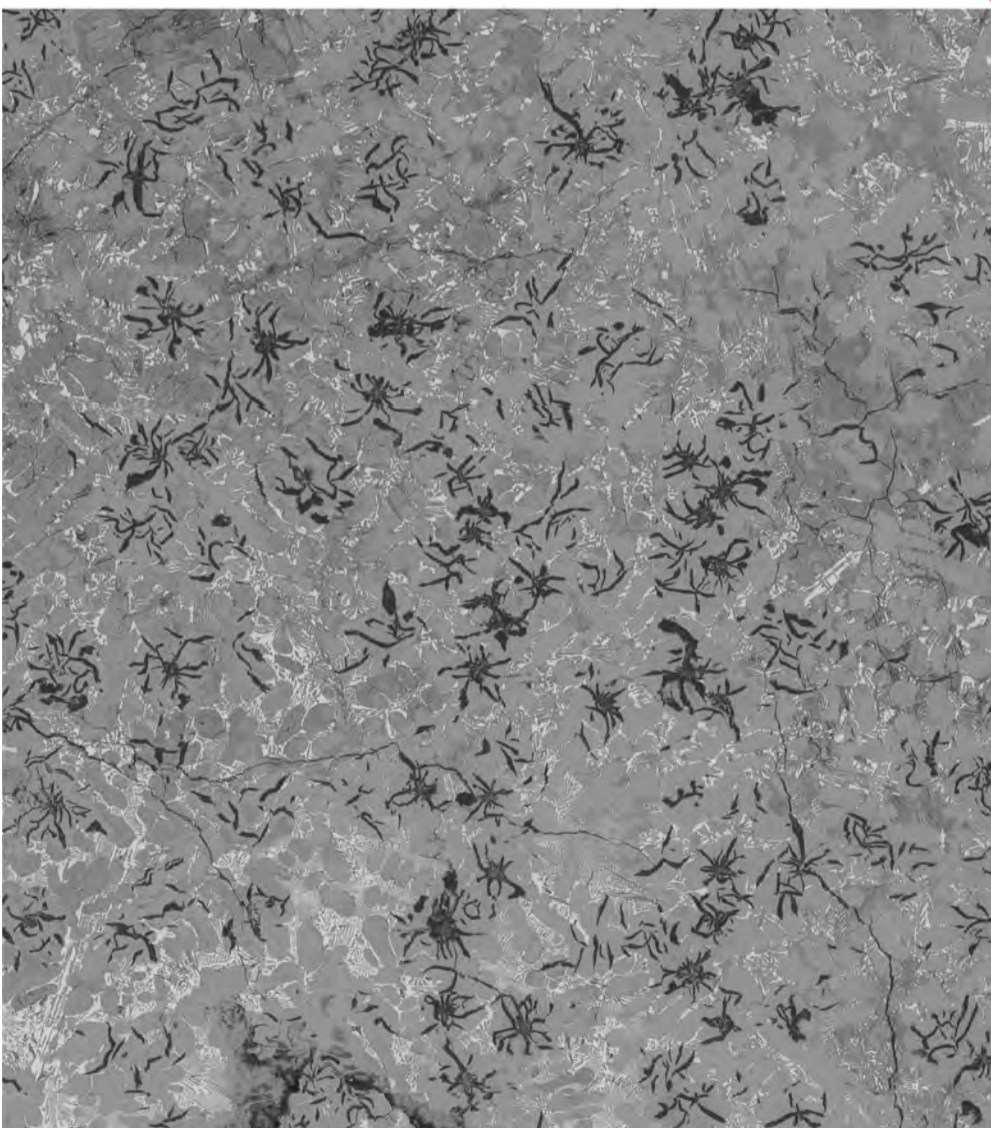
Cobalt	Fe	FeO(Fe40-50)	FeO(Fe60-70)
Copper	FeO(Fe30-40)	FeO(Fe50-60)	FeO(Fe70-80)
FeO(Fe80-90)	Lead	Phosphate/phosphide	Zinc
FeO(Fe90-100)	Manganese	Titanium	Not Analysed

# BMB5895

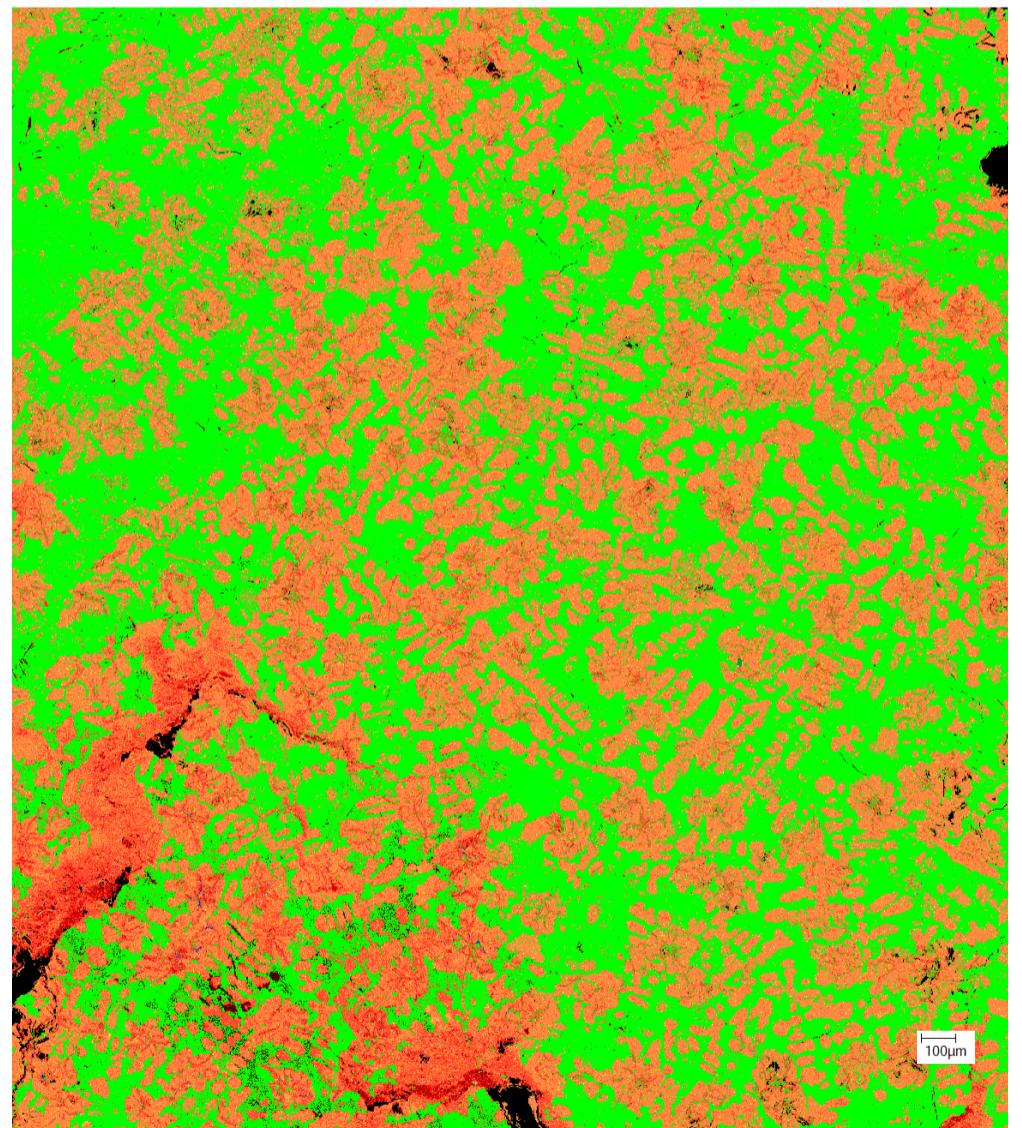


Optical microscopy image

BSE image

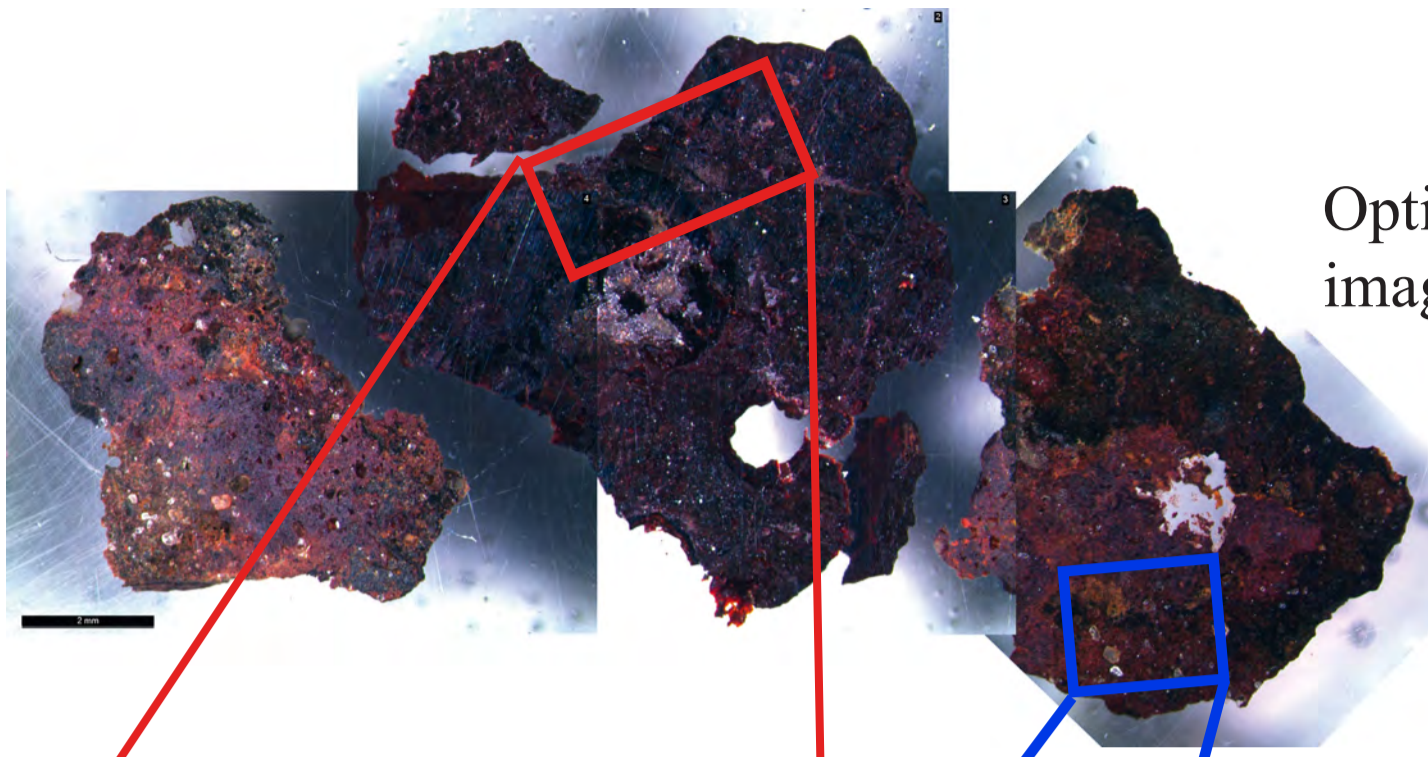


Mineral phases image



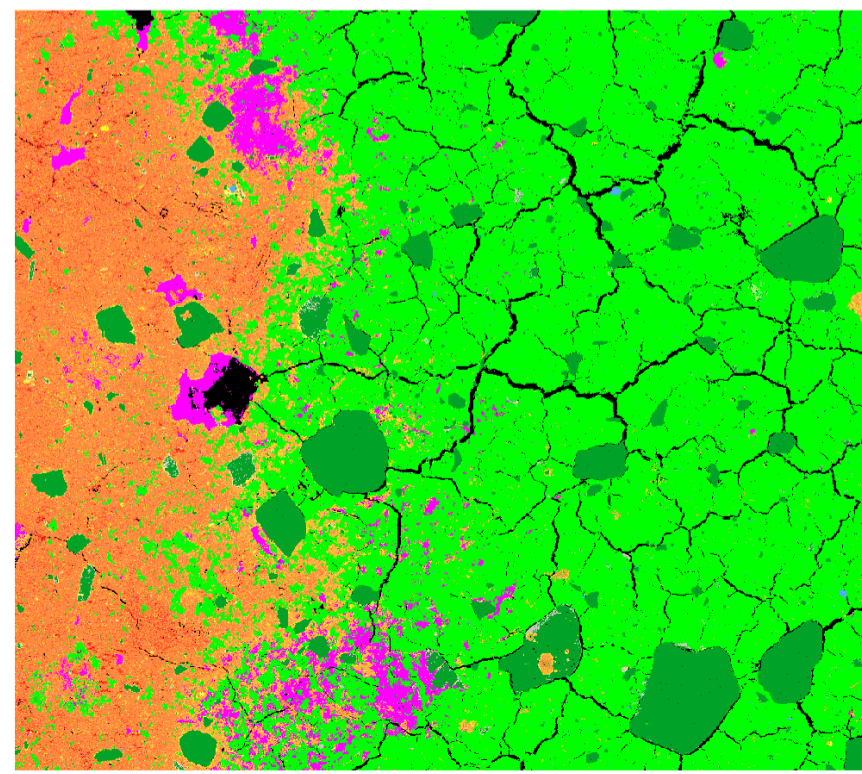
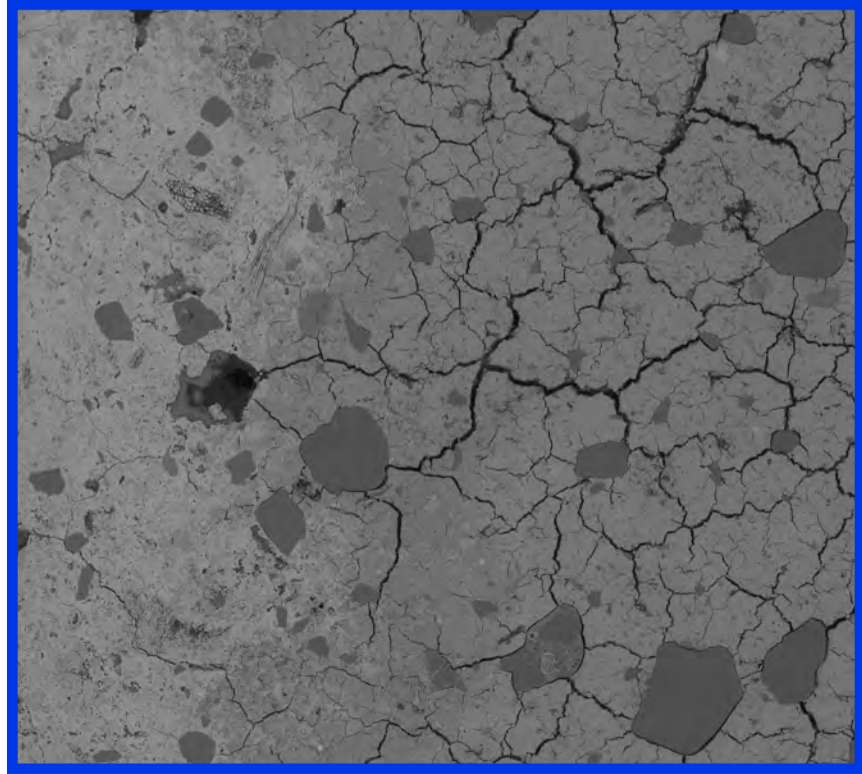
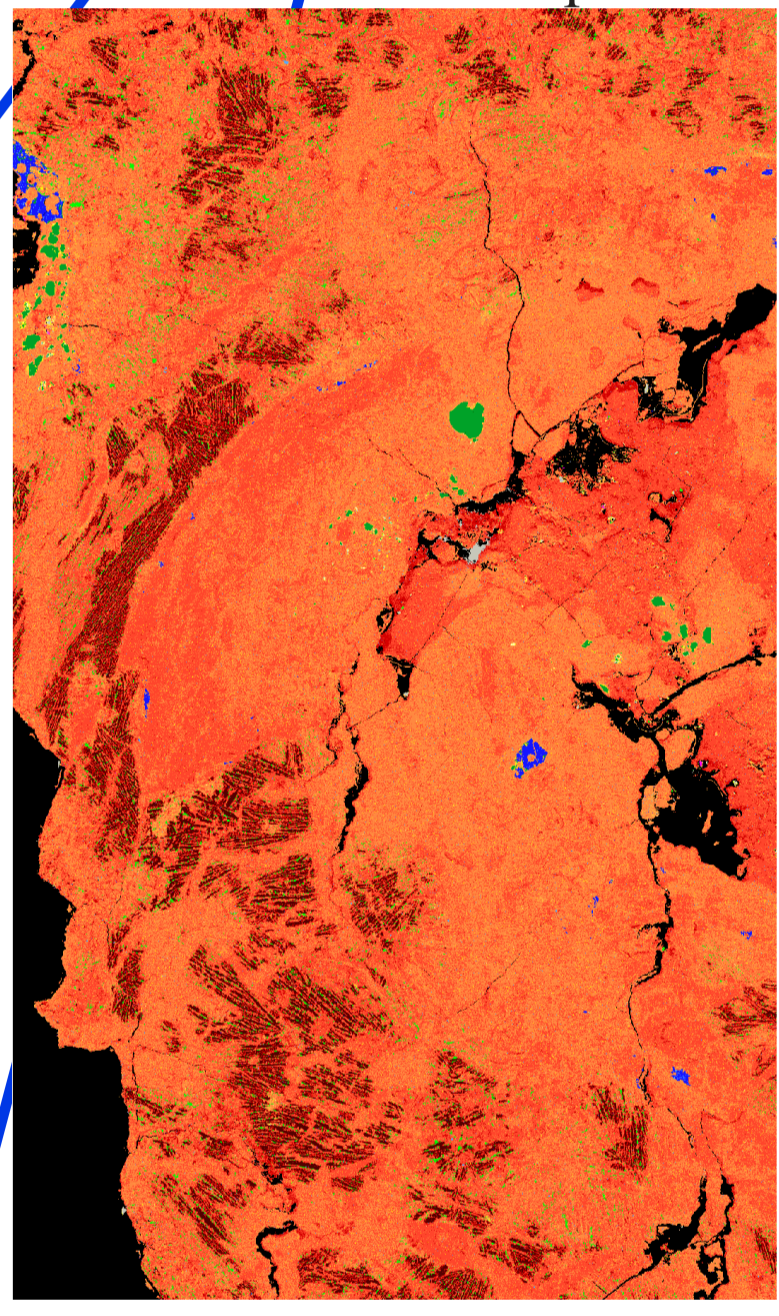
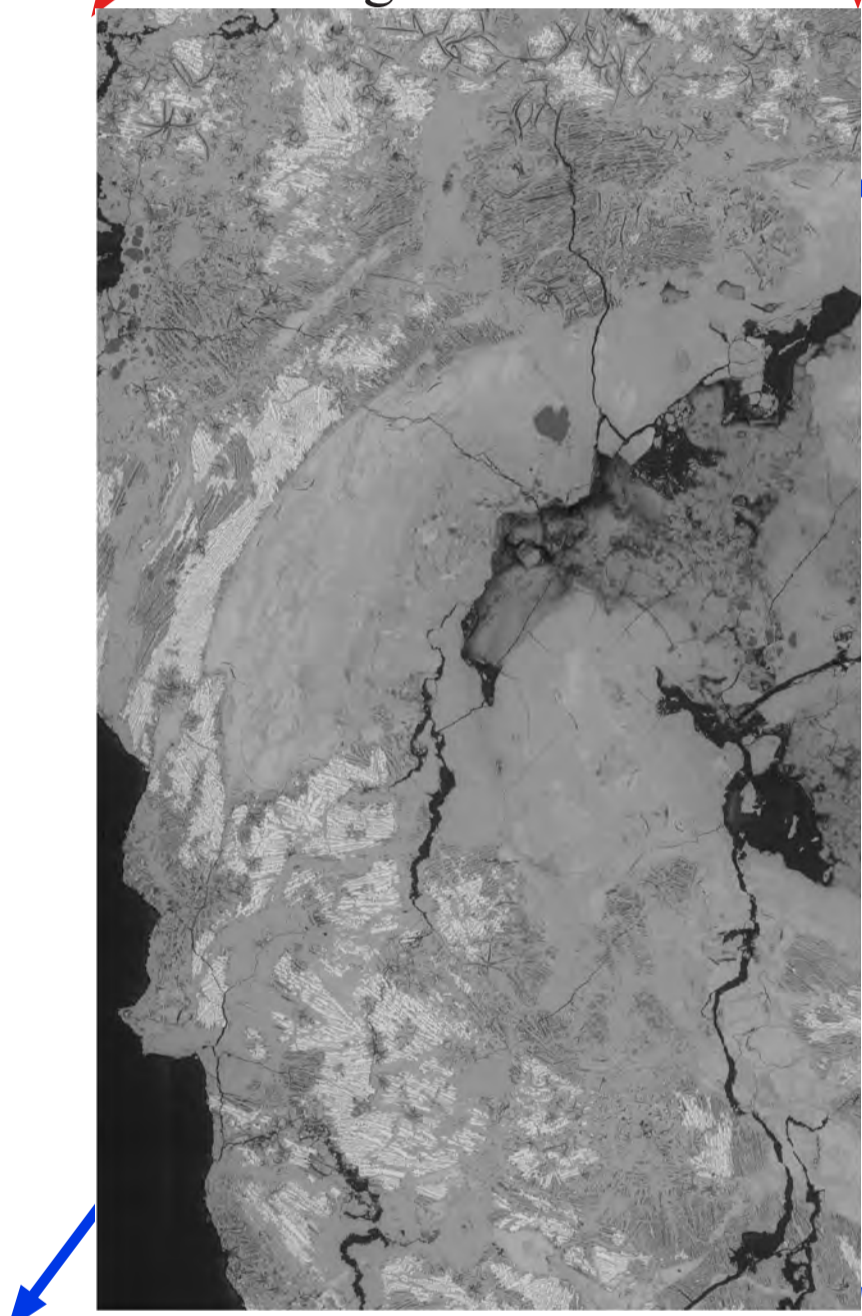
Chromium	Cobalt	Copper	Fe	FeO(Fe30-40)	FeO(Fe40-50)	FeO(Fe50-60)
FeO(Fe60-70)	FeO(Fe70-80)	FeO(Fe80-90)	Fe-Si-O	Lead	Manganese	Nickel
Phosphate/phosphide	Sulphate/Sulphide	Tin	Titanium	Vanadium	Zinc	Not Analysed

Optical microscopy image



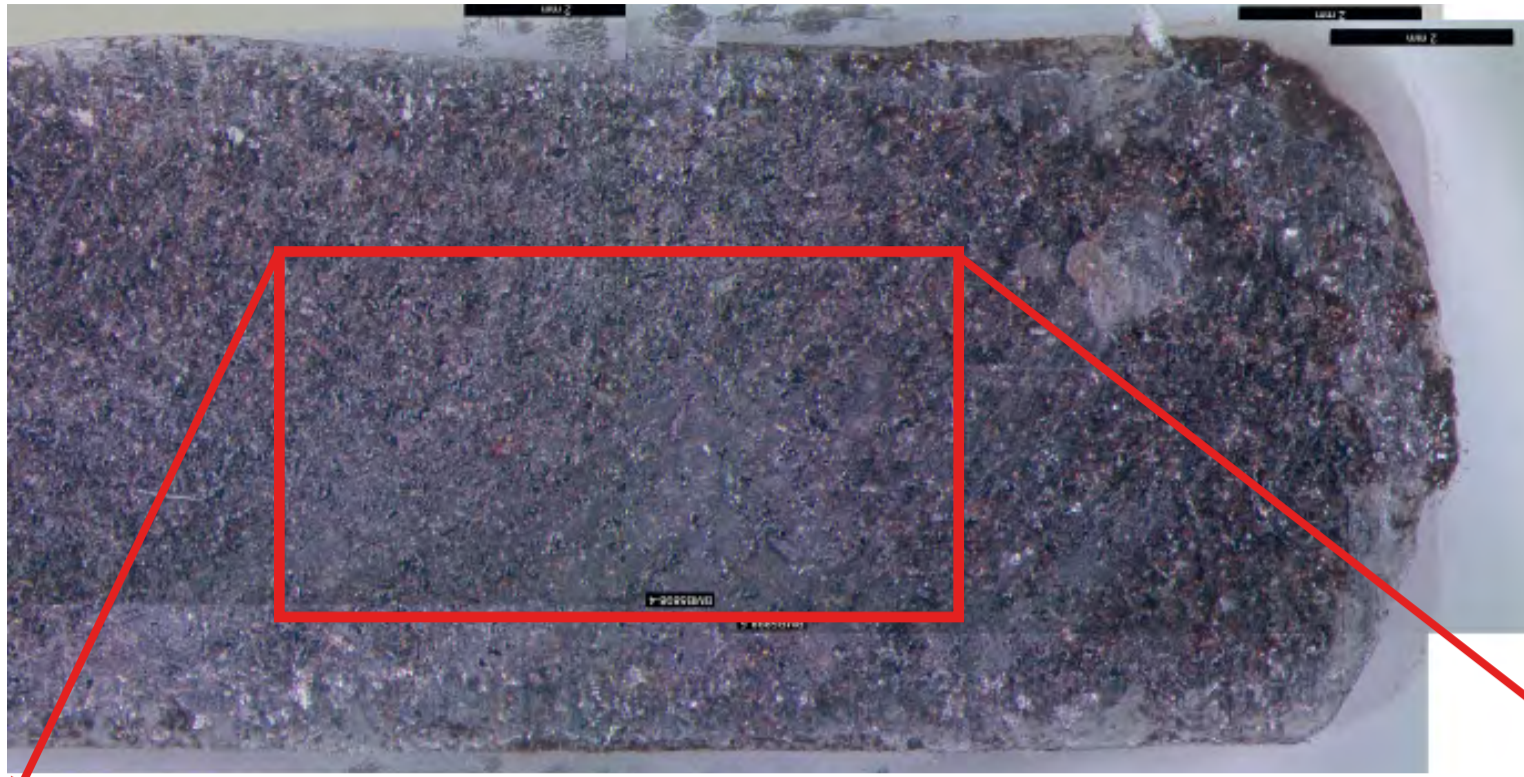
BSE images

Mineral phases images



Chromium	FeO(Fe30-40)	FeO(Fe90-100)	Manganese
Copper	FeO(Fe40-50)	Fe-Si-O	Nickel
Fe	FeO(Fe50-60)	Lead	Phosphate/phosphide
	FeO(Fe60-70)		Silicate/quartz
	FeO(Fe70-80)		Sulphate/Sulphide
	FeO(Fe80-90)		Tin
			Titanium
			Zinc
			Not Classified

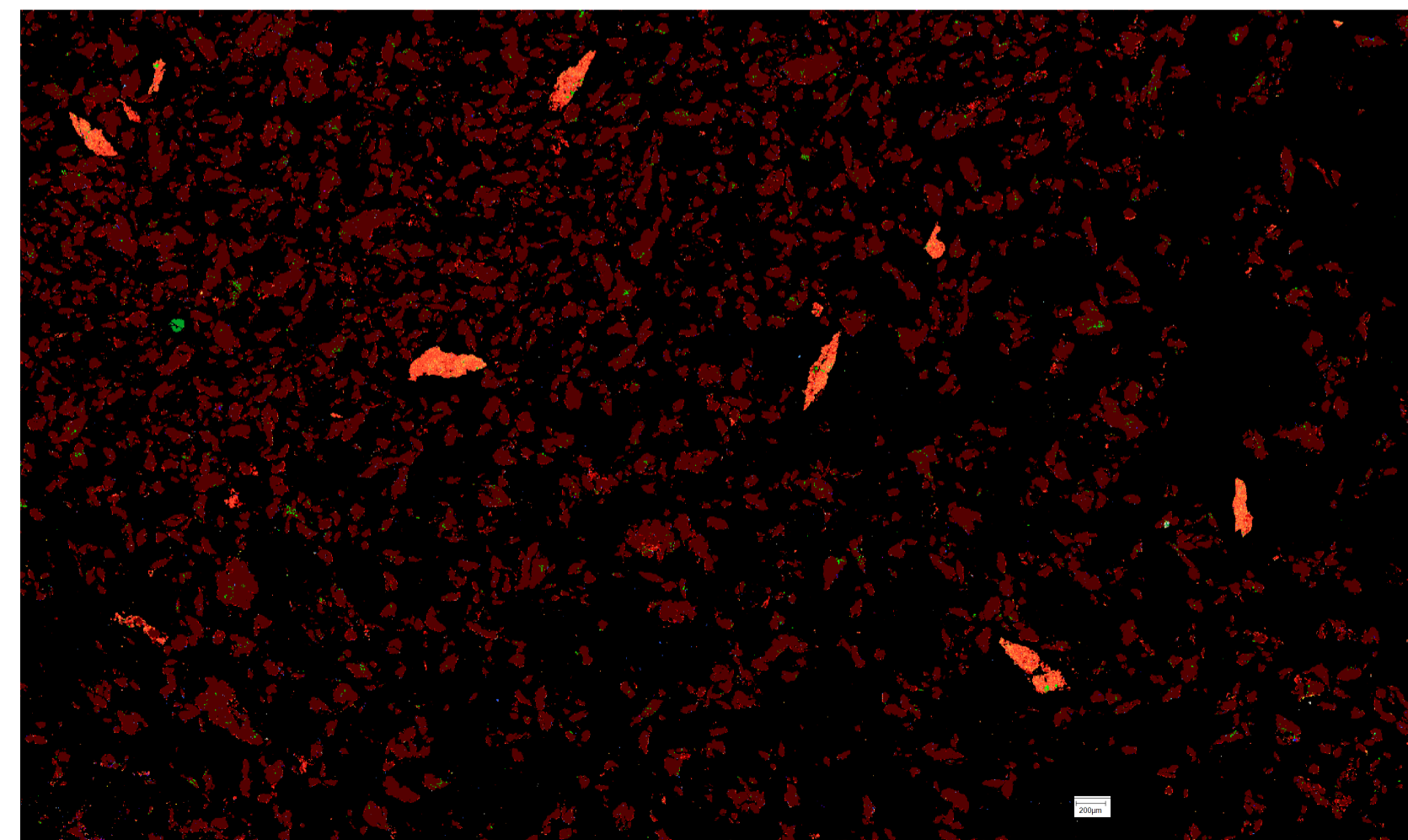
# BMB5898



Optical microscopy image



BSE image



Mineral phases image

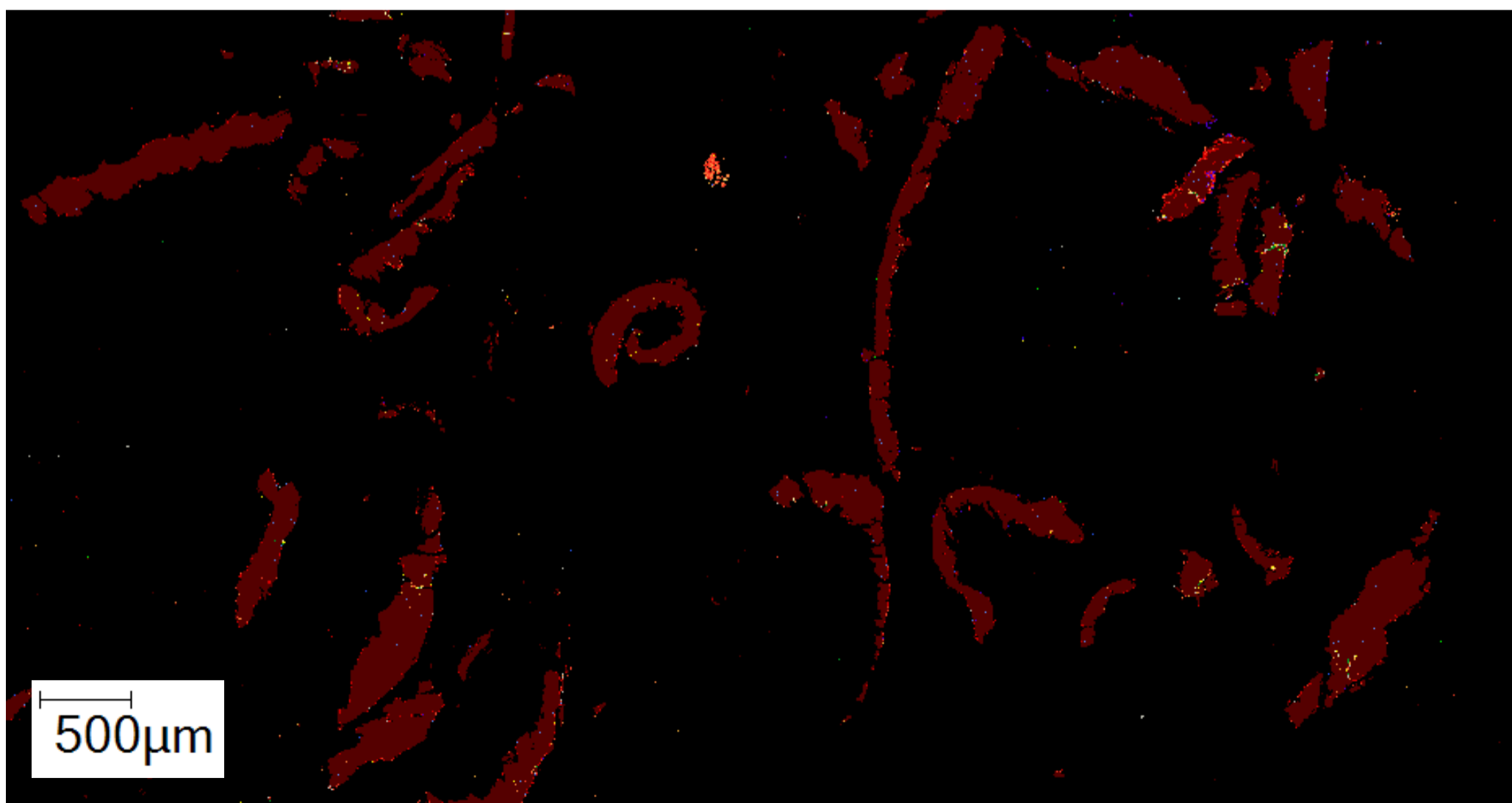
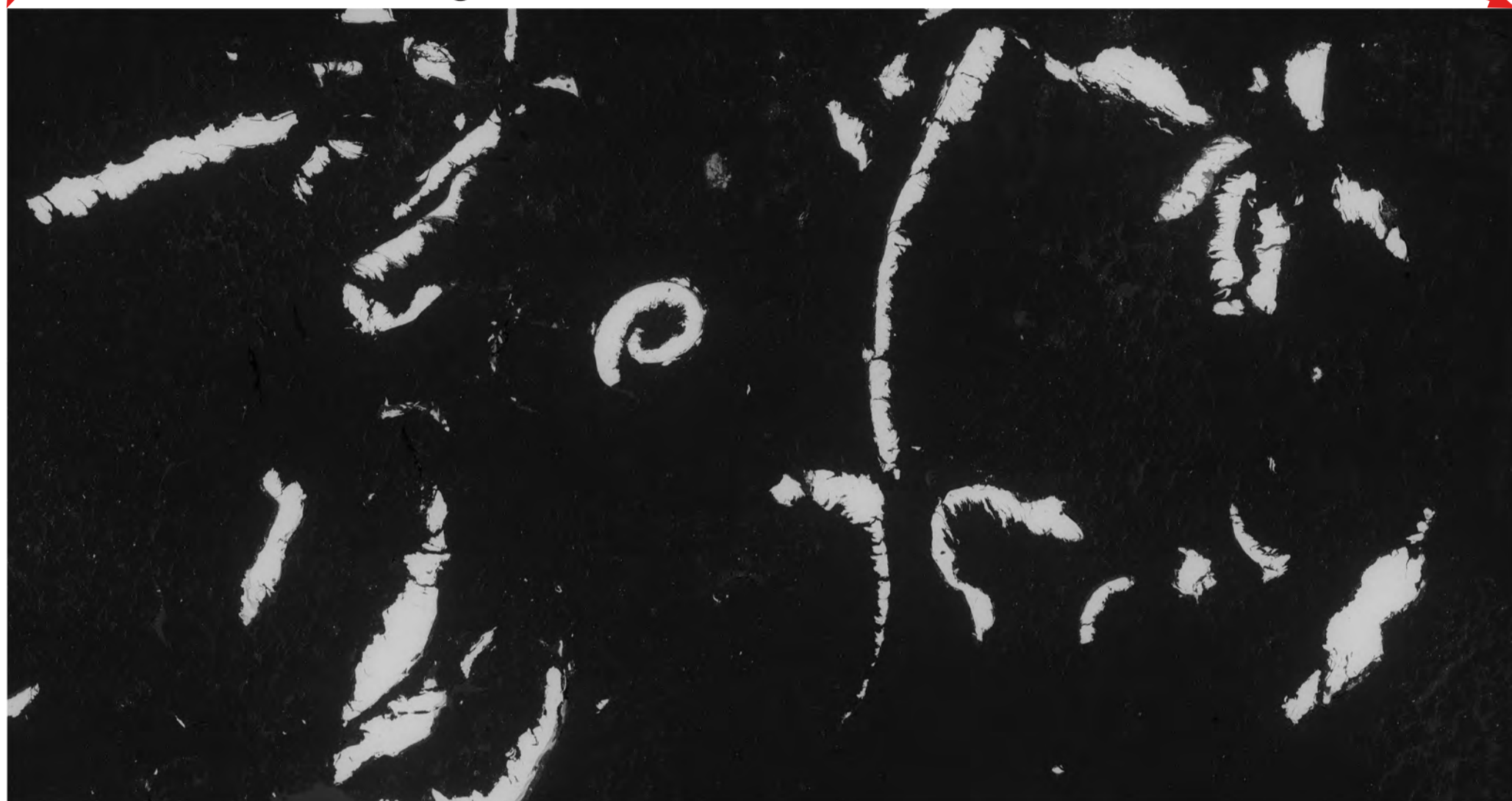
Chromium	Cobalt	Copper	Fe	FeO(Fe30-40)	FeO(Fe40-50)	FeO(Fe50-60)	FeO(Fe60-70)
FeO(Fe70-80)	FeO(Fe80-90)	FeO(Fe90-100)	Fe-Si-O	Lead	Manganese	Nickel	Phosphate/phosphide
Silicate/quartz	Sulphate/Sulphide	Tin	Titanium	Vanadium	Zinc	Not Classified	Unclassified

BMB5899



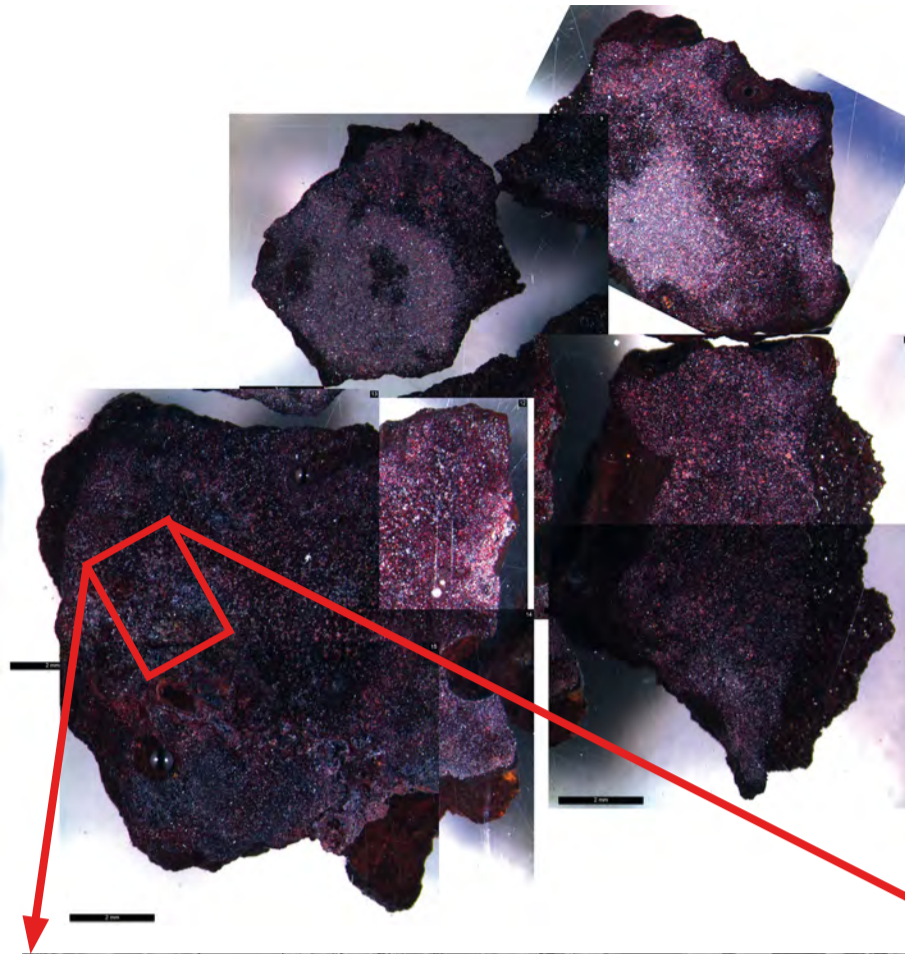
Optical microscopy image

BSE image

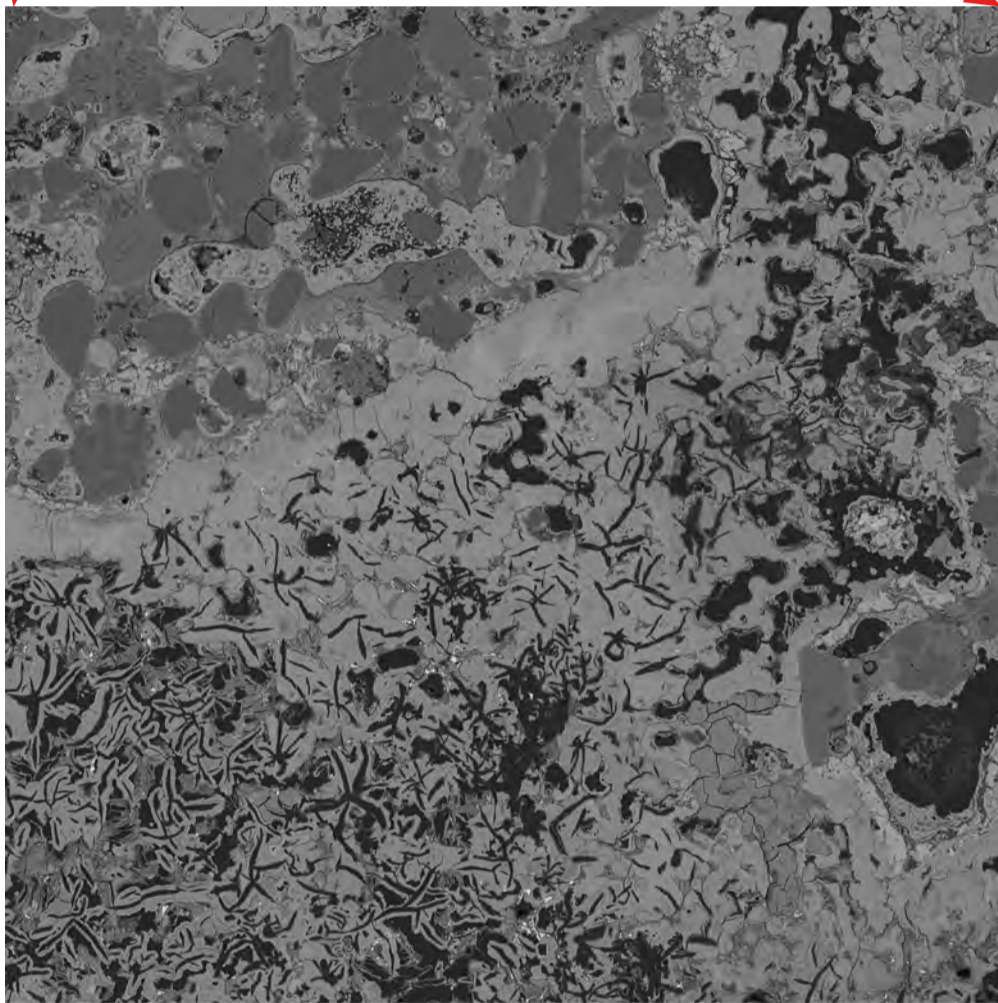


Chromium	FeO(Fe30-40)	FeO(Fe60-70)	FeO(Fe90-100)	Manganese	Silicate/quartz	Titanium
Copper	FeO(Fe40-50)	FeO(Fe70-80)	Fe-Si-O	Nickel	Sulphate/Sulphide	Zinc
Fe	FeO(Fe50-60)	FeO(Fe80-90)	Lead	Phosphate/phosphide	Tin	Not Classified

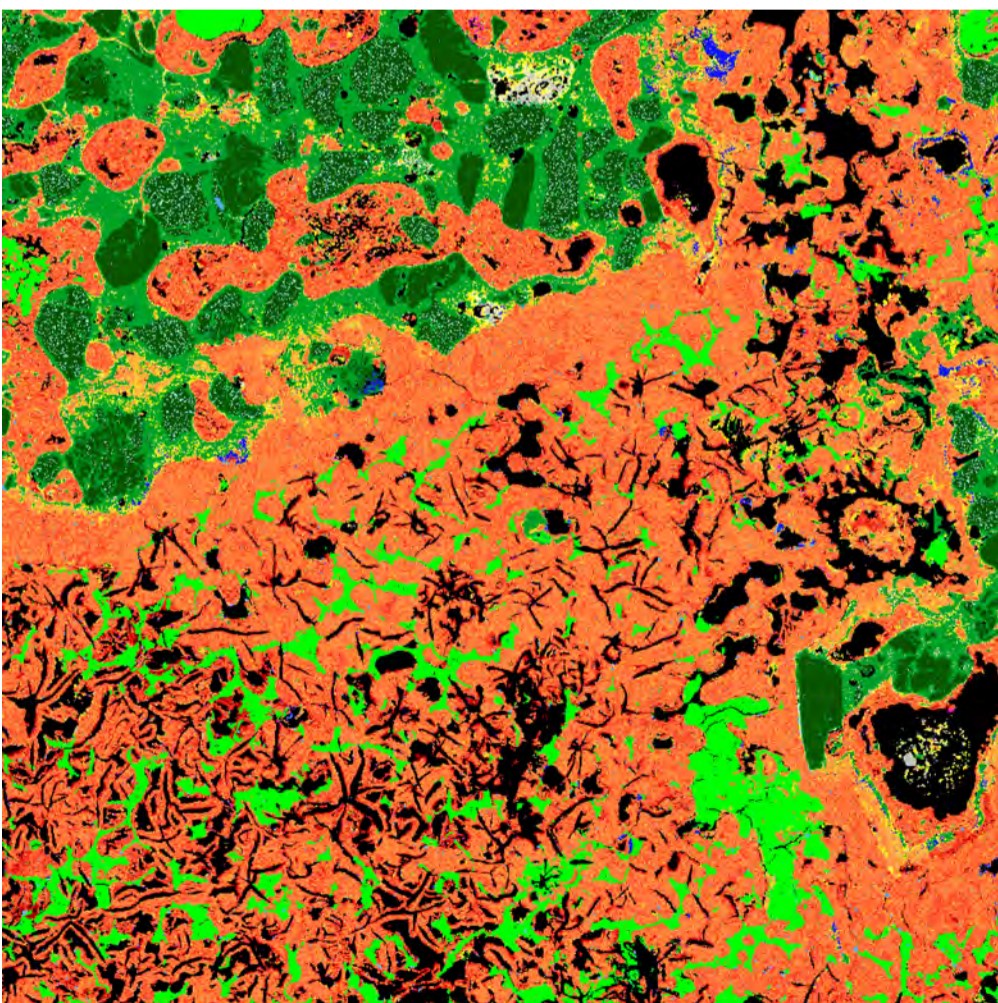
# BMB5903



Optical microscopy image



BSE image



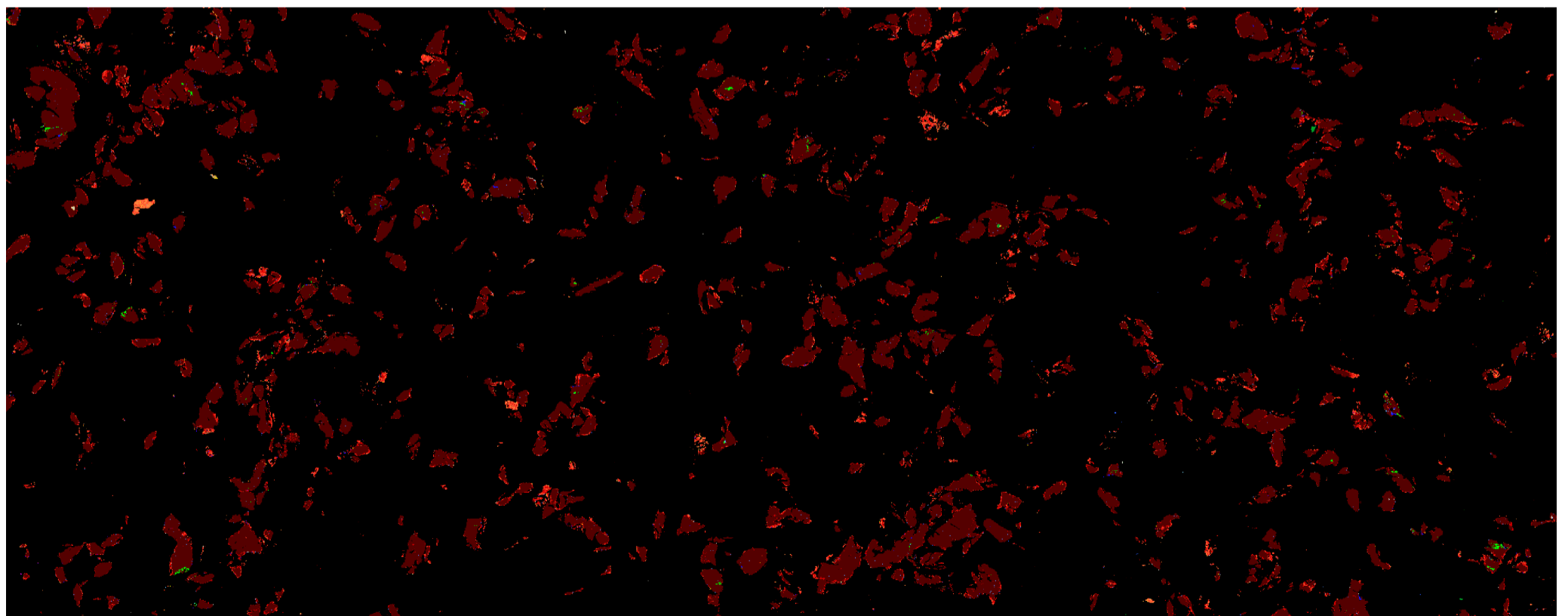
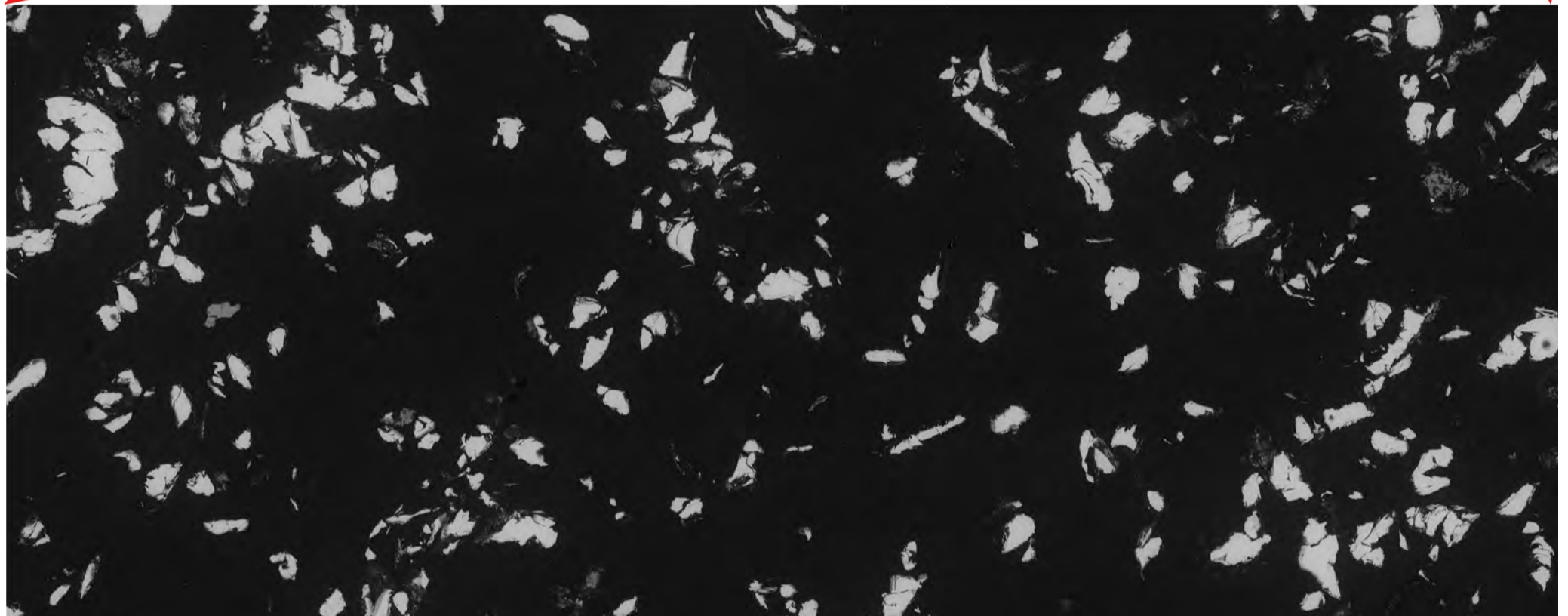
Mineral phases image

# BMB5904

Optical microscopy image



BSE image

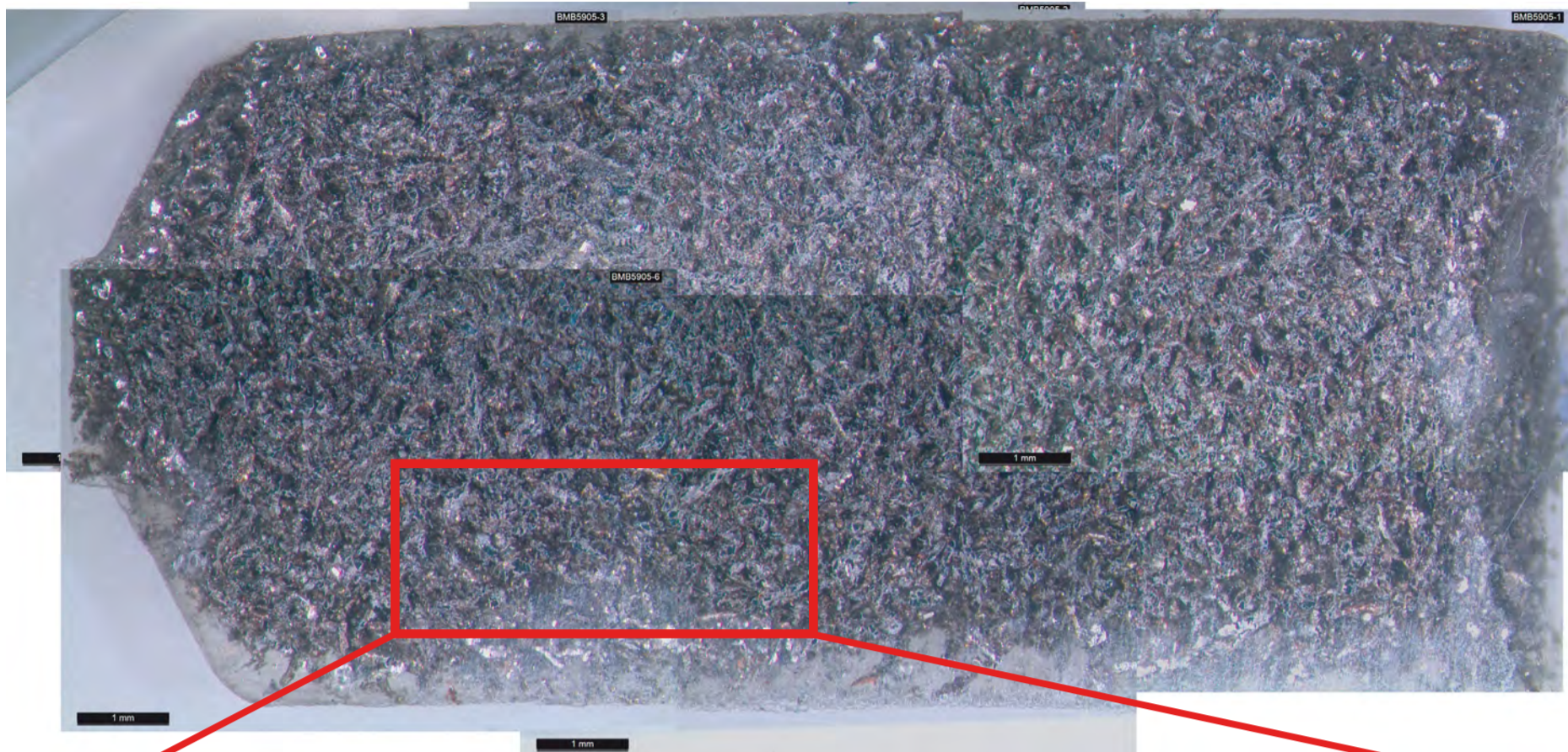


Chromium	Cobalt	Copper	Fe	FeO(Fe30-40)	FeO(Fe40-50)	FeO(Fe50-60)	FeO(Fe60-70)	FeO(Fe70-80)	FeO(Fe80-90)	FeO(Fe90-100)	200µm
Fe-Si-O	Lead	Manganese	Nickel	Phosphate/phosphide	Silicate/quartz	Sulphate/Sulphide	Tin	Titanium	Vanadium	Zinc	Not Classified

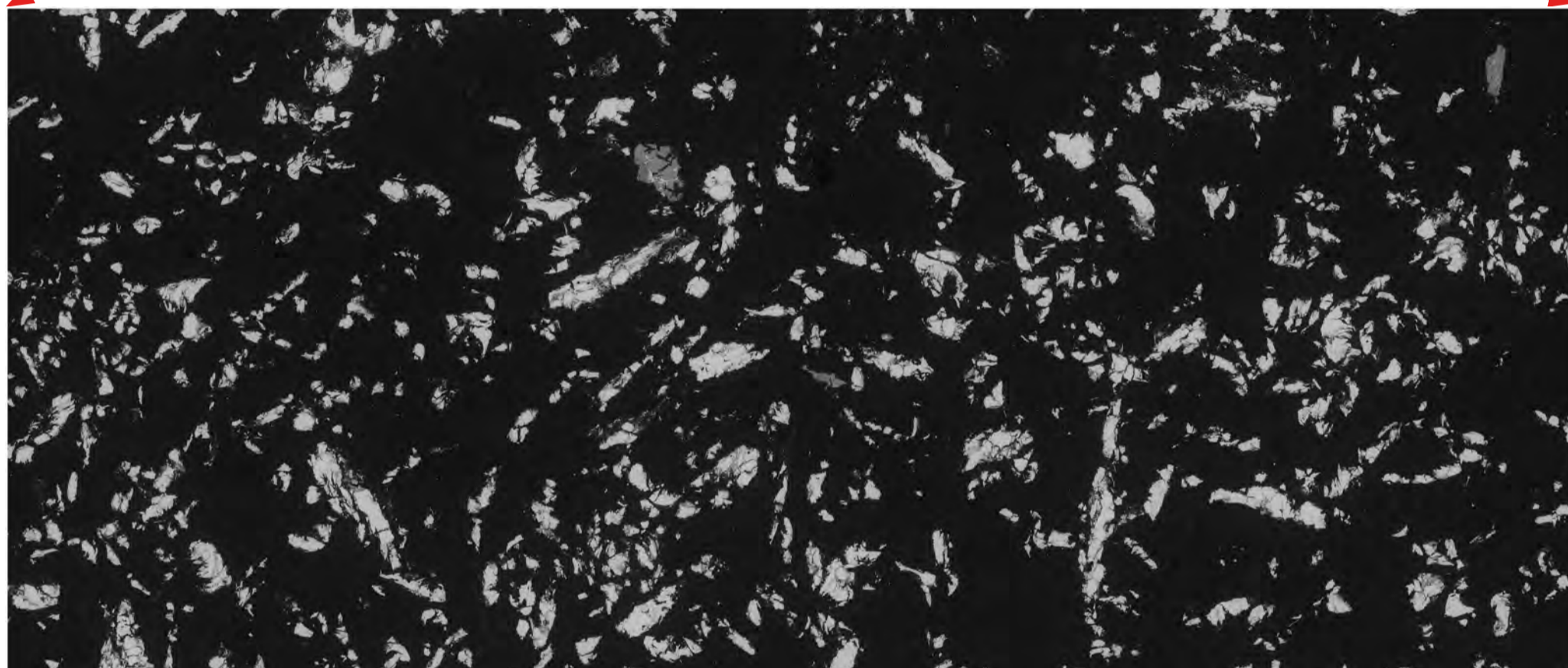
Mineral phases image

Optical microscopy image

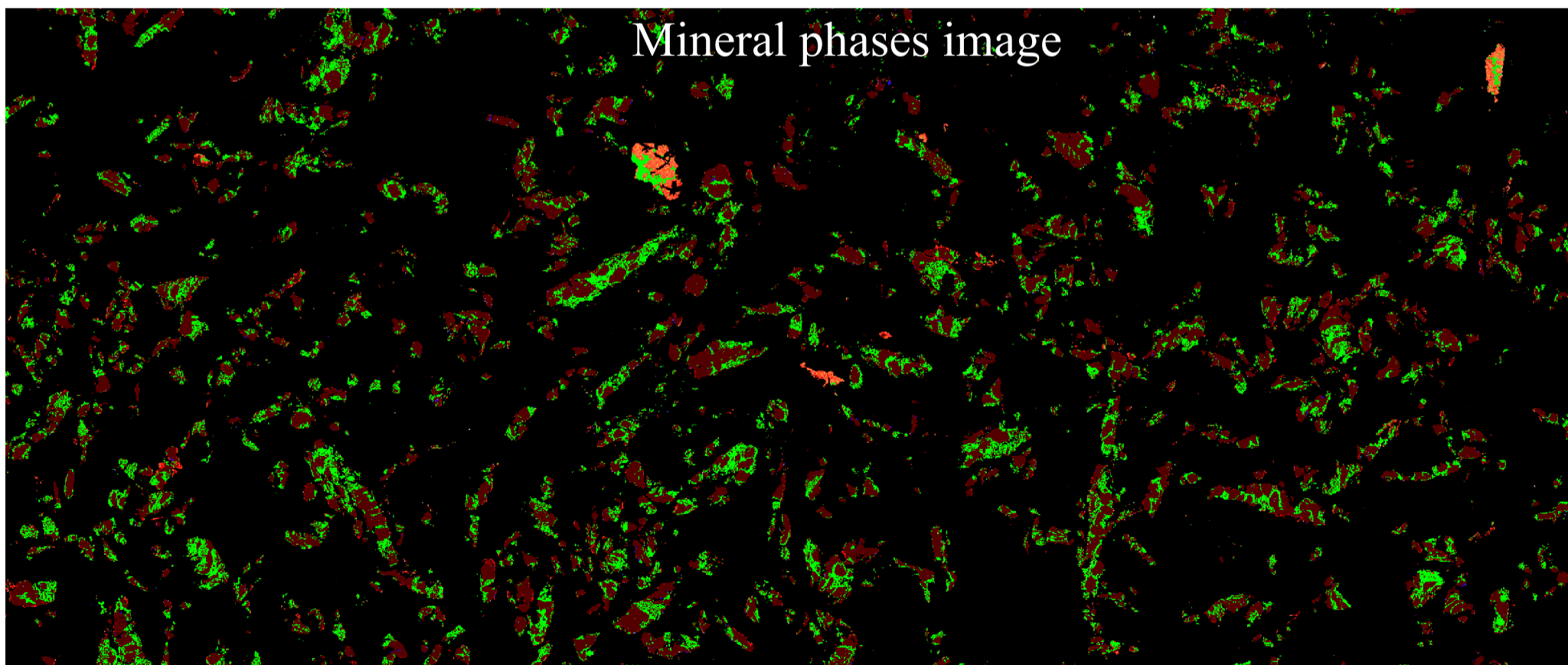
BMB5905



BSE image



Mineral phases image



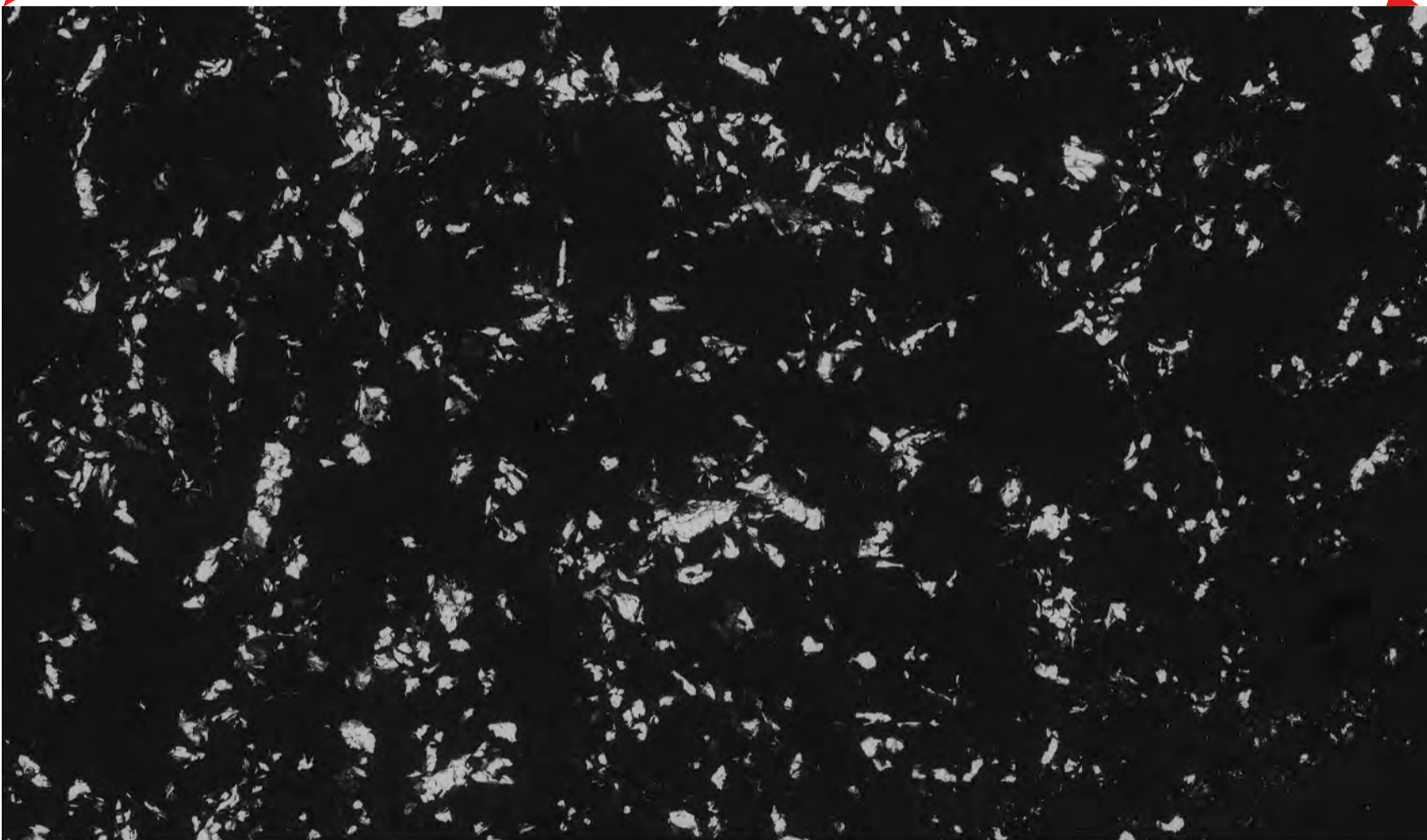
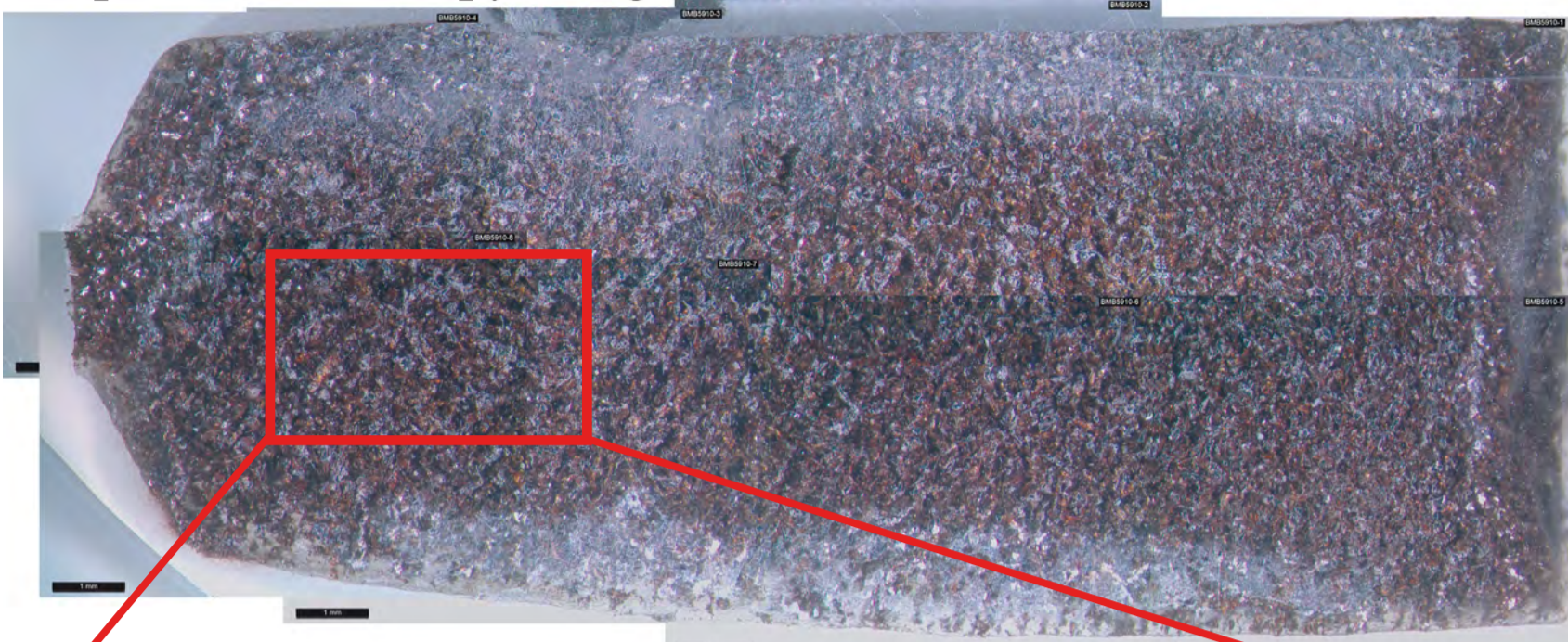
Chromium	Cobalt	Copper	Fe	FeO(Fe30-40)	FeO(Fe40-50)	FeO(Fe50-60)	FeO(Fe60-70)
FeO(Fe70-80)	FeO(Fe80-90)	FeO(Fe90-100)	Fe-Si-O	Lead	Manganese	Nickel	Phosphate/phosphide
Sulphate/Sulphide	Tin	Titanium	Vanadium	Zinc	Not Analysed	Not Classified	Unclassified

200µm

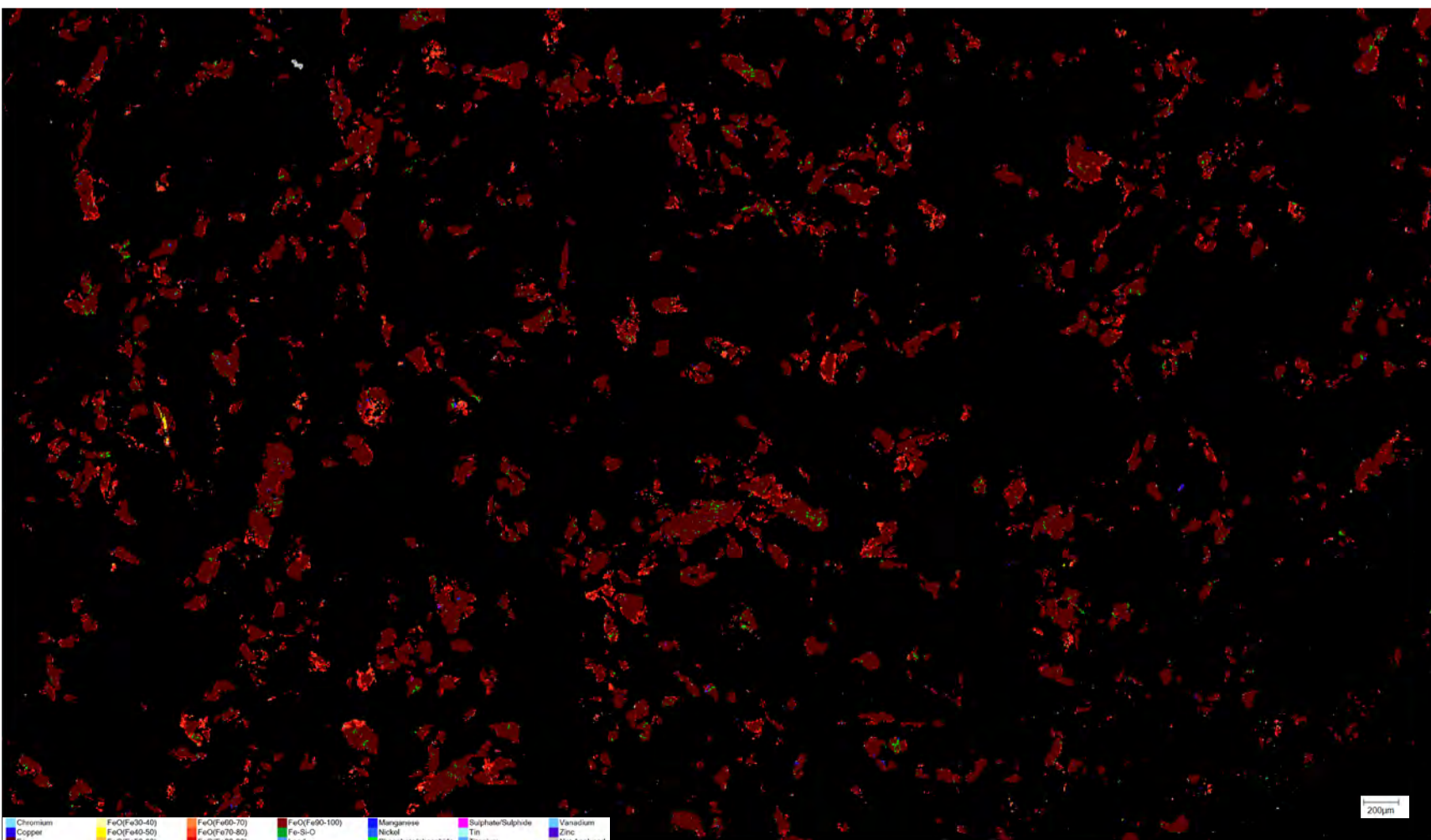


Optical microscopy image

BMB5910



BSE image



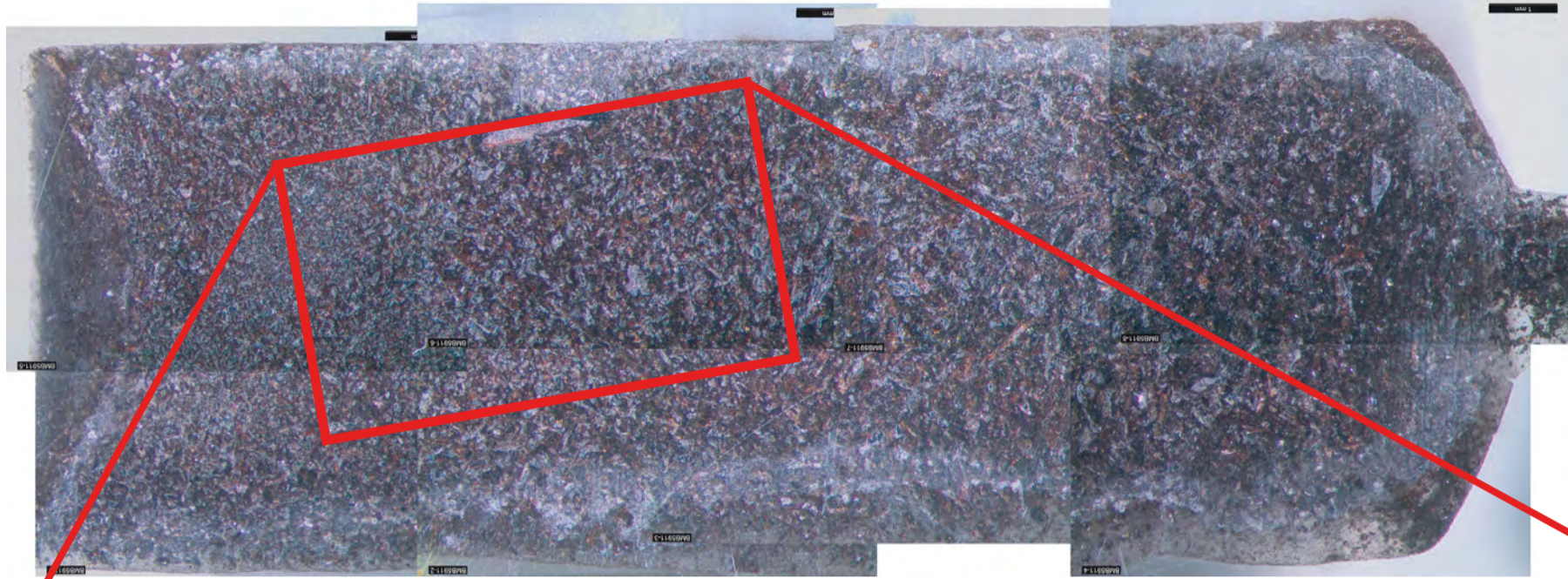
Mineral phases image

Chromium  
Copper  
Fe  
FeO(Fe30-40)  
FeO(Fe40-50)  
FeO(Fe50-60)  
FeO(Fe60-70)  
FeO(Fe70-80)  
FeO(Fe80-90)  
FeO(Fe90-100)  
Fe-Si-O  
Lead  
Manganese  
Nickel  
Phosphates/phosphide  
Titanium  
Vanadium  
Zinc  
Not Analyzed

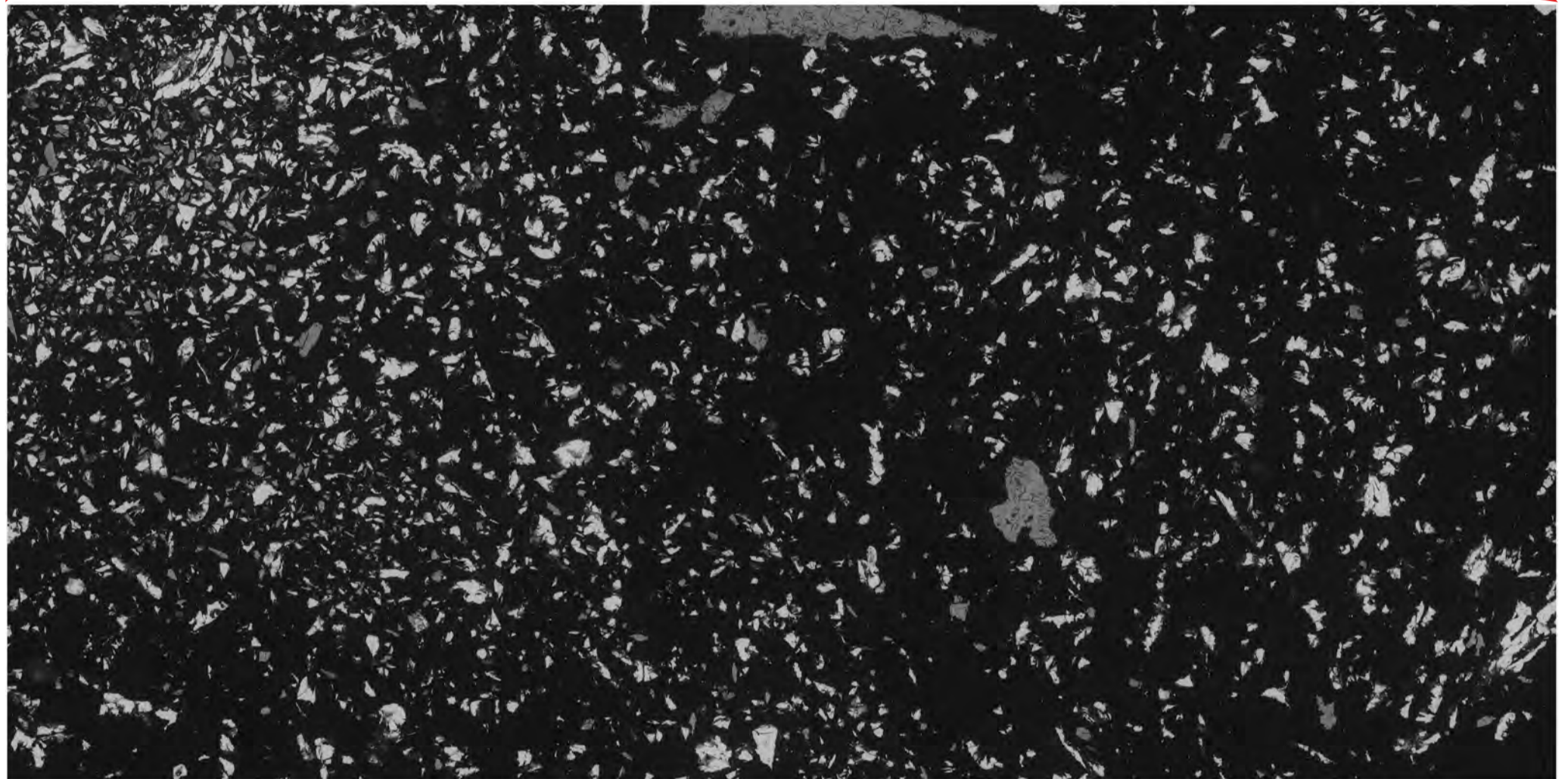
200µm

Optical microscopy image

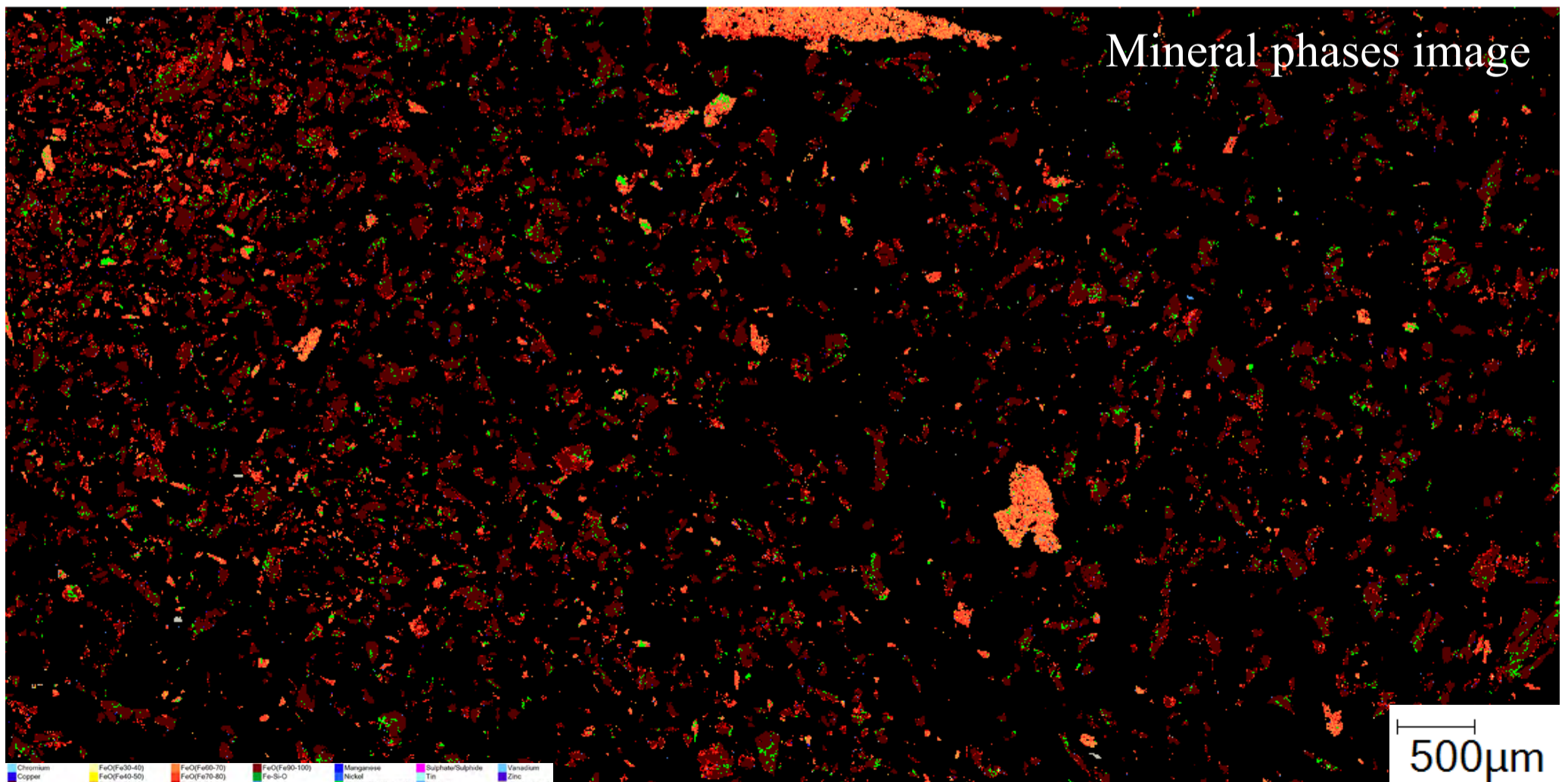
BMB5911



BSE image

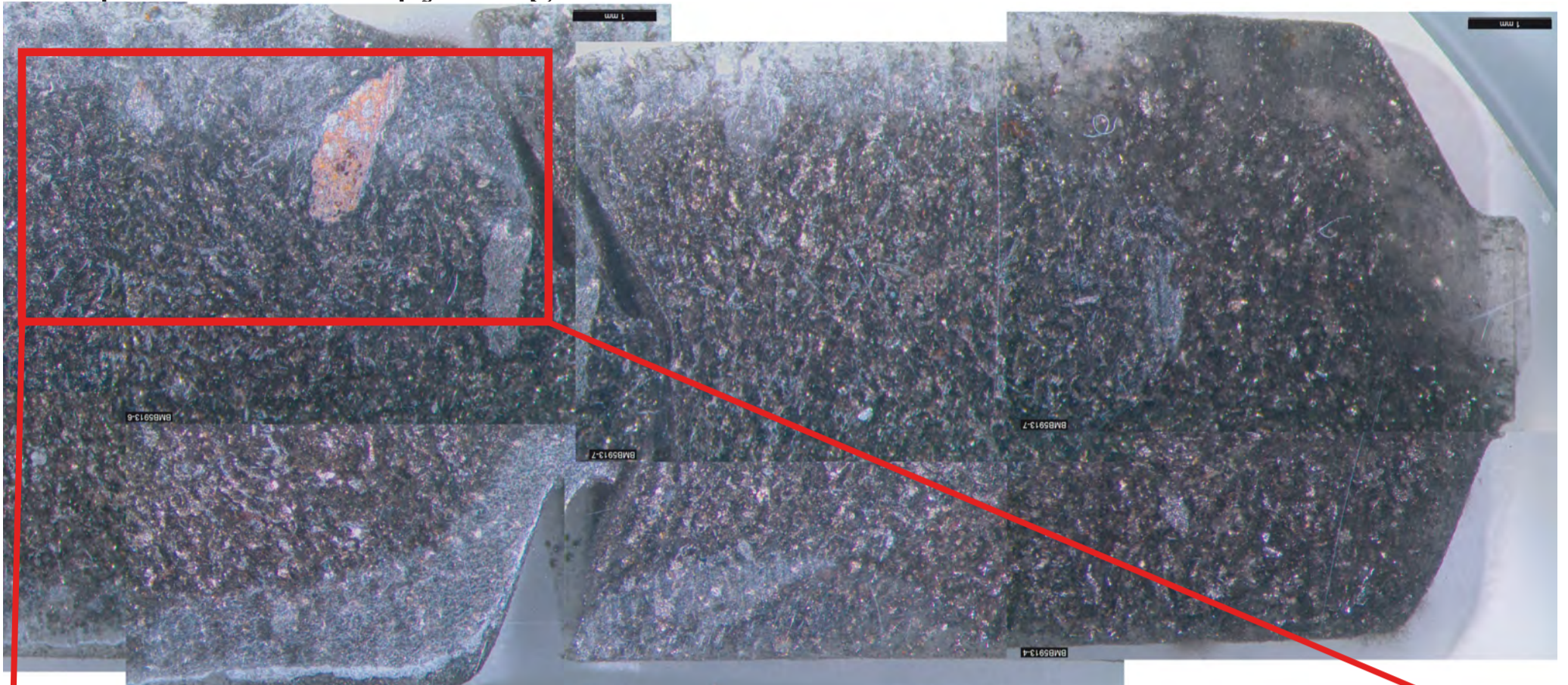


Mineral phases image

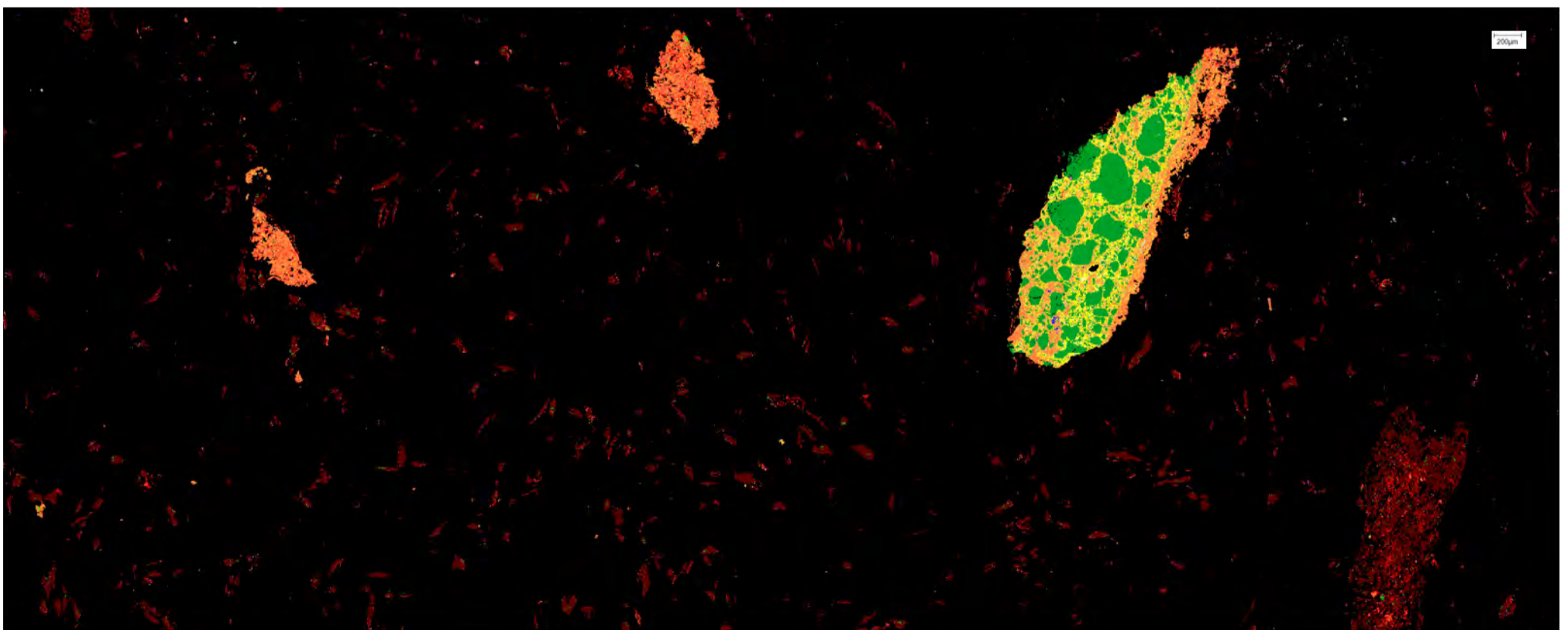
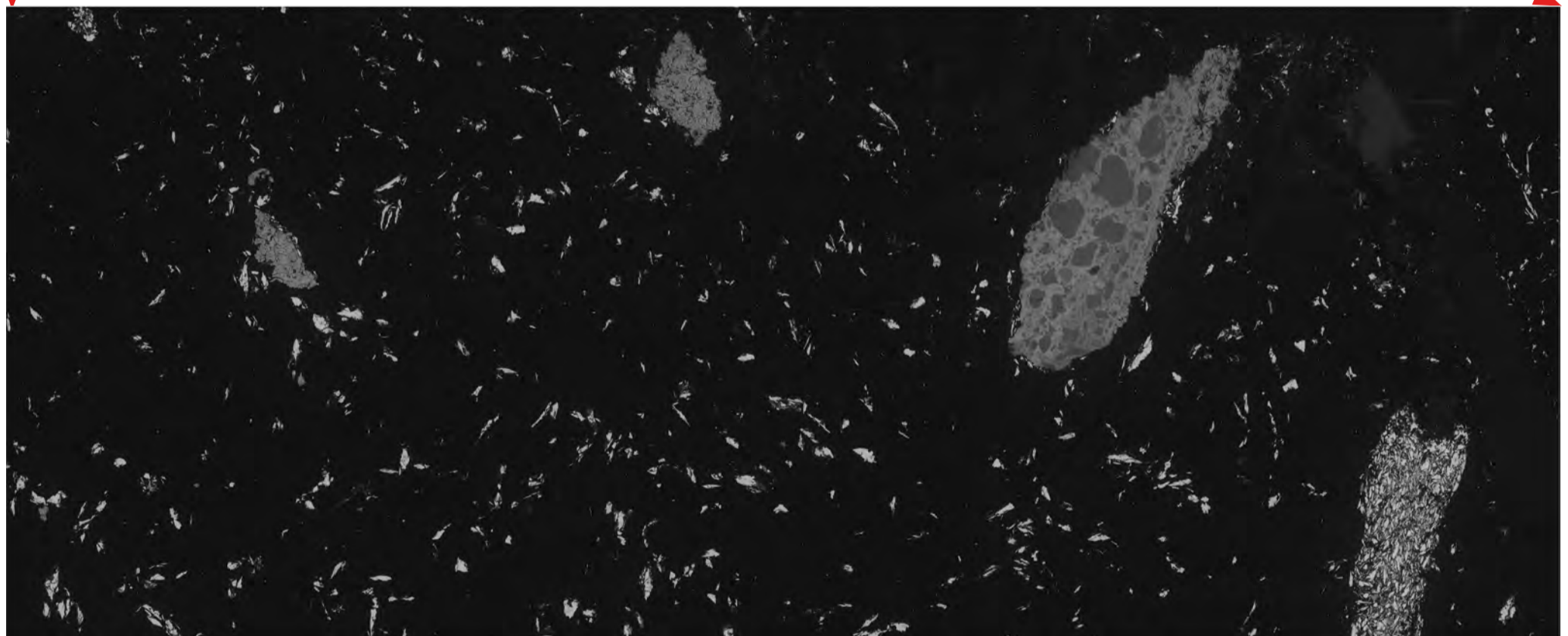


Optical microscopy image

BMB5913



BSE image

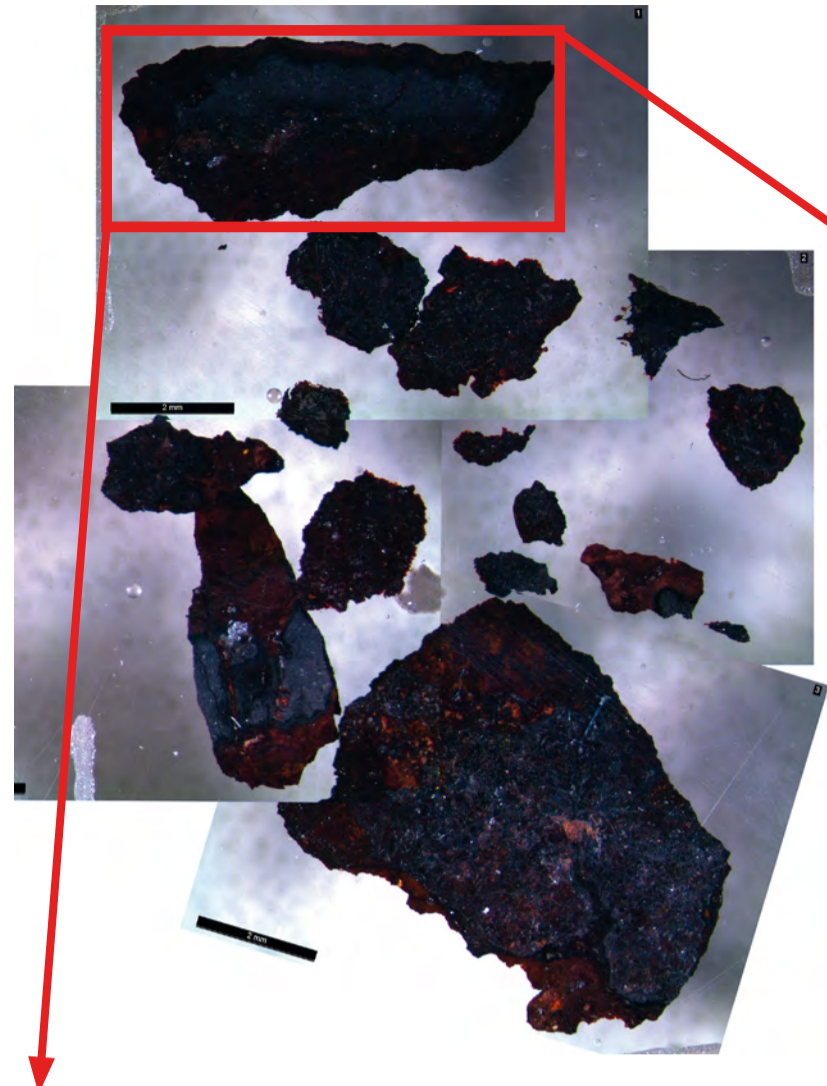


Chromium	FeO(Fe30-40)	FeO(Fe60-70)	FeO(Fe90-100)	Manganese	Sulphate/Sulphide	Vanadium
Copper	FeO(Fe40-50)	FeO(Fe70-80)	Fe-Si-O	Nickel	Tin	Zinc
Fe	FeO(Fe50-60)	FeO(Fe80-90)	Lead	Phosphate/phosphide	Titanium	Not Analysed

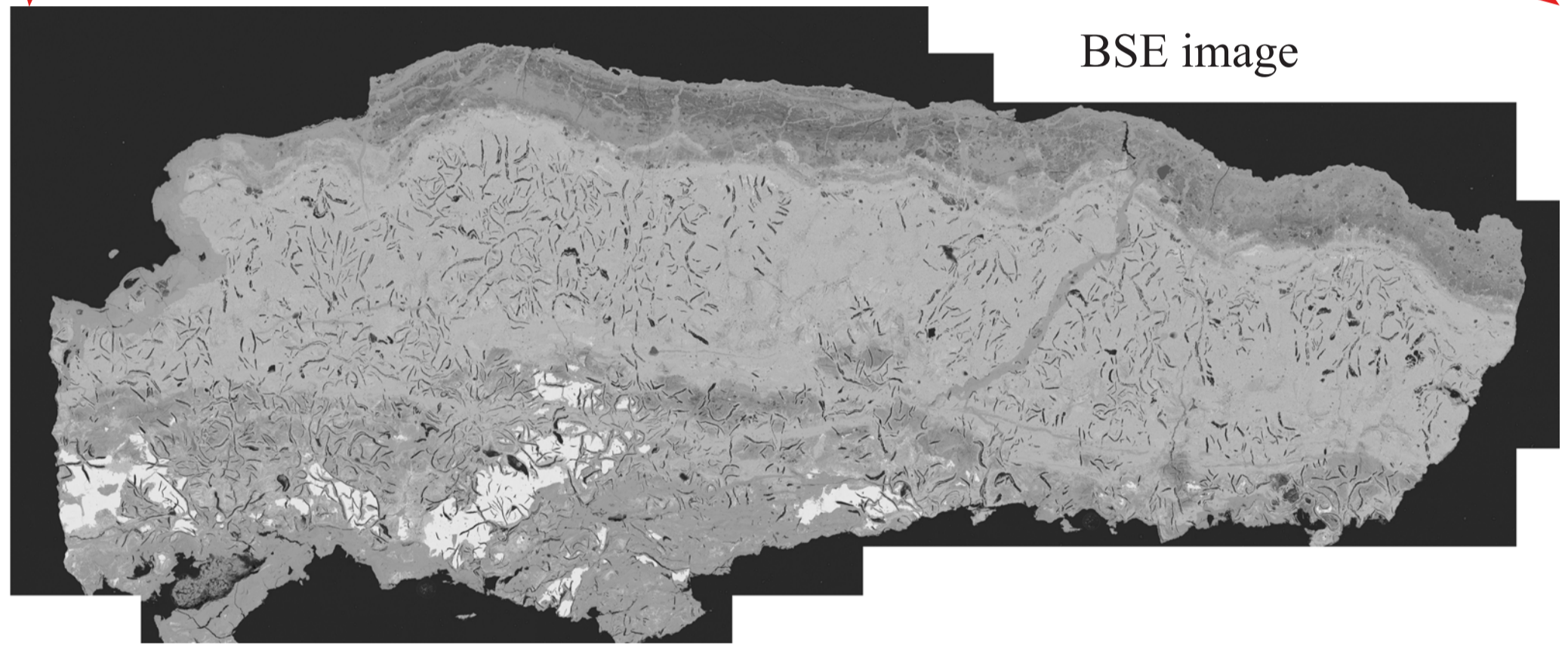
Mineral phases image

BMB5923

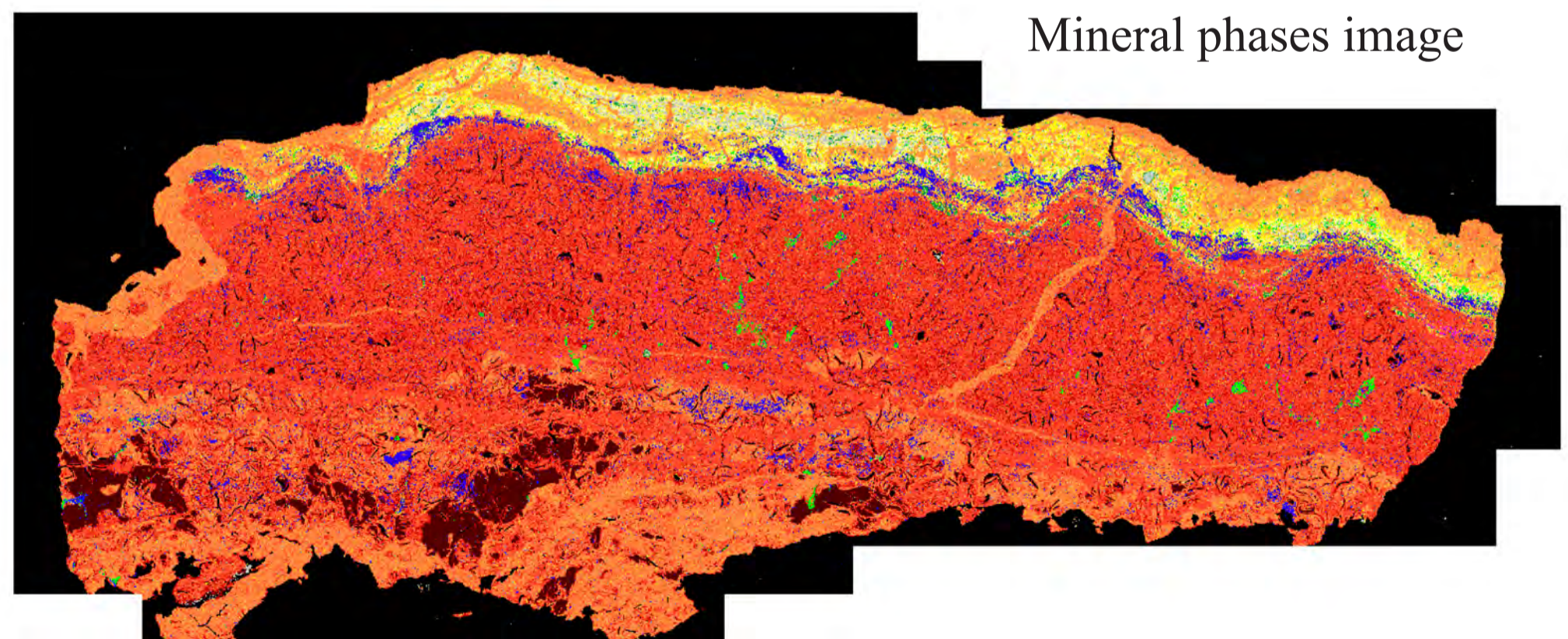
Optical microscopy image



BSE image



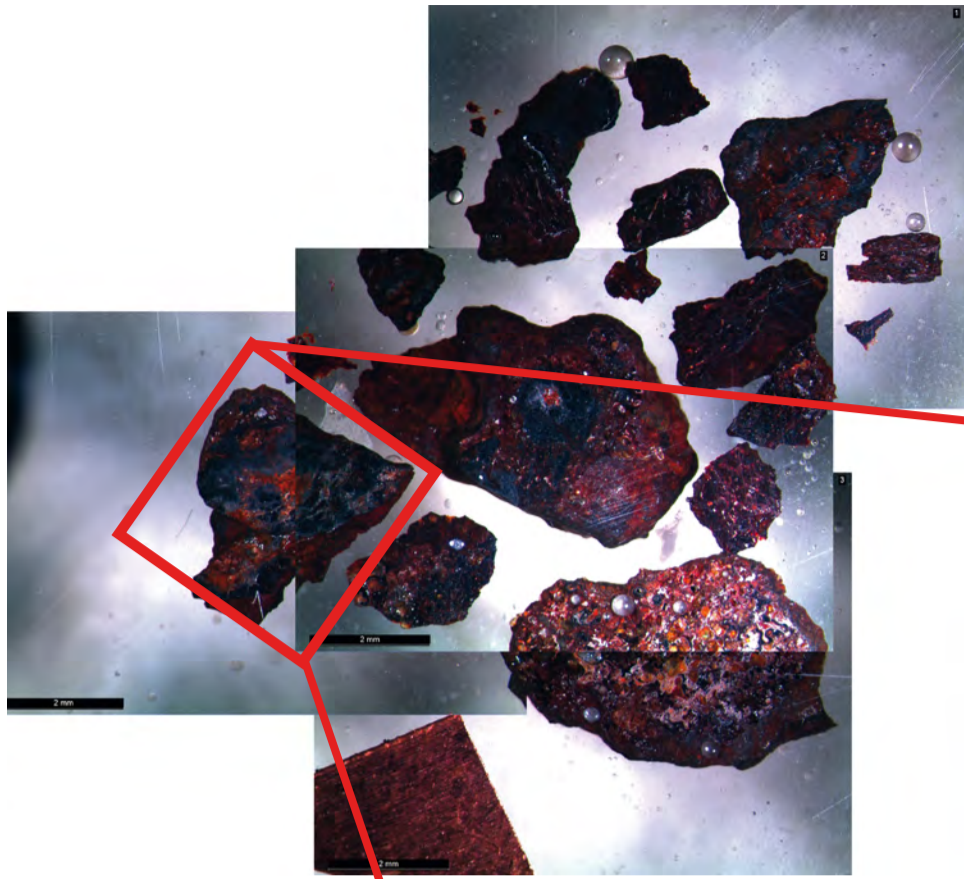
Mineral phases image



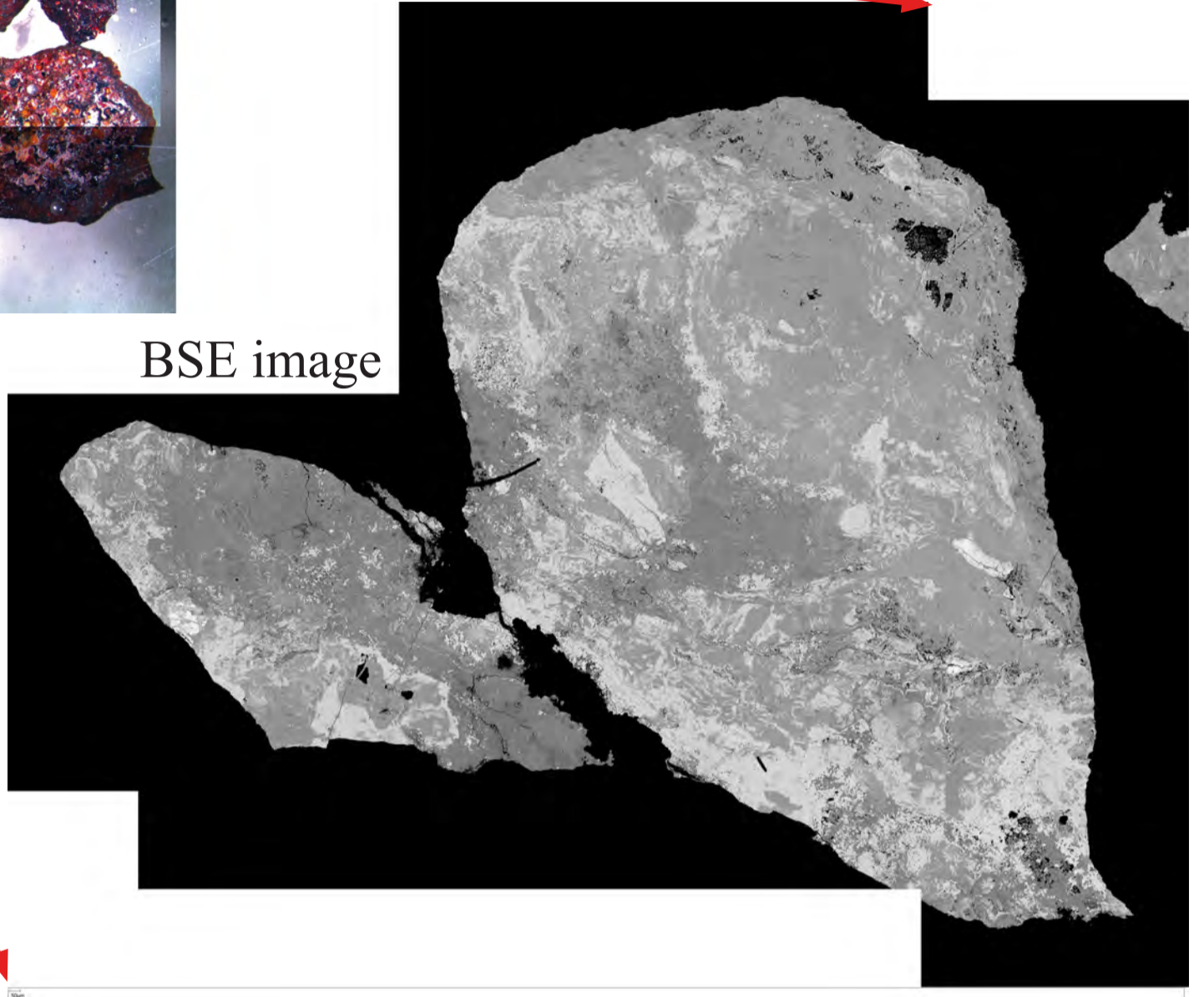
Chromium	FeO(Fe30-40)	FeO(Fe60-70)	FeO(Fe90-100)	Manganese	Sulphate/Sulphide	Vanadium
Copper	FeO(Fe40-50)	FeO(Fe70-80)	Fe-Si-O	Nickel	Tin	Zinc
Fe	FeO(Fe50-60)	FeO(Fe80-90)	Lead	Phosphate/phosphide	Titanium	Not Analysed

# BMB5930

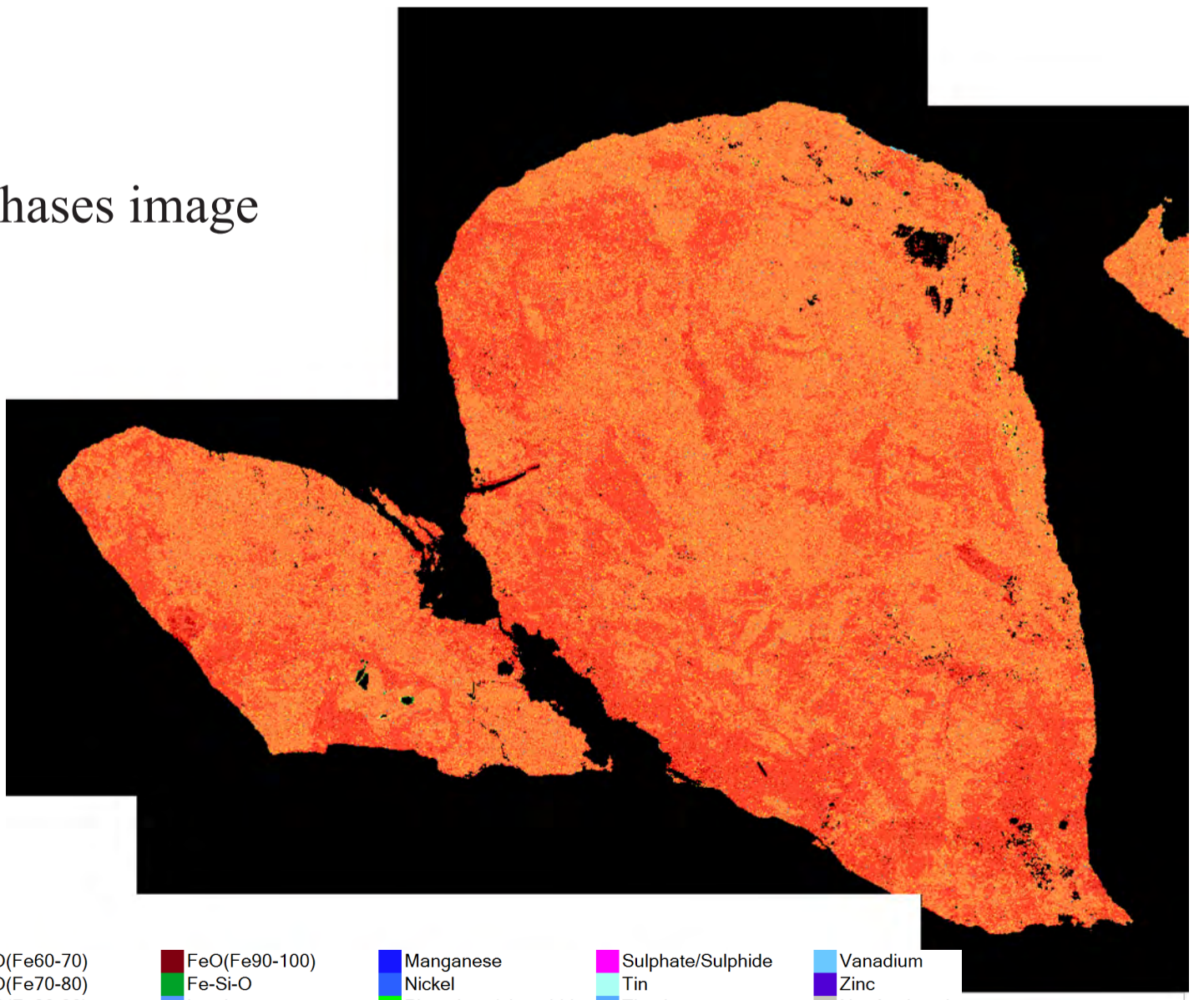
Optical microscopy image



BSE image

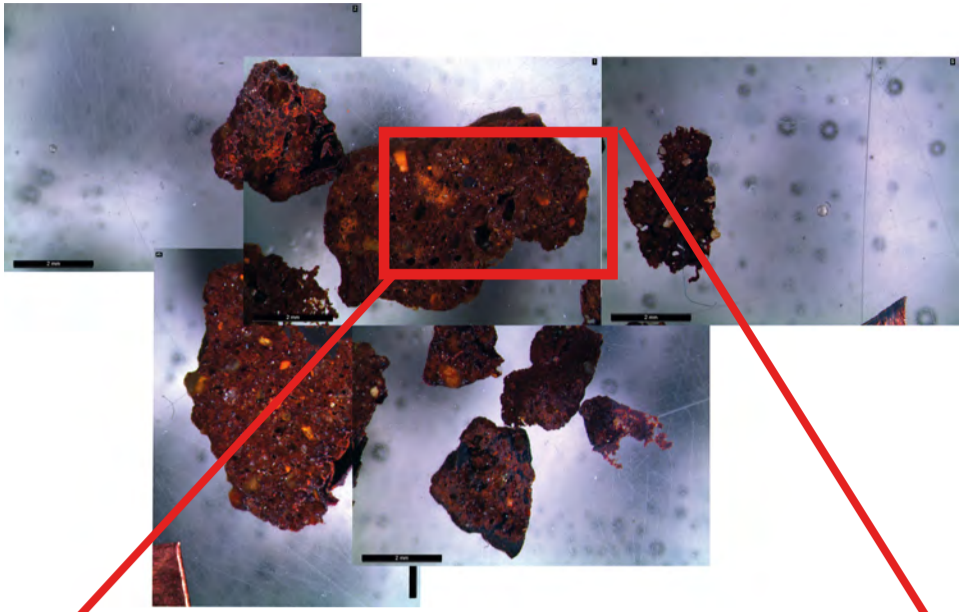


Mineral phases image



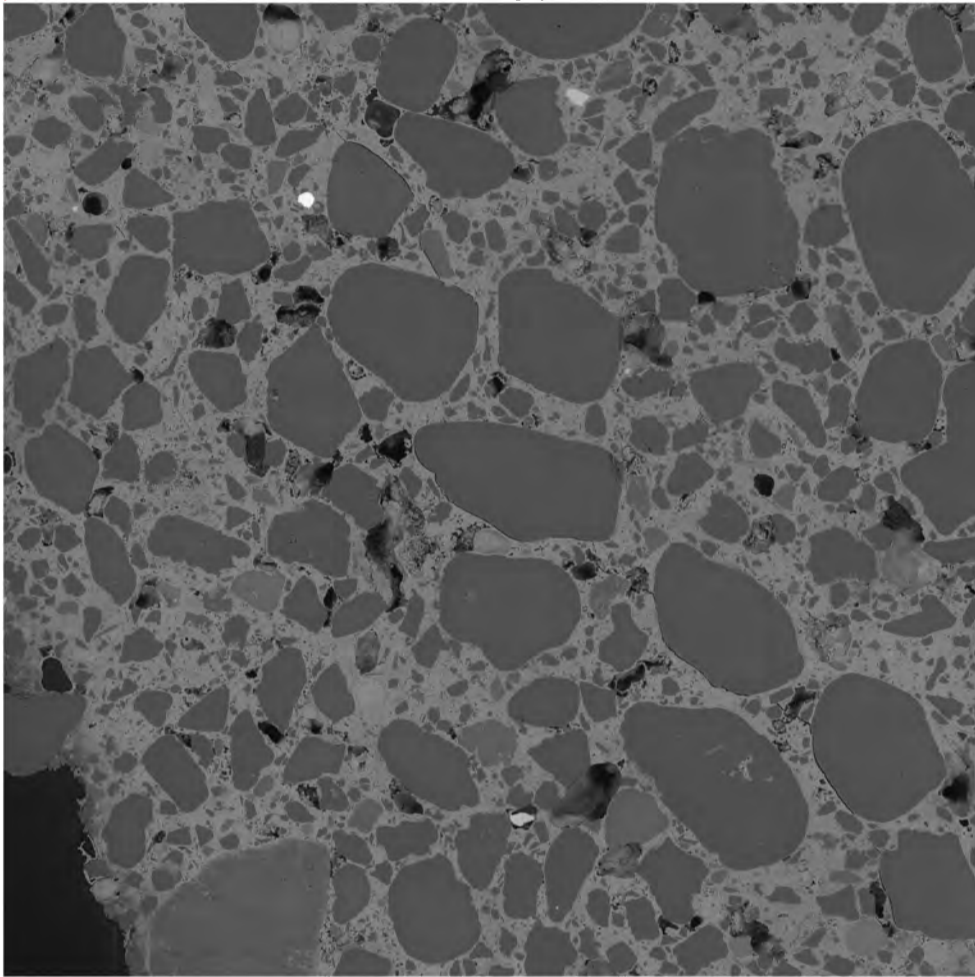
Chromium	FeO(Fe30-40)	FeO(Fe60-70)	FeO(Fe90-100)	Manganese	Sulphate/Sulphide	Vanadium
Copper	FeO(Fe40-50)	FeO(Fe70-80)	Fe-Si-O	Nickel	Tin	Zinc
Fe	FeO(Fe50-60)	FeO(Fe80-90)	Lead	Phosphate/phosphide	Titanium	Not Analysed

Optical microscopy image

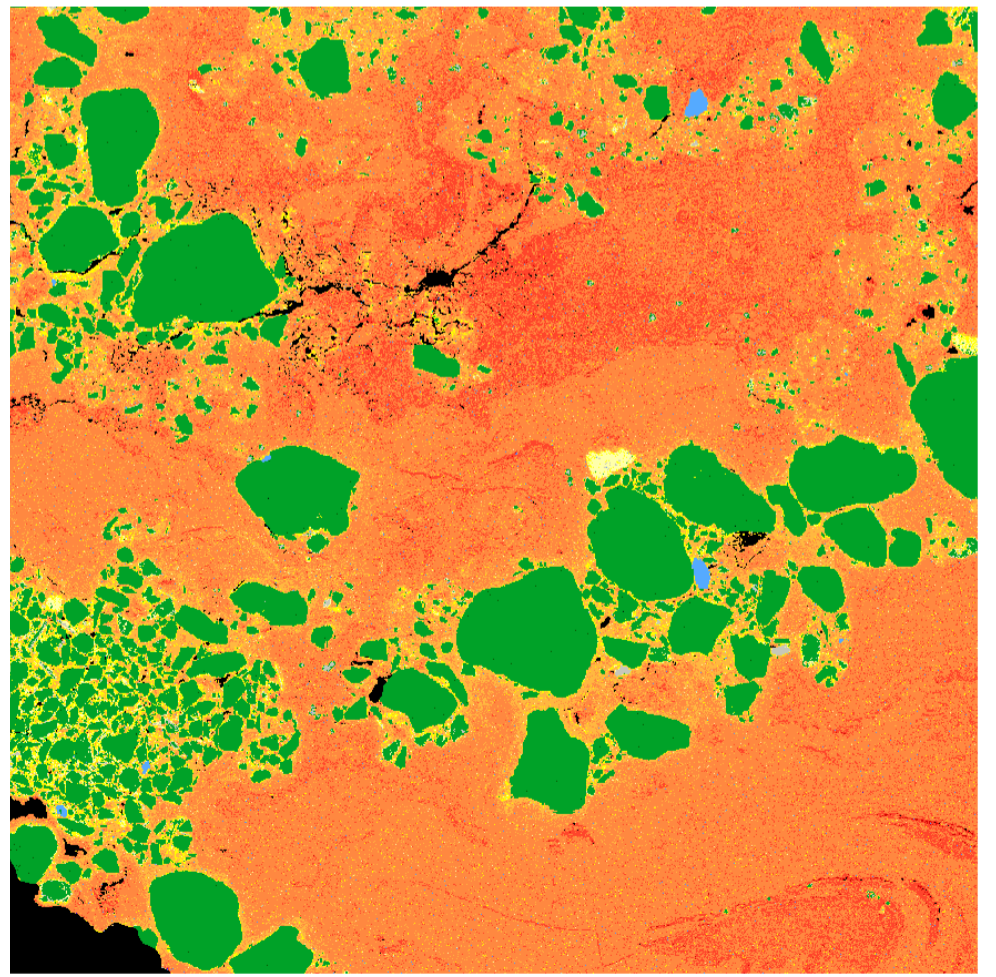
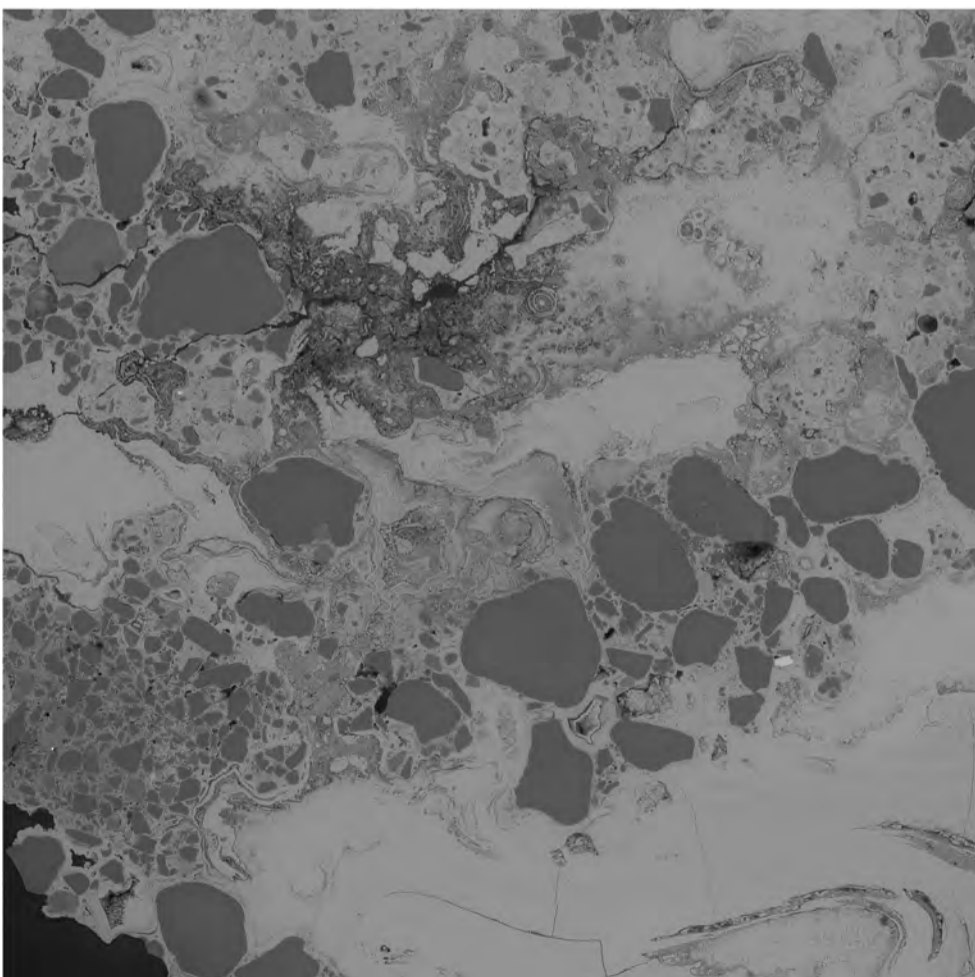
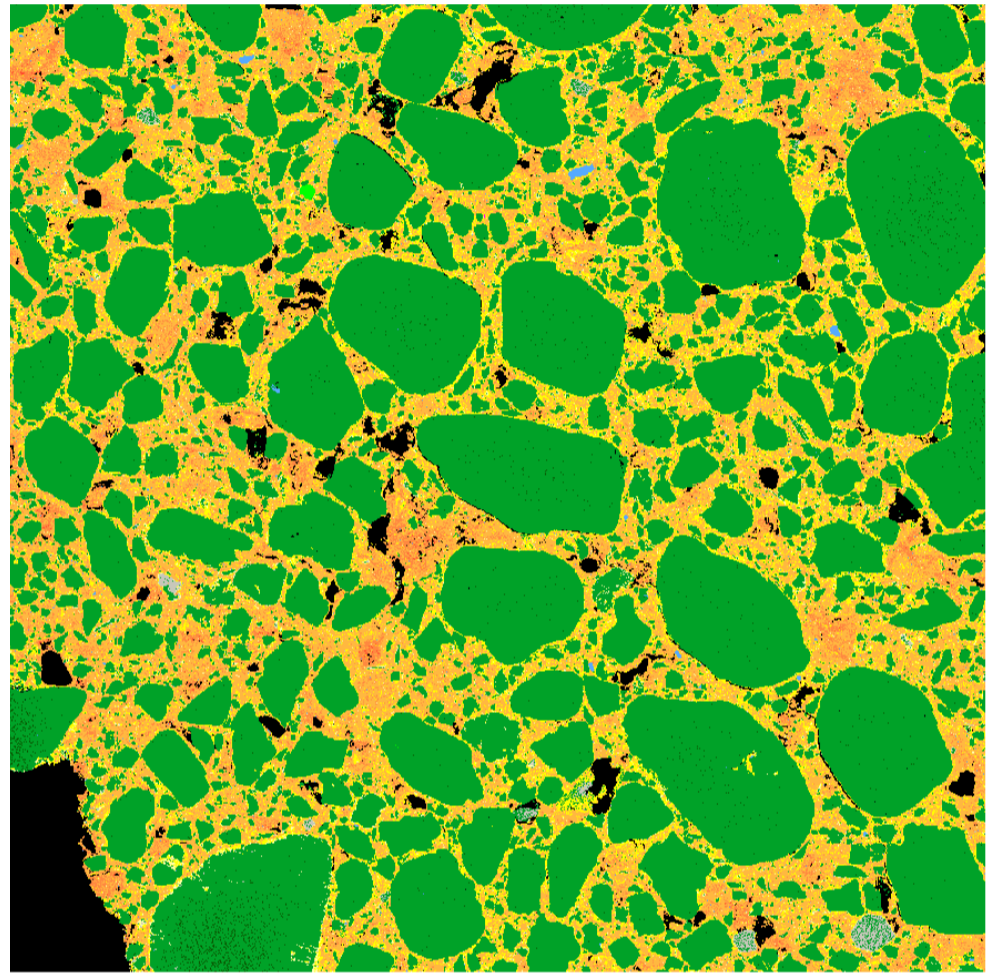


BMB5933

BSE images



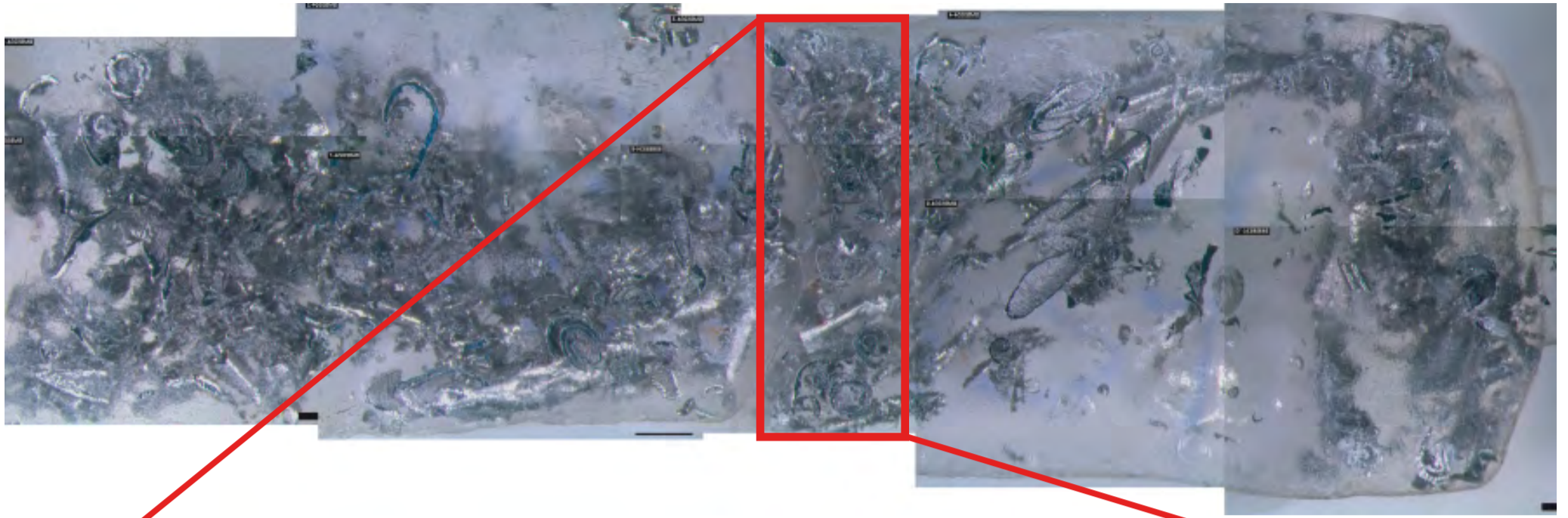
Mineral phases image



Chromium	FeO(Fe30-40)	FeO(Fe60-70)	FeO(Fe90-100)	Manganese	Sulphate/Sulphide	Vanadium
Copper	FeO(Fe40-50)	FeO(Fe70-80)	Fe-Si-O	Nickel	Tin	Zinc
Fe	FeO(Fe50-60)	FeO(Fe80-90)	Lead	Phosphate/phosphide	Titanium	Not Analysed

100µm

Optical microscopy image



BSE image



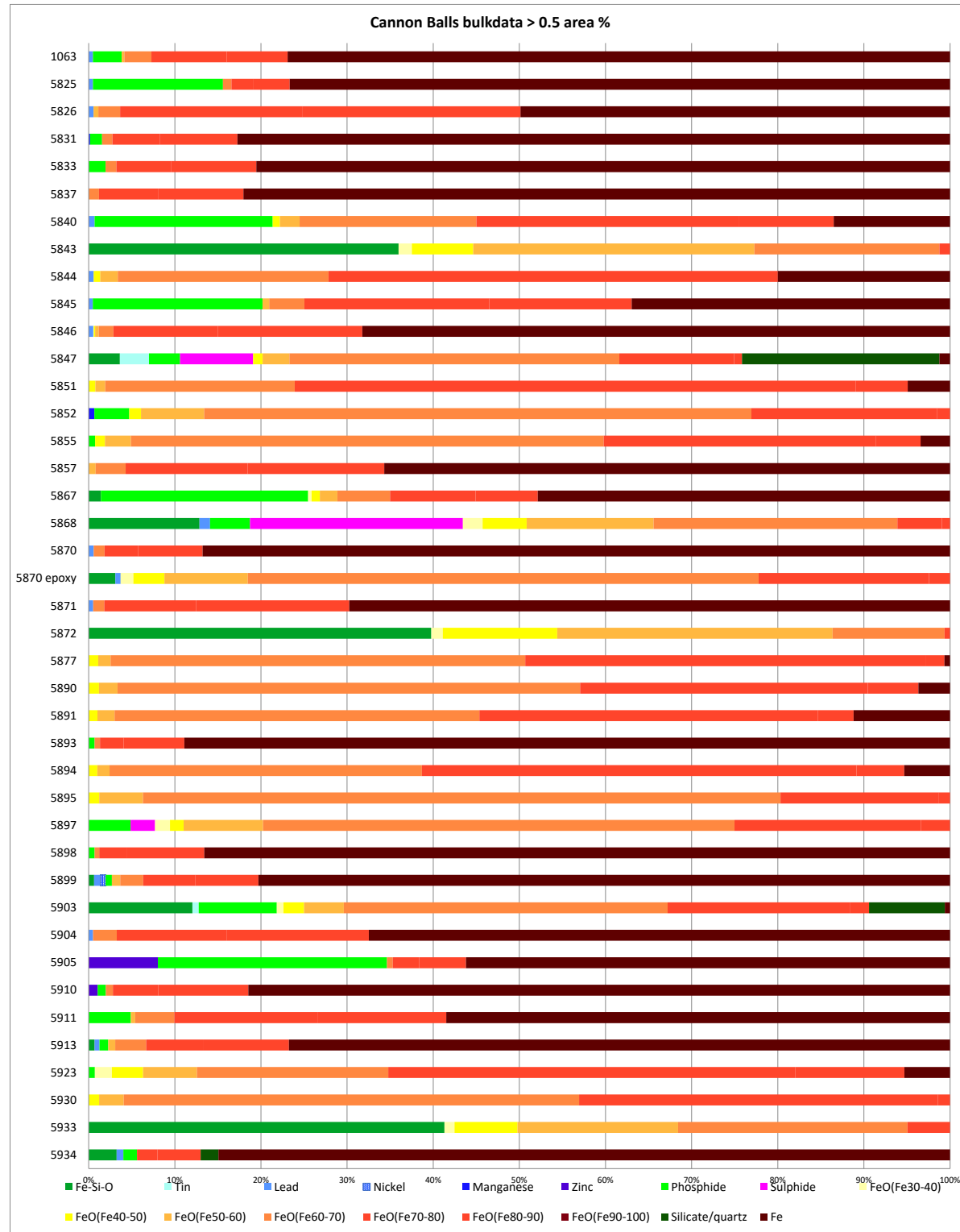
Mineral phases image



Chromium	FeO(Fe30-40)	FeO(Fe60-70)	FeO(Fe90-100)	Manganese	Sulphate/Sulphide	Vanadium
Copper	FeO(Fe40-50)	FeO(Fe70-80)	Fe-Si-O	Nickel	Tin	Zinc
Fe	FeO(Fe50-60)	FeO(Fe80-90)	Lead	Phosphate/phosphide	Titanium	Not Analysed

Appendix C - Bulk SEM data

	5934	5933	5930	5923	5913	5911	5910	5905	5904	5903	5899	5898	5897	5895	5894	5893	5891	5890	5877	5872	5871	5870 epoxy	5870	5868	5867	5857	5855	5852	5851	5847	5846	5845	5844	5843	5840	5837	5833	5831	5826	5825	1063				
Fe	77.52021553	0	0	5.310278	76.74708	58.48619	82.32867	61.10902	67.47945	0.599882	79.45084	86.58021	0	0	5.31909	88.32181	11.20277	3.669135	0.655547	0	69.74897	0	86.77664	0	47.86405	65.67895	3.4237	0	4.909277	1.240917	68.23129	36.95758	19.98831	0	13.49587	82.04109	80.54077	82.74479	49.87224	76.66237	76.90977				
FeO(Fe30-4)	1.158419	0	1.972687	0	0	0	0	0	0	0.772632	0	0	1.722653	0	0	0	0	0	0	0	1.333082	0	1.476648	0	2.28385	0.407073	0	0	0	0.04892	0	0	1.550246	0	0	0	0	0	0	0	0	0			
FeO(Fe40-5)	7.323726	1.203816	3.624167	0	0	0	0	0	2.385672	0	0	1.593454	1.229369	1.004302	0	1.020915	1.188012	1.106319	13.28525	0	3.605769	0	5.111474	0.957525	0	1.14707	1.364494	0.780801	1.103352	0.151652	0	0.75979	7.110139	0.831037	0	0	0	0	0	0	0	0			
FeO(Fe50-6)	18.63183	2.870206	6.252279	0.80262	0.502769	0	0	0	4.627058	0.974314	0	9.216193	5.072726	1.413284	0	1.984451	2.156766	1.434163	31.96455	0	9.684066	0	14.73627	2.031755	0.798972	3.022257	7.327877	1.129804	3.111776	0.428051	0.76686	2.030976	32.65209	2.291711	0	0	0	0.556547	0	0.311446	0	0			
FeO(Fe60-7)	0	26.6339	52.86825	22.21133	3.593339	4.549799	0.821017	0.733404	2.747143	37.58622	2.627694	0.540594	54.7373	74.01107	36.27027	0.626909	42.3485	53.70852	48.13953	12.99859	1.293169	59.30632	1.256874	28.30343	6.113881	3.491159	54.87859	63.54171	22.00398	38.30944	1.702419	4.093784	24.46669	21.48404	20.53212	1.192497	1.259439	1.203303	2.520214	0.993252	3.14041				
FeO(Fe70-8)	2.156334255	4.943802	41.6595	47.27853	6.591632	16.60971	5.346964	3.317454	12.79326	21.21922	5.96398	3.23789	21.66236	18.33708	50.45194	2.73268	39.3208	33.38887	46.54953	0.636132	10.67397	19.78022	3.92773	5.165851	9.9287	14.1557	31.57235	21.52498	65.11054	13.32816	12.10528	21.45356	37.5	1.215729	30.51516	6.913801	6.325072	5.5407	21.2083	2.570324	8.755083				
FeO(Fe80-9)	4.582210214	0	1.398224	12.63539	9.986623	14.95476	10.55309	5.915213	16.47082	2.173009	7.263065	8.95173	3.359173	1.349859	5.541118	6.984408	4.122571	5.8887	2.114912	0	17.76662	2.438187	7.462687	0.951604	7.22062	15.86827	5.213264	1.532448	6.065599	0.904702	16.78204	16.54426	14.66978	0.015509	10.96884	9.852613	9.913334	8.961856	25.27565	4.192888	7.055109				
FeO(Fe90-10)	0	0	0	0	0	0	0	0	0	0	0	0	0	0	0	0	0	0	0	0	0	0	0	0	0	0	0	0	0	0	0	0	0	0	0	0	0	0	0	0	0	0	0		
Fe-Si-O	2.964959721	41.30883	0	0	0.691914	0	0	0	0	12.03619	0.620018	0	0	0	0	0	0	0	0	0	39.7824	0	3.090659	0	12.86025	1.412392	0	0	0	0	0	0	3.618932	0	0	0	0	0	0	0	0	0	0	0	
Lead	0.700808642	0	0	0	0.558144	0	0	0	0.509324	0	0.708592	0	0	0	0	0	0	0	0	0	0.517268	0.576067	1.223491	0	0	0	0	0	0	0.540567	0.484211	0.584454	0	0.680517	0	0	0	0	0.567048	0.492835	0.497448	0	0		
Manganese	0	0	0	0	0	0	0	0	0	0	0	0	0	0	0	0	0	0	0	0	0	0	0	0	0	0	0	0	0	0	0	0	0	0	0	0	0	0	0	0	0	0	0		
Nickel	0	0	0	0	0	0	0	0	0	0	0.620018	0	0	0	0	0	0	0	0	0	0	0	0	0	0	0	0	0	0	0	0	0	0	0	0	0	0	0	0	0	0	0	0	0	
Phosphide	1.45525681	0	0	0.715342	1.028645	4.896762	0.950258	28.92491	0	9.062991	0.708592	0.689577	4.866494	0	0	0.68317	0	0	0	0	0	0	0	0	4.649266	24.06401	0	0.742768	4.044539	0	3.596394	0	19.69974	0	0	20.68476	0	1.961381	1.392057	0	15.08833	3.330738	0	0	
Silicate/qu.	1.88679254	0	0	0	0	0	0	0	0	8.796561	0	0	0	0	0	0	0	0	0	0	0	0	0	0	0	0	0	0	0	0	0	0	0	0	0	0	0	0	0	0	0	0	0	0	
Sulphide	0	0	0	0	0	0	0	0	0	0	0	0	2.842377	0	0	0	0	0	0	0	0	0	0	0	0	0	0	0	0	0	0	0	0	0	0	0	0	0	0	0	0	0	0	0	0
Tin	0	0	0	0	0	0	0	0	0	0.740552	0	0	0	0	0	0	0	0	0	0	0	0	0	0	0	0	0	0	0	0	0	0	0	0	0	0	0	0	0	0	0	0	0	0	
Zinc	0	0	0	0	0	0	1.063	8.733	0	0	0	0	0	0	0	0	0	0	0	0	0	0	0	0	0	0	0	0	0	0	0	0	0	0	0	0	0	0	0	0	0	0	0	0	





#### Appendix D. LA-SF-ICP-MS operating and data acquisition parameters

<b>Laser ablation system</b>	<b>New Wave Research NWR213 solid state Nd:YAG laser with aperture imaging</b>
Laser wavelength	213 nm (Nd:YAG)
Laser mode	Q-switched (Nd:YAG)
Nominal pulse width	4 ns (Nd:YAG)
Repetition rate	10 Hz
Spot sizes (diameter)	25 $\mu\text{m}$
Energy density on sample	3.4-3.5 J/cm <sup>2</sup> (homogenized energy distribution)
Ablation cell	standard TV2 cell with custom sample holder
Ablation cell gas flow rates	421-481 ml/min He
Tubing for gas flow	Tygon S3 B44-3 and S-50 HL
Laser beam focus	Fixed at sample surface

<b>ICP-MS</b>	<b>Thermo-Fisher Scientific ELEMENT 2 double-focusing magnetic sector-field ICP-MS with Jet interface system</b>
Interface cones	Ni Jet sampler (X-cone) and H-type skimmer cone
Detector type	single-collector discrete dynode electron multiplier
Detector mode	cross-calibrated pulse counting and analogue
Detector vacuum	10 <sup>-7</sup> mbar (during analysis)
Mass resolution	300 (low resolution)
Scan type	E-scan
Detection mode	Both
Integration type	Average
Aquisition mode	Time resolved analysis
Argon gas flow rates (l/min):	
Plasma	16
Auxiliary	0.70
Sample	0.896-0.902
RF power	1400 W
Lenses (V):	
Extraction	-2000
Focus	-848
X-Deflection	2.00
Y-Deflection	-4.25
Shape	120
SEM potential	2500 V

<b>Data acquisition and processing</b>	
Isotopes measured	<sup>45</sup> Sc, <sup>47</sup> Ti, <sup>51</sup> V, <sup>53</sup> Cr, <sup>55</sup> Mn, <sup>57</sup> Fe, <sup>59</sup> Co, <sup>65</sup> Cu, <sup>66</sup> Zn, <sup>95</sup> Mo, <sup>120</sup> Sn, <sup>121</sup> Sb, <sup>139</sup> La, <sup>140</sup> Ce, <sup>141</sup> Pr, <sup>146</sup> Nd, <sup>147</sup> Sm, <sup>153</sup> Eu, <sup>157</sup> Gd, <sup>159</sup> Tb, <sup>163</sup> Dy, <sup>165</sup> Ho, <sup>166</sup> Er, <sup>169</sup> Tm, <sup>172</sup> Yb, <sup>175</sup> Lu, <sup>178</sup> Hf, <sup>182</sup> W, <sup>202</sup> Hg, <sup>208</sup> Pb
Sampling time (ms)	10 ms for all elements except the lanthanides (La-Lu, 15 ms) and Hf (15 ms)
Search & integration window (%/%)	0/80 for all elements
Samples per peak	10 for all elements
Oxide production rate	Tuned to $\leq 0.1\%$ UO <sub>2</sub> ( <sup>254</sup> UO <sub>2</sub> / <sup>238</sup> U)
Analysis duration	Preablation (5 impulses) followed by 60 s. blank, 40 s. ablation and 40 s. washout.
Software for data reduction	lolite vers. 2.5 (Hellstrom et al. 2008)
External standardization	BCR-2 (glass) as primary standard with NIST-612, NIST-614, BHVO2 glasses and the E363 pressed powder pellet as secondary standards. E363 was also used to verify the FeO concentration of BCR-2 and the other standards.
Internal standard isotopes	<sup>57</sup> Fe





BM5837	Zircon_Sample-182-FIN2	Fe-rich	70000	-0.17	0.14	1100	2200	290	410	25	10	1600	3400	12.6	1.5	15.2	1.7	4.4	0.47	35	31	0.63	0.32	7.6	2.4	-0.018	0.019	0.013	0.029	-0.004	0.015	-0.005	0.027	-0.00309	0.0009	-0.00046	0.00013	0.17	0.44	0.013	0.043	-0.013	0	0.0038	0.0099	0.015	0.075	0.0025	0.0054	0.022	0.05	0.0073	0.0091	0.045	0.058	3.3	2.1	60	180	0.057	0.028
--------	------------------------	---------	-------	-------	------	------	------	-----	-----	----	----	------	------	------	-----	------	-----	-----	------	----	----	------	------	-----	-----	--------	-------	-------	-------	--------	-------	--------	-------	----------	--------	----------	---------	------	------	-------	-------	--------	---	--------	--------	-------	-------	--------	--------	-------	------	--------	--------	-------	-------	-----	-----	----	-----	-------	-------

\* Fe is used as internal standard reference, thus of assumed abundance, here set to FeO = 96 with FeO for FeO-100 phases, and then use FeO = FeO3 = 0.8981.

BM5840	Zircon_Sample-247-FIN2	Fe-rich	70000	0.13	0.12	168	49	80	30	142	35	840	870	6420	550	20900	3200	177	39	14.11	0.63	6	2.9	35	16	1.08	0.12	2.46	0.76	0.254	0.079	1.31	0.27	0.191	0.039	0.013	0.013	0.28	0	0.026	0.012	0.227	0	0.04	0.017	0.1	0.051	0.013	0.0068	0.046	0.033	0.009	0.003	0.047	0.048	4.28	0.61	1700	380	7.8	2.4
--------	------------------------	---------	-------	------	------	-----	----	----	----	-----	----	-----	-----	------	-----	-------	------	-----	----	-------	------	---	-----	----	----	------	------	------	------	-------	-------	------	------	-------	-------	-------	-------	------	---	-------	-------	-------	---	------	-------	-----	-------	-------	--------	-------	-------	-------	-------	-------	-------	------	------	------	-----	-----	-----

BM5840	Zircon_Sample-248-FIN2	Fe-rich	70000	0.082	0.086	57	63	83	107	142	35	840	870	6420	550	20900	3200	177	39	14.11	0.63	6	2.9	35	16	1.08	0.12	2.46	0.76	0.254	0.079	1.31	0.27	0.191	0.039	0.013	0.013	0.28	0	0.026	0.012	0.227	0	0.04	0.017	0.1	0.051	0.013	0.0068	0.046	0.033	0.009	0.003	0.047	0.048	4.28	0.61	1700	380	7.8	2.4
--------	------------------------	---------	-------	-------	-------	----	----	----	-----	-----	----	-----	-----	------	-----	-------	------	-----	----	-------	------	---	-----	----	----	------	------	------	------	-------	-------	------	------	-------	-------	-------	-------	------	---	-------	-------	-------	---	------	-------	-----	-------	-------	--------	-------	-------	-------	-------	-------	-------	------	------	------	-----	-----	-----

\* Fe is used as internal standard reference, thus of assumed abundance, here set to FeO = 96 with FeO for FeO-100 phases, and then use FeO = FeO3 = 0.8981.

BM5844	Zircon_Sample-189-FIN2	Fe-rich	70000	0.075	0.04	7.6	8.3	12.8	8.8	5.09	9.4	11.4	8.5	9.1	2.4	46	19	8	10	30.4	1.6	6.4	0.88	30	6.1	-0.0061	0.0006	-0.002	0.01	0.0018	0.005	0.019	0.006	0.01	0.013	0.004	0.014	0.04	0.096	0.0099	0.0024	-0.008	0	-0.00036	0.00089	0.0005	0.0076	0.0027	0.0022	0.011	0.023	0.0028	0.0079	-0.0005	0.00055	0.011	0.65	830	130	0.383	0.074
--------	------------------------	---------	-------	-------	------	-----	-----	------	-----	------	-----	------	-----	-----	-----	----	----	---	----	------	-----	-----	------	----	-----	---------	--------	--------	------	--------	-------	-------	-------	------	-------	-------	-------	------	-------	--------	--------	--------	---	----------	---------	--------	--------	--------	--------	-------	-------	--------	--------	---------	---------	-------	------	-----	-----	-------	-------

\* Fe is used as internal standard reference, thus of assumed abundance, here set to FeO = 96 with FeO for FeO-100 phases, and then use FeO = FeO3 = 0.8981.

BM5844	Zircon_Sample-190-FIN2	Fe-rich	70000	0.005	0.045	13.8	6.5	8.9	9.8	7	3.5	17.9	3.5	2.09	0.68	67	15	2.99	0.69	57.8	6.3	11.3	1.1	141	35	0.006	0.026	0.004	0.009	0.074	0.006	0.009	0.015	0.048	0.013	0.003	0.009	-0.1	0.2	-0.0032	0.0028	-0.002	0.003	0.0023	-0.018	0.0079	-0.00007	0.00062	0.011	0.025	0.001	0.004	-0.0005	0.00055	0.011	0.65	830	130	0.383	0.074
--------	------------------------	---------	-------	-------	-------	------	-----	-----	-----	---	-----	------	-----	------	------	----	----	------	------	------	-----	------	-----	-----	----	-------	-------	-------	-------	-------	-------	-------	-------	-------	-------	-------	-------	------	-----	---------	--------	--------	-------	--------	--------	--------	----------	---------	-------	-------	-------	-------	---------	---------	-------	------	-----	-----	-------	-------

BM5844	Zircon_Sample-191-FIN2	Fe-rich	70000	0.032	0.039	18.1	9.5	9.1	25	9.4	3.4	69	2.8	2.18	0.77	170	48	1.9	7	10	24.3	2.8	31	59	18	0.006	0.01	0.013	0.027	0.0043	-0.014	0.008	0.009	0.011	0.041	0.048	-0.04	0.12	0.015	0.0046	-0.004	0	0.0017	0.004	0.002	0.014	0.00048	0.00018	0.0017	0.001	0.22	0.39	210	400	0.36	0.2
--------	------------------------	---------	-------	-------	-------	------	-----	-----	----	-----	-----	----	-----	------	------	-----	----	-----	---	----	------	-----	----	----	----	-------	------	-------	-------	--------	--------	-------	-------	-------	-------	-------	-------	------	-------	--------	--------	---	--------	-------	-------	-------	---------	---------	--------	-------	------	------	-----	-----	------	-----



Table with 28 columns: BM1587, Zircon\_Sample-078.FIN2, Fe-rich, 70000, 4.6, 8, 140, 130, 7.8, 4.6, -13, 34, 1340, 200, 4.9, 4.3, 1.29, 0.54, 12.3, 4, 4, 0.7, 1.7, -0.2, 0.49, 0.39, 0.3, 1.35, 0.58, 4.1, 1.5, 0.51, 0.23, 3.4, 1.2, 0.7, 0.43, 0.13, 0.11, 0.9, 0.67, 0.057, 0.084, 0.32, 0, 0.18, 0.17, 0.25, 0.16, 0.13, 0.2, 0.41, 0.38, 0.021, 0.023, 0.28, 0.44, 0.48, 0.36, 140, 180, 0.93, 0.41

\* Fe is used as internal standard reference, thus of assumed abundance, here set to FeO = 56 wt% FeO for FeO-100 phases, and then use FeO + Fe2O3 = 0.89881.

Table with columns: BM1585, Analysis#, Phase, [CONCENTRATIONS], and 48 columns of numerical data.

\* Fe is used as internal standard reference, thus of assumed abundance, here set to FeO = 56 wt% FeO for FeO-100 phases, and then use FeO + Fe2O3 = 0.89881.

Table with columns: BM1582, Analysis#, Phase, [CONCENTRATIONS], and 48 columns of numerical data.

\* Fe is used as internal standard reference, thus of assumed abundance, here set to FeO = 56 wt% FeO for FeO-100 phases, and then use FeO + Fe2O3 = 0.89881.

Table with columns: BM1585, Analysis#, Phase, [CONCENTRATIONS], and 48 columns of numerical data.







BM5872	Zircon_Sample_201.FIN2	70000	70000	34000	40000	55000	-7000	17000	-50000	25000	-14000	79000	18000	46000	14000	13000	-1300	13000	25000	40000	17000	-2100	4200	2100	2100	1700	600	1300	-1800	2300	40000	8000	120	200	-1100	8100	-700	2100	-300	-240	-480	-1100	3600	13	39	1200	3300	-400	1100	-6000	10000	-600	3900	110	170	0	2700
BM5872	Zircon_Sample_202.FIN2	70000	40000	14000	60000	130000	-500	13000	-19000	25000	-14000	79000	18000	46000	14000	13000	-1300	13000	25000	40000	17000	-2100	4200	2100	2100	1700	600	1300	-1800	2300	40000	8000	120	200	-1100	8100	-700	2100	-300	-240	-480	-1100	3600	13 <td>39</td> <td>1200</td> <td>3300</td> <td>-400</td> <td>1100</td> <td>-6000</td> <td>10000</td> <td>-600</td> <td>3900</td> <td>110</td> <td>170</td> <td>0</td> <td>2700</td>	39	1200	3300	-400	1100	-6000	10000	-600	3900	110	170	0	2700

\* Fe is used as internal standard reference, thus of assumed abundance, here set to FeO = 96 wt% FeO for FeO30 phases, and then use FeO = Fe2O3 + 0.89881.

BM5877	Analysis #	Phase	Fe [ppm]	Zr [ppm]	U [ppm]	Th [ppm]	Pa [ppm]	Sc [ppm]	Y [ppm]	Hf [ppm]	Ta [ppm]	Nb [ppm]	K [ppm]	Ca [ppm]	Mg [ppm]	Al [ppm]	Si [ppm]	Ti [ppm]	Mn [ppm]	Fe [ppm]	Zr [ppm]	U [ppm]	Th [ppm]	Pa [ppm]	Sc [ppm]	Y [ppm]	Hf [ppm]	Ta [ppm]	Nb [ppm]	K [ppm]	Ca [ppm]	Mg [ppm]	Al [ppm]	Si [ppm]	Ti [ppm]	Mn [ppm]	Fe [ppm]	Zr [ppm]	U [ppm]	Th [ppm]	Pa [ppm]	Sc [ppm]	Y [ppm]	Hf [ppm]	Ta [ppm]	Nb [ppm]	K [ppm]	Ca [ppm]	Mg [ppm]	Al [ppm]	Si [ppm]	Ti [ppm]	Mn [ppm]	Fe [ppm]	Zr [ppm]	U [ppm]	Th [ppm]	Pa [ppm]	Sc [ppm]	Y [ppm]	Hf [ppm]	Ta [ppm]	Nb [ppm]	K [ppm]	Ca [ppm]	Mg [ppm]	Al [ppm]	Si [ppm]	Ti [ppm]	Mn [ppm]
BM5877	Zircon_Sample_007.FIN2	Fe-rich	70000	0.011	0.092	12	6.6	60.9	4.1	33.8	3.7	656	34	13.37	0.35	20.5	2.3	0.42	0.41	26.8	1.8	1.88	0.64	2.09	0.51	0.06	0.14	0.011	0.073	0.007	0.012	0.011	0.004	-0.016	0.044	0.024	0.02	-0.28	0.49	-0.017	0.019	0.11	0	0.006	0.012	0.09	0.17	0.0031	0.0066	0.012	0.037	0.016	0.022	-0.086	0.051	1.36	0.33	132	54	0.028	0.18									

\* Fe is used as internal standard reference, thus of assumed abundance, here set to FeO = 96 wt% FeO for FeO30 phases, and then use FeO = Fe2O3 + 0.89881.

BM5880	Analysis #	Phase	Fe [ppm]	Zr [ppm]	U [ppm]	Th [ppm]	Pa [ppm]	Sc [ppm]	Y [ppm]	Hf [ppm]	Ta [ppm]	Nb [ppm]	K [ppm]	Ca [ppm]	Mg [ppm]	Al [ppm]	Si [ppm]	Ti [ppm]	Mn [ppm]	Fe [ppm]	Zr [ppm]	U [ppm]	Th [ppm]	Pa [ppm]	Sc [ppm]	Y [ppm]	Hf [ppm]	Ta [ppm]	Nb [ppm]	K [ppm]	Ca [ppm]	Mg [ppm]	Al [ppm]	Si [ppm]	Ti [ppm]	Mn [ppm]	Fe [ppm]	Zr [ppm]	U [ppm]	Th [ppm]	Pa [ppm]	Sc [ppm]	Y [ppm]	Hf [ppm]	Ta [ppm]	Nb [ppm]	K [ppm]	Ca [ppm]	Mg [ppm]	Al [ppm]	Si [ppm]	Ti [ppm]	Mn [ppm]	Fe [ppm]	Zr [ppm]	U [ppm]	Th [ppm]	Pa [ppm]	Sc [ppm]	Y [ppm]	Hf [ppm]	Ta [ppm]	Nb [ppm]	K [ppm]	Ca [ppm]	Mg [ppm]	Al [ppm]	Si [ppm]	Ti [ppm]	Mn [ppm]
BM5880	Zircon_Sample_072.FIN2	Fe-rich	70000	0.04	0.13	0	1.6	14.1	2.3	1.3	1.4	311	20	12.75	0.82	11.2	8	2.1	0.69	1.7	1.5	8.59	0.57	9.3	1.7	0.09	0.13	0.012	0.033	0.004	0.018	0.01	0.17	0.044	0.099	0.025	0.027	0.02	0.19	0.042	0.065	0.02	0	0.047	0.008	0.042	0.095	0.014	0.013	-0.0084	0.0016	0.009	0.014	0.03	0.03	111	11.1	1.6	120	160	0.044	0.058								

\* Fe is used as internal standard reference, thus of assumed abundance, here set to FeO = 96 wt% FeO for FeO30 phases, and then use FeO = Fe2O3 + 0.89881.

BM5881	Analysis #	Phase	Fe [ppm]	Zr [ppm]	U [ppm]	Th [ppm]	Pa [ppm]	Sc [ppm]	Y [ppm]	Hf [ppm]	Ta [ppm]	Nb [ppm]	K [ppm]	Ca [ppm]	Mg [ppm]	Al [ppm]	Si [ppm]	Ti [ppm]	Mn [ppm]	Fe [ppm]	Zr [ppm]	U [ppm]	Th [ppm]	Pa [ppm]	Sc [ppm]	Y [ppm]	Hf [ppm]	Ta [ppm]	Nb [ppm]	K [ppm]	Ca [ppm]	Mg [ppm]	Al [ppm]	Si [ppm]	Ti [ppm]	Mn [ppm]	Fe [ppm]	Zr [ppm]	U [ppm]	Th [ppm]	Pa [ppm]	Sc [ppm]	Y [ppm]	Hf [ppm]	Ta [ppm]	Nb [ppm]	K [ppm]	Ca [ppm]	Mg [ppm]	Al [ppm]	Si [ppm]	Ti [ppm]	Mn [ppm]	Fe [ppm]	Zr [ppm]	U [ppm]	Th [ppm]	Pa [ppm]	Sc [ppm]	Y [ppm]	Hf [ppm]	Ta [ppm]	Nb [ppm]	K [ppm]	Ca [ppm]	Mg [ppm]	Al [ppm]	Si [ppm]	Ti [ppm]	Mn [ppm]
BM5881	Zircon_Sample_007.FIN2	Fe-rich	70000	-0.128	0.072	4.6	3	5.35	0.33	3.6	1.5	7330	260	4.33	1	2.12	0.92	1.47	0.59	3.06	0.91	0.9	0.72	9.9	1	-0.021	0.054	0.009	0.022	-0.006	0.013	0.002	0.096	0.17	0.021	0.029	0.28	0.39	-0.027	0.026	-0.044	0	-0.01	0.012	0.05	0.11	0.004	0.0082	0.032	0.061	0.008	0.011	0.035	0.082	1.02	0.25	90	110	0.115	0.068										

Sample	Analysis #	Phase	Fe [ppm]	Zn [ppm]	Zr [ppm]	... (total 44 elements)																																																								
BMB891	Zrcon_Sample-048.FIN2	Fe-rich	70000	0.18	0.11	1.2	1.8	3.4	1.3	6.1	1.3	18700	400	4.66	0.76	3.96	0.69	1.2	0.62	0.7	1.5	0.51	0.14	3.5	0.49	0.05	0.17	-0.011	0.041	0.002	0.042	0.02	0.15	-0.003	0.088	0.026	0.062	0.5	0.15	0.032	0.032	0	0	0.1311	0.0078	0.008	0.08	0.16	0.018	0.028	0.028	0.04	0.14	0.2	0.1	0.17	1.13	0.24	-40	110	0.1	0.12
BMB891	Zrcon_Sample-049.FIN2	Fe-rich	70000	0.012	0.029	35.9	7.6	20.3	2.6	8.31	0.7	13700	1200	13.02	0.69	14.6	6	0.19	0.19	4.3	1	0.75	0.12	21.9	1.7	-0.001	0.017	0.008	0.015	0.003	0.0039	-0.026	0.071	0.013	0.285	0.026	0.002	0.076	0.085	-0.0055	0.066	0.036	0	0	0.076	0.0088	0.006	0.006	0.042	0.002	0.026	0.008	0.003	-0.013	0.012	3.3	0.65	170	230	0.42	0.12	

\* Fe is used as internal standard reference, thus of assumed abundance, here set to Fe0 = 96 with Fe0 for FeH90-100 phases, and then use Fe0 = Fe203 = 8.9981.

Sample	Analysis #	Phase	Fe [ppm]	Zn [ppm]	Zr [ppm]	... (total 44 elements)																																																						
BMB891	Zrcon_Sample-247.FIN2	Fe-rich	70000	0	0.11	4.8	1.6	23.4	1.9	18.1	2.4	54	11.7	1.6	16.5	1.9	1.5	1.2	6.38	0.47	0.79	0.39	0.19	1.71	0.16	0.04	0.013	-0.049	0.044	0.018	0.02	0.2	0.1	0.045	0.097	0.01	0.41	0.43	-0.054	0.046	-0.068	0	0	0.027	0.01	0.29	-0.038	0.0078	0.08	0.042	0.028	0.048	-0.053	0.08	0.989	0.09	16	0.1	0.1	0.01
BMB891	Zrcon_Sample-248.FIN2	Fe-rich	70000	-0.02	0.12	15.6	7.8	70	11	33.3	4	630	42	12.2	1.2	10.39	0.99	2.47	0.69	18.8	1.1	0.86	0.5	3.3	0.46	-0.009	0.079	0.018	0.07	0.012	0.028	0.013	0.1	0.048	0.043	0.012	0.11	0.1	0.166	0.048	0.002	-0.02	0.1	0.1	0.024	0.055	0.042	0.11	0.11	0.02	0.09	2.1	0.84	77	0.7	0.3	0.019			

\* Fe is used as internal standard reference, thus of assumed abundance, here set to Fe0 = 96 with Fe0 for FeH90-100 phases, and then use Fe0 = Fe203 = 8.9981.

Sample	Analysis #	Phase	Fe [ppm]	Zn [ppm]	Zr [ppm]	... (total 44 elements)																																																							
BMB894	Zrcon_Sample-007.FIN2	Fe-rich	70000	0.092	0.52	12.4	2.1	21.1	6.2	20.7	2.5	12600	1600	27.1	6	35.3	7	0.86	0.36	2.57	0.73	1.45	0.49	42.7	8.7	0.006	0.033	0.003	0.017	-0.014	0.016	0.035	0.061	0.06	0.54	-0.0086	0.0028	-0.24	0.27	0.008	0.025	0.01	0.048	0.0095	-0.001	0.093	0.023	0.049	0.029	0.023	0.046	0.0061	-0.003	0.021	4.6	1.4	70	180	0.12	0.19	
BMB894	Zrcon_Sample-008.FIN2	Fe-rich	70000	0.028	0.075	20.8	8	36.8	4.7	23.8	5.1	10000	1500	25	26	47	19	0.69	0.11	6.2	2.6	2.8	1.1	31	20	0.033	0.009	0.012	0.025	0.0015	0.0079	-0.02	0.11	0	0.044	0.009	0.008	-0.14	0.22	-0.006	0.013	0.027	0	0.012	0.009	-0.092	0.019	0.00314	0.00045	0.006	0.051	-0.00209	0.00012	0.006	0.041	5.2	1.1	40	130	0.28	0.21

\* Fe is used as internal standard reference, thus of assumed abundance, here set to Fe0 = 96 with Fe0 for FeH90-100 phases, and then use Fe0 = Fe203 = 8.9981.

Sample	Analysis #	Phase	Fe [ppm]	Zn [ppm]	Zr [ppm]	... (total 44 elements)																																																								
BMB894	Zrcon_Sample-072.FIN2	Fe-rich	70000	0.069	0.51	436	96	97	27	95	20	4880	680	230	72	44	1.2	0.43	0.28	0.14	0.11	0.1	0.013	0.017	0.004	0.022	0.024	0.011	0.0018	0.008	0.04	0.04	0.081	0.082	-0.00178	0.00017	0.01	0.12	-0.072	0.007	0.014	-0.011	0.029	0.027	0.02	0.045	0.049	0.008	0.024	0.006	0.033	0.016	0.027	0.027	0.002	0.047	1.48	0.33	110	210	0.1	0.067
BMB894	Zrcon_Sample-073.FIN2	Fe-rich	70000	0.001	0.091	580	130	28	90	18	4660	700	120	30	1.05	0.71	1.8	1.1	2.1	1.5	0.51	0.15	1.4	0.6	0.01	0.02	0.01	0.011	0.016	0.01	0.02	0.011	0.04	0.18	0.11	0.015	0.062	0.17	0.1	0.011	0.016	0.001	0.028	0.02	0.01	0.012	0.009	0.008	0.009	0.004	0.015	0.02	0.1	0.1	0.002	0.019						



Sample	Analysis #	Phase	Fe [ppm]	2s	3s	Ti [ppm]	2s	V [ppm]	2s	Cr [ppm]	2s	Mn [ppm]	2s	Co [ppm]	2s	Cu [ppm]	2s	Zn [ppm]	2s	Mg [ppm]	2s	Sr [ppm]	2s	La [ppm]	2s	Ce [ppm]	2s	Pr [ppm]	2s	Nd [ppm]	2s	Sm [ppm]	2s	Eu [ppm]	2s	Gd [ppm]	2s	Tb [ppm]	2s	Dy [ppm]	2s	Ho [ppm]	2s	Er [ppm]	2s	Tm [ppm]	2s	Yb [ppm]	2s	Lu [ppm]	2s	Hf [ppm]	2s	W [ppm]	2s	Mo [ppm]	2s	Pb [ppm]	2s		
BMS989	Zircon_Sample-255-FIN2	Fe-rich	700000	0.11	0.11	2.1	8.4	3.65	3.31	5.1	5.7	140	14	67.4	7.1	83	18	7.1	6.6	25.1	7.1	4.2	1.7	5.7	1.7	0.07	0.01	0.029	0.094	0.01	0.03	0.03	0.16	0.09	0.24	0.038	0.041	-0.22	0.67	0.032	0.034	-0.024	0	-0.005	0.02	-0.04	0.11	0.003	0.013	-0.03	0.11	0.025	0.021	0.136	0.18	0.316	0.074	24	70	0.09	0.17

\* Fe is used as internal standard reference, thus of assumed abundance, here set to FeO + Si wts FeO for FeO-130 phases, and then use FeO + Fe2O3 + 0.899Fe1.

Sample	Analysis #	Phase	Fe [ppm]	2s	3s	Ti [ppm]	2s	V [ppm]	2s	Cr [ppm]	2s	Mn [ppm]	2s	Co [ppm]	2s	Cu [ppm]	2s	Zn [ppm]	2s	Mg [ppm]	2s	Sr [ppm]	2s	La [ppm]	2s	Ce [ppm]	2s	Pr [ppm]	2s	Nd [ppm]	2s	Sm [ppm]	2s	Eu [ppm]	2s	Gd [ppm]	2s	Tb [ppm]	2s	Dy [ppm]	2s	Ho [ppm]	2s	Er [ppm]	2s	Tm [ppm]	2s	Yb [ppm]	2s	Lu [ppm]	2s	Hf [ppm]	2s	W [ppm]	2s	Mo [ppm]	2s	Pb [ppm]	2s		
BMS989	Zircon_Sample-081-FIN2	Fe-rich	700000	0.075	0.054	3.0	390	302	26	1548	63	4050	200	763	27	165	15	6.5	1.8	45.9	1	1.57	0.13	1	0.11	0.19	0.12	1.33	0.24	0.189	0.039	0.83	0.21	0.198	0.072	0.014	0.077	0.137	0.064	0.061	0.0075	0.228	0	0.443	0.074	0.137	0.037	0.049	0.003	0.031	0.035	0.021	0.048	0.002	0.016	2.83	0.3	590	770	0.258	0.038

\* Fe is used as internal standard reference, thus of assumed abundance, here set to FeO + Si wts FeO for FeO-130 phases, and then use FeO + Fe2O3 + 0.899Fe1.

Sample	Analysis #	Phase	Fe [ppm]	2s	3s	Ti [ppm]	2s	V [ppm]	2s	Cr [ppm]	2s	Mn [ppm]	2s	Co [ppm]	2s	Cu [ppm]	2s	Zn [ppm]	2s	Mg [ppm]	2s	Sr [ppm]	2s	La [ppm]	2s	Ce [ppm]	2s	Pr [ppm]	2s	Nd [ppm]	2s	Sm [ppm]	2s	Eu [ppm]	2s	Gd [ppm]	2s	Tb [ppm]	2s	Dy [ppm]	2s	Ho [ppm]	2s	Er [ppm]	2s	Tm [ppm]	2s	Yb [ppm]	2s	Lu [ppm]	2s	Hf [ppm]	2s	W [ppm]	2s	Mo [ppm]	2s	Pb [ppm]	2s
BMS989	Zircon_Sample-150-FIN2	Fe-rich	700000	0.013	0.048	8.3	7	166	21	15.8	2.2	1450	130	161.7	7.4	139	12	3.61	0.41	3.7	2	3.14	0.46	0.49	0.23	0.011	0.039	0.07	0.14	0.018	0.031	0.029	0.093	-0.01	0.16	0.015	0.014	0.03	0.29	0	0.01	0.039	0.05	0.25	-0.009	0.011	0.01	0.17	0.024	0.049	-0.012	0.077	0.65	0.12	-10	130	0.059	0.055	

\* Fe is used as internal standard reference, thus of assumed abundance, here set to FeO + Si wts FeO for FeO-130 phases, and then use FeO + Fe2O3 + 0.899Fe1.

Sample	Analysis #	Phase	Fe [ppm]	2s	3s	Ti [ppm]	2s	V [ppm]	2s	Cr [ppm]	2s	Mn [ppm]	2s	Co [ppm]	2s	Cu [ppm]	2s	Zn [ppm]	2s	Mg [ppm]	2s	Sr [ppm]	2s	La [ppm]	2s	Ce [ppm]	2s	Pr [ppm]	2s	Nd [ppm]	2s	Sm [ppm]	2s	Eu [ppm]	2s	Gd [ppm]	2s	Tb [ppm]	2s	Dy [ppm]	2s	Ho [ppm]	2s	Er [ppm]	2s	Tm [ppm]	2s	Yb [ppm]	2s	Lu [ppm]	2s	Hf [ppm]	2s	W [ppm]	2s	Mo [ppm]	2s	Pb [ppm]	2s
BMS989	Zircon_Sample-072-FIN2	Fe-rich	700000	0.079	0.091	2.6	4.1	8.97	0.69	7.9	4	1054	43	8.04	0.89	4.7	0.54	4.5	0.14	3.6	0.9	0.34	0.16	0.062	0.051	0.041	0.062	0.028	0.068	0.012	0.024	-0.02	0.12	0.047	0.037	0.016	0.1	0.5	0.013	0.011	0	0.0045	0.0088	-0.003	0.046	-0.00046	0.0011	0.008	0.086	0.0071	0.0098	0.024	0.029	0.138	0.041	120	220	0.01	0.019



Table with 4 columns: Sample, Analysis #, Phase, and a large grid of numerical data representing various elemental concentrations for Fe and FeO.

\* Fe is used as internal standard reference, thus of assumed abundance, here set to Fe = 56 with FeO for FeO 100 phases, and then use FeO = FeO3 x 0.89881.

Table with 4 columns: Sample, Analysis #, Phase, and a large grid of numerical data representing various elemental concentrations for Fe and FeO.

\* Fe is used as internal standard reference, thus of assumed abundance, here set to Fe = 56 with FeO for FeO 100 phases, and then use FeO = FeO3 x 0.89881.

Table with 4 columns: Sample, Analysis #, Phase, and a large grid of numerical data representing various elemental concentrations for Fe and FeO.

\* Fe is used as internal standard reference, thus of assumed abundance, here set to Fe = 56 with FeO for FeO 100 phases, and then use FeO = FeO3 x 0.89881.

Table with 4 columns: Sample, Analysis #, Phase, and a large grid of numerical data representing various elemental concentrations for Fe and FeO.

